

Higgs Phenomenology in the Standard Model and Beyond

A Dissertation Presented

by

Bryan Jonathan Field

to

The Graduate School

in Partial Fulfillment of the

Requirements

for the Degree of

Doctor of Philosophy

in

Physics

Stony Brook University

May 2005

Copyright © by
Bryan Jonathan Field
2005

Stony Brook University

The Graduate School

Bryan Jonathan Field

We, the dissertation committee for the above candidate for the Doctor of Philosophy degree, hereby recommend acceptance of this dissertation.

John Smith

C.N. Yang Institute for Theoretical Physics, Stony Brook University
Dissertation Director

George Sterman

C.N. Yang Institute for Theoretical Physics, Stony Brook University
Chairman of Dissertation

Christopher Jacobsen

Department of Physics, Stony Brook University

Sally Dawson

High Energy Theory Group
Department of Physics, Brookhaven National Laboratory

This dissertation is accepted by the Graduate School.

Dean of the Graduate School

Abstract of the Dissertation

Higgs Phenomenology in the Standard Model and Beyond

by

Bryan Jonathan Field

Doctor of Philosophy

in

Physics

Stony Brook University

2005

The way in which the electroweak symmetry is broken in nature is currently unknown. The electroweak symmetry is theoretically broken in the Standard Model by the Higgs mechanism which generates masses for the particle content and introduces a single scalar to the particle spectrum, the Higgs boson. This particle has not yet been observed and the value of its mass is a free parameter in the Standard Model. The observation of one (or more) Higgs bosons would confirm our understanding of the Standard Model.

In this thesis, we study the phenomenology of the Standard Model Higgs boson and compare its production observables to those of the Pseudoscalar Higgs boson and the lightest scalar Higgs boson of the Minimally Supersymmetric Standard Model. We study the production at both the Fermilab Tevatron and the future CERN Large Hadron Collider (LHC). In the first part of the thesis, we present the results of our calculations in the framework of perturbative QCD. In the second part, we present our resummed calculations.

For my parents, Margaret and Christopher, who never got to see this...
... and for my Angeliki, who understood.

Contents

List of Figures	xiii
List of Tables	xiv
Preface	xv
Acknowledgements	xx
Cirriculum Vitæ	xxi
1 Introduction	1
1.1 Standard Model	2
1.2 SM as a Field Theory	5
1.2.1 Symmetries	5
1.2.2 Gauge Invariance	6
1.2.3 Goldstone bosons	9
1.3 Electroweak Symmetry Breaking	9
1.3.1 Higgs mechanism	10
1.3.2 Bounds on Higgs mass	13
1.4 SM Lagrangian	19
1.4.1 Feynman rules	20
1.4.2 Polarizations, gauges, and ghosts	22
1.5 Quantum Chromodynamics (QCD)	24
1.5.1 Quark Model	24
1.5.2 Regularization and renormalization	25
1.5.3 Running of α_s and pQCD	28
1.6 Partons, Hadrons, and Observables	30
1.6.1 Lowest order cross-section	32
1.6.2 Higher order cross-sections	34
1.7 Resummation	40
1.8 Why supersymmetry?	41

1.8.1	MSSM	44
1.9	HQET	47
1.10	SM predictions	49
1.11	Roadmap ahead	51
I	Higgs Phenomenology in pQCD	52
2	Distinguishing scalar from pseudoscalar Higgs production at the LHC	53
2.1	Introduction	53
2.2	Effective Lagrangian	54
2.3	Observables and Moments	55
2.4	Conclusions	61
3	NLO corrections to differential cross sections for pseudoscalar Higgs boson production	64
3.1	Introduction	64
3.2	Effective Lagrangian	65
3.3	Kinematics	67
3.4	Corrections	68
3.5	Conclusions	74
4	Scalar and Pseudoscalar Higgs Boson Plus One Jet Production at the LHC and Tevatron	78
4.1	Introduction	78
4.2	Partonic Processes - Heavy Quark Effective Theory	80
4.3	Partonic Processes - Full Theory	83
4.3.1	Gluon fusion ($gg \rightarrow g\Phi$)	83
4.3.2	Quark-antiquark annihilation ($q\bar{q} \rightarrow g\Phi$)	85
4.3.3	HQET Matrix Elements	85
4.3.4	Small Quark Mass Limit	86
4.4	Observables	87
4.5	Numerical Results	88
4.5.1	Standard Model	88
4.5.2	Minimal Supersymmetric Standard Model	88
4.6	Conclusions	92

II	Resummation and the Higgs Boson	100
5	Next-to-leading Log Resummation of Scalar and Pseudoscalar Higgs Boson Differential Cross-Sections at the LHC and Tevatron	101
5.1	Introduction	101
5.2	Heavy Quark Effective Theory	102
5.2.1	Scalar Higgs Matrix Elements	104
5.2.2	Pseudoscalar Higgs Matrix Elements	109
5.3	Resummation	111
5.3.1	Formalism	112
5.3.2	Matching	114
5.3.3	Higgs Resummation	115
5.4	Results and Conclusions	120
6	Higgs Boson Resummation via Bottom-Quark Fusion	132
6.1	Introduction	132
6.2	Setup	134
6.3	Resummation	135
6.4	Results and Conclusions	138
	Bibliography	153
A	Cross-sections and widths	154
A.1	Cross-section	154
A.2	Width	155
B	The Clifford Algebra	156
B.1	Algebra and Group Theory	157
C	Group Theory	160
C.1	$SU(2)$	160
C.2	$SU(3)$	160
D	Loop Integrals	162
D.1	Feynman parametrization	162
D.2	Tensor Reduction	163
E	Mathematical Reference	164
E.1	Euler Gamma	164
E.2	Beta function	164
E.3	Dilogarithms	165

E.4 Expansions	165
--------------------------	-----

List of Figures

1.1	Spontaneous symmetry breaking.	11
1.2	Sample Higgs-Higgs scattering diagrams.	15
1.3	Theoretical Higgs mass limits.	16
1.4	WW scattering (sample diagrams).	18
1.5	Electroweak fit for the SM Higgs mass (February 2005).	19
1.6	Parton Model.	32
1.7	Drell-Yan W^\pm production (sample diagrams).	33
1.8	Phase space singularities.	38
1.9	Self energy mass corrections.	42
1.10	Effective gluon-gluon-Higgs vertex.	48
1.11	Function $ F_{1/2} ^2$ approaches the HQET limit.	49
1.12	Tevatron Run II and LHC total cross-sections.	50
2.1	Total cross-sections for scalar and pseudoscalar Higgs plus two jets. These curves are for the LHC with the cuts described in the text.	56
2.2	Normalized transverse momentum spectrum of the scalar or pseudoscalar Higgs production channels plus two jets. The Higgs mass for both the scalar and pseudoscalar is 120 GeV. Note that the pseudoscalar Higgs has been displaced down by 10% to allow the two curved to be distinguished. These curves are for the LHC with the cuts described in the text.	57
2.3	Normalized opening angle in the center-of-momentum frame between the Higgs and the highest p_t jet for the scalar and pseudoscalar Higgs production channels plus two jets. The Higgs mass for both the scalar and pseudoscalar is 120 GeV. Note that the pseudoscalar Higgs has been displaced down by 20% to allow the two curved to be distinguished. These curves are for the LHC with the cuts described in the text.	58

2.4	Normalized integrated moment $\alpha[a_1]$ for the scalar and pseudo-scalar Higgs plus two jets. The center curve shows what the observable would look like if both of the processes were to be measured at the same time with degenerate masses. The splitting between the two different production channels is clear at all mass scales with a statistical uncertainty of about 5%. These curves are for the LHC with the cuts described in the text. . .	60
3.1	The ratio R in Eq. (3.46) plotted as a function of p_T for $\sqrt{S} = 14$ TeV and $\mu^2 = p_T^2 + m_B^2$ with $m_H = m_{A^0} = 120$ GeV/c ² ; $R^{\text{LO}}(M_t = \infty)$ (dotted line), $R^{\text{LO}}(M_t = 173.4)$ (solid line) $R^{\text{NLO}}(m_t = \infty)$ (dot-dashed line) $R^{\text{NLO}}(M_t = 173.4)$ (dashed line).	75
3.2	The transverse momentum distribution $d\sigma_A/dp_T$ with $\mu^2 = p_T^2 + M_{A^0}^2$, $M_{A^0} = 91.9$ GeV/c ² , $\tan\beta = 0.5$; $\sqrt{S} = 14$ TeV (solid line), $\sqrt{S} = 2$ TeV (dashed line).	76
3.3	The rapidity distribution $d\sigma_{A^0}/dy$ calculated from the integral of $d^2\sigma_{A^0}/(dp_T dy)$ between $8 p_{T,\text{min}} > p_T > p_{T,\text{min}}$ and $p_{T,\text{min}} = 30$ GeV/c. Input parameters are $\mu^2 = p_{T,\text{min}}^2 + M_{A^0}^2$, $M_{A^0} = 91.9$ GeV/c ² , $\tan\beta = 0.5$; $\sqrt{S} = 14$ TeV (solid line), $\sqrt{S} = 2$ TeV (dashed line).	77
4.1	Sample Higgs plus one jet diagrams. Figures 4.1a,b are the gg diagrams, 4.1c is the $q\bar{q}$ channel, and 4.1d is the $q\bar{q}$ channel. All quarks contribute to the loops. The crossed and charge conjugate diagrams are not shown. There are a total of 12 gg diagrams and 2 for each of the $q\bar{q}$ and $q\bar{q}$ sub-processes. . . .	81
4.2	The squared matrix elements, $ \mathcal{M} ^2$, evaluated at $\hat{s} = 4m_\Phi^2$ and $\hat{u} = \hat{t}$ for the three different channels, (gg , $q\bar{q}$, $q\bar{q}$), normalized to the squared matrix elements in the HQET for scalar and pseudoscalar (with $g_A = 1$) Higgs plus jet production. We include only the top quark loops. The solid line is the scalar, whereas the dashed line is the pseudoscalar.	84
4.3	Transverse momentum distributions for the SM Higgs boson plus one jet production at the LHC with $M_H = 120$ GeV/c ² for the different channels. The curves labeled ‘Top’ (‘Bot’) include <i>only</i> the top (bottom) quark loops.	89
4.4	Transverse momentum distributions for the SM Higgs (H) plus one jet and for a pseudoscalar (A^0) plus one jet in the full theory with only the top-quark loops included and in the HQET at the LHC for $M_\Phi = 120$ GeV/c ² . We assume $g_A = 1$	90

4.5	The transverse momentum distributions for the MSSM pseudo-scalar Higgs boson for $\tan \beta = 30, 40, 50$ and $M_{A^0} = 120 \text{ GeV}/c^2$ at the Tevatron including the top and bottom quark loops. The top, middle, and bottom lines in the top graph are the curves for $\tan \beta = 50, 40, 30$ respectively. Below is the fraction of the process that comes from each of the different channels. The curves at $p_t = 250 \text{ GeV}/c$ from top to bottom are the qg , gg , and $q\bar{q}$ channels respectively.	91
4.6	Cross-section for the production of the MSSM pseudoscalar Higgs boson plus one jet for different values of $\tan \beta$ at the LHC for $M_{A^0} = 120 \text{ GeV}/c^2$ integrated for $p_t > 30 \text{ GeV}/c$ using the full theory matrix elements. The top and bottom labels show what the contribution of the top and bottom quark would be alone. In the region $4 < \tan \beta < 8$ the total cross-section is not represented well by either the top or bottom matrix elements alone. In the experimentally accessible region, the total cross-section at the Tevatron is dominated by the bottom loop so only the bottom contribution is shown for $\tan \beta > 30$	93
4.7	Cross-section for the production of the MSSM lightest scalar Higgs boson plus one jet for different values of $\tan \beta$ integrated for $p_t > 30 \text{ GeV}/c$ using the full theory matrix elements. The top and bottom labels show what the contributions of the top and bottom quark would be alone. In the experimentally accessible region, the total cross-section at the Tevatron is dominated by the bottom loop, so only the bottom contribution is shown for $\tan \beta > 30$. Below is the corresponding mass of the lightest scalar for $M_{A^0} = 120 \text{ GeV}/c^2$	94
5.1	The transverse momentum spectrum for the scalar and pseudo-scalar Higgs boson at the LHC for $ y \leq 2.5$. The p_t distribution peaks at approximately 15 GeV . The resummed curve is the NLL resummation, and the perturbative curve is the NLO fixed order calculation. The NLO fixed order calculation diverges in the negative direction at small p_t . This piece of the differential cross-section is not shown for clarity. These two curves cross at approximately $p_t = 100 \text{ GeV}/c$ and stay very close thereafter.	121

5.2	The transverse momentum spectrum for the scalar and pseudo-scalar Higgs boson at the Tevatron for $ y \leq 2.5$. The p_t distribution peaks at approximately 10 GeV. The resummed curve is the NLL resummation, and the perturbative curve is the NLO fixed order calculation. The NLO fixed order calculation diverges in the negative direction at small p_t . This piece of the differential cross-section is not shown for clarity. These two curves cross at approximately $p_t = 80$ GeV/c and stay very close thereafter.	122
5.3	The effects of increasing Higgs mass on the transverse momentum spectrum at the LHC for $ y \leq 2.5$. The $M_H = 250$ GeV/c ² curve peaks at approximately 23 GeV/c. We can clearly see that the resummed curve peaks at higher p_t with increasing Higgs mass and that the width of the resummed distribution becomes wider with increasing Higgs mass.	123
5.4	This is the scale uncertainty in the transverse momentum spectrum for the pseudoscalar Higgs boson. The upper figure shows the variation on the differential cross-section at its peak near 15 GeV/c over a scale variation of an order of magnitude. The upper figure shows both the MRST and CTEQ parton distribution function. The lower figure shows the variation over the whole spectrum when the scale is varied by a factor of two. It is easy to see that the largest scale uncertainty is at the peak value.	124
5.5	The uncertainty due to the parton distribution functions for the CTEQ 6.1M parton distribution functions. The resummation is done for the gg initial state only and therefore has the largest PDF uncertainty. A $q\bar{q}$ initial state would have a smaller PDF uncertainty.	125
6.1	Diagrams needed for the $b\bar{b}$ initial state resummed differential cross-section. Figure 6.1a is the lowest order production channel and couples differently for different Higgs bosons. Figure 6.1b is the virtual correction to the lowest order process. Figure 6.1c is the lowest order graph contributing to the differential cross-section. The crossed graph is not shown.	134

6.2	Figure 6.2a shows the errors associated with the CTEQ6.1M PDF set. The variation is approximately 8 – 12%. Figure 6.2b show the variation of the renormalization and factorization scale for a factor of 1/4 and 4. These scales were chosen because there has been great interest [169–172] in the scale $\mu = M_\Phi/4$. We find this variation to be approximately 20%.	139
6.3	The movement of the peak of the differential distribution (at 15 GeV) for a variation in the scale by a factor of 10.	140

List of Tables

1.1	The elementary particles of the Standard Model.	3
1.2	The gauge structure of the Standard Model.	4
1.3	QCD Feynman rules.	21
1.4	Group structure of chiral superfields and gauge multiplets in the MSSM.	45
4.1	Higgs-fermion couplings in the MSSM and the dependence of the matrix element-squared on the couplings. \mathcal{M}_t and \mathcal{M}_b represent contributions from top- and bottom- quark loops, respectively. The α parameter is the angle that diagonalizes the CP-even Higgs squared-mass matrix.	80
B.1	Clifford algebras in even dimensions.	158
C.1	Non-vanishing $SU(3)$ structure constants.	161

Preface

I have always felt it is important to put things in perspective, especially in physics. Especially at the beginning. Reading a paper or attending a seminar is very different from talking with someone about why a certain problem was considered, especially if the results were unexpected. Oftentimes I would hear in a talk about a different problem that was being studied that inspired the current research or that much of the work for a current problem had been accomplished under different circumstances, but I have never read about it in the scientific literature because these sorts of observations would be out of place in a journal. This thesis presents my research, but I would like put it in context. I began graduate school at Stony Brook in 1999 and it has proved to be an incredible time to be a physicist in training.

While I have been in graduate school, the Large Electron-Positron Collider (LEP) at CERN saw an indication (5 events) for the existence of the Higgs Boson (see Ref. [1]) which later turned out to be statistically insignificant. After running for eleven years LEP was turned off and removed from its tunnels underneath France and Switzerland to make room for the Large Hadron Collider (LHC). The mass of the top quark, which was discovered right as I began my bachelors degree, was measured at the Tevatron with higher and higher precision leading to a better (albeit indirect) prediction for the Higgs mass. This new top mass moved the prediction for the Higgs mass from formally “ruled-out” to (informally) “just around the corner”. This excitement however has been tempered by luminosity problems at Fermilab. The U.S. Higgs community is breathing a collective (but good-natured) sigh of frustration as we watch these problems and our hopes slip away for an American collider seeing a Higgs signal before the completion of the European LHC, currently expected in 2007. In the end, it is the science that will be remembered. Which collider sees the signal is not the most pressing problem, but everyone agrees that the sooner a signal is seen the better. I cannot think anyone would be disappointed if the Tevatron discovered the Higgs and the LHC found supersymmetry. We’ll all have to wait and see, seeing something is always better than seeing nothing.

However, I have skipped ahead. Let me move back to the first indication of a Higgs signal at LEP in September 2000. I was taking Quantum Field Theory (QFT) from my Stony Brook adviser Jack Smith, with whom I was interested in working. He told us about the tantalizing hint of a Higgs signal and what it would mean to find the Higgs boson and also what it would mean if the signal was accurate and the collider was shut down to build the LHC as scheduled before confirming the Higgs signal. I still remember his words, “If they are wrong, they will write it on their tombstones.” At the time, the Higgs seemed close enough to taste and an excellent topic to study.

While the Higgs was looming large, a new semester began and so came another QFT course. As the semester began, the $(g - 2)_\mu$ experiment at Brookhaven National Laboratory released the first analysis of their data set [2]. This was an extraordinary paper because in its final few paragraphs, it predicted that the discrepancy between theory and experiment was due to the effects of a supersymmetric particle with a mass between 120 – 400 GeV. The halls and offices at Stony Brook and Brookhaven were buzzing with interest and excitement, but it was hard to describe this excitement to my family. If physicists could measure something with such incredible precision (roughly being able to measure the distance between New York and Tokyo with an error bar less than 18 feet) it was difficult to explain why it was so exciting that we were expecting a number different by a few fractional parts per million. I suppose I’m not the only one with difficulties describing my work to my family, and this is still an open question. I went to speak with Jack and told him of my interest in $(g - 2)_\mu$. With the release of this first paper, we had learned in his class about the different contributions to $(g - 2)_\mu$ and which were considered to be under good theoretical control and which contributions still needed work.

Jack showed me another paper [3] that had quickly followed the $(g - 2)_\mu$ results which claimed that perhaps the disagreement between theory and experiment was not as large as previously thought. Although we had initially thought that this would make an ideal summer project for my oral exam, we later decided that it would have been too difficult for me to tackle by myself over the summer while Jack worked with collaborators in Europe. We decided on a project involving the Higgs boson instead dealing with helicity amplitudes to check a calculation already underway. It was later shown that there was an error in the original $(g - 2)_\mu$ theoretical analysis involving a specific sub-process [4] that brought the difference between theory and experiment to a more reasonable level making the Higgs project much more attractive in hindsight. The problem in the theoretical analysis for $(g - 2)_\mu$ was a fundamental one and will be discussed later in this thesis. In short, it is important

to understand the metric in a calculation and what it means to do a calculation on a computer and not on a chalkboard. Since the first findings of the Brookhaven experiment there has been a constant repartee between theory and experiment about the size of each of their respective error bars. It is a little odd that our community cares more about the error bars than the central value. Currently there is agreement of about 1.4 standard deviations (when different data sets are included in the theory calculation), which is considered moderately acceptable by the particle physics community.

While particle physics was becoming more familiar to me, I also was exploring large-scale structures in my breadth courses. I took General Relativity (GR) with the very accomplished theorist Martin Roček opposite my first class in QFT. At the time, the geometry of the universe was still very much an open question. Near the end of the semester, there was the report of a measurement of the power spectrum of the Cosmic Microwave Background (CMB) from a hot-air balloon flown over Antarctica [5]. This was very interesting because with the precision the cosmological parameters had just been measured one could use the words “precision cosmology” in the same sentence without laughing (or being laughed at). Martin had told us a story of a cosmology paper that, due to a computational error, had to be replaced after changing their results by a factor of 10^{60} . However, this correction did not change the conclusions of the paper. The comparisons with $(g-2)_\mu$ are left to the reader. Needless to say, more precision was needed in cosmology.

After years of research using the usual astrophysical methods for measuring the cosmological parameters, there were still enormous error bars on all the important quantities. Many had error bars so large, the sign of the quantity was still unknown. Worse yet, cosmologists had formed camps with their own preferred central values of all the important parameters used in their papers. This new paper from the Boomerang balloon experiment with its high precision measurements allowed the community to move beyond these limitations.

Buoyed by my experience with GR, I signed up for Cosmology the next semester, taught by an astronomer who had made many important contributions to cosmology, Amos Yahil. Although the previous analysis was not lost on our class, it was the longer paper showing the complete analysis [6] that turned heads in the astronomy community at Stony Brook. I had chosen to do my final class project on the Microwave Anisotropy Probe (now known as the Wilkinson Microwave Anisotropy Probe or WMAP), a NASA satellite designed to improve the previous COBE measurements of the CMB [7].

The Antarctic balloon had scooped the WMAP results by two years for much less money and much less lead time. The current WMAP results [8] are spectacular in their own right (the satellite is still taking data and follow-up

missions are planned). The most amazing result that the probe revealed is that the part of the universe that we can see (the baryonic matter) makes up only roughly 3% of the energy density of the universe. The probe also told us more about dark matter in a more quantitative way, the existence of which was not a surprise from what is known from rotation curves of galaxies and clusters. The big WMAP surprise was the dark energy. Dark energy, according to WMAP, made up 70% of the energy density of our universe. I would say that this stands as the most embarrassing measurement in all of physics. In contrast to dark matter, physicists do not even have a good candidate for understanding dark energy. It is simply not possible to overstate the impact these results are having on the particle physics community. The future certainly holds that progress in both the high-energy and cosmological communities will be tied together to resolve this problem.

In between learning of a possible Higgs signal and writing these words, I learned the day-to-day skills of a theorist in a very intense way from my involvement with the High Energy Group at Brookhaven National Laboratory. I met my Brookhaven adviser, Sally Dawson, taking a course she taught at Stony Brook in Electroweak Symmetry Breaking. Sally and I began working together that summer after I returned from a summer school in Colorado and have continued working together ever since. The High Energy Group at Brookhaven complimented the group at Stony Brook in many ways and vice-versa. Overall, the differences in the ambiance of a National Laboratory and a research university are the most striking, and are perhaps best left for another time.

It would be professionally derelict of me not to at least mention the other great theoretical revolution during my time at Stony Brook, the verification that neutrinos are massive. Although WMAP also had something to say about the mass of neutrinos, it was the oscillation experiments at KEK [9] that first grabbed my attention (albeit well after they were published) after seeing a colloquium on the subject. Between the Higgs and $(g-2)_\mu$ talks at Stony Brook and Brookhaven, neutrino masses complete the triumvirate of phenomenology talks I have attended. What I remember most about the neutrinos is that they were a large piece of the puzzle standing in the way of understanding the Standard Solar Model (SSM) of the great theorist John Bahcall.

Dr. Bahcall came to Stony Brook to give a talk about neutrinos and the SSM to a general audience which I attended with great interest. It was at his talk that I came to an understanding of all these varied subjects and his talk in particular seemed to bring everything together for me. I would like to close this reflection by sharing these thoughts.

We use particle physics to understand the universe, great and small. We

thought we understood particle physics well enough to say that an incredibly small discrepancy in the $(g-2)_\mu$ measurement was the signature of an entirely new sector of physics that changes the very nature of space-time, when all the while 70% of the universe was “missing” from our understanding, both theoretically and observationally. As an analogy, one could say the current situation in physics would be equivalent to a statement by a biologist that the terrestrial ecosystem was understood so well as to make precise predictions on human evolution without ever knowing anything of the life in our oceans, or even that they existed at all. The most dangerous thing is what we do not know that we do not know. And like the drunk man looking for his car keys under the street light because that is where he can see, so do I approach my research. This is an exploration of what we can see where we can see it. We do not yet understand our universe, but hopefully, this work will be a small ray of light under which we can look for physics.

Bryan J. Field
Coram, New York
April 12, 2005

Acknowledgements

I owe a great debt to many people. First and foremost, I need to thank my wife Angeliki for her patience, love, and insight while I was consumed by other things. I would also like to thank my brother, Adam, who has always set the intellectual bar for me, and my sister, Ingrid, for putting up with my antics and keeping me grounded. I need to thank my Aunt Phyllis and Uncle Doug who have filled a great void in my life and for the advice they have given.

Beyond my family, I have been fortunate enough to interact with other great graduate students in the C.N. Yang Institute for Theoretical Physics. Thank you Tibor, my mentor, Carola, and Neil for all the insight, conversations, and encouragement. Also, I would like to thank a colleague of mine, Maria Elena Tejada-Yeomans, who helped me understand physics on a whole new level. I cannot forget my other graduate friends, Sean and Shawn, with whom I've had so much fun, and Jack Laiho, my office-mate at Brookhaven. Thank you all.

Many faculty members have helped me understand modern physics during my time at Stony Brook. I would like to thank Robert Shrock, George Sterman, and Peter van Nieuwenhuizen. I would also like to thank the astronomy group for not throwing the particle physicist out of their talks and for answering all of my questions. I have also been fortunate enough to have the dream team of scientific advisors. I am extremely indebted to Jack Smith and Sally Dawson.

Finally, I would like to personally thank Pat Peiliker for helping me get through it all when I needed help.

Cirriculum Vitæ

- B. Field “*Distinguishing scalar from pseudoscalar Higgs production at the LHC*”, Phys. Rev. D **66** 114007 (2002) [hep-ph/0208262]
- B. Field, J. Smith, M.E. Tejeda-Yeomans, and W.L. van Neerven “*NLO corrections to differential cross sections for pseudo-scalar Higgs boson production.*”, Phys. Lett. B **551** 137-145 (2003) [hep-ph/0210369]
- B. Field, S. Dawson, and J. Smith “*Scalar and pseudoscalar Higgs boson plus one jet production at the LHC and Tevatron.*”, Phys. Rev. D **69** 074013 (2004) [hep-ph/0311199]
- B. Field “*Next-to-leading Log Resummation of Scalar and Pseudoscalar Higgs Boson Differential Cross-Sections at the LHC and Tevatron*”, Phys. Rev. D **70** 054008 (2004) [hep-ph/0405219]
- B. Field “*Higgs Boson Resummation via Bottom-Quark Fusion*”, [hep-ph/0407254]
- B. Field “*Associated production of A^0 and Z^0 bosons and rare pseudo-scalar Higgs decays*”, [hep-ph/0502195]

Chapter 1

Introduction

This thesis will explore the collider phenomenology of the Standard Model (SM) Higgs boson and the Higgs bosons of the Minimally Supersymmetric Standard Model (MSSM). We will begin by reviewing several concepts and notations so that our results can be cast in a uniform light. There is a balance that has to be reached in our introduction to particle physics. This presentation is in no way a replacement for textbook knowledge [10–12, 14] on the subject, but is merely a recapitulation of some of the topics and issues that will be of importance to Higgs research.

We will begin with a brief review of what is known about the SM, and then move on to how to incorporate this knowledge into our theoretical understanding. The current picture of Electroweak Symmetry Breaking (EWSB) will be described as well as the electroweak and strong sectors of the SM. We will then discuss current theoretical and experimental bounds on the SM Higgs.

Supersymmetry will be introduced next as a way of coming to the Minimally Supersymmetric Standard Model. We will determine how the introduction of supersymmetry changes the Higgs sector and a brief discussion of parameters in the SM and MSSM. Finally, we will introduce the Heavy Quark Effective Theory (HQET) for Higgs phenomenology and show how it can simplify Higgs calculations.

Also, it should be noted that when the phrase “Standard Model” is used, one is referring to a very specific model with specific assumptions and a specific method of breaking the electroweak symmetry. A more appropriate phrase might be the “Minimal Standard Model”. This assumption will be implicit in our description of the Standard Model throughout this work with any exceptions noted.

A word on confusion

It has been said that what cannot be impressed upon students of particle physics is the confusion of the time when the discoveries that led to the creation of our current outlook on particle physics were made. It took more than a generation of great work by thousands of physicists to construct the Standard Model and there are countless ways to communicate their results. The SM will be presented in a way that (hopefully) makes it the easiest to understand without appearing to come to the right answer in the first pass and will be approached a few times from different perspectives. This mix of experimental observation and mathematical insight should give us the proper framework to understand the results presented.

Finally, when approached with a high level of mathematical rigor one can begin with unitarity or with renormalizability as the basis of a gauge field theory. A complete theory cannot be formulated with just one or the other, at some point the two methods will converge and both unitarity and renormalizability will be needed to find a usable theory. Each will be used when it best suits the situation.

1.1 Standard Model

Any viable theory of electroweak interactions must explain several qualitative experimental facts. We need to understand why the W^\pm bosons only couple to left-handed fermions (and right-handed anti-fermions), why the Z^0 boson couples differently to left-handed fermions and right-handed fermions but the photon couples with the same charge to both right- and left-handed fermions. There are also very stringent experimental tests limiting the relative strengths of fermion–anti-fermion–vector couplings as well as the ratio of the W^\pm and Z^0 boson masses. The electroweak sector of the SM incorporates all of these features and tests into a spontaneously broken gauge theory [15–17].

The Standard Model contains our best formulation to date in understanding particle physics phenomenology. The SM does have a few short-comings, but should be considered overall as an excellent description of nature. It is represented as an Abelian and non-Abelian spontaneously broken gauge theory that is unitary and renormalizable at its fundamental level based on a compact Lie algebra group structure. Its interactions are described by a complicated Lagrangian with several components.

$$\mathcal{L}_{\text{SM}} = \mathcal{L}_{\text{QCD}} + \mathcal{L}_{\text{EW}} + \mathcal{L}_{\text{gauge-fixing}} + \mathcal{L}_{\text{ghost}}. \quad (1.1)$$

Quarks 3 Colors	u^a up	c^a charm	t^a top	γ photon	Force Carriers
	$(d')^a$ down	$(s')^a$ strange	$(b')^a$ bottom	g^a gluon	
Leptons	ν_e electron neutrino	ν_μ muon neutrino	ν_τ tau neutrino	Z^0 Z boson	
	e electron	μ muon	τ tau	W^\pm W bosons	

Table 1.1: The elementary particles of the Standard Model.

We choose to break the SM Lagrangian into four basic parts. We have the strong interactions, the electroweak interactions, the gauge-fixing terms, and the ghost interactions. This is the proper setup for perturbative calculations. This Lagrangian taken with the observation that only colorless particles are seen in nature leads us to construct the SM.

Our understanding of the SM is predicated on our ability to measure its physical parameters in experiments. In this the age of precise measurements and monumental experiments, we need an equally precise theoretical understanding of the SM to understand the features and drawbacks of our current description of the universe. This is why the calculation of radiatively corrected observables is so important to our understanding of particle physics.

If the SM were a play, its known cast of characters is often depicted as in Table (1.1). Here we see that there are six known quarks (fractionally charged fermions) that appear in three different colors (corresponding to the index a). Three (colorless) charged leptons, each with a corresponding neutrino (also a lepton) and four force carriers for the three forces of the SM. By definition, the SM is a theory without gravitational interactions, because of this we will freely speak of three forces instead of four and leave gravity to the theory of General Relativity and its very successful phenomenological record. The strong force is carried by the gluon (of which there are 8 colored combinations), the electromagnetic force is carried by the familiar photon (γ) and the weak force is carried by the Z^0 and W^\pm bosons. Although this table is familiar, it hides some of the important details of the SM.

First, the SM contains right- and left-handed particles that appear in gauge singlets, doublets, and triplets. A better representation of the SM particles can be written

$$\psi_i = \begin{pmatrix} \nu_i \\ l_i^- \end{pmatrix}_L \quad i = e, \mu, \tau; \quad q_L^a = \begin{pmatrix} u_i \\ d_i' \end{pmatrix}_L \quad i = u(d), c(s), t(b)$$

	$SU(3)_c$	$SU(2)_L$	$U(1)_Y$
ψ_i	1	2	$-\frac{1}{2}$
l_R^-	1	1	-1
q_L^a	3	2	$+\frac{1}{6}$
u_R^a	$\bar{3}$	1	$+\frac{2}{3}$
$(d')_R^a$	$\bar{3}$	1	$-\frac{1}{3}$

Table 1.2: The gauge structure of the Standard Model.

$$[\nu_R], l_R^-, u_R^a, (d')_R^a, W^\pm, Z^0, \gamma, g, [H]. \quad (1.2)$$

In the top row are the $SU(2)_L$ left-handed doublets. The ψ_i field is a doublet of the left handed neutrinos and (negatively) charged leptons arranged by family. The ψ_i fields are $SU(3)_c$ singlets. The left-handed (colored) quark fields appear in $SU(2)_L$ doublets and are $SU(3)_c$ triplets. On the bottom we have $SU(2)_L$ singlets for the right-handed leptons and quarks. The vector bosons interact with the quarks and leptons and also have self-interactions. We can already see that there is a need for a method to systematically describe the particle interactions and their relative strengths.

Since we are going to construct the SM based on its group properties, we need to know how each of the fields transform under the group transformations as shown in Table (1.2). This will also help us when we try to expand the structure of the SM. We must make sure not to ruin what has already been built.

The right-handed neutrino is in square brackets because whereas there is compelling evidence that they exist in nature (neutrino oscillations [9] and neutrinoless double-beta decay [18, 19] point to non-zero neutrino masses), a right-handed neutrino is not needed by the SM and we will in fact define the SM as a model where right-handed neutrinos are absent and not concern ourselves with this complication any further. However, the Higgs boson (H) is missing from the SM and is needed to make it complete (without a change in our understanding). The SM Higgs is an $SU(2)_L$ doublet and a singlet under $SU(3)_c$.

We also note in this more complete description that the down-type quarks have different weak and mass eigenstates. It is a convention that the down type quarks mix. The quark mixing is defined by the Cabibbo-Kobayashi-Maskawa (CKM) matrix [20, 21],

$$\begin{pmatrix} d' \\ s' \\ b' \end{pmatrix}^a = \begin{pmatrix} V_{ud} & V_{us} & V_{ub} \\ V_{cd} & V_{cs} & V_{cb} \\ V_{td} & V_{ts} & V_{tb} \end{pmatrix} \begin{pmatrix} d \\ s \\ b \end{pmatrix}^a. \quad (1.3)$$

There are several ways to parametrize this quark mixing, but the values of the array elements have to be determined experimentally. The standard parametrization utilizes three angles and one complex phase to describe \mathcal{CP} violation. It should also be noted that this matrix is defined to be unitary in the SM, and deviations from unitarity are considered an extension to the SM in much the same way as right-handed neutrinos. The Higgs boson is in square brackets because it has not been discovered as of yet.

1.2 SM as a Field Theory

We have several empirical facts and observations about the particle and force content of the SM. Now we need to understand how to codify this understanding into our mathematical description of the SM in a systematic way so that we can make testable predictions. To do this, we will need a few more tools and some more mathematical observations. The SM is built on broken and unbroken symmetries, so this must be formalized first.

1.2.1 Symmetries

A Lagrangian (\mathcal{L}) is said to be invariant under a discrete or continuous symmetry group G if

$$U \in G, \quad U^{-1} \mathcal{L} U = \mathcal{L}. \quad (1.4)$$

We are interested in continuous symmetries based on Lie algebras. This implies that we can write the unitary matrix as

$$U = \exp(i\alpha Q), \quad (1.5)$$

where α is a continuous group parameter (allowing the transformation to be continuously transformed to back to the origin) and Q is a generator of the group. Furthermore, Q is hermitian ($Q = Q^\dagger$).

There are different observed realizations of this kind of symmetry. An exact symmetry (also known as a Wigner-Weyl symmetry) is a symmetry where the vacuum state is also invariant under the symmetry. Examples of this kind of symmetry are charge and color which are not believed to be broken or approximate in nature.

There can be physical states of a theory that are irreducible representations but may not be the states of the Lagrangian. Quark mixing is an example of this kind of symmetry where a diagonalization of the physical states must be performed for meaningful calculations to be performed. We will also eventually see this kind of symmetry in the Higgs sector of the MSSM as well as in its squark sector.

We can also have an approximate symmetry like isospin symmetry. The masses of the proton and neutron are not identical, but we can use them to estimate the violation of isospin symmetry. We find that $(m_n - m_p)/(m_n + m_p) < 10^{-3}$ making isospin symmetry a good symmetry if not an exact one. Another example would be the $SU(3)_F$ symmetry from lattice QCD and the small strangeness violation in the weak interactions. Both are forms of approximate symmetries.

Finally, we could have a situation where the Lagrangian is invariant under a group transformation, but the states of the theory do not transform as irreducible representations of the group. This leads to spontaneous symmetry breaking and is the basis of the Higgs mechanism which will be discussed at the appropriate time.

1.2.2 Gauge Invariance

To understand gauge invariance we will explore a few examples to see where our results lead us. We will begin with an Abelian gauge symmetry for simplicity, we have electromagnetism in mind to guide our calculation. Let us begin with a very general (complex scalar) Lagrangian,

$$\mathcal{L} = |\partial\varphi|^2 - m^2|\varphi|^2 - \lambda|\varphi|^4, \quad |\varphi|^2 = \varphi^\dagger\varphi, \quad |\partial\varphi|^2 = (\partial^\mu\varphi^\dagger)(\partial_\mu\varphi). \quad (1.6)$$

and we want this Lagrangian to be invariant under

$$\varphi \rightarrow \varphi' = U\varphi, \quad U \in U(1) : U = \exp(-i\theta Q). \quad (1.7)$$

If θ is independent of x (the space-time coordinate) then this is a global symmetry. We will promote this symmetry to a local symmetry by allowing $U = U(x)$ and $\theta = \theta(x)$.

When we check the terms in the potential, we find that they are gauge invariant by direct calculation

$$\varphi^\dagger\varphi \rightarrow \varphi'^\dagger\varphi' = \varphi^\dagger U^\dagger U \varphi = \varphi^\dagger\varphi, \quad (1.8)$$

but we do not find the same for the kinetic term,

$$\begin{aligned} \partial^\mu\varphi^\dagger\partial_\mu\varphi' &= (\partial^\mu e^{iQ\theta}\varphi^\dagger)\partial_\mu(e^{-iQ\theta}\varphi) \\ &= [iQ\partial^\mu\theta e^{iQ\theta}\varphi^\dagger + e^{iQ\theta}\partial^\mu\varphi^\dagger][-iQ\partial_\mu\theta e^{iQ\theta}\varphi + e^{-iQ\theta}\partial_\mu\varphi] \\ &\neq |\partial\varphi|^2. \end{aligned} \quad (1.9)$$

Here we need to introduce a covariant derivative to “correct” the kinetic term and make the Lagrangian gauge invariant. If we define a covariant derivative in terms of a new gauge field (A_μ) with its own transformation properties,

$$D_\mu = \partial_\mu - ieQA_\mu, \quad A_\mu \rightarrow A'_\mu = A_\mu - \frac{1}{e}\partial_\mu\theta, \quad (1.10)$$

we have a solution to our problem,

$$\begin{aligned}
D'_\mu \varphi' &= (\partial_\mu - ieQA'_\mu)(e^{-iQ\theta} \varphi) \\
&= -iQ\partial_\mu \theta e^{-iQ\theta} \varphi + e^{-iQ\theta} \partial_\mu \varphi - ieQ(A_\mu - \frac{1}{e} \partial_\mu \theta) e^{-iQ\theta} \varphi \\
&= e^{-iQ\theta} (\partial_\mu - ieQA_\mu) \varphi = UD_\mu \varphi.
\end{aligned} \tag{1.11}$$

We can also see that this would work without the factor of e , but we would lose the physics in our problem. It is the gauge coupling that makes this a physics problem and not a geometric one. We can also see that it was important that the scalar field be complex. In fact, the complex nature of the scalar field tells us that it is charged and therefore interacts with this new gauge field, the photon. We need to add a kinetic term for the gauge field to our Lagrangian. If we define the field strength tensor as

$$F_{\mu\nu} = \partial_\mu A_\nu - \partial_\nu A_\mu, \tag{1.12}$$

then we can not only verify that the field strength is gauge invariant but we can add a new (normalized) term to our Lagrangian describing the new gauge particle,

$$\mathcal{L} = |D\varphi|^2 - m^2|\varphi|^2 - \lambda|\varphi|^4 - \frac{1}{4}F_{\mu\nu}F^{\mu\nu}. \tag{1.13}$$

We can also ask if we should add a mass term for the gauge field. The answer is no, because it would irreparably break the gauge invariance we just imposed,

$$\frac{m^2}{2}A_\mu A^\mu \rightarrow \frac{m^2}{2}\left(A_\mu - \frac{1}{e}\partial_\mu \theta\right)\left(A^\mu - \frac{1}{e}\partial^\mu \theta\right), \tag{1.14}$$

thus local gauge invariance forbids a mass term for the gauge field. This would appear to be a good thing, because we want a massless photon in our theory, but this requirement is too strong for our own good. We can not seem to have any non-scalar mass terms in our gauge theory. This problem will be solved by the Higgs mechanism, but we should first explore a non-Abelian gauge theory.

Non-Abelian gauge theories, also known as Yang-Mills theories [22], are based on groups with non-commutative generators. In the interest of future developments, we will consider the gauge group $G = SU(N)$, later to be understood to be $SU(2)_L$ and $SU(3)_c$.

We will need some of the properties of the Lie algebra to understand the analysis better. We will let φ^i be our particle fields in the fundamental representation of the gauge group, and a^i will be our group parameters. We will define our Lie algebra with real structure constants and the order (the number of generators of the group) and rank (the number of generators that can be

simultaneously diagonalized and therefore commute¹) of our gauge group are written as

$$[T_i, T_j] = iC_{ijk}T_k, \quad \mathcal{O}(SU(N)) = N^2 - 1, \quad r(SU(N)) = N - 1. \quad (1.15)$$

We will define our gauge transformation as

$$\varphi^i \rightarrow U_j^i \varphi^j, \quad i = 1, \dots, N. \quad (1.16)$$

Our transformation matrix then takes the more complicated form

$$U = \exp \left\{ -i \sum_{j=1}^{\mathcal{O}(G)} T_j a^j \right\}. \quad (1.17)$$

For the group $SU(2)_L$ we would have $T_j = \frac{1}{2}\sigma_j$, where σ_j are the Pauli matrices and are normalized as $\text{Tr}(T_i T_j) = \frac{1}{2}\delta_{ij}$. For the group $SU(3)$ we have the usual λ_j Gell-Mann matrices (see Appendix C).

The kinetic and mass terms in our (complex scalar) Lagrangian will have a little more structure to them, but are in principle the same. For instance,

$$(\partial_\mu \varphi)^\dagger (\partial^\mu \varphi) = (\partial_\mu \varphi_1^\dagger, \dots, \partial_\mu \varphi_{N^2-1}^\dagger) \begin{pmatrix} \partial^\mu \varphi_1 \\ \vdots \\ \partial^\mu \varphi_{N^2-1} \end{pmatrix}. \quad (1.18)$$

Now we can construct a Lagrangian and reuse our procedure to find the covariant derivative. We find (quite generically),

$$D_\mu = (\partial_\mu \mathbb{1} - ig\vec{T} \cdot \vec{A}_\mu), \quad D_\mu \varphi_R = [\partial_\mu \mathbb{1}_{\dim(R) \times \dim(R)} - ig\mathcal{D}_R(\vec{T}) \cdot \vec{A}_\mu] \varphi_R \quad (1.19)$$

where the \mathcal{D}_R implies a generic representation (darstellung) for the group generators. Proceeding, we can find the variation of the gauge field and the form of the field strength tensor for a non-Abelian gauge group,

$$A_\mu^j \rightarrow A_\mu'^j = A_\mu^j - \frac{1}{g} \partial_\mu \theta^j + C_{kl}^j \theta^k A_\mu^l, \quad (1.20)$$

$$F_{\mu\nu}^j = \partial_\mu A_\nu^j - \partial_\nu A_\mu^j + gC_{kl}^j A_\mu^k A_\nu^l, \quad (1.21)$$

which regain their usual Abelian structure when the structure constants vanish (the generators commute) and we have taken g to be the coupling constant of the new gauge group.

¹These generators are also known as the Cartan sub-algebra after Élie-Joseph Cartan.

Finally, we must ask what happens when we have the direct product (\otimes) of several groups like we do in the standard model. For the group structure $G = SU(3)_c \otimes SU(2)_L \otimes U(1)_Y$, our Lagrangian and covariant derivative have the form

$$\mathcal{L} \supset -\frac{1}{4} \sum_i^8 G_{\mu\nu}^i G^{i,\mu\nu} - \frac{1}{4} \sum_j^3 F_{\mu\nu}^j F^{j,\mu\nu} - \frac{1}{4} \sum_{\text{none}} F_{\mu\nu} F^{\mu\nu} \quad (1.22)$$

$$D_\mu = \left[\partial_\mu (\mathbb{1}_{\text{color}} \otimes \mathbb{1}_{SU(2)} \otimes \mathbb{1}_Y) - ig_3 \sum_i^8 T_{SU(3)}^i C_\mu^i - ig_2 \sum_j^3 T_{SU(2)}^j A_\mu^j - ig_1 \left(\frac{Y}{2} \right) B_\mu \right] \quad (1.23)$$

There are some generic comments to be made. Making the Lagrangian gauge invariant added a gauge field to the Lagrangian, and that gauge field had a universal gauge coupling to the other fields. This is an important phenomenological result as it increases the predictive capacity of the theory. Each gauge group adds a coupling constant.

1.2.3 Goldstone bosons

Before moving on to how the electroweak symmetry is broken in the SM, we need to introduce one final piece of information, the Nambu-Goldstone theorem [23, 24]. Simply stated, the theorem tells us what should happen when a continuous symmetry is broken in a Lagrangian.

The theorem says: if you have a (manifestly Lorentz invariant) Lagrangian under a continuous symmetry group G , but the generators of the group (the group elements) do not leave the vacuum invariant (there is spontaneous symmetry breaking) then there exists massless, spin-0 particles in the spectrum, and there is a 1:1 correspondence between these broken generators and these bosons.

Without revealing too much of what is to come, this theorem tells us why we might expect a Higgs boson, but not why it might be massive or how any of the other particles acquire their mass. As a side note, one might ask if Goldstone fermions can exist in nature. Some theories introduce these objects, but they are absent in the SM and the MSSM.

1.3 Electroweak Symmetry Breaking

How do we build the SM Lagrangian from scratch? We start with a massless gauge invariant Lagrangian, break the electroweak symmetry so the particle

spectrum acquires mass, and we can then proceed with the interactions.

Thus far, we have described observations of the SM, but it is difficult to proceed without introducing the formalism behind the current incarnation of EWSB. To do this we need to take a step backwards and show how, so now is the time to discuss the Higgs mechanism in all its glory.

One may also ask when the electroweak symmetry was broken. If we view the SM as our fundamental theory (and not as a low-energy effective theory of a larger theory) then we can back the evolution of the universe up to where the electroweak phase transition was expected to have occurred and we find that the universe was cool enough to undergo a phase transition at around 10^{-10} s after the big-bang, well after inflation would have ended and well before nuclear matter would have become confined at around 10^{-6} s. So we should be concerned only with the spontaneously broken version of the SM.

1.3.1 Higgs mechanism

The Higgs mechanism [25–31], as it is known in the literature, is the means by which the electroweak symmetry is broken in the SM. In the SM, we will introduce a single complex scalar $SU(2)_L$ doublet Φ ,

$$\Phi = \begin{pmatrix} \phi^+ \\ \phi^0 \end{pmatrix}. \quad (1.24)$$

The scalar sector of the Lagrangian then will be (some authors normalize this Lagrangian differently)

$$\mathcal{L} = |D_\mu \Phi|^2 - \mu^2 |\Phi|^2 - \lambda |\Phi|^4. \quad (1.25)$$

If there is a phase-transition that makes $\mu^2 < 0$, then $\Phi = \begin{pmatrix} 0 \\ 0 \end{pmatrix}$ is no longer a local minimum, it is a local maximum of the potential. This can be seen in the change in the scalar potential in Figure (1.1). There now exist degenerate minima with

$$\Phi^\dagger \Phi = v^2/2, \quad v = \sqrt{-\mu^2/2\lambda}, \quad \mu^2 < 0, \quad (1.26)$$

and we can see that the vacuum expectation value (VEV) of the field Φ can be chosen to be real and the neutral component of the Higgs field. The VEV has the dimensions of mass,

$$\langle 0 | \Phi | 0 \rangle = \begin{pmatrix} 0 \\ v/\sqrt{2} \end{pmatrix}. \quad (1.27)$$

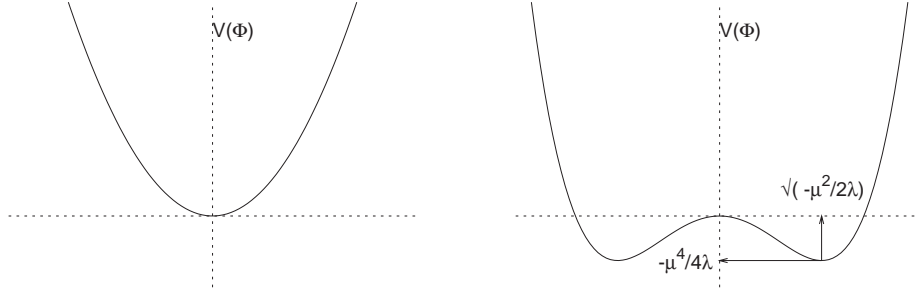


Figure 1.1: Spontaneous symmetry breaking.

Because we are breaking the symmetry down to $SU(2)_L \otimes U(1)_Y \rightarrow U(1)_{\text{EM}}$, we put the VEV in the neutral component of the Higgs field so it will not couple to the photon. If the Higgs field were complex it could be made real by a suitable $SU(2)_L$ transformation without a loss in generality. Since the Higgs field has two complex, or four real degrees of freedom, we will write Φ as a phase times two real valued fields,

$$\Phi = \exp \left\{ \frac{iG^a(x)\sigma^a}{2v} \right\} \begin{pmatrix} 0 \\ \frac{v+H(x)}{\sqrt{2}} \end{pmatrix}, \quad (1.28)$$

where $G^a(x)$ ($a = 1, 2, 3$) and $H(x)$ are each real scalar fields. The G^a are the would-be Nambu-Goldstone bosons corresponding to the broken $SU(2)_L \otimes U(1)_Y \rightarrow U(1)_{\text{EM}}$ generators. The Nambu-Goldstone bosons can be removed by choosing the unitary gauge. This is equivalent to removing the exponential from our definition of Φ . We will not make this simplification, as most of our results use the Feynman gauge. The label “would-be” will be defined in a moment.

We will replace the field Φ in our Lagrangian and expand out all the interactions to see what happens. We write our Lagrangian and covariant derivative as

$$\mathcal{L} = |D_\mu \Phi|^2 - \mu^2 |\Phi|^2 - \lambda |\Phi|^4 - \frac{1}{4} F_{\mu\nu}^j F^{j,\mu\nu} - \frac{1}{4} F_{\mu\nu} F^{\mu\nu}, \quad (1.29)$$

$$D_\mu = \left[\partial_\mu - ig_2 \frac{\sigma^j}{2} A_\mu^j - ig_1 \left(\frac{Y}{2} \right) B_\mu \right], \quad (1.30)$$

where σ^j are the Pauli matrices for the $SU(2)_L$ sub-group. Here we need to work out the dot product (sum over j) between the Pauli matrices and the $SU(2)_L$ gauge bosons to multiply the column vector for our new representation of Φ when we expand the covariant derivative in the potential. It will

be convenient to introduce a spherical representation of the gauge bosons to simplify our notation

$$A_\mu^\pm \equiv \frac{A_\mu^1 \mp iA_\mu^2}{\sqrt{2}}. \quad (1.31)$$

Now we can work out an explicit representation for the matrices in the covariant derivative. We find

$$\begin{aligned} \frac{g_2}{2} \begin{pmatrix} A^3 & \sqrt{2}A^+ \\ \sqrt{2}A^- & -A^3 \end{pmatrix} + \frac{g_1}{2} \begin{pmatrix} B & 0 \\ 0 & B \end{pmatrix} \\ = \frac{1}{2} \begin{pmatrix} g_2A^3 + g_1B & \sqrt{2}g_2A^+ \\ \sqrt{2}g_2A^- & -g_2A^3 + g_1B \end{pmatrix}. \end{aligned} \quad (1.32)$$

If we let $Z = (g_2A^3 - g_1B)/\sqrt{g_2^2 + g_1^2}$, then

$$(D_\mu\varphi)^\dagger(D^\mu\varphi) \rightarrow \frac{v^2}{8} \left[2g_2^2A^-A^+ + 2(g_2^2 + g_1^2)Z \right] \quad (1.33)$$

$$= \frac{v^2}{4} \left[g_2^2(|A^-|^2 + |A^+|^2) + (g_2^2 + g_1^2)Z \right], \quad (1.34)$$

and we have generated mass terms for the three bosons (recall that the VEV has units of mass) when we identify the A^\pm gauge bosons with the W^\pm gauge bosons and the Z with the Z^0 ,

$$M_{W^+}^2 = M_{W^-}^2 = \frac{g_2^2v^2}{4}, \quad M_Z^2 = \frac{(g_2^2 + g_1^2)v^2}{4}. \quad (1.35)$$

We can now define the weak mixing angle, θ_w , to make our transformation more convenient as,

$$\frac{g_1}{g_2} = \tan \theta_w, \quad \frac{M_W^2}{M_Z^2} = \frac{g_2^2}{g_2^2 + g_1^2} = \cos^2 \theta_w. \quad (1.36)$$

Therefore, we can see that after SSB, the Z^0 boson and the photon are mixtures of the former $SU(2)_L$ and $U(1)_Y$ gauge bosons rotated by the weak mixing angle,

$$Z = A^3 \cos \theta_w - B \sin \theta_w \quad (1.37)$$

$$\gamma = B \cos \theta_w + A^3 \sin \theta_w, \quad \text{no mass term.} \quad (1.38)$$

The photon received no mass term in the new Lagrangian and remains exactly massless. Experimentally, the value of the weak mixing angle (as defined by the on-shell masses of the vector bosons) is found to be

$$\sin^2 \theta_w \equiv 1 - \frac{M_W^2}{M_Z^2} = 0.2223(11). \quad (1.39)$$

Let's count the degrees of freedom before and after spontaneous symmetry breaking (SSB). Before we had three massless $SU(2)_L$ gauge bosons (each with two degrees of freedom) and one $U(1)_Y$ massless gauge boson and the four components of the complex doublet. That makes $3 \times 2 + 1 \times 2 + 4 = 12$. After SSB, we have three massive vector bosons (with three degrees of freedom), a massless photon and a Higgs boson with one degree of freedom. That makes $3 \times 3 + 1 \times 2 + 1 = 12$. It is said that the gauge bosons have “eaten” the would-be Goldstone bosons to gain their masses. This is where the phrase would-be comes from, they would be present if they were not eaten by the gauge bosons.

In the SM, the Higgs mechanism has only one free parameter, the mass of the Higgs boson itself. All the other couplings are determined. The value for the VEV is determined from muon decays and it is related to the Fermi constant,

$$\frac{G_F}{\sqrt{2}} = \frac{g_2^2}{8M_W^2} = \frac{1}{2v^2}, \quad (1.40)$$

and has a value of $v^2 = (\sqrt{2}G_F)^{-1} = (246 \text{ GeV})^2$.

At this point, we should discuss what happened in the strong sector. It is very nice that the gauge bosons became massive and the photon remained massless, but we also know there are fermion masses that need to be accounted for. The mass of the fermions come from their coupling to the Higgs boson. Generically, this mass term comes from the Yukawa term in the strong sector Lagrangian,

$$\mathcal{L}_{\text{Yukawa}} = \sum_i^{\text{fermions}} -\frac{y_i}{\sqrt{2}}(v + H)\bar{\psi}_i\psi_i = -\frac{y_i v}{\sqrt{2}}\bar{\psi}_i\psi_i - \frac{y_i}{\sqrt{2}}H\bar{\psi}_i\psi_i. \quad (1.41)$$

We can see that if we let $y_i = \sqrt{2}m_i/v$, then the Higgs couples to fermions like m_i/v . We can clearly see that the Yukawa couplings have to be tuned to the known masses of the fermions, and that the Higgs mechanism does not predict the values for the fermion masses. Now the common statement “the Higgs couples to mass” is clear. The coupling of the Higgs is proportional to the mass of the particle over the VEV. So the Higgs couples stronger to more massive particles. This will be very important to our phenomenological studies of the Higgs boson. For instance, we can now see that the top quark is the most important interaction in the strong sector of the SM.

1.3.2 Bounds on Higgs mass

Now that we have seen EWSB and have determined that the Higgs mechanism is testable, is there anything we can say about the free parameter left in our

theory, the mass of the Higgs? The (normalized) scalar potential before SSB could be written

$$V(\Phi) = \frac{m^2}{2}\Phi^2 + \frac{\lambda}{4}\Phi^4, \quad (1.42)$$

and after EWSB we find,

$$V(H) = \frac{M_H^2}{2}H^2 + \frac{M_H^2}{2v}H^3 + \frac{M_H^2}{8v^2}H^4. \quad (1.43)$$

The Higgs mass can be written

$$M_H = \sqrt{2\lambda}v, \quad (1.44)$$

which does not tell us the value of the Higgs mass, nor the strength of its self interactions. It is this parameter λ that is not predicted in the SM but we will continue to be interested in the mass of the Higgs boson as it is the physical parameter. We can also see in the potential that the self-couplings of the Higgs are also proportional to the Higgs mass. The Higgs has generated its own mass, a property that may be missing from other spurious (as-yet unknown) scalar particles that may be discovered. Verifying this for the potential is important to verifying the Higgs is the SM Higgs. This will be discussed later.

The question we must ask next is can we derive limits on the Higgs mass from internal consistency of the SM and what do we already know from past and continuing particle physics experiments? Theoretically, we can calculate the corrections to the λ parameter and see what it can tell us, as well as any other processes that may tell us something about a limit on the Higgs mass. Experimentally, we will review the current state of affairs.

Theoretical limits

The internal consistency of the SM can be tested generically in two ways. We need to find when the SM violates unitarity and when the theory becomes trivial. One of these limits is stronger than the other and we will see that when it is derived.

To begin, can the Higgs be infinitely heavy? The answer is no and that may seem to violate the decoupling theorem [33], but upon careful inspection we see that the decoupling theorem does not apply to particles that couple proportional to their mass, like the SM Higgs. Just how heavy the Higgs can be and still be perturbative is a good place to start accessing this question.

Although we will talk about diagrams and Feynman rules more in detail later (the confused reader can find some more details in Appendix A), let us jump ahead and find the perturbative limit. Consider $HH \rightarrow HH$ elastic

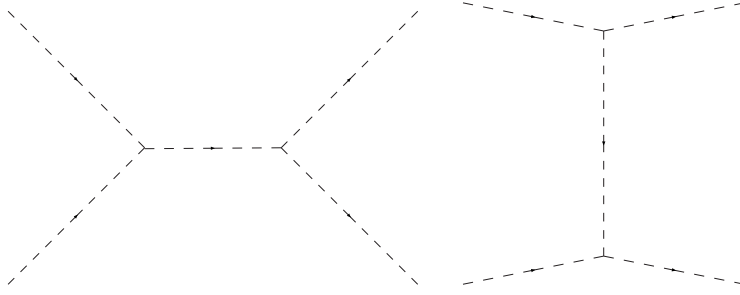


Figure 1.2: Sample Higgs-Higgs scattering diagrams.

scattering as shown in Figure (1.2). Since this is a $2 \rightarrow 2$ process we can write out most of our results without too much difficulty. The tree level amplitude is very simple,

$$i\mathcal{M}_{\text{tree}} = -6i\lambda. \quad (1.45)$$

When we add the one loop corrections in $n = 4 - 2\epsilon$ dimensions, we can see that the coupling constant λ takes on corrections that can be interpreted (at this order) as a geometric series that depends on the interaction energy Q^2 ,

$$i\mathcal{M} = -6i\lambda + \frac{27\lambda^2}{8\pi^2} \int_0^1 dx \left[\Gamma(\epsilon) \left(M_H^2 + x^2 Q^2 - x Q^2 \right)^\epsilon \right] \quad (1.46)$$

$$= -6i\lambda \left(1 + \frac{9\lambda}{16\pi^2} \log \left(\frac{Q^2}{M_H^2} \right) \right) + \dots \quad (1.47)$$

$$= \frac{6i\lambda}{1 - \frac{9\lambda}{8\pi^2} \log \frac{Q}{M_H}} \equiv 6i\lambda(Q). \quad (1.48)$$

The problem here is that the amplitude becomes infinite before $Q \rightarrow \infty$. We also see that the denominator can become zero for a certain value of the energy. This is known as the Landau pole. We can turn this limit around to bound the Higgs mass from above. Without the $\lambda\phi^4$ interaction the theory is trivial (has no interactions) so we must require the coupling to be finite and positive up to some cut-off scale Λ where the theory could in principle be saved by the introduction of new physics,

$$\frac{1}{\lambda(\Lambda)} > 0, \quad \implies \quad M_H^2 = 2\lambda v^2 < \frac{16\pi^2 v^2}{9 \log(\Lambda/v)}. \quad (1.49)$$

So if no new physics emerges before the Planck scale (10^{16} GeV) then the Higgs mass must be lighter than 180 GeV in what we have considered so far in the SM. A better upper bound is found when more particles and interactions are included (the most important is the super-heavy top quark because

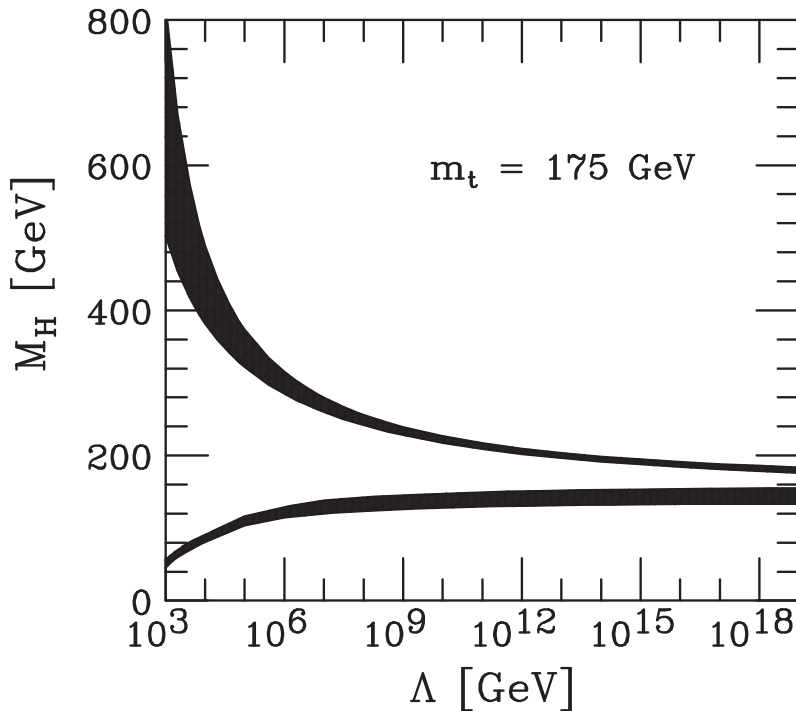


Figure 1.3: Theoretical Higgs mass limits.

the Higgs couples to mass). These interactions change our geometric series into coupled differential equations familiar to the study of the renormalization group. The detailed results will be presented in a moment.

We can also ask if there is a minimum Higgs mass permissible in the SM. The answer is also yes because the coupling constant λ has to be positive or else the electroweak vacuum would not be broken or would become unstable and our SSB potential would not be bound from below. In simple terms, we must have

$$V(v) < V(0), \quad (1.50)$$

for the vacuum to be broken and stable. In much the same way we can find the relation

$$M_H^2 > \frac{3v^2}{2\pi^2} \left(\frac{m_t}{v}\right)^4 \log\left(\frac{\Lambda^2}{v^2}\right). \quad (1.51)$$

If we also run the scale out to the Planck scale, then we see that the Higgs has to be heavier than 140 GeV for the SM to be a complete theory out to the Planck scale.

We can represent these limits graphically as in Figure (1.3). The upper [34] and lower limits [35] use all available information and show the uncertainty in

the calculation. Figure (1.3) was taken from Ref. [36]. This is not to say that the Higgs has to be found within this range of masses. In fact, it may be more interesting if it is not. This would imply that there is more physics at a high scale.

Finally, there is one other limit we can mention theoretically and it is weaker than the other criteria we have found so far. For $2 \rightarrow 2$ elastic scattering,

$$\frac{d\sigma}{d\Omega} = \frac{1}{64\pi^2 s} |\mathcal{M}|^2. \quad (1.52)$$

It is also possible to decompose any scattering amplitude into partial waves and make sure they all obey the optical theorem. The amplitude can be written

$$\mathcal{M} = 16\pi \sum_{l=0}^{\infty} (2l+1) P_l(\cos\theta) a_l, \quad (1.53)$$

where the P_l are the Legendre polynomials and a_l are the spin- l partial waves. In this manner, the total cross-section can be written as the sum over the partial waves

$$\sigma = \frac{8\pi}{s} \sum_{l=0}^{\infty} \sum_{l'=0}^{\infty} (2l+1)(2l'+1) a_l a_{l'}^* \int_{-1}^1 d(\cos\theta) P_l(\cos\theta) P_{l'}(\cos\theta) \quad (1.54)$$

$$= \frac{16\pi}{s} \sum_{l=0}^{\infty} (2l+1) |a_l|^2. \quad (1.55)$$

The optical theorem [37,38] (See Ref. [39] for historical review) states that the total cross-section must be equal to the (normalized) imaginary part of the far-forward scattering amplitude

$$\sigma = \frac{1}{s} \text{Im}[\mathcal{M}(\theta = 0)], \quad (1.56)$$

so we can see that $|\text{Re}(a_l)| < \frac{1}{2}$, or this series will diverge. We are interested in the limit far from the Higgs mass pole, so we will only need the first partial wave to satisfy unitarity, $|a_0^0| < 1$. We can now examine different scattering amplitudes to see what this limit can tell us about the Higgs mass. The best limit on this Higgs mass comes from WW scattering [40]. This may seem like an academic exercise, but this process takes place in nature inside $e^+e^- \rightarrow \nu\bar{\nu}H$ and $q\bar{q} \rightarrow q\bar{q}H$ diagrams. The WW scattering process can be simplified by using the ‘‘Electroweak Equivalence Theorem’’ which is proved in the preceding reference. We can see the diagrams in Figure (1.4).

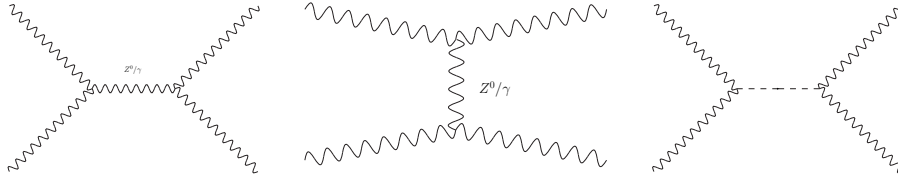


Figure 1.4: WW scattering (sample diagrams).

If we consider the longitudinally polarized W^\pm scattering, we find the amplitude can be written

$$i\mathcal{M}(W_L^+W_L^- \rightarrow W_L^+W_L^-) = -i\frac{M_H^2}{v^2} \left(\frac{s}{s - M_H^2} + \frac{t}{t - M_H^2} \right) \quad (1.57)$$

$$\rightarrow -2i\frac{M_H^2}{v^2} \quad s, t \gg M_H^2. \quad (1.58)$$

We can convert our (high-energy) amplitude into the $J = 0$ partial wave with the following transformation

$$a_0^0(W_L^+W_L^- \rightarrow W_L^+W_L^-) \equiv \frac{1}{16\pi s} \int_{-s}^0 |\mathcal{M}| dt \quad (1.59)$$

$$= \frac{M_H^2}{8\pi v^2} < \frac{1}{2} \quad (1.60)$$

$$\Rightarrow M_H < \sqrt{4\pi}v = 870 \text{ GeV}. \quad (1.61)$$

It is important to emphasize that this is not a constraint on the theory, but to the application of the theory. It is best to say that if the Higgs were heavier than this mass limit then the Higgs sector of the SM would not be perturbative and we would need different formalisms to calculate physical observables.

Experimental limits

Twice a year, the LEP Electroweak Working Group (EWWG) releases the results of precision fits to the current electroweak observables. Included in this analysis is a plot known in the Higgs community as the “blue-band” plot [32]. This plot shows what value of the Higgs mass best fits the data set if the SM was chosen by nature. The plot released for the Winter 2005 conferences (meaning February 2005) is shown in Figure (1.5).

According to this plot, the best fit Higgs mass is $M_H = 126_{-48}^{+73}$ GeV. The precision with which the Higgs mass can be fit is dictated by the fact that the Higgs mass comes in logarithmically to the radiative corrections to

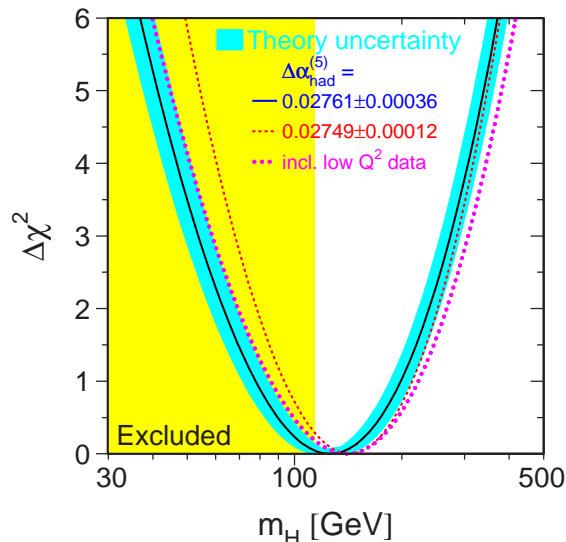


Figure 1.5: Electroweak fit for the SM Higgs mass (February 2005).

the electroweak observables. What can also be said is that the Higgs mass $M_H < 280$ GeV at 95% confidence level.

This (relatively light) bound on the Higgs mass combined with the theoretical limitations increases the possibility of the Higgs boson (if it exists in nature) being discovered in the near future at the Large Hadron Collider (LHC) which has a reach to discover a Higgs boson(s) up to a mass of roughly 1 TeV.

1.4 SM Lagrangian

Now, that we see how the SM Lagrangian can be constructed, we are ready to see what we have. For our purposes, it is not necessary to write out the entire Lagrangian as we are mostly interested in the dynamics of the strong sector and its interactions with the Higgs field. We are interested in the strong sector because strong corrections tend to be larger than electroweak corrections because the coupling constant is much larger, $\alpha_s \gg \alpha$. Although it is not a hard and fast rule, in many known cases for Higgs production, the electroweak corrections have the opposite sign from the strong corrections making both important.

The strong sector Lagrangian can be written as

$$\mathcal{L}_{\text{QCD}} = -\frac{1}{4}G_{\mu\nu}^a G^{\mu\nu,a} + \sum_f \bar{\psi}_{f,i}(i\not{D}_{ij} - m_f\delta_{ij})\psi_{f,j}. \quad (1.62)$$

The ‘‘Feynman slash’’ notation stands for a contraction of a vector and a γ matrix, $\not{A} = \gamma_\mu A^\mu$. The gamma matrices form a special kind of algebra called a Clifford algebra (see Appendix B) that is particularly relevant to our discussions of the pseudoscalar Higgs. In brief, the gamma matrices are defined by the following relation,

$$\{\gamma^\mu, \gamma^\nu\} = \gamma^\mu\gamma^\nu + \gamma^\nu\gamma^\mu \equiv 2\eta^{\mu\nu}, \quad (1.63)$$

where $\eta^{\mu\nu}$ is the space time metric (usually this is written as $g^{\mu\nu}$, which the author prefers to reserve for applications in curved space). The QCD part of the covariant derivative can be written

$$D_{ij}^\mu = \partial^\mu\delta_{ij} - igA^{\mu,a}T_{ij}^a, \quad (1.64)$$

where $A^{\mu,a}$ is the gluon field with a color index a . We define the $SU(3)_c$ generators T_{ij}^a and the group structure constants

$$[T^a, T^b] = if_{abc}T^c. \quad (1.65)$$

More information about group theory can be found in Appendix C. Finally, the field strength for the gluon self-interactions

$$F_{\mu\nu}^a = \partial_\mu A_\nu^a - \partial_\nu A_\mu^a + gf_{abc}A_\mu^b A_\nu^c. \quad (1.66)$$

We are being rather cavalier with raising and lowering the group indices because we have a trivial orthonormal Killing metric in the SM. This is not always true for more exotic groups.

1.4.1 Feynman rules

Once a Lagrangian has been formulated for a given theory, the Feynman rules can be deduced. It is the Feynman rules that are important in perturbative calculations. There are several ways to derive Feynman rules, in both operator language and the path integral formalism. We will skip these derivations as they are a bit tedious and technical for our uses and simply list the Feynman rules for QCD.

The Feynman rules for QCD can be found in Table (1.3). These allow us to generate the mathematical expressions for scattering cross-sections if we remember to add the appropriate spinor and polarization vectors to the matrix elements for the external particles.

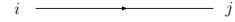
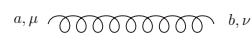
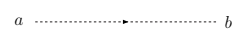
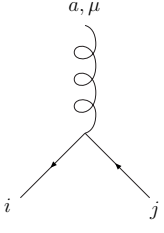
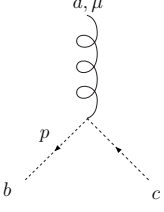
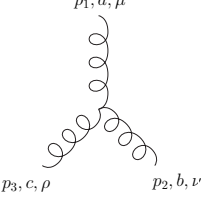
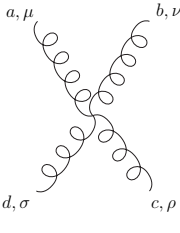
	$\frac{i(\not{p}+m)}{p^2-m^2+i\epsilon}\delta_{ij}$
	$\frac{-i\delta^{ab}}{p^2+i\epsilon}\left[\eta^{\mu\nu} - (1-\xi)\frac{p^\mu p^\nu}{p^2}\right]$
	$\frac{-i\delta^{ab}}{p^2+i\epsilon}$
	$-ig_3\gamma^\mu(T^a)_{ij}$
	$g_3 f^{abc} p^\mu$
	$-g_3 f^{abc} [(p_1-p_2)^\rho \eta^{\mu\nu} + (p_2-p_3)^\mu \eta^{\nu\rho} + (p_3-p_1)^\nu \eta^{\mu\rho}]$
	$-ig_3^2 [f^{abe} f^{cde} (\eta^{\nu\sigma} \eta^{\mu\rho} - \eta^{\mu\sigma} \eta^{\nu\rho}) + f^{ace} f^{bde} (\eta^{\rho\sigma} \eta^{\mu\nu} - \eta^{\mu\sigma} \eta^{\nu\rho}) + f^{ade} f^{cbe} (\eta^{\nu\sigma} \eta^{\mu\rho} - \eta^{\rho\sigma} \eta^{\mu\nu})]$

Table 1.3: QCD Feynman rules.

1.4.2 Polarizations, gauges, and ghosts

Since we have tried so hard to build a massive theory out of a massless one, we are led to wonder if there is any more information about a gauge theory hidden in the differences between massive and massless particles. The answer is yes. Let us briefly explore those differences to solidify our understanding.

We observe two kind of photons, thus two degrees of freedom (polarizations). However, the photon is a vector field (A^μ), which has four components. One of these degrees of freedom is removed by the Ward [41–45] identity $k^\mu \epsilon_\mu^i(k) = 0$, making the polarizations orthonormal. This condition is good in any Lorentz frame. However, if we start in a state where the unphysical third polarization is zero, there exists a Lorentz frame where the physical polarizations mix with the unphysical one which is unacceptable. Gauge invariance comes to the rescue.

Even in classical electrodynamics, we know that the physics does not change when we redefine the fields as $A_\mu \rightarrow A'_\mu = A_\mu + \partial_\mu \Lambda$ for any (arbitrarily differentiable real field) Λ . When we define the field via a Fourier transform, the Λ field cancels the unphysical polarization. So gauge invariance implies that the physics remains the same if we add an arbitrary amount of a new field to the photon field. In retrospect, this suggests that ghost fields will need to be introduced in non-Abelian gauge theories when gauge invariance is lost (and it unfortunately has to be lost to define the gluon propagator).

In the massive case, the problem is more subtle. Massive particles have three polarizations, so Lorentz invariance is not an issue, we can mix freely the three states. The problem is that we cannot arrive at the massless result from the massive result simply by taking the mass to zero.

A theory with massless vector particles, such as QED or QCD, must be gauge invariant or the theory is not Lorentz invariant. Theories with massive vector particles need gauge invariance or else the theory is not renormalizable. We will touch on this shortly.

We have built a gauge invariant Lagrangian from the beginning. When we try to quantize this theory though, we find that the gluon field A_μ^a has a freedom to be changed by a total derivative and still leave the Lagrangian gauge invariant which helped us to understand its two polarizations. However, we will need to eliminate this freedom to define a perturbative propagator. To eliminate this freedom of the gauge transformation, we need to add a constraint to the gluon field in the form of a gauge-fixing term.

We could choose a Lorentz condition ($\partial^\mu A_\mu^a = 0$), or we could choose the Coulomb gauge ($\partial_i A_i^a = 0$), or the axial gauge ($n \cdot A^a = 0$, with $n^2 = 1$), or even the temporal gauge ($A_0^a = 0$). Beyond these there are even more exotic choices. To make our calculations easier, we will employ the Lorentz gauge,

so we add the gauge-fixing term

$$\mathcal{L}_{\text{gauge-fixing}} = -\frac{1}{2\xi}(\partial_\mu A^{\mu,a})^2. \quad (1.67)$$

The parameter ξ is called the gauge parameter. The addition of this term breaks gauge invariance but it allows for a definition of a perturbative framework to perform calculations that include gluons. Any physical observable will not depend on the value of the gauge parameter so we can choose something convenient. Some examples include $\xi = 0$ (Landau gauge), $\xi = 1$ (Feynman gauge), and $\xi \rightarrow \infty$ (Unitary gauge). The reasons for these choices are clear in the gluon propagator.

The full perturbative gluon propagator with Lorentz indices (μ, ν) and color indices (a, b) at each end and momentum p can be written in the Lorentz gauge as

$$\Gamma_{ab}^{\mu\nu}(p) = \frac{i\delta^{ab}}{p^2 + i\epsilon} \left[-\eta^{\mu\nu} + (1 - \xi) \frac{p^\mu p^\nu}{p^2 + i\epsilon} \right]. \quad (1.68)$$

All of our calculations are done in the Feynman gauge where the second term in the gluon propagator is missing.

There is one further complication. Even when the gauge-fixing term is added there is still an issue with the number of polarizations for the gluons. The $SU(3)_c$ vector bosons (gluons) are massless and so they should have only two degrees of freedom. One possible way to get this desired result is to add the so called Fadeev-Popov ghost fields. Ghosts are anti-commuting scalar fields that must be added to loop diagrams in the Lorentz gauge² to cancel the unphysical polarizations. We can write

$$\mathcal{L}_{\text{ghost}} = (\partial_\mu (\chi^a)^*) (\partial^\mu \delta_{ab} - g f_{abc} A^{\mu,c}) \chi^b. \quad (1.69)$$

It is important to understand that ghosts should be thought of as a prescription, and not an actual particle. Furthermore, χ^* has nothing to do with χ . As ghost fields did not play an important role in our research, we will leave them now and simply summarize our strong Lagrangian

$$\begin{aligned} \mathcal{L} = & -\frac{1}{4} G_{\mu\nu}^a G^{\mu\nu,a} + \sum_f \bar{\psi}_{f,i} (i\not{D}_{ij} - m_f \delta_{ij}) \psi_{f,j} \\ & - \frac{1}{2\xi} (\partial^\mu A_\mu^a)^2 + (\partial_\mu \chi^{a*}) D_{ab}^\mu \chi^b. \end{aligned} \quad (1.70)$$

To summarize, ghost fields must be included as internal lines, but never as external particles. They do not correspond to physical particles, but occur in

²Ghosts do not couple to the physical fields in the axial gauge.

diagrams to correct violations in unitarity that would otherwise arise due to the form of the vector boson propagators. This fact was put best by M. Veltman when he wrote, “The proof of that fact is really the central part of gauge field theory.” This property of gauge theories is remarkable and cannot be stressed enough, even if it plays a small role in the current research being presented.

Ward identities

Since they were mentioned in the last section, we need a formal definition of the Ward identities. There are actually several identities that belong to the framework of Ward identities, sometimes called Ward-Takahashi identities. However, we are only interested in one of them in our calculations.

When there are external particles with polarization vectors ϵ_μ , the matrix elements can be written generically as,

$$\mathcal{M} \equiv \epsilon_{\mu_1}(k_1) \cdots \epsilon_{\mu_N}(k_N) \mathcal{M}^{\mu_1 \cdots \mu_N}. \quad (1.71)$$

The Ward identity tells us that if any of the momenta of the polarization vectors are substituted for the polarization vector itself, then the matrix elements are reduced to zero.

$$k_{\mu_1}^1 \cdots \epsilon_{\mu_N}(k_N) \mathcal{M}^{\mu_1 \cdots \mu_N} = \cdots = \epsilon_{\mu_1}(k_1) \cdots k_{\mu_N}^N \mathcal{M}^{\mu_1 \cdots \mu_N} = 0. \quad (1.72)$$

This relation is an incredibly powerful tool in checking the results of a particular calculation at any intermediate stage before proceeding.

1.5 Quantum Chromodynamics (QCD)

We will now turn our discussion to the strong sector of the SM and leave behind the electroweak interactions. Strong corrections to collider observables tend to be larger than their electroweak counterparts and in some ways, they are simpler to calculate because there are fewer interactions in the strong sector, although one would not be out of line in saying that strong interactions are more complicated in their form.

1.5.1 Quark Model

The current theory of strong interactions began in the early 1960’s with the quark model [46, 47]. This model predicted that all strongly interacting particles are composed of more fundamental constituents called quarks which were fractionally charged fermions that carried an additional quantum number dubbed ‘color’.

Generically, particles that participate in strong interactions are called Hadrons and they have been observed in fermionic (baryon) and bosonic (meson) states. With the exception of exotic particles³, this implies that baryons are bound states of three quarks (qqq) and mesons are bound states of two quarks ($q\bar{q}$). It was the discovery of the $\Delta^{++}(uuu)$ baryon that called for the addition of the color quantum number to save the Fermi-Dirac statistics. Historically, the three colors introduced were labeled red, white, and blue but were changed to a more neutral red, blue, and green. In the end, the labels are irrelevant.

From what we have learned about the field theory of the SM, we know that the strong sector is invariant under local $SU(3)_c$ transformations. We find that quarks transform in the fundamental representation and anti-quarks according to the conjugate representation. Gluon transform in the adjoint representation. Therefore, to form color singlet states, mesons are $q_a\bar{q}^a$ and baryons are $\epsilon^{abc}q_aq_bq_c$ color combinations.

We are interested in the high-energy behavior of the strong force, where the theory becomes asymptotically free and we are able to make a diagrammatic approach to our problems. We will leave behind the idea of bound quarks for now.

1.5.2 Regularization and renormalization

Regularization and renormalization are the central concern of Feynman diagrams with loops with are needed to calculate higher order corrections to any physical observable.

Given the Feynman rules for any Lagrangian, we can write down all the diagrams for a given physical observable to any desired order. The problem lies in trying to evaluate these mathematical expressions in $D = 4$ dimensions where divergencies develop in generically two ways.

Ultraviolet (UV) divergencies are due to the singular behavior of loop graphs at large loop momenta. These are removed systematically, order by order, by redefining the parameters in the Lagrangian by an infinite shift⁴.

Infrared (IR) divergencies occur when the propagators in a loop graph pass through zero in an unregulated way. This does not happen with massive quark loops, but does occur with massless quarks or gluon loops. We know that quarks are not truly massless, but are sometimes treated as such

³There is some theoretical interest in a so-called dibaryon, an object with six bound quarks, but none have been experimentally detected. Also, recently there has been evidence of a five quark bound state [48] called the $\Theta^+(1540)$. There is nothing in the quark model that prevents these configurations, but these exotic particle will be ignored in our current discussion.

⁴In the SM, we employ multiplicative renormalization exclusively for this purpose.

to simplify calculations. These types of divergencies cancel for appropriately defined quantities and can mostly be predicted for loop graphs. This will be elaborated on more later.

The means by which a Lagrangian is renormalized and the divergencies removed requires a regularization prescription. We will employ dimensional regularization, where the dimension of the graphs are taken to be non-integer, specifically we will calculate in $D = 4 - 2\epsilon$ dimensions.

Dimensional Regularization

When we calculate diagrams in $D = 4 - 2\epsilon$ dimensions, UV and IR divergencies are well behaved and appear as $1/\epsilon$ poles. Here we treat the amplitude as an analytic function in D dimensions and let $D \rightarrow 4$ when a finite answer (when all the poles cancel) is found. This actually presents a computational challenge to our Clifford algebra, but those subtleties will be addressed in Appendix B.

We need to work out an example to see all that this regularization procedure entails. After introducing the Feynman parameters and after the tensor reduction has been preformed (see Appendix D), we are left with integrals of the form

$$I = \int_{-\infty}^{+\infty} \frac{d^4 l}{(2\pi)^4} \frac{1}{(l^2 - \Delta + i\epsilon)^m}, \quad (1.73)$$

where m is a positive integer and the Δ parameter is combination of invariant masses and other kinematic variables. The denominator of this integral has poles in the complex l_0 plane at $(\mp\sqrt{l^2 + \Delta} \pm \epsilon')$. First, we will Wick rotate the integration contour to integrate this integral in Euclidean space instead of Minkowski space, and change to polar coordinates. So we have the replacements

$$l_0 \rightarrow il_0^E, \quad d^4 l \rightarrow id^4 l^E \quad (1.74)$$

$$d^4 l^E = d\Omega_4 (l^E)^3 dl^3 = 2\pi^2 (l^E)^3 dl^3. \quad (1.75)$$

Our integral becomes

$$I \xrightarrow{\text{WR}} i(-1)^m \int d\Omega_4 \int_0^\infty dl^E \frac{(l^E)^3}{[(l^E)^2 + \Delta]^m}, \quad (1.76)$$

$$\xrightarrow{\text{DR}} i(-1)^m \int d\Omega_D \int_0^\infty dl^E \frac{(l^E)^{D-1}}{[(l^E)^2 + \Delta]^m}, \quad (1.77)$$

$$= \frac{i(-1)^2}{2} \Delta^{D/2-m} \frac{\Gamma(m - D/2)\Gamma(D/2)}{\Gamma(m)}. \quad (1.78)$$

The details of how this integral is solved is in Appendix E. We can generalize this integral to an arbitrary power of the loop momentum squared,

$$I^{\alpha\beta} = \int_{-\infty}^{\infty} \frac{d^D l}{(2\pi)^D} \frac{(l^2)^\alpha}{(l^2 - \Delta + i\epsilon)^\beta}, \quad (1.79)$$

$$= i(-1)^{\alpha+\beta} \frac{\pi^{D/2}}{\Gamma(D/2)} \frac{\Gamma(\alpha + D/2)\Gamma(\beta - \alpha - D/2)}{\Gamma(\beta)\Delta^{\beta-\alpha-D/2}}. \quad (1.80)$$

This integral was derived assuming $D/2 < m$, so the integral converges. However, dimensional regularization changes more than just the loop integrals. From the beginning to end, all the aspects of the calculation are done in D dimensions. The loop integrals change, as does the Clifford algebra, the phase space integral, and the action. Here is where we find the introduction of the renormalization scale. The action is now written,

$$\mathcal{S} = \int d^D x \mathcal{L}. \quad (1.81)$$

The action is dimensionless, so the Lagrangian has to compensate for the change in the measure. This imposes a dimension on the coupling constant. If we let $D = 4 - 2\epsilon$, then

$$g \rightarrow \mu_R^\epsilon g, \quad (1.82)$$

where μ_R has units of mass and is the renormalization scale.

Renormalization

Renormalization is one of the great feats of gauge field theory. The theoretical framework behind renormalization is considerable, and will not be considered here. In short, the coupling and mass parameters in our Lagrangian are to be considered “bare” parameters and do not correspond to the physical (measured) values. When UV poles are found to exist, it is possible to redefine the parameters in our theory to remove these poles by shifting them by a formally infinite amount. This is done in a multiplicative way,

$$\psi_{0,f}^i \rightarrow Z^{1/2} \psi_{f,R}^i \quad (1.83)$$

$$A_{0,\mu}^a \rightarrow Z_A^{1/2} A_{\mu,R}^a \quad (1.84)$$

$$\chi_0^a \rightarrow Z_\chi^{1/2} \chi_R^a \quad (1.85)$$

$$g_0 \rightarrow Z_g g_R \quad (1.86)$$

$$m_0 \rightarrow Z_m m_R \quad (1.87)$$

$$\xi_0 \rightarrow Z_A \xi_R, \quad (1.88)$$

where the subscripts denote bare and renormalized quantities. We note that the gauge parameter is renormalized by the same factor as the gluon fields to keep the gauge-fixing term in the Lagrangian consistent.

Any serious candidate for a model of the universe needs to be renormalizable to correctly predict physical observables. However, there is some ambiguity as to what to absorb into the renormalization. Typically, radiative corrections have some commonly occurring finite terms appearing with the UV poles. The prescription used to subtract the divergencies and any finite terms is known as the renormalization scheme. Different schemes are appropriate to different kinds of calculations. We will use the modified minimal subtraction scheme, written $\overline{\text{MS}}$. In this scheme, we remove the commonly occurring factors of 4π and the Euler-Mascheroni constant ($\gamma_E = 0.5772\dots$) by defining the $\overline{\text{MS}}$ UV pole in terms of the bare pole as

$$\frac{1}{\bar{\epsilon}} = (4\pi)^\epsilon \exp(-\epsilon\gamma_E) \frac{1}{\epsilon}. \quad (1.89)$$

The dependence on the renormalization scale and scheme would lead one to think that our results will depend on the choices made, making the results inconsistent for the same physical observable. To ensure that this is not true, the behavior of the renormalized quantities are restricted when changing from one scale to another. Mathematically, the physical observables change according to scale and scheme according to a set of coupled differential equations known as the renormalization group equations⁵. These equations allow our results to be independent from the parameter μ_R , but we will come back to that assertion. Briefly, this is a goal of a calculation, not a reality.

1.5.3 Running of α_s and pQCD

To best understand perturbative QCD (pQCD), the best statement that can be made is that “everything runs”. The preceding comments about renormalization and the renormalization group effect all aspects of a calculation and make the values of all the parameters change in calculable ways.

If we consider a physical observable which depends on the energy scale, $R(Q)$, we would assume that there exists a limiting value for R independent of Q . This is not the case because the perturbation series requires renormalization to remove ultraviolet divergencies. The renormalization procedure is done at a scale μ , so our physical observable must depend on the ratio Q^2/μ^2 .

The μ parameter seems to be arbitrary, it was not mentioned in the QCD Lagrangian, but the scale μ must be chosen to define the theory at the quantum

⁵The choice of the word group is as unfortunate as it is historic.

(loop) level. Therefore our calculations should have results that are independent of the scale μ . In actuality, this is a goal and not a requirement and any residual dependence for a physical observable on the scale μ tells us about the expected size of higher order corrections. If we use the renormalization group equation we can define this independence precisely as,

$$\mu^2 \frac{d}{d\mu^2} R(Q^2/\mu^2, \alpha_s) = \left[\mu^2 \frac{\partial}{\partial \mu^2} + \mu^2 \frac{\partial \alpha_s}{\partial \mu^2} \frac{\partial}{\partial \alpha_s} \right] R \equiv 0, \quad (1.90)$$

here the scale μ need not be the renormalization scale, but we will identify it as such for convenience. We will simplify this equation by using the common notation

$$t = \ln\left(\frac{Q^2}{\mu^2}\right), \quad \beta(\alpha_s) = \mu^2 \frac{\partial \alpha_s}{\partial \mu^2}, \quad (1.91)$$

and we have in the end (remember t is not a time coordinate),

$$\left[-\frac{\partial}{\partial t} + \beta(\alpha_s) \frac{\partial}{\partial \alpha_s} \right] R(e^t, \alpha_s) = 0. \quad (1.92)$$

This equation can now we solved order by order leading to the running of the coupling constant.

The β function

The running of the coupling is controlled by the renormalization group equation,

$$Q^2 \frac{\partial \alpha_s}{\partial Q^2} = \beta(\alpha_s). \quad (1.93)$$

If we expand the β function itself into a perturbative expansion,

$$\beta(\alpha_s) = -b\alpha_s^2(1 + b'\alpha_s + b''\alpha_s^2 + \mathcal{O}(\alpha_s^3)), \quad (1.94)$$

then we can find exact (for the first few orders) or numeric solutions to the renormalization group equation and see how the coupling constant changes. The first few terms are equal to (see Appendix C for the Casimir invariants)

$$b = \frac{(11C_A - 2n_f)}{12\pi} = \frac{(33 - 2n_f)}{12\pi}, \quad (1.95)$$

$$b' = \frac{(12C_A^2 - 5C_A n_f - 3C_F n_f)}{2\pi(11C_A - 2n_f)} = \frac{(153 - 19n_f)}{2\pi(33 - 2n_f)}, \quad (1.96)$$

$$\begin{aligned} b'' &= \frac{(2857C_A^3 + (54C_F^2 - 615C_F C_A - 1415C_A^2)n_f + (66C_F + 79C_A)n_f^2)}{288\pi^2(11C_A - 2n_f)} \\ &= \frac{(77139 - 15099n_f + 325n_f^2)}{288\pi^2(33 - 2n_f)}, \end{aligned} \quad (1.97)$$

where n_f is the number of light flavors ($n_f = 5$ in this thesis). If we look at the expansion again and the form of b , we see that the β function is negative for $n_f \leq 16$.

Asymptotic freedom

In electromagnetism, we have a very simple structure for the β function. For one fermion flavor we have

$$\beta_{\text{QED}}(\alpha) = \frac{1}{3\pi}\alpha^2 + \dots, \quad (1.98)$$

so the strength of the coupling becomes greater at higher energy. This solution is very simple to understand. Higher energy interactions we able to penetrate deeper into the charge cloud screening the electron. Experimentally, we were able to see α become larger at different energy scales like $\alpha^{-1}(0) = 137.035$, $\alpha^{-1}(M_\tau^2) = 133.498$, and $\alpha^{-1}(M_Z^2) = 127.918$. However, the β function is negative⁶ in QCD, so the coupling becomes smaller at high energy. This effect is known as “asymptotic freedom and infrared slavery”.

At high energies in QCD, our perturbation theory becomes better and better and at small energies we have a confining behavior. This allows for the construction of the parton model which will be discussed next.

1.6 Partons, Hadrons, and Observables

We can go no further without defining our physical observables and going through an example to show how our machinery works. We will typically be interested in differential cross-sections because this is the quantity that is measured at colliders. From time to time we will also be interested in the total (integrated) cross-sections because it is useful in determining the number of events expected for a certain energy. Our first example happens to be a total cross-section because it is simpler to calculate the corrections to a $2 \rightarrow 1$ process as an illustration.

Scattering and factorization

We will be dealing with partonic cross-sections in this thesis, but we do not build parton colliders. We build hadron colliders. The Fermilab Tevatron

⁶It is interesting that what this meant was not immediately seen. Moreover, it is interesting to note how many people were working on this problem and failed to find the negative β function.

collides protons on anti-protons and the CERN Large Hadron Collider will collide protons on protons.

The connection between hadron-hadron scattering and parton-parton scattering is encoded in the parton model and the factorization theorem [49]. We can write our hadronic observable as follows,

$$d\sigma(P_1, P_2) = \sum_{ij} \int f_{i/1}(x_1, \mu_F^2) \otimes d\hat{\sigma}_{ij} \otimes f_{j/2}(x_2, \mu_F^2), \quad (1.99)$$

where the $d\sigma$ means that this can be a differential quantity that we are predicting. The functions $f_{a/H}(x, \mu_F^2)$ are known as the parton distribution functions (PDFs). These must be measured experimentally. The quantity $dx f_{a/H}$ should be interpreted as the probability⁷ that a parton a will be found in hadron H carrying a momentum fraction between x and $x + dx$. This probability interpretation is the reason we have written the partonic quantity between the functions as in ordinary quantum mechanics even though the PDFs are real functions and this is not needed. Also we have used the ‘ \otimes ’ symbol to drive home the fact that this is a convolution. Pictorially, we can think of this relation as depicted in Figure (1.6). We can understand this equation as integrating over all the allowable momentum configurations that allow for the partonic production process to occur. There are kinematic limits to consider in these derivations that will be explored in Appendix A.

It is the hard scattering (differential) cross-section that can be calculated with pQCD. However, the separation of the short and long distance physics with the factorization theorem requires the introduction of a factorization scale μ_F . As with the renormalization scale, the more terms that are included reduce the dependence on the factorization scale. In practice, both of these scales are often set equal, $\mu = \mu_F = \mu_R$, but this depends on the specifics of the calculation.

Observables

It is a truism that to get a Lorentz invariant answer you must ask a Lorentz invariant question. The same is true for physical observables. We must make sure that we are asking a question that has a physical answer. One needs to ask an IR safe question to get an IR safe answer. Can a detector tell the difference between a direct production process ($ab \rightarrow X$) and the same process with a soft gluon in the final state? This is a loaded question and we cannot

⁷Parton distribution functions lose this interpretation at higher orders due to the absorption of IR poles. However, it can still be approximately thought of in these terms.

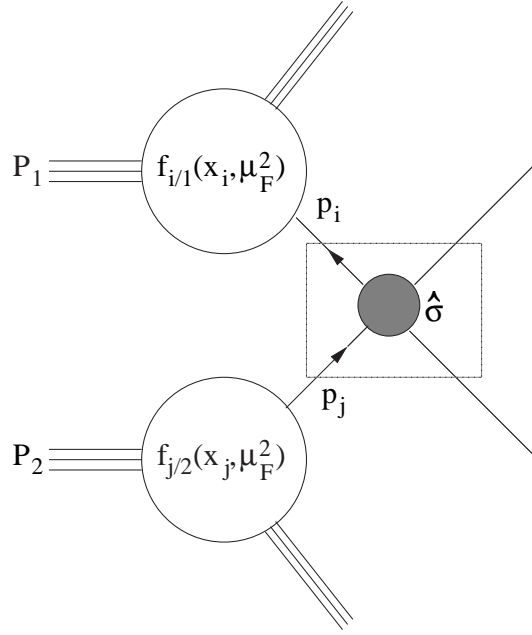


Figure 1.6: Parton Model.

put the cart before the horse. We will work out an example and show how all of this fits together.

We will examine the Drell-Yan production, $p\bar{p} \rightarrow W^+ + X$. We will refer to Figure (1.7) for our diagrams and momentum assignments.

1.6.1 Lowest order cross-section

At the partonic level, the Drell-Yan process (with momentum assignment) is $q(p_1)\bar{q}(p_2) \rightarrow W^+(q)$. If we consider only the scattering of valence quarks then we would have more accurately $u\bar{d} \rightarrow W^+$ and $\bar{u}d \rightarrow W^-$, however, the W^\pm is not directly seen so we will ignore this complication for the time being and return to it when we talk about fragmentation functions. The application of the Feynman rules (the weak vector bosons couple like $V - A$) gives,

$$i\mathcal{M} = \bar{v}(p_2) \frac{ig_2}{\sqrt{2}} \gamma_\mu \frac{(1 - \gamma_5)}{2} u(p_1) \epsilon(q). \quad (1.100)$$

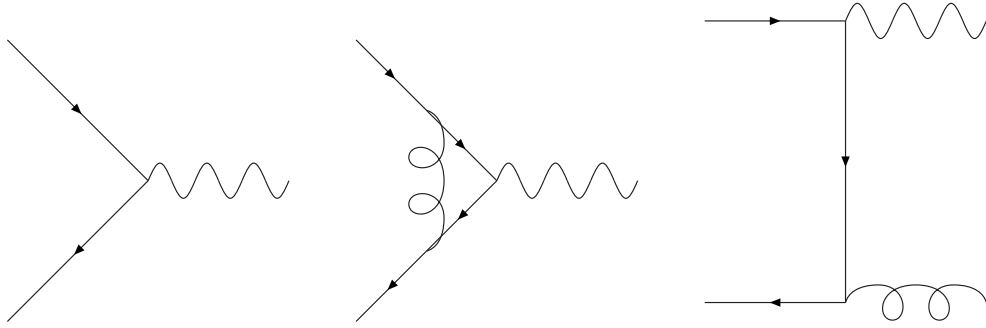


Figure 1.7: Drell-Yan W^\pm production (sample diagrams).

The color and spin averaged⁸ matrix elements can be written,

$$|\overline{\mathcal{M}}|^2 = \frac{N_c}{4N_c^2} \left(\frac{g_2}{\sqrt{2}} \right)^2 \text{Tr} [\not{p}_2 \gamma_\mu P_L \not{p}_2 \gamma_\nu P_L] \left(-\eta^{\mu\nu} + \frac{q^\mu q^\nu}{M_W^2} \right), \quad (1.101)$$

where $N_c = 3$ is the number of colors, $P_L = (1 - \gamma_5)/2$ is the left projection operator, and the final term involving the metric is the summation of the polarization vectors.

Right away in this calculation we are confronted with what to do with the γ_5 in D dimensions. For this very simple calculation we will simply use the naïve γ_5 prescription, but this will not always be the case. A detailed look at the γ_5 problem can be found in Appendix B.

If we use the usual Mandelstam variables and let $\hat{s} = (p_1 + p_2)^2 = 2p_1 \cdot p_2$ (massless initial state quarks), then the trace can be written in $D = 4 - 2\epsilon$ dimensions as,

$$\text{Tr} [\not{p}_2 \gamma_\mu P_L \not{p}_2 \gamma_\nu P_L] = 2\hat{s}(1 - \epsilon), \quad (1.102)$$

so we can write out total partonic cross-section as

$$\begin{aligned} \hat{\sigma} &= \frac{\pi g_2^2}{4N_c \hat{s}} (1 - \epsilon) \delta(1 - \hat{s}/M_W^2), \\ &= \hat{\sigma}^{(0)}(1 - \epsilon) \delta(1 - \hat{s}/M_W^2). \end{aligned} \quad (1.103)$$

We see that at the tree (Born) level, the process has a clean $\epsilon \rightarrow 0$ limit. The ϵ terms in the Born cross-section are important to higher order corrections as they could be contracted with a $1/\epsilon$ term yielding a finite term in the product so these terms cannot be ignored in general.

⁸We have averaged over 2 quark polarizations. In D dimensions, gluons have to be averaged over $(D - 2)$ polarizations.

1.6.2 Higher order cross-sections

At the lowest order, we are free to simply calculate our partonic cross-section at tree level and plug them into a computer program to convolute it with the PDFs to find a physical cross-section. However, if we want to reproduce data, we will need to add some more information about fragmentation functions, jet algorithms, detector limitations, et cetera. Whereas the PDFs relate the hard scattering matrix elements into hadronic scattering, fragmentation functions (and jet algorithms to some extent) convert the outgoing partons into hadronized information.

We also have the as-yet unresolved issue of the left over IR poles. Here we will show that there are subtraction terms present to remove these poles order by order. In short, these IR poles (which will manifest themselves as collinear singularities) will be absorbed as splitting functions in the higher order parton distribution functions and fragmentation functions. The IR poles cancel based on a very general theorem [50–52] known as either the Kinoshita-Lee-Nauenberg or Bloch-Nordsieck theorem, and they are required to completely cancel due to the factorization theorems.

We will seek to define an IR safe observable⁹, which we will call ω (also known in the literature as H , presumably to stand for hadronic information). This function will be defined order by order in our calculations. We can start by remembering that the lowest order cross-section is IR safe as the Born level cross-section has no poles. If we write out all the possible places the IR poles could be absorbed (up to ‘higher twist’ terms which will be ignored here represented by the last term) we find,

$$\sigma^{(0)} = \underbrace{f^{(0)}}_{\text{pdf}} \otimes \underbrace{\omega^{(0)}}_{\text{observable}} \otimes \underbrace{d^{(0)}}_{\text{fragmentation}} + \mathcal{O}(\Lambda_{\text{QCD}}^2/Q^2), \quad (1.104)$$

so we indeed see

$$\sigma^{(0)} = \omega^{(0)}, \quad \Rightarrow f^{(0)} = d^{(0)} = 1. \quad (1.105)$$

So at the lowest order, we recover what we already knew, that the lowest order observable is the same as the partonic cross-section. The superscripts here refer to the order of the calculation. PDFs and fragmentation functions are also fit order by order in the coupling constant, and as we are about to see, at higher orders the PDFs and fragmentation functions also absorb the left-over IR poles of the calculation.

We can continue this order by order to find the IR safe physical observable

⁹Many thanks to Fred Olness for finally elucidating this to the author.

at next-to-leading order (NLO),

$$\begin{aligned}\sigma^{(1)} &= f^{(1)} \otimes \omega^{(0)} \otimes d^{(0)} + f^{(0)} \otimes \omega^{(1)} \otimes d^{(0)} + f^{(0)} \otimes \omega^{(0)} \otimes d^{(1)} \\ &= f^{(1)} \otimes \omega^{(0)} + \omega^{(1)} + \omega^{(0)} \otimes d^{(1)}.\end{aligned}$$

By adding what we already know about the lowest order (LO) observable, we can write,

$$\omega^{(1)} = \sigma^{(1)} - f^{(1)} \otimes \sigma^{(0)} - \sigma^{(0)} \otimes d^{(1)} \quad (1.106)$$

So we can see that any collinear poles that are left in the partonic $\sigma^{(1)}$ function can be removed by suitable redefinition of the higher order PDFs and/or fragmentation functions. These redefinitions are referred to as splitting functions and they are analogous to our renormalization group equation, they tell us how the PDFs evolve with energy scale. The splitting functions are perturbative functions that are described by the Dokshitzer-Gribov-Lipatov-Altarelli-Parisi (DGLAP) formalism [53–56]. The entire machinery behind PDF evolution is well beyond the scope of our problem, but we will list the splitting functions for later reference (the labeling of the subscript appears backwards, but is in agreement with the convention),

$$P_{q \leftarrow q}^{(1)}(z) = C_F \left(\frac{1+z^2}{1-z} \right)_+, \quad (1.107)$$

$$P_{q \leftarrow g}^{(1)}(z) = \frac{1}{2}(z^2 + (1-z)^2). \quad (1.108)$$

We will define the + subscript in a minute.

The $\sigma^{(1)}$ function itself is free of UV poles because it is defined as the appropriate combination of virtual and real-emission corrections and can be renormalized,

$$\begin{aligned}\sigma^{(1)} &= \int \left[\langle \mathcal{M}^{(1)} | \mathcal{M}^{(0)} \rangle + \langle \mathcal{M}^{(0)} | \mathcal{M}^{(1)} \rangle \right]_2 \text{dPS}_2 \\ &+ \int \left[\langle \mathcal{M}^{(0)} | \mathcal{M}^{(0)} \rangle \right]_3 \text{dPS}_3,\end{aligned} \quad (1.109)$$

where the subscript refers to the number of particles in the final state and the superscript on the amplitude refers to the order of the diagrams (tree level, one-loop, et cetera). This will be made clearer in the next section. We can continue this process to define the next-to-next-to-leading order (NNLO) observable along the same lines,

$$\begin{aligned}\sigma^{(2)} &= f^{(2)} \otimes \omega^{(0)} \otimes d^{(0)} + f^{(0)} \otimes \omega^{(2)} \otimes d^{(0)} + f^{(0)} \otimes \omega^{(0)} \otimes d^{(2)} + \\ &f^{(1)} \otimes \omega^{(1)} \otimes d^{(0)} + f^{(1)} \otimes \omega^{(0)} \otimes d^{(1)} + f^{(0)} \otimes \omega^{(1)} \otimes d^{(1)},\end{aligned} \quad (1.110)$$

and insert what we know from the LO and NLO expressions to find

$$\begin{aligned} \omega^{(2)} = & \sigma^{(2)} - f^{(2)} \otimes \sigma^{(0)} - \sigma^{(0)} \otimes d^{(2)} + f^{(1)} \otimes f^{(1)} \otimes \sigma^{(0)} + \sigma^{(0)} \otimes d^{(1)} \otimes d^{(1)} \\ & + f^{(1)} \otimes \sigma^{(0)} \otimes d^{(1)} - f^{(1)} \otimes \sigma^{(1)} - \sigma^{(1)} \otimes d^{(1)}. \end{aligned} \quad (1.111)$$

Again, the $\sigma^{(2)}$ function is appropriately defined as

$$\begin{aligned} \sigma^{(2)} = & \int \left[\langle \mathcal{M}^{(2)} | \mathcal{M}^{(0)} \rangle + \langle \mathcal{M}^{(0)} | \mathcal{M}^{(2)} \rangle + \langle \mathcal{M}^{(1)} | \mathcal{M}^{(1)} \rangle \right]_2 \text{dPS}_2 \\ & + \int \left[\langle \mathcal{M}^{(1)} | \mathcal{M}^{(0)} \rangle + \langle \mathcal{M}^{(0)} | \mathcal{M}^{(1)} \rangle \right]_3 \text{dPS}_3 \\ & + \int \left[\langle \mathcal{M}^{(0)} | \mathcal{M}^{(0)} \rangle \right]_4 \text{dPS}_4. \end{aligned} \quad (1.112)$$

We could continue this recursion indefinitely, the procedure is very straight forward, but is of little practical value. At the next level (NNNLO) we would need to know the PDFs at the same level. The NNLO PDFs were just recently completed (meaning the splitting functions were recently calculated [57, 58]) and it is doubtful that the NNNLO calculation will be available any time in the foreseeable future.

Now that we have our machinery, let us return to our Drell-Yan calculation and see how it put it to use.

Virtual corrections

The virtual contributions at this order take in account the interference of the loop diagrams with the LO diagram as shown in Figure (1.7).

The virtual (loop) corrections to this process can be written

$$\hat{\sigma}_V^{(1)} = \hat{\sigma}^{(0)} \frac{\alpha_s}{2\pi} \delta(1 - \tau) \left(\frac{4\pi\mu_R}{M_W^2} \right)^\epsilon \frac{\Gamma(1 - \epsilon)}{\Gamma(1 - 2\epsilon)} C_F \left\{ -\frac{2}{\epsilon^2} - \frac{3}{\epsilon} - 8 + 4\zeta_2 \right\}, \quad (1.113)$$

where $\tau = M_W^2/\hat{s}$. The prefactor involving $4\pi\mu_R$ and the Γ -functions are common to all the higher order corrections and will be dropped from the expression. These poles occur when the momenta in the denominator of the loop diagrams vanish.

Real emissions

The real emissions taken are again tree-level at this order in the perturbation series. The extra external line adds a power of the coupling constant and is therefore the same order as the virtual corrections. There are many different

real emissions for this process. We can have the emission of real gluons in the quark-quark initial state as well as real (anti-)quarks in the gluon-(anti-)quark initial state. All of these permutations contribute to the physical observable, but we will examine just the real gluon emission for the sake of brevity and simply state the other results. The problem will arise when one of these real emissions become soft ($k^\mu \rightarrow 0$) or collinear ($k^\mu \parallel p^\mu$).

This becomes clear when we look at the kinematics. Let's look at the real emissions in the rest frame of the W -boson. If we assign the momentum,

$$W^+(Q) \rightarrow q(p_1) \bar{q}(p_2) g(p_3), \quad (1.114)$$

then we can define the energy fractions x_i as

$$x_i = \frac{2E_i}{\sqrt{s}} = \frac{2p_i \cdot Q}{s}, \quad x_i > 0, \quad (1.115)$$

which are not to be confused with the parton energy fractions. With this normalization we see

$$\sum_i x_i = \frac{2(\sum_i p_i) \cdot Q}{s} = 2. \quad (1.116)$$

Because of conservation of energy, only two of the fractions are independent. We can also define the angle between any two of the partons like

$$\begin{aligned} (Q - p_3)^2 &= (p_1 + p_2)^2 \\ \Rightarrow s - 2Q \cdot p_3 &= s(1 - x_3) = 2E_1 E_2 (1 - \cos \theta_{12}). \end{aligned} \quad (1.117)$$

We can then continue this process to find expressions for all the angles in terms of all the energy fractions,

$$2(1 - x_1) = x_2 x_3 (1 - \cos \theta_{23}), \quad (1.118)$$

$$2(1 - x_2) = x_3 x_1 (1 - \cos \theta_{31}), \quad (1.119)$$

$$2(1 - x_3) = x_1 x_2 (1 - \cos \theta_{12}). \quad (1.120)$$

Since all the energy fractions $x_i < 1$, this means that there are three configurations where the partons become soft, $x_i \rightarrow 0$, and three configurations where the partons become collinear,

$$x_1 \rightarrow 1 \iff \theta_{23} \rightarrow 0, \quad (1.121)$$

$$x_2 \rightarrow 1 \iff \theta_{31} \rightarrow 0, \quad (1.122)$$

$$x_3 \rightarrow 1 \iff \theta_{12} \rightarrow 0. \quad (1.123)$$

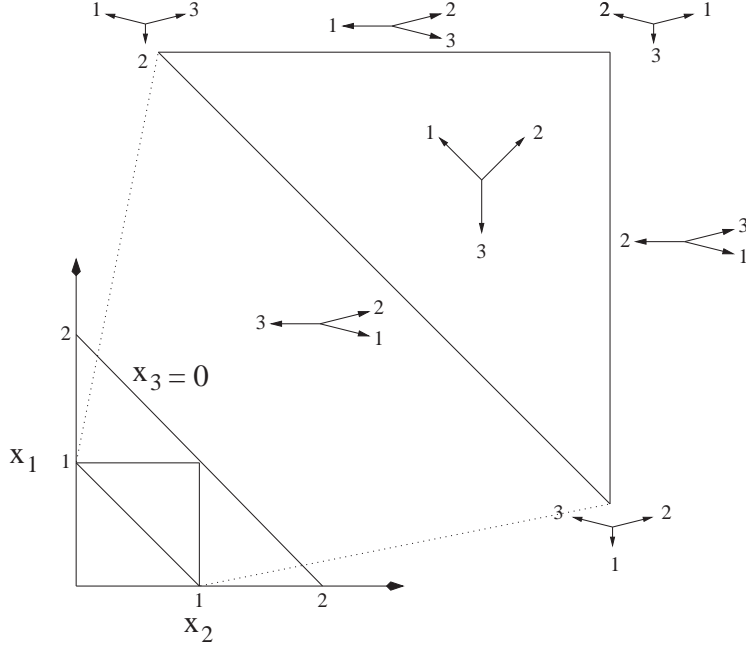


Figure 1.8: Phase space singularities.

Graphically, we can see this occurring at the borders of phase space in Figure (1.8). We can see a soft singularity when two particles are back to back and a collinear singularity when two particles are parallel.

When we try to integrate over all of the phase space we will pick up IR poles where the partons are soft or collinear. We find,

$$\hat{\sigma}_R = \hat{\sigma}_0 \frac{\alpha_s}{2\pi} C_F \left\{ \frac{2}{\epsilon^2} \delta(1-\tau) - \frac{2}{\epsilon} \frac{1+\tau^2}{(1-\tau)_+} + 4(1+\tau^2) \left(\frac{\ln(1-\tau)}{1-\tau} \right)_+ - 2 \frac{1+\tau^2}{1-\tau} \ln \tau \right\}, \quad (1.124)$$

where we have introduced the “plus” distribution to regulate the singularity at $\tau = 1$ smoothly. We define this as,

$$\int_0^1 dz \left(\frac{f(z)}{1-z} \right)_+ = \int_0^1 dz \frac{f(z) - f(1)}{1-z}, \quad (1.125)$$

which removes the singular point. In our case, this is a threshold effect and should not be of too much concern for our illustration.

When we add the virtual and real corrections we see that the double pole

cancels immediately and we are left with the following result,

$$\hat{\sigma}_{\text{V+R}} = \hat{\sigma}_0 \frac{\alpha_s}{2\pi} C_F \left\{ -\frac{2}{\epsilon} \left(\frac{1+\tau^2}{1-\tau} \right)_+ - 2 \frac{1+\tau^2}{1-\tau} \ln \tau + 4(1+\tau^2) \left(\frac{\ln(1-\tau)}{1-\tau} \right)_+ + \left(4\zeta_2 - 8 \right) \delta(1-\tau) \right\}, \quad (1.126)$$

where we have combined the left-over IR poles into one term. We can now see the structure of the IR pole and see that it corresponds to the quark-quark splitting function¹⁰. If we define our higher order PDF in terms of this splitting function and rely on the universal nature of the IR poles that appear in calculations, we have

$$f_{q/q}^{(1)}(z) = -\frac{1}{\epsilon} \frac{1}{2} (4\pi e^{\gamma_E})^\epsilon P_{q \leftarrow q}^{(1)}(z), \quad (1.127)$$

where we can see our PDF notation corresponds to getting a quark out of a quark (q/q), which is precisely what the splitting function describes.

Physical observable

Following our procedure of defining an IR safe observable, we have

$$\begin{aligned} \omega_{q\bar{q}}^{(1)} &= \hat{\sigma}^{(1)} - f_{q \leftarrow q}^{(1)} \otimes \hat{\sigma}_{q\bar{q}}^{(0)} \\ &= \hat{\sigma}^{(0)} \frac{\alpha_s}{2\pi} \left\{ P_{q \leftarrow q}^{(1)}(\tau) \ln \left(\frac{M_W^2}{\mu^2} \right) + C_F \left[-2 \frac{1+\tau^2}{1-\tau} \ln \tau + 4(1+\tau^2) \left(\frac{\ln(1-\tau)}{1-\tau} \right)_+ + \left(4\zeta_2 - 8 \right) \delta(1-\tau) \right] \right\}, \end{aligned} \quad (1.128)$$

$$(1.129)$$

which if we take $\mu = M_W$ and remove the α_s factor, this simplifies as

$$\omega_{q\bar{q}}^{(1)} = \hat{\sigma}^{(0)} C_F \left\{ -\frac{1+\tau^2}{1-\tau} \ln \tau + 2(1+\tau^2) \left(\frac{\ln(1-\tau)}{1-\tau} \right)_+ + \left(2\zeta_2 - 4 \right) \delta(1-\tau) \right\}. \quad (1.130)$$

We can do this for the other initial states and combine our results for a

¹⁰This definition is scheme dependent. As mentioned, we will employ the $\overline{\text{MS}}$ scheme.

final prediction

$$\begin{aligned}
\sigma_{hh'}^{\text{NLO}} = & \sum_{f=q,\bar{q}} \int dx_1 dx_2 f_{f/h}(x_1, \mu^2) \left[\sigma^{(0)} \delta(1 - \tau) \right] f_{\bar{f}/h'}(x_2, \mu^2) \\
& + \sum_{f=q,\bar{q}} \int dx_1 dx_2 f_{f/h}(x_1, \mu^2) \left[\frac{\alpha_s(\mu^2)}{\pi} \omega_{f\bar{f}}^{(1)}(\tau) \right] f_{\bar{f}/h'}(x_2, \mu^2) \\
& + \left\{ \sum_{f=q,\bar{q}} \int dx_1 dx_2 f_{f/h}(x_1, \mu^2) \left[\frac{\alpha_s(\mu^2)}{\pi} \omega_{fG}^{(1)}(\tau) \right] f_{G/h'}(x_2, \mu^2) + (x_1 \leftrightarrow x_2) \right\}.
\end{aligned} \tag{1.131}$$

When one carefully makes sure that all the constants, couplings, and distributions run at the appropriate level, this procedure gives predictions that match the data quite well.

1.7 Resummation

We carefully studied the IR properties of the total cross-section, but as was mentioned earlier, we are primarily interested in the differential cross-section. To that end, our Born level cross-sections are $2 \rightarrow 2$ processes (the particles recoil off one another to give the outgoing particles transverse momentum). However, we have already seen one kind of problem with the introduction of the plus distribution. There are energy configurations which pose problems to our computational formalism. There also appear to be singular corrections when the transverse momentum (p_T) of an outgoing particle goes to zero. We can generically write these corrections as

$$\text{threshold} \sim \alpha_s^n \frac{\ln^{2n-1}(1 - \tau)}{(1 - \tau)}, \quad \text{recoil} \sim \frac{\alpha_s^n}{p_t^2} \ln^{2n-1} \frac{M_W^2}{p_t^2}. \tag{1.132}$$

In the second half of this thesis we will be interested in the recoil (or p_t singular corrections) and what we can do to make reliable predictions at small values of the transverse momentum. The formalism that allows for predictions at small p_t is known as resummation. This formalism is described in detail when it is used and will not be introduced here. However we will present a motivation for our future results based on our Drell-Yan calculation. Experimentally, we note that at small values of p_t , the differential cross-section goes like $\exp(-p_t^2)$. Since our LO prediction was off by a K -factor ($d\sigma^{\text{NLO}} = K d\sigma^{\text{LO}}$), if we assume that the corrections form a series,

$$K = 1 + \frac{2\pi\alpha_s}{3}(\dots) + \dots \Rightarrow \exp(2\pi\alpha_s/3), \tag{1.133}$$

where the arrow introduced the resummation formalism. Lets look at the exact calculation and see where this assumption enters.

When we look at the differential cross-section for $q\bar{q} \rightarrow W^\pm g$, we find that the correction has a singular log correction as predicted. But we can resum that large logarithm into our assumption that repeated soft-gluon emission will make the result finite. We can write,

$$\begin{aligned} \int_0^s \frac{d\sigma}{d\tau dy dp_t^2} dp_t^2 &= \left(\frac{d\sigma}{d\tau dy} \right)_{\text{Born}} + \mathcal{O}(\alpha_s) \\ \int_0^{p_t^2} \frac{d\sigma}{d\tau dy dp_t^2} dp_t^2 &= \left(\frac{d\sigma}{d\tau dy} \right)_{\text{Born}} \times \left\{ 1 - \int_{p_t^2}^s \frac{4\alpha_s \ln s/p_t^2}{3\pi p_t^2} dp_t^2 \right\} \\ &= \left(\frac{d\sigma}{d\tau dy} \right)_{\text{Born}} \times \left\{ 1 - \frac{2\alpha_s}{3\pi} \ln^2 \frac{s}{p_t^2} \right\} \\ &= \left(\frac{d\sigma}{d\tau dy} \right)_{\text{Born}} \times \exp \left\{ -\frac{2\alpha_s}{3\pi} \ln^2 \frac{s}{p_t^2} \right\}, \end{aligned} \quad (1.134)$$

which is finite as $p_t \rightarrow 0$. This is the well-known Sudakov double logarithm. When we differentiate our previous expression we find that the observable behaves like,

$$\frac{d\sigma}{d\tau dy dp_t^2} = \left(\frac{d\sigma}{d\tau dy} \right)_{\text{Born}} \times \frac{4\alpha_s \ln s/p_t^2}{3\pi p_t^2} \times \exp \left\{ -\frac{2\alpha_s}{3\pi} \ln^2 \frac{s}{p_t^2} \right\}. \quad (1.135)$$

Although there are some details missing, we will leave our computational machinery now and examine what might lie beyond the SM.

1.8 Why supersymmetry?

So far, we have only sung the praises of the SM, but is there anything wrong with the SM? The answer to that question depends on what one considers a problem. Experimentally, the SM represents the known data extremely well. However, we are only a few years away from seeing data from a new energy regime and it would not be out of line to prepare some extended theories before the data come rolling in.

However, there are some theoretical reasons for extensions to the SM. We will present one motivation from the Higgs sector of the SM having to do with radiative corrections to the Higgs mass. It would seem that every paper that deals with supersymmetry has its own favorite reason, so we will stick with the topic at hand, the Higgs.

The Higgs is a unique particle in the SM, a fundamental scalar that disobeys the decoupling theorem. If we calculate radiative corrections to the

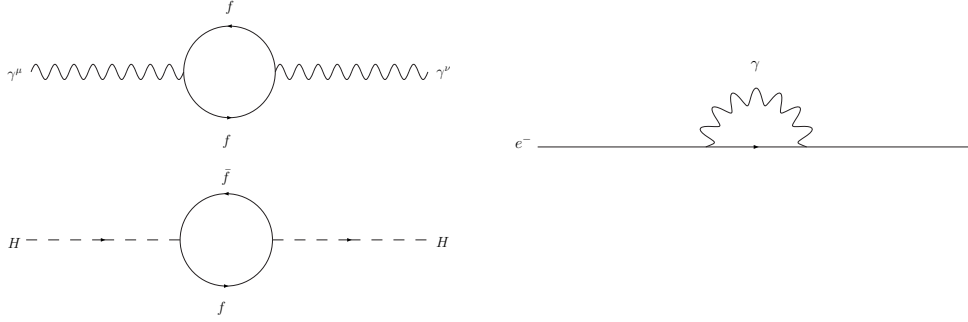


Figure 1.9: Self energy mass corrections.

masses of different SM particles, as shown in Figure (1.9), we find different classes of results. The two-point function for the photon (at zero external momentum) with a fermion loop can be written as,

$$\begin{aligned}
 \Pi_{\gamma\gamma}^{\mu\nu}(0) &= - \int \frac{d^4k}{(2\pi)^4} \text{Tr} \left[(-ie\gamma^\mu) \frac{i(\not{k} + m_f)}{k^2 - m_f^2 + i\epsilon} (-ie\gamma^\nu) \frac{i(\not{k} + m_f)}{k^2 - m_f^2 + i\epsilon} \right] \\
 &= -4e^2 \int \frac{d^4k}{(2\pi)^4} \frac{2k^\mu k^\nu - \eta^{\mu\nu}(k^2 - m_f^2)}{(k^2 - m_f^2 + i\epsilon)^2} \\
 &= 0.
 \end{aligned} \tag{1.136}$$

This integral vanishes in dimensional regularization. Moreover, there is an exact $U(1)$ gauge invariance that makes the photon massless at all orders of perturbation theory. It would be suspect if the photon developed a mass radiatively.

What about the opposite correction, a fermion with a photon in what is sometimes called a sunset graph. We find,

$$\begin{aligned}
 \Pi_{ff}(0) &= \int \frac{d^4k}{(2\pi)^4} \text{Tr} \left[(-ie\gamma_\mu) \frac{i(\not{k} + m_f)}{k^2 - m_f^2 + i\epsilon} (-ie\gamma_\nu) \frac{-i\eta^{\mu\nu}}{k^2} \right] \\
 &= -e^2 \int \frac{d^4k}{(2\pi)^4} \frac{\text{Tr}(\gamma_\mu(\not{k} + m_f)\gamma^\mu)}{k^2(k^2 - m_f^2 + i\epsilon)} \\
 &= -4e^2 m_f \int \frac{d^4k}{(2\pi)^4} \frac{1}{(k^2 - m_f^2 + i\epsilon)}.
 \end{aligned} \tag{1.137}$$

Now this is a formally divergent integral. However, if we use a regulator (in this case a cut-off) and set it at a very high scale, the Planck scale for instance, and we can see the size of the mass correction for the electron,

$$\delta m_e \sim \frac{2\alpha}{\pi} \log \frac{M_{\text{Pl}}}{m_e} \sim 0.24 m_e. \tag{1.138}$$

This is a modest mass correction, but there is more here than meets the eye. There is a symmetry here that is hidden. In the massless limit, the model is chirally invariant, $\psi \rightarrow \psi' = \exp(i\gamma_5\varphi)\psi$. If this were an exact symmetry, the correction would vanish. In fact, the opposite is true. This symmetry is broken by the mass.

The problem with the SM manifests itself with the mass corrections to the Higgs. If we let the $f\bar{f}H$ coupling be λ_f generically, then the two-point function is

$$\begin{aligned}\Pi_{HH}^f(0) &= -N_c \int \frac{d^4k}{(2\pi)^4} \text{Tr} \left[\left(i \frac{\lambda_f}{\sqrt{2}} \right) \frac{i(\not{k} + m_f)}{k^2 - m_f^2 + i\epsilon} \left(i \frac{\lambda_f}{\sqrt{2}} \right) \frac{i(\not{k} + m_f)}{k^2 - m_f^2 + i\epsilon} \right] \\ &= -2N_c \lambda_f^2 \int \frac{d^4k}{(2\pi)^4} \left[\frac{1}{k^2 - m_f^2 + i\epsilon} + \frac{2m_f^2}{(k^2 - m_f^2 + i\epsilon)^2} \right].\end{aligned}$$

The first term is quadratically divergent. If we follow the same prescription as with the electron and pick a large cut-off at the Planck scale then the ‘‘correction’’ is 30 orders of magnitude larger than the Higgs mass itself (for $M_H < 1$ TeV). This correction is independent of the Higgs mass and the correction does not vanish with a vanishing Higgs mass. There are no hidden symmetries here.

This fact is often stated that there is nothing in the SM that protects the Higgs mass. Now, the critical issue here is what we make of this divergence. There is absolutely nothing wrong with removing this quadratic divergence with a large counter-term. If we think of the SM as a field theory, this is a fair move. However, one is led to ask if there is a way to correct this within the model itself. Without belaboring the mechanics of this, a supersymmetric model protects the mass of the Higgs boson by introducing scalar partners for all the fermions (these particles are usually represented with a tilde). If we make the couplings

$$\tilde{\lambda}_f = -\lambda_f^2, \tag{1.139}$$

then the Higgs mass correction has more diagrams and we get a more reasonable result. We now have the renormalized result,

$$\begin{aligned}\Pi_{HH}^{f+\tilde{f}}(0) &= \frac{i\lambda_f^2 N_c}{16\pi^2} \left[-2m_f^2 \left(1 - \log \frac{m_f^2}{\mu^2} \right) + 4m_f^2 \log \frac{m_f^2}{\mu^2} \right. \\ &\quad \left. + 2m_{\tilde{f}}^2 \left(1 - \log \frac{m_{\tilde{f}}^2}{\mu^2} \right) - 4m_{\tilde{f}}^2 \log \frac{m_{\tilde{f}}^2}{\mu^2} \right. \\ &\quad \left. - |A_f|^2 \log \frac{m_{\tilde{f}}^2}{\mu^2} \right],\end{aligned} \tag{1.140}$$

where A_f is the unknown coupling for the $H\tilde{f}\tilde{f}^*$ vertex. We can see that for degenerate masses and $A_f \rightarrow 0$, the correction vanishes. This would imply a hidden symmetry, a supersymmetry. However, we know nothing a priori about the masses of these scalar particles and their coupling (in this model). We also find that not only are the quadratic divergencies canceled, but as long as the differences in the fermion and scalar masses squared remains small (on the order of the weak scale), then the weak scale itself is protected from loop corrections from these heavy particles, phenomenologically a great boon.

1.8.1 MSSM

If we accept supersymmetry into our theory, we have to add it to the SM without breaking what we have built so far. It is not as simple as adding very heavy particles that decouple, there are observables that have more delicate dependences. Our measurements of electroweak observables are quite good, so we must somehow add supersymmetry in a way that it is difficult to see. Skeptics may argue that this is a reason to ignore supersymmetry, but we will move on.

The first fact that must be accommodated, the ρ -parameter has been determined experimentally to be very close to unity,

$$\rho = \frac{M_W^2}{M_Z^2 \cos^2 \theta_w} = 0.9998_{-0.0005}^{+0.0008}, \quad (1.141)$$

which implies that it must be exactly unity at tree level and only picks up radiative corrections that move it away from unity. Only Higgs doublets and singlets generate a tree-level ρ -parameter of unity¹¹.

The second major constraint is the suppression of flavor changing neutral currents (FCNCs). In the SM, quarks do not flavor change at a $q\bar{q}Z^0/\gamma$ vertex (at tree level). We want this to be true in our supersymmetric model as well. One way to do this is to have all the fermions of one charge couple to only one Higgs doublet. Since there are two differently charged fermions in nature, we are led to two Higgs doublets, one that couples to up-type quarks and another that couples to down-type quarks as well as to the charged fermion sector. It should also be noted (but not elaborated) that this structure also prevents the occurrence of anomalies in the theory. Although it should be noted that supersymmetry is not needed for a doublet model, but supersymmetry adds some constraints to the model and makes it more predictive in many respects.

The MSSM is a model that incorporates two Higgs doublets with two VEVs that give masses to the up and down sectors separately. We will concentrate on

¹¹Here we have ignored exotic combinations of weak isospin.

Superfield	$SU(3)_c$	$SU(2)_L$	$U(1)_Y$	Content
\hat{Q}	3	2	$+\frac{1}{6}$	$(u_L, d_L), (\tilde{u}_L, \tilde{d}_L)$
\hat{U}^c	$\bar{\mathbf{3}}$	1	$-\frac{2}{3}$	u_R, \tilde{u}_R^*
\hat{D}^c	$\bar{\mathbf{3}}$	1	$+\frac{1}{3}$	d_R, \tilde{d}_R^*
\hat{L}	1	2	$-\frac{1}{2}$	$(\nu_L, e_L), (\tilde{\nu}_L, \tilde{e}_L)$
\hat{E}^c	1	1	$+1$	\bar{e}_R, \tilde{e}_R^*
\hat{H}_1	1	2	$-\frac{1}{2}$	(H_1, \tilde{h}_1)
\hat{H}_2	1	2	$+\frac{1}{2}$	(H_2, \tilde{h}_2)
\hat{G}^a	8	1	0	g, \tilde{g}
\hat{W}^i	1	3	0	$W_i, \tilde{\omega}_i$
\hat{B}	1	1	0	B, \tilde{b}

Table 1.4: Group structure of chiral superfields and gauge multiplets in the MSSM.

the physics of the Higgs sector of the MSSM, and introduce the other sectors only as needed. There is a great deal of mathematical machinery surrounding supersymmetry, most of which we will not need. We will simply construct the most general interactions given our constraints.

Before we move through the mathematics, we should say what we are going to do in words. We will more than double our particle spectrum with the addition of supersymmetry so we need a systematic way of creating Feynman rules. We will end up with the normal SM field and the supersymmetric fields which are usually called by the same name with an ‘s’ prepended to the particle name. For instance, a supersymmetric top quark is a stop squark¹². Leptons have super-partners called sleptons and so on. There are more exotic name in the gauge sector, including winos, binos, and generically gauginos.

Supersymmetric theories are constructed from supermultiplets. Using the superfields in Table (1.8.1), we can build a superpotential, W , and use it to create all the supersymmetric interactions. From a superpotential, we can write the Lagrangian potential like,

$$\mathcal{L}_W = - \sum_i \left| \frac{\partial W}{\partial \phi_i} \right|^2 - \frac{1}{2} \sum_{ij} \left[\frac{\partial^2 W}{\partial \phi_i \partial \phi_j} \psi_i \psi_j + \text{c.c.} \right], \quad (1.142)$$

where the ϕ fields are the scalars and the ψ fields are the fermions in the model. The superpotential is holomorphic as it only depends on the fields and

¹²I would like to point out that this leaves us in a strange situation for the strange quark. The options sstrange or super-strange both seem a little too strange. Typographically, $\tilde{\text{s}}$ trange would work, but is difficult to enunciate.

not their charge conjugates. The most general superpotential we can write in $SU(3)_c \otimes SU(2)_L \otimes U(1)_Y$ is

$$\begin{aligned}
W = & -\epsilon_{ij\mu} \hat{H}_1^i \hat{H}_2^j + \epsilon_{ij} \left[\lambda_L \hat{H}_1^i (\hat{L}^c)^j \hat{E}^c + \lambda_D \hat{H}_1^i \hat{Q}^j \hat{D}^c + \lambda_U \hat{H}_2^j \hat{Q}^i \hat{U}^c \right] \\
& + \epsilon_{ij} \left[\lambda_1 \hat{L}^i \hat{L}^j \hat{E}^c + \lambda_2 \hat{L}^i \hat{Q}^j \hat{D}^c \right] + \lambda_3 \hat{U}^c \hat{D}^c \hat{D}^c.
\end{aligned} \tag{1.143}$$

Here the (i, j) indices are $SU(2)_L$ indices. There is much to be said about all the different interactions in this model. To fully explore this model we would have to introduce several topics we have skipped in field theory, in particular, auxiliary fields and this does not seem appropriate, so we will simply present the Higgs sector.

We will take our two Higgs doublets to have components

$$H_1 = \begin{pmatrix} (\phi_1^0)^* \\ -\phi_1^- \end{pmatrix}, \quad H_2 = \begin{pmatrix} \phi_2^+ \\ \phi_2^0 \end{pmatrix}, \tag{1.144}$$

and we break the electroweak symmetry like,

$$\langle H_1 \rangle = \begin{pmatrix} v_1 \\ 0 \end{pmatrix}, \quad \langle H_2 \rangle = \begin{pmatrix} 0 \\ v_2 \end{pmatrix}. \tag{1.145}$$

We define the ratio of these two VEVs as $\tan \beta = v_2/v_1$. This procedure results in five physical Higgs bosons, two charged (H^\pm), one light and one heavy scalar (h^0, H^0), and one pseudoscalar (A^0). Like the SM Higgs, not all of the MSSM Higgs' can decouple from the theory. Given the parameter space, the lightest scalar, h^0 , can only be so heavy. The h^0 Higgs at its heaviest is light compared to the SM weight limit, only becoming as massive as around 130 GeV in one extreme corner of parameter space.

Phenomenologically speaking, the Higgs sector of the MSSM is very interesting because the different Higgs bosons couple to the SM particles in distinct ways. Beyond the obvious presence of the charged Higgs, the differences between the lightest scalar in the MSSM and the SM Higgs make the case for a careful study of the collider signatures of the two bosons. Remember that the lightest scalar does not decouple and could therefore be confused with a SM Higgs. Moreover, the pseudoscalar Higgs couples in an even more exotic and intriguing way. It couples proportionally to the free parameter $\tan \beta$ and therefore its production could be greatly enhanced. For these reasons we have chosen to study the lightest scalar and pseudoscalar of the MSSM and compare the collider signatures to the SM Higgs boson.

Counting parameters

Why might one be skeptical of supersymmetry? We must make clear that so far there is no smoking gun for supersymmetry. Theoretically, it has many intriguing properties, but has so far avoided experimental detection, a critical requirement for a falsifiable theory of nature. What we do know is that if supersymmetry exists in nature, it is badly broken. We do not see scalar partners to all the known SM particles, so the supersymmetric masses must be quite heavy and therefore split from their SM partners. Any attempts to identify two known particles as superpartners has failed.

In the SM, we have 20 free parameters (as defined with massless neutrinos). We have the strength of the three gauge couplings as measured at some scale, the masses of the three lepton generations, two vector boson masses, six quark masses, three CKM angles and one \mathcal{CP} violating phase, and the mass of the Higgs. The final parameter to make the 20 has not been mentioned, it is the QCD θ_{QCD} parameter. If we were to add massive neutrinos, we would pick up another ten, the three neutrino masses, three mixing angles and another phase bringing the grand total to 30 parameters.

The MSSM introduces a minimum of an additional 114 free parameters without describing how supersymmetry is broken (a problem in itself, usually soft supersymmetry breaking terms are added to the Lagrangian by hand although more exotic mechanisms exist). These consist of seven three by three hermitian mass matrices for the super-partners (with massive neutrinos), three additional mixing matrices, three gaugino masses, and three of five additional parameters to constrain the masses of the five Higgs bosons.

One is forced to ask if we have gained anything in this bargain. In the end, this is impossible to answer on a chalkboard. We do not get to pick how nature chose her particle content. However, we should take statements that the MSSM fits experimental data better than the SM with a grain of salt. It rightfully should, it has more than one hundred additional parameters to float.

1.9 HQET

Now that we have introduced the SM and the MSSM in all their glory and shown how to calculate physical quantities we argue that the full theory is too complicated to calculate higher order corrections to most processes involving the Higgs boson. This is because at a Hadron collider, the Higgs is produced at lowest order in a loop diagram. So the virtual corrections start at two loops with several mass scales. One might say that it is a nightmare to calculate observables in the full SM Higgs. Moreover, NLO corrections have typically

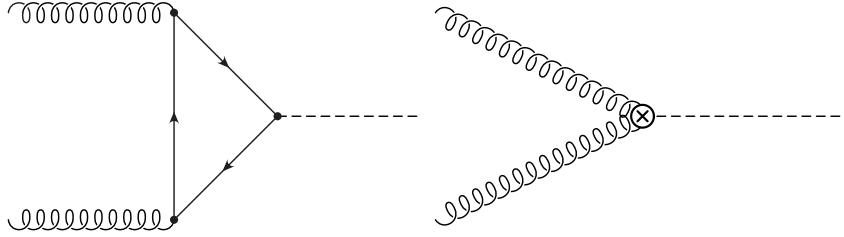


Figure 1.10: Effective gluon-gluon-Higgs vertex.

been found to be large, so even more corrections need to be calculated to understand the theoretical uncertainty of the calculations. NNLO corrections in the full theory are almost a Herculean task.

However, it is possible to obtain reliable results by integrating the top quark out of our theory (remember the Higgs couples to mass so the top quark is the most important in the SM) and be left with an effective theory where the Higgs couples directly to gluons and thereby lower the complexity of the calculation at each level. One is still left with calculating the order by order correction to the effective coupling, but better one difficult calculation than several. To see this, look at the partonic process $gg \rightarrow H$ through a top quark loop as shown in Figure (1.10). The total partonic cross-section can be written,

$$\hat{\sigma}_0(gg \rightarrow H) = \frac{\alpha_s^2}{1024\pi v^2 \hat{s}} \left| \sum_q F_{1/2}(\tau_q) \right|^2 \delta(1 - \hat{s}/M_H^2), \quad (1.146)$$

where

$$\tau_q \equiv 4M_q^2/M_H^2, \quad F_{1/2} = -2\tau_q[1 + (1 - \tau_q)f(\tau_q)], \quad (1.147)$$

and

$$f(\tau_q) = \begin{cases} \left[\sin^{-1}(1/\sqrt{\tau_q}) \right]^2 & \tau_q \geq 1 \\ -\frac{1}{4} \left[\log \left(\frac{1+\sqrt{1-\tau_q}}{1-\sqrt{1-\tau_q}} \right) - i\pi \right]^2 & \tau_q < 1. \end{cases} \quad (1.148)$$

It is interesting that when $\tau_q \rightarrow \infty$, the $F_{1/2}$ function approaches its limit very quickly, as seen in Figure (1.11). Mathematically, the limit is simple to find,

$$\lim_{\tau_q \rightarrow \infty} F_{1/2} = -\frac{4}{3}. \quad (1.149)$$

We see that the function is very well represented by the limit when the square of the mass of the Higgs is two and a half times lighter than the heaviest quark. Now, the top quark has a mass of around 178 GeV, meaning that for

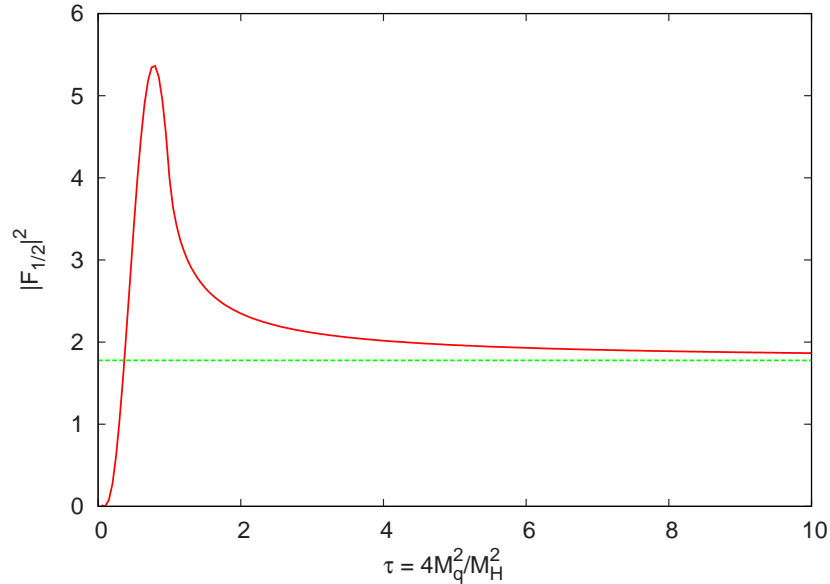


Figure 1.11: Function $|F_{1/2}|^2$ approaches the HQET limit.

a Higgs as heavy as 112 GeV this is an excellent approximation that should deteriorate as the Higgs mass becomes heavier. However, this approximation works well beyond this limit in practice as has been shown by direct calculation. It represents the full calculation to within a few percent for Higgs masses up to several hundred GeV.

1.10 SM predictions

Finally, we would like to show what is currently known about Higgs production at both the Tevatron during Run II and the future LHC. Because of the different energies involved, the SM Higgs is primarily produced via different mechanisms at the two colliders. There is a large catalog of completed, public calculations that are available as shown in Figure (1.12) (from Ref. [59]). The Tevatron collides protons on anti-protons at $\sqrt{S} = 1.96$ TeV, whereas the LHC will be a proton-proton collider at $\sqrt{S} = 14$ TeV. Shown is a collection of all the radiatively corrected observables for the different colliders. These graphs represent our current best understanding of Higgs production and are the combined work of several groups over a number of years.

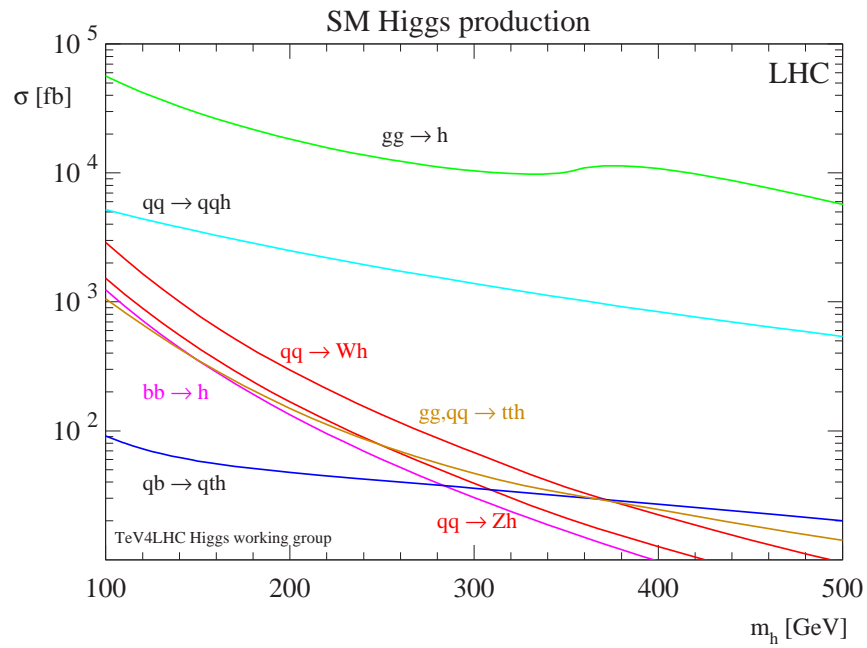
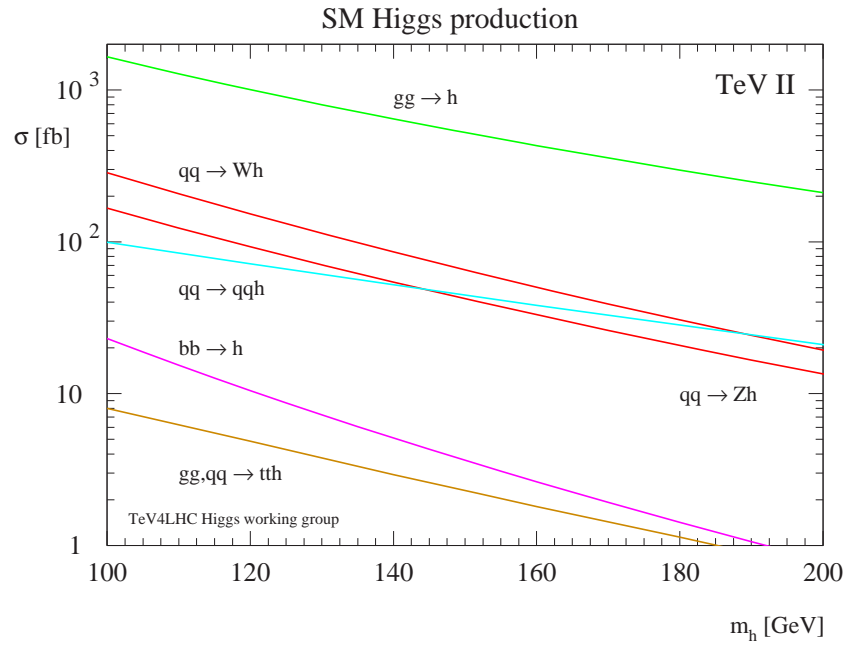


Figure 1.12: Tevatron Run II and LHC total cross-sections.

1.11 Roadmap ahead

The main body of this thesis is comprised of five of my research papers on Higgs production in pQCD and within the framework of resummation. These papers were done in collaboration with several colleagues, who are listed both as authors and in the acknowledgments.

Part I

Higgs Phenomenology in pQCD

Chapter 2

Distinguishing scalar from pseudoscalar Higgs production at the LHC

In this letter we examine the production channels for the scalar or pseudoscalar Higgs plus two jets at the CERN Large Hadron Collider (LHC). We identify possible signals for distinguishing between a scalar and a pseudoscalar Higgs boson.

2.1 Introduction

The Higgs mechanism is responsible for electroweak symmetry breaking in the Standard Model (SM). The experimental lower limit on the Higgs mass is approximately 114 GeV [60–63]. There are many models that contain more than one Higgs boson in various numbers of doublets. In the Minimal Supersymmetric Standard Model (MSSM) there are two Higgs doublets that give five physical Higgs bosons: two neutral (H_1^0, H_2^0), two charged H^\pm , and one neutral pseudoscalar A (for review see [64]). In the MSSM the mass limits change slightly with the lightest of the two neutral scalars H_1^0 (afterwards referred to as simply H) having a mass greater than about 91 GeV and the pseudoscalar being more massive than roughly 92 GeV [65].

Finding one or more Higgs bosons is the top priority of high energy physics programs around the world. A subset of Higgs bosons in some doublet models may be experimentally difficult to distinguish. The characteristics of the scalar H and pseudoscalar A Higgs boson within the MSSM are of particular interest.

We study the production of both a scalar and pseudoscalar Higgs in association with two jets in hadron collisions. At the LHC the primary processes

that produce a Higgs plus two jets are $gg \rightarrow ggH$ and $qq \rightarrow qqH$, accounting for approximately 60%(40%) of the total cross-section respectively. The same is true for the production of the pseudoscalar. Other channels that contribute to the total cross-section include $qq \rightarrow ggH$ and $qq \rightarrow qqH$, although these channels have been shown to add very little to the total cross-section. In the following calculations, only the two dominant channels were considered as the other channels are negligible.

Total cross-sections of the scalar and pseudoscalar plus two jets exist [66–68] at the lowest order. Total cross-sections for the inclusive production have been calculated at NLO for the scalar [69,70] and for the pseudoscalar [71] and at NNLO for the scalar [72–76] and for the pseudoscalar [77,78]. If we define the K-factor to be the ratio of the higher order cross-section to the lowest order, the rate increase at the LHC at NNLO for the scalar inclusive processes [74] was reported to be $K^{\text{NNLO}}(\text{pp} \rightarrow \text{H} + \text{X}) = 2 - 2.2$ and for pseudoscalar the K-factor [75] can be determined to be $K^{\text{NNLO}}(\text{pp} \rightarrow \text{A} + \text{X}) = 2 - 2.3$ in the mass range $M_{H,A} = 100 - 200$ GeV. The total cross-section and the differential cross-section for a scalar Higgs plus one jet has been calculated by [68,72,73,79,80] and the total rate was also shown to increase substantially. The NLO corrections to pseudoscalar plus one jet have not yet been computed. In all of the processes cited above the rates increased by comparable amounts. We expect our estimates of the Higgs plus two jets rates to be conservative, however, since our proposed observable is normalized to the cross-section, we do not expect major changes to occur in our analysis at higher orders.

In this letter, we propose a technique for distinguishing between a scalar and a pseudoscalar Higgs when produced in association with two jets by means of a splitting that occurs in a specific integrated operator moment. This distinction is important both experimentally and theoretically in order to separate the two kinds of events and understand the properties of these particles which would otherwise be very difficult due to the similarity in their physical observables.

2.2 Effective Lagrangian

We work in the limit that the top quark is much heavier than the Higgs boson [69–71, 81–83], integrating out the top quark and neglecting all the other quarks that would normally appear in the loop diagrams. This has been shown to be an excellent approximation and remains very good even when the Higgs mass is heavier than the mass of the top quark. In general this approximation is considered to be a good one when $M_{H,A} < 2m_t$. We consider Higgs bosons lighter than 200 GeV. The effective Lagrangian used in the scalar

case is defined as

$$\mathcal{L}_{\text{eff}}^H = -\frac{1}{4}g_H H G_{\mu\nu}^a G^{a,\mu\nu} \quad (2.1)$$

where $g_H = \alpha_s/3\pi v$. $G_{\mu\nu}^a$ is the field-strength tensor for the gluons. The vacuum expectation value (vev) of the Higgs field is determined in the usual way as $v^2 = (\sqrt{2}G_F)^{-1}$ and is numerically equal to approximately 246 GeV. For the pseudoscalar case we let the Higgs couple to the quarks with a γ_5 and the effective Lagrangian¹ can be written as

$$\mathcal{L}_{\text{eff}}^A = \frac{1}{4}g_A A G_{\mu\nu}^a \tilde{G}^{a,\mu\nu} \quad (2.2)$$

where $g_A = \alpha_s/2\pi v$. Here $\tilde{G}_{\mu\nu}^a = 1/2\epsilon^{\mu\nu\rho\sigma}G_{\rho\sigma}^a$ is the dual of the gluon field-strength tensor.

This effective Lagrangian generates a scalar Higgs coupling to two, three, and four gluons or a pseudoscalar coupling to two or three gluons. The four gluon coupling to a pseudoscalar vertex vanishes via the Jacobi identity as it is proportional to a completely antisymmetric combination of structure constants. The Feynman rules for these effective theories can be found in [66] (for the scalar) and [67] (for the pseudoscalar).

2.3 Observables and Moments

We present our results for the LHC with $\sqrt{S} = 14$ TeV. We have used the CTEQ6L parton distribution functions [84] with $\Lambda_5^{\text{LO}} = 226$ MeV with a one-loop running of α_s for consistency with a value of $\alpha_s(M_Z) = 0.137$. The transverse momentum (p_t) was constrained to be more than 25 GeV for the Higgs and each of the two jets. Also the rapidity was constrained to be $|y| < 2.5$ for all the outgoing particles. The separation of the jets was restricted to be $\Delta R \equiv \sqrt{\Delta\phi^2 + \Delta\eta^2} \geq 0.7$.

The total cross-section of these two channels are shown in Fig. (2.1). These cross-sections agree exactly with those in the literature [66,67] once the problems with the effective coupling constants are remedied. When plotted in this linear fashion it is interesting to note the differences in the dependence of the

¹There is some confusion over the coupling constant for the pseudoscalar case in the literature. The correct coupling is found in Ref. [71]. There is an extra factor of 1/4 in Ref. [67] leading to a cross-section 16 times too small for the pseudoscalar case. It seems that the 1/4 from the effective Lagrangian was incorporated into the coupling constant by mistake. The Feynman rules in both papers are correct if the coupling constant from Ref. [71] paper is used.

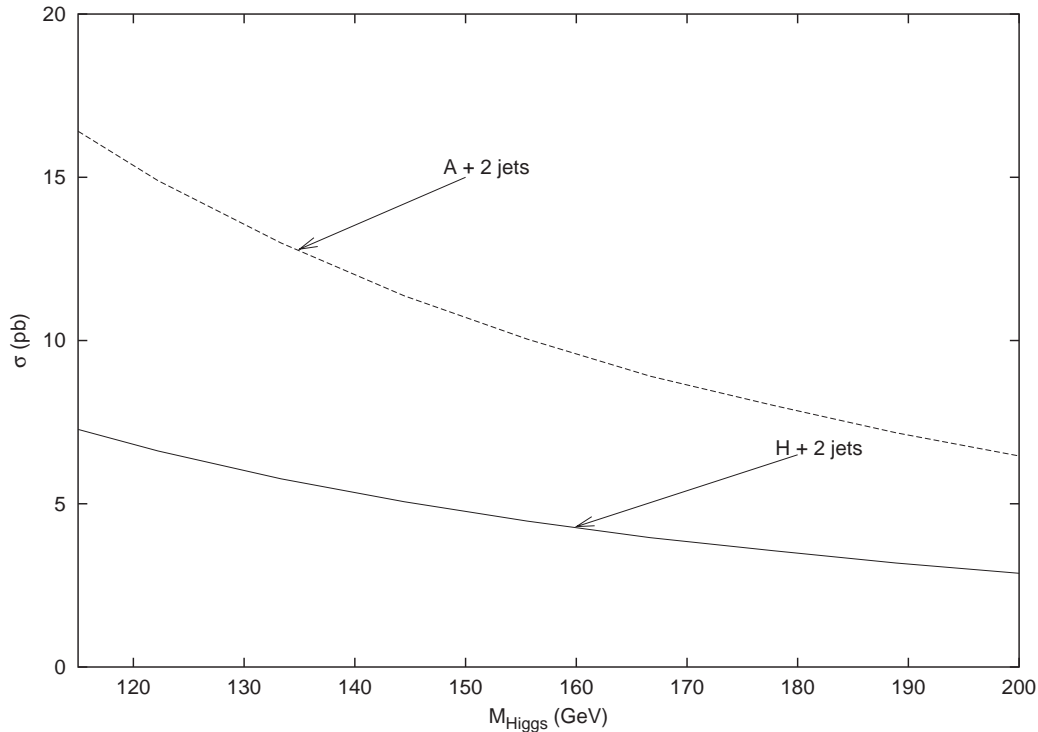


Figure 2.1: Total cross-sections for scalar and pseudoscalar Higgs plus two jets. These curves are for the LHC with the cuts described in the text.

cross-sections on the mass of the Higgs boson. Both total cross-sections lose more than two-thirds of their value from 100 – 200 GeV and appear in the approximate ratio of $(g_H/g_A)^2 = 4/9$ due to the similarity in their matrix elements.

Fig. (2.2) shows the normalized transverse momentum spectrum of both the production channels. The pseudoscalar Higgs p_t spectrum was displaced down by 10% to allow the two curves to be distinguished. If this had not been done, the curves would lie virtually on top of one another. Fig. (2.3) shows the center-of-momentum angle between the Higgs and the highest p_t jet for the two reactions. This shows what would be expected naïvely, that the Higgs prefers to come out back-to-back with the highest p_t jet. Once again, the pseudoscalar curve has been scaled down by 20% to allow both curves to be seen clearly. No significant differences between these curves were found.

The authors of [85] presented a technique for determining the CP nature of the Higgs boson in $t\bar{t}H$ production based on certain weighted moments of the cross-section. The cross-section integral was weighted by operators \mathcal{O}_{CP} . The six operators presented in [85] are scalar and cross products of the momentum

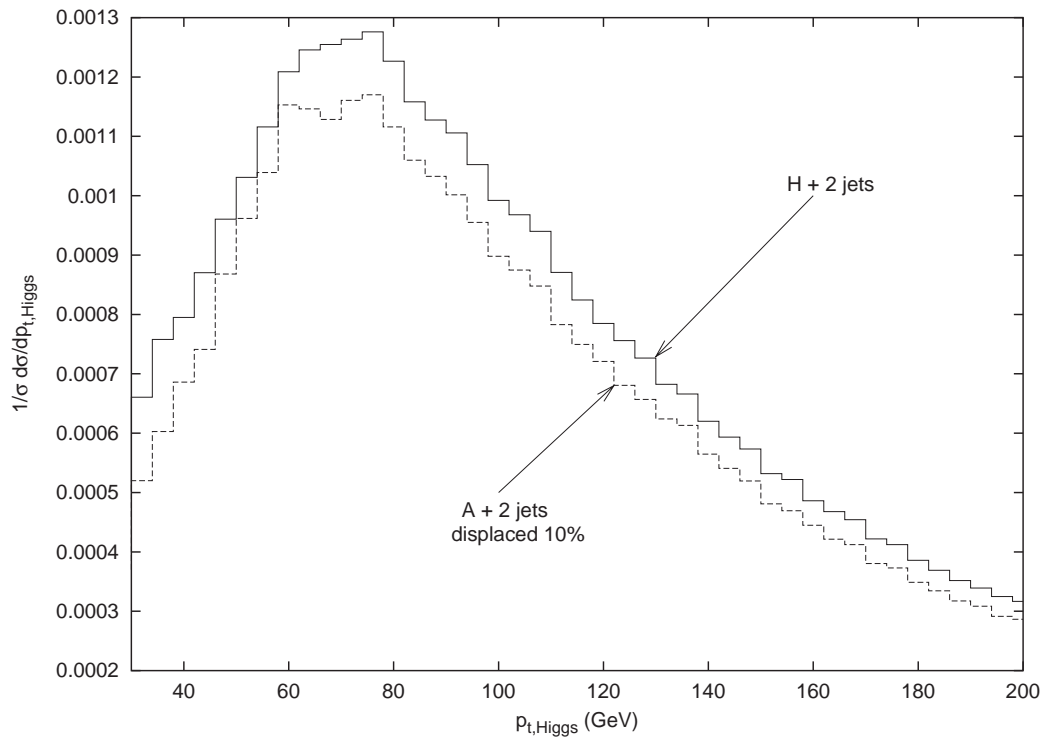


Figure 2.2: Normalized transverse momentum spectrum of the scalar or pseudoscalar Higgs production channels plus two jets. The Higgs mass for both the scalar and pseudoscalar is 120 GeV. Note that the pseudoscalar Higgs has been displaced down by 10% to allow the two curves to be distinguished. These curves are for the LHC with the cuts described in the text.

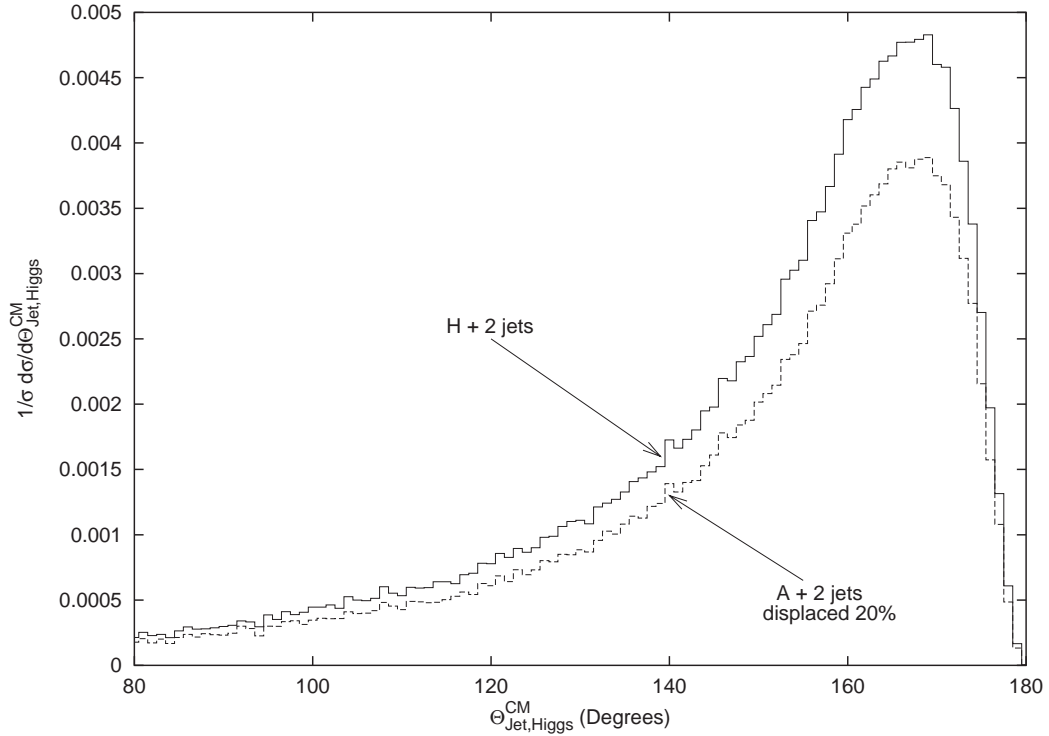


Figure 2.3: Normalized opening angle in the center-of-momentum frame between the Higgs and the highest p_t jet for the scalar and pseudoscalar Higgs production channels plus two jets. The Higgs mass for both the scalar and pseudoscalar is 120 GeV. Note that the pseudoscalar Higgs has been displaced down by 20% to allow the two curves to be distinguished. These curves are for the LHC with the cuts described in the text.

of the outgoing particles (in this case the massive top quarks). We propose using the same test for the massless quarks and gluons that make up the jets. All of these weighted moments were examined as well as some novel ones and the only operator from these sets that produced a significant difference between the scalar and the pseudoscalar signals was the operator [85]

$$a_1 = \frac{(\vec{p}_1 \times \hat{z}) \cdot (\vec{p}_2 \times \hat{z})}{|(\vec{p}_1 \times \hat{z}) \cdot (\vec{p}_2 \times \hat{z})|} \quad (2.3)$$

when it was integrated and normalized as prescribed below

$$\alpha[\mathcal{O}_{CP}] \equiv \frac{1}{\sigma} \int \mathcal{O}_{CP} d\sigma dPS \quad (2.4)$$

where p_1 and p_2 are the momentum of the two jets and \hat{z} is the axis of the beam. The a_1 operator is sensitive to the cosine of the angle between the transverse momentum vectors of the two jets. Distinguishing between the two jets is not important as this moment is invariant under $1 \leftrightarrow 2$. Another combination of momentum in the above equations that was considered was to use the moment operators presented in [85] with $p_1 = p_{\text{Higgs}}$ and p_2 the momentum of the highest p_t jet. However, this yielded no differences in the integrated moments making this definition of little use for these channels.

Fig. (2.4) shows the results of this integration as a function of the Higgs mass. If we consider a conservative estimate of 100 fb^{-1} of integrated luminosity at the LHC and take a branching ratio of approximately 10^{-3} as an order of magnitude for the decay of the Higgs to a pair of photons, then the $\alpha[a_1]$ observable will have a statistical uncertainty of about 5%, making these two signals distinguishable at all mass scales. With this conservative estimate on the integrated luminosity we would expect to see about 600 scalar events and 1000 pseudoscalar events for a Higgs mass of 120 GeV in this channel for this Higgs decay. These numbers are supported by a more detailed analysis using the actual branching ratios calculated using HDECAY [86] in the $\tan \beta = 1$ limit for the pseudoscalar.

This integrated moment showed a modest (30%) splitting at all Higgs mass scales from 100 – 200 GeV. The pseudoscalar does not show much mass dependence. However, the scalar integrated moment rises slightly with increasing Higgs mass. This effect might also be useful as another method for constraining the mass of the scalar Higgs boson. The splitting in Fig. (2.4) helps to remove the problems created by the degeneracy in the physical observable of the scalar and the pseudoscalar. If the two signals could not be separated, the doublet structure of the model would not be easily measured. In the case of the MSSM this would mean that part of the supersymmetric signal might

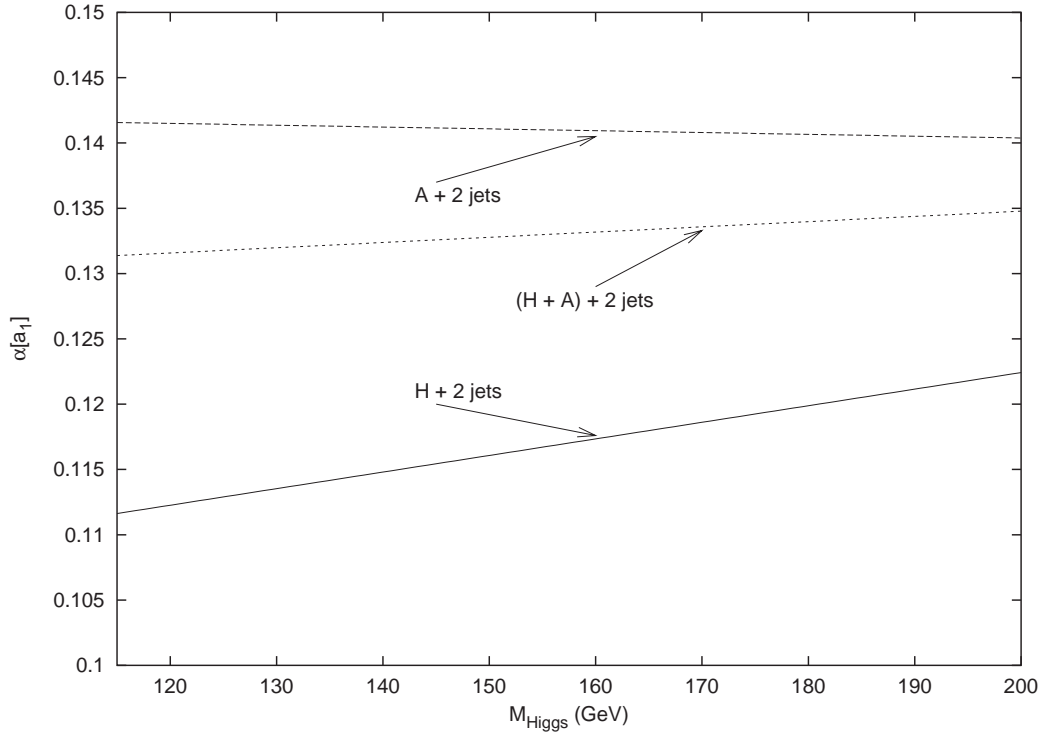


Figure 2.4: Normalized integrated moment $\alpha[a_1]$ for the scalar and pseudo-scalar Higgs plus two jets. The center curve shows what the observable would look like if both of the processes were to be measured at the same time with degenerate masses. The splitting between the two different production channels is clear at all mass scales with a statistical uncertainty of about 5%. These curves are for the LHC with the cuts described in the text.

be lost or the mass of the scalar Higgs may be determined incorrectly if the pseudoscalar events were wrongly identified as scalar events.

Separating the two signals is theoretically intriguing because it appears to be one of the only ways to predict a difference between the scalar and pseudo-scalar events of this nature at the LHC by means other than the magnitude of their cross-section. This is also interesting experimentally as it leads to the possibility of separating the two kinds of Higgs events with the added bonus that the z momentum is not needed in this analysis.

2.4 Conclusions

The production channels of the scalar or pseudoscalar Higgs plus two jets were found to have many similarities in their physical observables and one important difference is the integrated moment $\alpha[a_1]$. This may help to reduce the difficulty in distinguishing between the two types of events at the LHC. The most important aspect of separating the two signals is to make sure that the doublet structure (the supersymmetric signal in the case of the MSSM) is not lost because of its small cross-section and its similarity to the scalar Higgs with respect to its physical observables or wrongly determining the mass of the scalar Higgs by misidentifying pseudoscalar events as scalar events. The proposed technique presented in this letter may enable these two signals to be separated after a full detector simulation is preformed.

Appendix A: Differences in the Amplitudes

It turns out that the differences in the scalar (or pseudoscalar) plus two jets amplitudes squared were very small. The differences will be presented using the helicity basis presented in [66, 67] to make for the most compact matrix elements squared. These matrix elements have been found to be in exact analytic agreement with the four dimensional matrix elements presented in [79]. We identify the momentum as follows (where X should be considered the Higgs for the process in question, playing the part of either the scalar or the pseudoscalar). All the momenta are outgoing.

$$q(p_1) + \bar{q}(p_2) \rightarrow g(-p_3) + g(-p_4) + X(-p_5) \quad (2.5)$$

$$g(p_1) + g(p_2) \rightarrow g(-p_3) + g(-p_4) + X(-p_5) \quad (2.6)$$

$$q(p_1) + \bar{q}(p_2) \rightarrow q(-p_3) + \bar{q}(-p_4) + X(-p_5). \quad (2.7)$$

In the following we define $S_{ab} = (p_a + p_b)^2 = 2p_a \cdot p_b$. Color factors have been included in the expression for the $qqggH(A)$ and $qqqqH(A)$ channels as

they affect the terms differently but not in the expression for the $ggggH(A)$ channel as there is one overall color factor for all the matrix elements squared. Here N is the number of colors. Color and spin averages have not been included nor have any coupling constants.

For the $qqggH(A)$ channel the difference in the scalar minus the pseudo-scalar amplitude squared was 15 terms out of 626. Setting the color factors to match those presented in [79], $C_O = (N^2 - 1)/N$ and $C_K = (N^2 - 1)N$ the difference was found to be

$$\begin{aligned}
|\mathcal{M}|_{qq \rightarrow ggH}^2 - |\mathcal{M}|_{qq \rightarrow ggA}^2 &= 2C_K - 6C_O \\
&+ \left(\left\{ \frac{4C_O}{S_{12}^2 S_{34}^2} \left[S_{13} S_{14} S_{23} S_{24} - S_{13}^2 S_{24}^2 \right] + 4C_O \frac{S_{13} S_{24}}{S_{12} S_{34}} \right. \right. \\
&\quad \left. \left. \frac{1}{S_{13} S_{24}} \left[C_O (S_{12} S_{34} - S_{14} S_{23}) + C_K (S_{14} S_{23} - S_{12} S_{34}) \right] \right\} \right. \\
&\quad \left. + \{3 \leftrightarrow 4\} \right). \tag{2.8}
\end{aligned}$$

For the $ggggH(A)$ channel the difference in the scalar minus the pseudo-scalar was 16 terms out of 2761. The overall color factor is $N^2(N^2 - 1)$. The difference was

$$\begin{aligned}
|\mathcal{M}|_{gg \rightarrow ggH}^2 - |\mathcal{M}|_{gg \rightarrow ggA}^2 &= 48 + \left(8 \left\{ \frac{1}{2} \frac{1}{S_{12}^2 S_{34}^2} \left[S_{13} S_{24} - S_{14} S_{23} \right]^2 \right. \right. \\
&\quad - \frac{1}{2} \frac{1}{S_{12} S_{34}} \left[S_{13} S_{24} + S_{14} S_{23} \right]^2 + \frac{1}{S_{13}^2 S_{24}^2} \left[S_{12} S_{34} - S_{14} S_{23} \right]^2 \\
&\quad \left. \left. - \frac{1}{S_{13} S_{24}} \left[S_{12} S_{34} + S_{14} S_{23} \right] \right\} + \{3 \leftrightarrow 4\} \right). \tag{2.9}
\end{aligned}$$

Finally, there are two cases for the $qqqqH(A)$ amplitude squared. If there are identical quarks allowed in the scattering process ($q\bar{q}q\bar{q}H(A)$) then there are two diagrams that contribute. The color factors here are $C_A = N$ and $C_F = (N^2 - 1)/2N$. The difference in the amplitudes squared is 19 out of 39 terms and is equal to

$$\begin{aligned}
|\mathcal{M}|_{qq \rightarrow qqH}^2 - |\mathcal{M}|_{qq \rightarrow qqA}^2 &= 4C_A C_F \left(2 - \frac{4}{C_A} + \frac{(S_{13} S_{24} - S_{14} S_{23})^2}{S_{12}^2 S_{34}^2} \right. \\
&\quad + \frac{(S_{14} S_{23} - S_{12} S_{34})^2}{S_{13}^2 S_{24}^2} - 2 \frac{S_{13} S_{24}}{S_{12} S_{34}} - 2 \frac{S_{12} S_{34}}{S_{13} S_{24}} \\
&\quad \left. + \frac{2}{C_A} \left(\frac{S_{12} S_{34} - S_{14} S_{23}}{S_{13} S_{24}} \right) + \{3 \leftrightarrow 4\} \right). \tag{2.10}
\end{aligned}$$

If a different quark pair is created ($q\bar{q}q'\bar{q}'H(A)$), then the difference is smaller as only one diagram is needed for the amplitude. Here 6 out of 10 terms survive and are equal to

$$|\mathcal{M}|_{qq \rightarrow qqH}^2 - |\mathcal{M}|_{qq \rightarrow qqA}^2 = 4C_F \left(1 + \left\{ \frac{(S_{13}S_{24} - S_{13}S_{24})^2}{S_{12}^2 S_{34}^2} - \frac{S_{13}S_{24} + S_{14}S_{23}}{S_{12}S_{34}} \right\} + \{3 \leftrightarrow 4\} \right). \quad (2.11)$$

It should also be noted that all these differences are invariant under $1 \leftrightarrow 2$.

Acknowledgments

The author would like to thank J. Smith, S. Dawson, R.P. Kauffman, S.V. Desai, W. Kilgore, F. Paige, and J. Laiho for their help and comments on this paper at all stages of its development. The author was partially supported by the National Science Foundation grant PHY-0098527 and the U.S. Department of Energy under Contract No. DE-AC02-98CH10886.

Chapter 3

NLO corrections to differential cross sections for pseudoscalar Higgs boson production

We have computed the full next-to-leading (NLO) QCD corrections to the differential distributions $d^2\sigma/(dp_T dy)$ for pseudoscalar Higgs (A^0) production at large hadron colliders. This calculation has been carried out using the effective Lagrangian approach which is valid as long as the mass of the pseudoscalar Higgs boson M_{A^0} and its transverse momentum p_T do not exceed the top-quark mass M_t . The shape of the distributions hardly differ from those obtained for scalar Higgs (H) production because, apart from the overall coupling constant and mass, there are only small differences between the partonic differential distributions for scalar and pseudoscalar production. Therefore there are only differences in the magnitudes of the hadronic differential distributions which can be mainly attributed to the unknown mixing angle β describing the pseudoscalar Higgs coupling to the top quarks.

3.1 Introduction

The scalar Higgs boson H , which is the corner stone of the Standard Model, is the only particle which has not yet been observed. Its discovery or its absence will shed light on the mechanism how particles acquire mass as well as answer questions about super-symmetric extensions of the Standard Model or about the compositeness of the existing particles and the Higgs boson. Among these two alternatives supersymmetry is the most appealing one, in particular the minimal supersymmetric extension of the standard model. The latter version contains two complex Higgs doublets instead of one and it is therefore

called the Two-Higgs-Doublet Model (2HDM). Here the scalar particle spectrum contains both the Higgs boson H and another neutral scalar boson h^0 . Furthermore it contains two charged scalar bosons H^\pm and a neutral pseudo-scalar Higgs boson A^0 . The tree-level masses are expressed in two independent parameters, namely the mass M_{A^0} and the ratio of the vacuum expectation values of the two Higgs doublets defined by $\tan\beta = v_2/v_1$ (see e.g. [64]). According to the experiments at LEP their parameter ranges are restricted so that $M_{A^0} < 91.9 \text{ GeV}/c^2$ and $0.5 < \tan\beta < 2.4$ [87–89] are excluded.

In this paper we study A^0 production which in lowest order proceeds via gluon-gluon fusion where the gluons are coupled to the A^0 via a heavy flavor triangular loop. This is similar to H -production except that now the coupling constant describing the interaction of the A^0 with the quarks depends on both the masses of the quarks and on the angle β . This follows from the 2HDM where the coupling constants of the up and down quarks behave like $g_{\text{up}} \sim M_u \cot\beta$ and $g_{\text{down}} \sim M_d \tan\beta$ respectively [64]. Since the effective Lagrangian approach below is only valid in the case the mass of the quark appearing in the triangular loop satisfies the condition $M_q \gg M_{A^0}$, the bottom quark is excluded. However then we have to require that in the 2HDM the coupling of the A^0 to the top-quark is stronger than to the bottom-quark which implies the condition

$$\frac{M_t}{M_b} \gg \tan^2\beta. \quad (3.1)$$

If we choose $M_b = 4.5 \text{ GeV}/c^2$ and $M_t = 173.4 \text{ GeV}/c^2$ one obtains the inequality $\tan\beta \ll 6.21$. In view of the experimental boundaries above one can conclude that the results of the calculation below can be only applied for the regions $\tan\beta < 0.5$ and $2.4 < \tan\beta < 6.21$.

3.2 Effective Lagrangian

In the effective Lagrangian approach scalar H -production is described by the Lagrangian density [69, 70, 90]

$$\mathcal{L}_{\text{eff}}^H = G_H \Phi^H(x) O(x), \quad \text{with} \quad O(x) = -\frac{1}{4} G_{\mu\nu}^a(x) G^{a,\mu\nu}(x), \quad (3.2)$$

whereas pseudoscalar A^0 production is obtained from [67, 71, 91–93]

$$\mathcal{L}_{\text{eff}}^A = \Phi^A(x) \left[G_A O_1(x) + \tilde{G}_A O_2(x) \right], \quad (3.3)$$

with,

$$O_1(x) = -\frac{1}{8} \epsilon_{\mu\nu\lambda\sigma} G_a^{\mu\nu}(x) G_a^{\lambda\sigma}(x), \quad (3.4)$$

$$O_2(x) = -\frac{1}{2} \partial^\mu \sum_{i=1}^{n_f} \bar{q}_i(x) \gamma_\mu \gamma_5 q_i(x), \quad (3.5)$$

where $\Phi^H(x)$ and $\Phi^A(x)$ are the scalar and pseudoscalar fields respectively and n_f denotes the number of light flavors. Up to NLO the operator $O_2(x)$ only contributes when it interferes with the operator $O_1(x)$ provided the quarks are massless. The effective couplings G_B ($B = H, A^0$) are determined by the top-quark triangular graph describing the decay process $B \rightarrow g + g$ in the limit $m_t \rightarrow \infty$

$$G_B^2 = 4\sqrt{2} \left(\frac{\alpha_s(\mu_r^2)}{4\pi} \right)^2 G_F \tau_B^2 F_B^2(\tau_B) \mathcal{C}_B^2 \left(\alpha_s(\mu_r^2), \frac{\mu_r^2}{M_t^2} \right), \quad \tau_B = \frac{4M_t^2}{M_B^2}, \quad (3.6)$$

where $B = H, A^0$ and the functions F_B are defined by

$$F_H(\tau) = 1 + (1 - \tau)f(\tau), \quad F_A(\tau) = f(\tau) \cot \beta, \quad (3.7)$$

$$\begin{aligned} f(\tau) &= \arcsin^2 \frac{1}{\sqrt{\tau}}, \quad \text{for } \tau \geq 1, \\ &= -\frac{1}{4} \left(\ln \frac{1 - \sqrt{1 - \tau}}{1 + \sqrt{1 - \tau}} + i\pi \right)^2, \quad \text{for } \tau < 1. \end{aligned} \quad (3.8)$$

In the large M_t -limit $F(\tau)$ behaves as

$$\lim_{\tau \rightarrow \infty} F_H(\tau) = \frac{2}{3\tau}, \quad \lim_{\tau \rightarrow \infty} F_A(\tau) = \frac{1}{\tau} \cot \beta. \quad (3.9)$$

Here M_B and M_t denote the masses of the (pseudo)scalar Higgs boson and the top quark respectively. The running coupling constant is given by $\alpha_s(\mu_r^2)$ where μ_r denotes the renormalization scale and G_F is the Fermi constant. The coefficient functions \mathcal{C}_B originate from the corrections to the top-quark triangular graph provided one takes the limit $m_t \rightarrow \infty$. We have presented the couplings G_B in Eq. (3.6) for general M_t on the Born level only in order to keep some part of the top-quark mass dependence. This is an approximation because the gluons which couple to the (pseudo)scalar Higgs boson via the top-quark loop in the partonic subprocesses are very often virtual. The virtual-gluon momentum dependence is neither described by $F_B(\tau)$ nor by \mathcal{C}_B . For on-mass-shell gluons the latter quantity has been computed in the large M_t

limit up to order α_s in [69, 70, 91, 92, 71, 67] and up to order α_s^2 in [90, 93]. For our NLO calculations we only need these coefficient functions corrected up to order α_s and they read

$$\mathcal{C}_H \left(\alpha_s(\mu_r^2), \frac{\mu_r^2}{M_t^2} \right) = 1 + \frac{\alpha_s^{(5)}(\mu_r^2)}{4\pi} (11) + \dots, \quad (3.10)$$

$$\mathcal{C}_A \left(\alpha_s(\mu_r^2), \frac{\mu_r^2}{M_t^2} \right) = 1, \quad (3.11)$$

where $\alpha_s^{(5)}$ is presented in a five-flavor number scheme. Notice that Eq. (3.11) holds in all orders because of the Adler-Bardeen theorem [94]. The effective Lagrangian approach has been successfully applied to compute the total cross section of scalar Higgs production in hadron-hadron collisions in NLO [69, 70] and NNLO [72, 74–76, 95]. In the case of pseudoscalar Higgs production this cross section was computed in NLO in [67, 71, 91, 92] and in NNLO in [77, 78].

3.3 Kinematics

In this paper we study the semi-inclusive reaction with one pseudoscalar Higgs boson A^0 in the final state which is given by

$$H_1(p_1) + H_2(p_2) \rightarrow A^0(-p_5) + 'X', \quad (3.12)$$

where H_1 and H_2 denote the incoming hadrons and X represents an inclusive hadronic final state. Further we define the following kinematical invariants

$$S = (p_1 + p_2)^2, \quad T = (p_1 + p_5)^2, \quad U = (p_2 + p_5)^2. \quad (3.13)$$

The latter two invariants can be expressed in terms of the transverse momentum p_T and rapidity y variables as

$$\begin{aligned} T &= M^2 - \sqrt{S} \sqrt{p_T^2 + m^2} \cosh y + \sqrt{S} \sqrt{p_T^2 + m^2} \sinh y, \\ U &= M^2 - \sqrt{S} \sqrt{p_T^2 + m^2} \cosh y - \sqrt{S} \sqrt{p_T^2 + m^2} \sinh y, \end{aligned} \quad (3.14)$$

where M is the mass of the pseudoscalar Higgs boson. The hadronic cross section is given by

$$\begin{aligned} S^2 \frac{d^2 \sigma^{H_1 H_2}}{dT dU}(S, T, U; M^2) &= \sum_{a,b=q,g} \int_{x_{1,\min}}^1 \frac{dx_1}{x_1} \int_{x_{2,\min}}^1 \frac{dx_2}{x_2} f_a^{H_1}(x_1, \mu^2) f_b^{H_2}(x_2, \mu^2) \\ &\times s^2 \frac{d^2 \sigma_{ab}}{dt du}(s, t, u; M^2, \mu^2), \end{aligned} \quad (3.15)$$

with,

$$x_{1,\min} = \frac{-U}{S + T - M^2}, \quad x_{2,\min} = \frac{-x_1(T - M^2) - M^2}{x_1 S + U - M^2}, \quad (3.16)$$

where s , t and u are the partonic analogues of S , T and U in Eq. (3.13) where p_1 and p_2 now represent the incoming parton momenta. Further $f_a^{\text{H}_i}$ denotes the parton density corresponding to hadron H_i and μ stands for the factorization scale which for convenience is set equal to the renormalization scale μ_r appearing in Eq. (3.6). The NLO corrections to the partonic cross section $d^2\sigma/(dt du)$ in the case of H -production based on the effective Lagrangian in Eq. (3.6) are presented in [79, 80]. Here we will give the corresponding results for the A^0 described by the Lagrangian in Eq. (3.3). The calculation proceeds in the same way as presented in [79].

3.4 Corrections

We use n -dimensional regularization in order to compute the loop and phase space integrals which contain ultraviolet, infrared and collinear singularities. However there is one extra complication in the pseudoscalar case. This concerns the Levi-Civita tensor in Eq. (3.3) which is essentially a four dimensional object. Here we follow the same prescription as in Eq. (4) in [77, 78] where the product of two Levi-Civita tensors is contracted in n -dimensions if one sums over dummy Lorentz indices. This prescription leads to an interference between diagrams carrying the vertex coming from the operator $O_1(x)$ and those carrying the vertex corresponding to the operator $O_2(x)$ in Eq. (3.3) (see [77]). The LO subprocesses contributing to the partonic cross section are given by

$$g + g \rightarrow g + A^0, \quad q + \bar{q} \rightarrow g + A^0, \quad q(\bar{q}) + g \rightarrow q(\bar{q}) + A^0. \quad (3.17)$$

The matrix elements squared do not differ from those derived for the scalar H provided $n = 4$, see [67, 71, 91, 92], which implies that the LO double differential partonic cross sections are the same for both bosons except for an overall constant given by $F_B(\tau)$ in Eq. (3.7). In NLO one has to compute the one-loop virtual corrections to the processes in Eq. (3.17) above and to add

the contributions from the following two-to-three-body reactions

$$g + g \rightarrow g + g + A^0, \quad (3.18)$$

$$g + g \rightarrow q_i + \bar{q}_i + A, \quad (3.19)$$

$$q + \bar{q} \rightarrow g + g + A^0, \quad (3.20)$$

$$q_1 + \bar{q}_2 \rightarrow q_1 + \bar{q}_2 + A^0 \quad q_1 \neq q_2, \quad (3.21)$$

$$q + \bar{q} \rightarrow q_i + \bar{q}_i + A^0 \quad q_i \neq q, \quad (3.22)$$

$$q + \bar{q} \rightarrow q + \bar{q} + A^0, \quad (3.23)$$

$$q_1 + q_2 \rightarrow q_1 + q_2 + A^0 \quad q_1 \neq q_2, \quad (3.24)$$

$$q + q \rightarrow q + q + A^0, \quad (3.25)$$

$$q(\bar{q}) + g \rightarrow q(\bar{q}) + g + A^0. \quad (3.26)$$

After renormalization of the strong coupling constant α_s and mass factorization which are carried out in the $\overline{\text{MS}}$ -scheme we obtain the NLO corrected coefficient functions according to the procedure in [79]. The coefficient functions are as long as in the case of H -production so that they cannot be explicitly presented. However the differences between the results for the H and the A^0 are so small that we can show them below. If we put for simplicity $G_H = G_A = G$ and $M_H = M_{A^0} = M$ the differences between the soft-plus-

virtual differential cross sections are given by

$$s^2 \frac{d^2 \sigma_{gg \rightarrow gA^0}^{\text{S+V}}}{dt du} - s^2 \frac{d^2 \sigma_{gg \rightarrow gH}^{\text{S+V}}}{dt du} = \pi \delta(s+t+u-M^2) G^2 \left(\frac{\alpha_s(\mu^2)}{4\pi} \right)^2 \frac{N}{(N^2-1)^2} \left[2|M_{gg \rightarrow gB}^{(1)}|^2 \right], \quad (3.27)$$

$$s^2 \frac{d^2 \sigma_{q\bar{q} \rightarrow gA^0}^{\text{S+V}}}{dt du} - s^2 \frac{d^2 \sigma_{q\bar{q} \rightarrow gH}^{\text{S+V}}}{dt du} = \pi \delta(s+t+u-M^2) G^2 \left(\frac{\alpha_s(\mu^2)}{4\pi} \right)^2 \frac{1}{N^2} \left[2C_A |M_{q\bar{q} \rightarrow gB}^{(1)}|^2 + (C_F - C_A) |MB_{q\bar{q} \rightarrow gB}^{(1)}|^2 \right], \quad (3.28)$$

$$s^2 \frac{d^2 \sigma_{qg \rightarrow qA^0}^{\text{S+V}}}{dt du} - s^2 \frac{d^2 \sigma_{qg \rightarrow qH}^{\text{S+V}}}{dt du} = \pi \delta(s+t+u-M^2) G^2 \left(\frac{\alpha_s(\mu^2)}{4\pi} \right)^2 \frac{1}{N(N^2-1)} \left[2C_A |M_{qg \rightarrow qB}^{(1)}|^2 + (C_F - C_A) |MB_{qg \rightarrow qB}^{(1)}|^2 \right]. \quad (3.29)$$

where we have added to the righthand side of Eqs. (3.28) and (3.29) the contributions coming from the interference of the graphs in Figs. 1b, 1d with those in Figs. 2b, 2d which are shown in [77]. The color factors of the group $SU(N)$ are given by $C_A = N$ and $C_F = (N^2 - 1)/(2N)$ and the Born matrix elements squared belonging to the processes in Eq. (3.17) are equal to

$$|M_{gg \rightarrow gB}^{(1)}|^2 = N(N^2 - 1) \frac{1}{stu} \left[s^4 + t^4 + u^4 + M^8 \right], \quad (3.30)$$

$$|M_{q\bar{q} \rightarrow gB}^{(1)}|^2 = C_A C_F \frac{1}{s} \left[t^2 + u^2 \right], \quad (3.31)$$

$$|M_{qg \rightarrow qB}^{(1)}|^2 = C_A C_F \frac{1}{u} \left[-s^2 - t^2 \right]. \quad (3.32)$$

The differences above can be wholly attributed to the virtual corrections and not to the soft gluon contributions which are the same for both H and A^0

production. These virtual corrections also entail some extra terms denoted by

$$|MB_{gg \rightarrow gB}^{(1)}|^2 = \frac{2}{3}N(N^2 - 1)\frac{M^2}{stu} \left[stu + M^2(st + su + tu) \right], \quad (3.33)$$

$$|MB_{q\bar{q} \rightarrow gB}^{(1)}|^2 = C_A C_F (-t - u), \quad (3.34)$$

$$|MB_{qg \rightarrow qB}^{(1)}|^2 = C_A C_F (s + t). \quad (3.35)$$

Denoting the two-to-three-body reactions by

$$a(p_1) + b(p_2) \rightarrow c(-p_3) + d(-p_4) + A^0(-p_5), \quad s_4 = (p_3 + p_4)^2, \quad (3.36)$$

then the differences between the partonic cross sections due to the subprocesses

in Eqs. (3.18)–(3.26) are equal to

$$s^2 \frac{d^2 \sigma_{gg \rightarrow gg A^0}^{\text{HARD}}}{dt du} - s^2 \frac{d^2 \sigma_{gg \rightarrow gg H}^{\text{HARD}}}{dt du} = \pi G^2 \left(\frac{\alpha_s(\mu^2)}{4\pi} \right)^2 \frac{N^2}{N^2 - 1} \left[-4 \ln \frac{tu - M^2 s_4}{(s_4 - t)(s_4 - u)} - \frac{17}{3} \right], \quad (3.37)$$

$$s^2 \frac{d^2 \sigma_{gg \rightarrow q\bar{q} A^0}^{\text{HARD}}}{dt du} - s^2 \frac{d^2 \sigma_{gg \rightarrow q\bar{q} H}^{\text{HARD}}}{dt du} = \pi G^2 \left(\frac{\alpha_s(\mu^2)}{4\pi} \right)^2 \frac{n_f}{N^2 - 1} \left[C_A \left\{ \frac{2}{3} \right\} + C_F \left\{ 2 \ln \frac{tu - M^2 s_4}{(s_4 - t)(s_4 - u)} + 2 \right\} \right], \quad (3.38)$$

$$s^2 \frac{d^2 \sigma_{q\bar{q} \rightarrow gg A^0}^{\text{HARD}}}{dt du} - s^2 \frac{d^2 \sigma_{q\bar{q} \rightarrow gg H}^{\text{HARD}}}{dt du} = \pi G^2 \left(\frac{\alpha_s(\mu^2)}{4\pi} \right)^2 \frac{C_A C_F}{N^2} \left[C_A \left\{ \frac{2}{3} \right\} + C_F \left\{ 2 \ln \frac{tu - M^2 s_4}{(s_4 - t)(s_4 - u)} + 2 \right\} \right], \quad (3.39)$$

$$s^2 \frac{d^2 \sigma_{q_1 \bar{q}_2 \rightarrow q_1 \bar{q}_2 A^0}^{\text{HARD}}}{dt du} - s^2 \frac{d^2 \sigma_{q_1 \bar{q}_2 \rightarrow q_1 \bar{q}_2 H}^{\text{HARD}}}{dt du} = \pi G^2 \left(\frac{\alpha_s(\mu^2)}{4\pi} \right)^2 \frac{C_A C_F}{N^2} \left[-2 \ln \frac{tu - M^2 s_4}{(s_4 - t)(s_4 - u)} - 1 \right], \quad (3.40)$$

$$s^2 \frac{d^2 \sigma_{q_1 \bar{q}_1 \rightarrow q_i \bar{q}_i A^0}^{\text{HARD}}}{dt du} - s^2 \frac{d^2 \sigma_{q_1 \bar{q}_1 \rightarrow q_i \bar{q}_i H}^{\text{HARD}}}{dt du} = \pi G^2 \left(\frac{\alpha_s(\mu^2)}{4\pi} \right)^2 \frac{(n_f - 1) C_A C_F}{N^2} \left[-\frac{2}{3} \right], \quad (3.41)$$

and,

$$\begin{aligned}
s^2 \frac{d^2 \sigma_{q\bar{q} \rightarrow q\bar{q} A^0}^{\text{HARD}}}{dt du} - s^2 \frac{d^2 \sigma_{q\bar{q} \rightarrow q\bar{q} H}^{\text{HARD}}}{dt du} = & \\
& \pi G^2 \left(\frac{\alpha_s(\mu^2)}{4\pi} \right)^2 \frac{C_F}{N^2} \left[C_A \left\{ -2 \ln \frac{tu - M^2 s_4}{(s_4 - t)(s_4 - u)} - \frac{5}{3} \right\} \right. \\
& + \frac{ss_4((s - M^2)^2 + s_4^2 - 2tu)}{8(s_4 - t)^2(s_4 - u)^2} + \frac{(s - M^2)^2 + s_4^2 - 2tu}{4(s_4 - t)(s_4 - u)} \\
& \left. + \frac{(s - M^2)^2 + s_4^2 - 2tu + 6ss_4}{4ss_4} \ln \frac{tu - M^2 s_4}{(s_4 - t)(s_4 - u)} + \frac{9}{4} \right], \quad (3.42)
\end{aligned}$$

$$\begin{aligned}
s^2 \frac{d^2 \sigma_{q_1 q_2 \rightarrow q_1 q_2 A^0}^{\text{HARD}}}{dt du} - s^2 \frac{d^2 \sigma_{q_1 q_2 \rightarrow q_1 q_2 H}^{\text{HARD}}}{dt du} = & \\
& \pi G^2 \left(\frac{\alpha_s(\mu^2)}{4\pi} \right)^2 \frac{C_A C_F}{N^2} \left[-2 \ln \frac{tu - M^2 s_4}{(s_4 - t)(s_4 - u)} - 1 \right], \quad (3.43)
\end{aligned}$$

$$\begin{aligned}
s^2 \frac{d^2 \sigma_{qq \rightarrow qq A^0}^{\text{HARD}}}{dt du} - s^2 \frac{d^2 \sigma_{qq \rightarrow qq H}^{\text{HARD}}}{dt du} = & \\
& \pi G^2 \left(\frac{\alpha_s(\mu^2)}{4\pi} \right)^2 \frac{C_F}{N^2} \left[C_A \left\{ -2 \ln \frac{tu - M^2 s_4}{(s_4 - t)(s_4 - u)} - 1 \right\} \right. \\
& \left. + \frac{s^2 + s_4^2}{4(s_4 - t)(s_4 - u)} \ln \frac{ss_4}{tu - M^2 s_4} - \frac{3}{2} \ln \frac{tu - M^2 s_4}{(s_4 - t)(s_4 - u)} \right], \quad (3.44)
\end{aligned}$$

$$\begin{aligned}
s^2 \frac{d^2 \sigma_{qg \rightarrow qg A^0}^{\text{HARD}}}{dt du} - s^2 \frac{d^2 \sigma_{qg \rightarrow qg H}^{\text{HARD}}}{dt du} = & \\
& \pi G^2 \left(\frac{\alpha_s(\mu^2)}{4\pi} \right)^2 \frac{1}{N} \left[C_A \left\{ -2 \ln \frac{tu - M^2 s_4}{(s_4 - t)(s_4 - u)} - 1 \right\} \right. \\
& \left. + C_F \left\{ \ln \frac{tu - M^2 s_4}{(s_4 - t)(s_4 - u)} - \frac{1}{2} \right\} \right], \quad (3.45)
\end{aligned}$$

where the meaning of the superscript HARD is explained in [79]. From these expressions we infer that the partonic cross sections (coefficient functions) for H and A^0 are equal in LO and almost equal in NLO. This means that apart from the overall normalisation due to the constant G_B there will not be any difference in the shapes of the double differential cross sections. We show this in Fig. (3.1) where we plot the ratio

$$R = \frac{d\sigma_{A^0}}{d\sigma_H}, \quad (3.46)$$

for $d\sigma_B = d\sigma_B/dp_T$ and proton-proton collisions at the LHC with $\sqrt{S} = 14$ TeV. For these and the next plots we have adopted the parton density set MRST98 (LO, lo05a.dat) [96] for the LO calculations with $\Lambda_5^{\text{NLO}} = 130.5$ MeV as input for the leading log running coupling constant. For the NLO cross sections we have chosen the set MTST99 (NLO, cor01.dat) [97] with $\Lambda_5^{\text{NLO}} = 220$ MeV as input for the next-to-leading log running coupling constant. Furthermore the factorization/renormalization scale is chosen to be $\mu^2 = \mu_r^2 = p_T^2 + M_B^2$. For the masses of the Higgs bosons we take $M_H = M_{A^0} = 120$ GeV/ c^2 and the top quark mass is set equal to $M_t = 173.4$ GeV/ c^2 . Further we have put $\tan\beta = 1$. In the case of an infinite top quark mass, (here we choose $M_t = 173.4 \times 10^3$ GeV/ c^2), we get $R^{\text{LO}} = 9/4$ irrespective of the values of m_H and m_{A^0} . This follows from Eq. (3.9) and the fact that the LO partonic cross sections are the same for H -production and A^0 -production. A finite M_t as given above introduces a small effect and one gets $R^{\text{LO}} = 2.31$ which amounts to a shift upwards of 0.06 (see Fig. (3.1)).

3.5 Conclusions

In NLO the partonic cross sections differ a little bit and $\mathcal{C}_H^2 = [1+22\alpha_s/(4\pi)] \mathcal{C}_A^2$ (see Eqs. 3.10–3.11). Therefore we expect a deviation from the R^{LO} result when m_t is taken infinite in both the LO and NLO reactions. However it turns out that both differences compensate each other. The NLO corrected partonic cross section for A^0 is larger than the one for H and one obtains an upward shift $\Delta R^{\text{NLO}} = 0.26$. The shift due to the coefficient function in Eq. (3.10) is negative and amounts to $\Delta R^{\text{NLO}} = -0.24$. Hence the actual value becomes $R^{\text{NLO}} = 2.27$ (see Fig. (3.1)) which is very close to $R^{\text{LO}} = 9/4$. If M_t is finite one gets again an upward shift of 0.06 like in LO and $R^{\text{NLO}} = 2.33$ (see Fig. (3.1)). One can make similar plots for the rapidity y distributions which yield the same ratios as shown in Fig. (3.1) for the p_T distributions.

The most important feature is that the ratios are independent of p_T and y showing the shape independence of the distributions on the parity of the Higgs boson (scalar versus pseudoscalar). This behaviour was discovered for both the (pseudo)scalar p_T distributions and for the opening angle distribution between the (pseudo)scalar bosons and the highest p_T -jet in the reaction $p + p \rightarrow (H \text{ or } A) + \text{jet} + \text{jet} + 'X'$ in Ref. [98].

From Fig. (3.1) and the observations made above it is clear that the ratios between the NLO and LO corrected cross sections (K -factors) are the same for H production and A^0 production. This also holds for the variation of the NLO cross sections with respect to the mass factorization/renormalization scales. They are given for H -production in [79,80] and we do not have to show

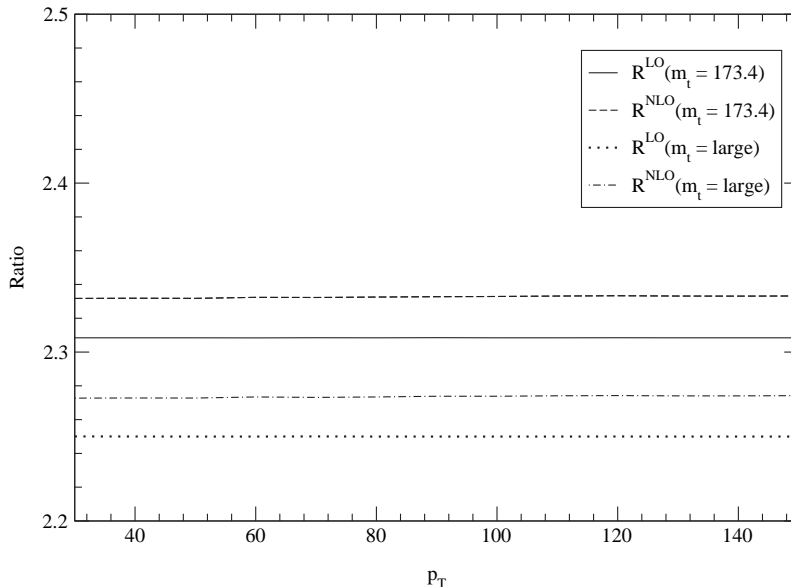


Figure 3.1: The ratio R in Eq. (3.46) plotted as a function of p_T for $\sqrt{S} = 14$ TeV and $\mu^2 = p_T^2 + m_B^2$ with $m_H = m_{A^0} = 120$ GeV/ c^2 ; $R^{\text{LO}}(M_t = \infty)$ (dotted line), $R^{\text{LO}}(M_t = 173.4)$ (solid line) $R^{\text{NLO}}(m_t = \infty)$ (dot-dashed line) $R^{\text{NLO}}(M_t = 173.4)$ (dashed line).

them again for A^0 production. In Fig. (3.2) we present the p_T distributions in NLO for A^0 -production in proton-antiproton collisions at $\sqrt{S} = 2$ TeV (Fermilab Tevatron, Run II) and in proton-proton collisions at $\sqrt{S} = 14$ TeV (LHC). Further we have chosen $m_A = 91.9$ GeV/ c^2 and $\tan\beta = 0.5$. The parton density set and the factorization scale are given above. From Fig. (3.2) we infer that the p_T -distributions decrease rather slowly as p_T increases and that the differential cross section for the Tevatron is two orders of magnitude smaller than the one predicted for the LHC. The latter observation also holds for the corresponding rapidity distributions shown in Fig. (3.3). They are obtained by integrating $d^2\sigma_A/(dp_T dy)$ over the range $p_{T,\text{min}} < p_T < 8 p_{T,\text{min}}$ with $p_{T,\text{min}} = 30$ GeV/ c . The cross section for $p_T > 8 p_{T,\text{min}}$ is negligible. Notice that the range of the rapidity for A^0 -production at the Tevatron is rather small.

Finally we want to comment on the relative importance of the partonic subprocesses contributing to the hadronic differential cross section in Eq. (3.15). For the LHC ($\sqrt{S} = 14$ TeV) the gg -channel dominates and the qg -subprocess contributes about one third of the cross section. This is because at these high energies the x -values of the gluon density $f_g^P(x)$ is so small that it becomes

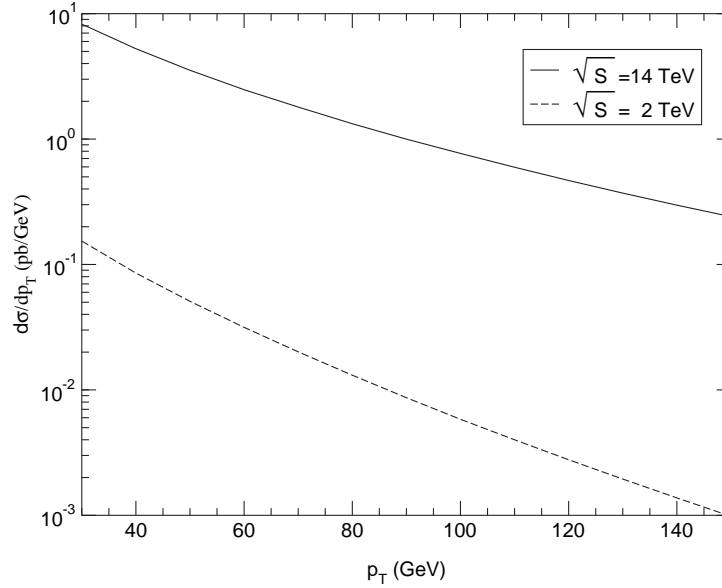


Figure 3.2: The transverse momentum distribution $d\sigma_A/dp_T$ with $\mu^2 = p_T^2 + M_{A^0}^2$, $M_{A^0} = 91.9$ GeV/ c^2 , $\tan\beta = 0.5$; $\sqrt{S} = 14$ TeV (solid line), $\sqrt{S} = 2$ TeV (dashed line).

much larger than the quark densities. At lower energies like $\sqrt{S} = 2$ TeV (Tevatron) the x -values are larger so that the valence quark densities also play a role. This explains why the contribution of the qg -subprocess is of the same magnitude as the one from the gg -channel for A^0 -production at the Tevatron.

Acknowledgments

We are indebted to V. Ravindran for discussions about the relevance of the operator $O_2(x)$. B. Field would like to thank S. Dawson and W. Kilgore for discussions on the pseudoscalar coupling.

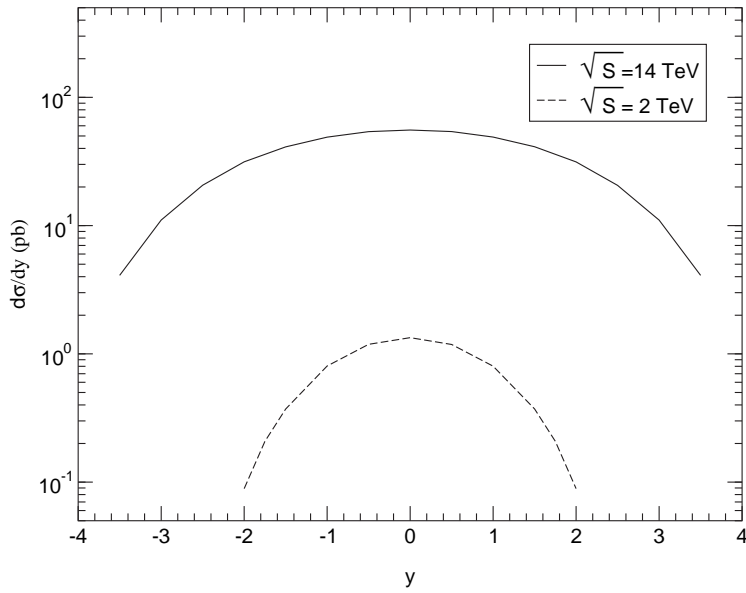


Figure 3.3: The rapidity distribution $d\sigma_{A^0}/dy$ calculated from the integral of $d^2\sigma_{A^0}/(dp_T dy)$ between $8 p_{T,\min} > p_T > p_{T,\min}$ and $p_{T,\min} = 30$ GeV/c. Input parameters are $\mu^2 = p_{T,\min}^2 + M_{A^0}^2$, $M_{A^0} = 91.9$ GeV/c², $\tan\beta = 0.5$; $\sqrt{S} = 14$ TeV (solid line), $\sqrt{S} = 2$ TeV (dashed line).

Chapter 4

Scalar and Pseudoscalar Higgs Boson Plus One Jet Production at the LHC and Tevatron

The production of the Standard Model (SM) Higgs boson (H) plus one jet is compared with that of the lightest scalar Higgs boson (h^0) plus one jet and that of the pseudoscalar Higgs boson (A^0) plus one jet. The latter particles belong to the Minimal Supersymmetric Model (MSSM). We include both top and bottom quark loops to lowest order in QCD and investigate the limits of small quark mass and infinite quark mass. We give results for both the CERN Large Hadron Collider (LHC) and the Fermilab Tevatron.

4.1 Introduction

The Higgs boson is the cornerstone of electroweak symmetry breaking in the Standard Model (SM). Particle physicists around the world have made the search for the Higgs boson the top priority in high energy experiments. However, there are several different candidate models in the Higgs sector. The Minimal Supersymmetric Standard Model (MSSM), which is a special case of the Two Higgs Doublet Model (2HDM), is of particular theoretical interest.

The Standard Model Higgs boson has been experimentally excluded by LEP searches for $e^+e^- \rightarrow ZH$ if its mass is lighter than $114 \text{ GeV}/c^2$ [99]. In the MSSM, the particle spectrum includes five physical Higgs bosons; a light and a heavy neutral scalar (h^0, H^0), two charged scalars (H^\pm), and a CP-odd pseudoscalar (A^0). The mass of the lightest scalar in the MSSM is excluded from being lighter than $91 \text{ GeV}/c^2$ [65], while the mass of the pseudoscalar M_{A^0} is experimentally excluded from being lighter than approximately

92 GeV/c². The ratio between the vacuum expectation values (VEVs) of the two neutral Higgs bosons of the MSSM is defined as $\tan\beta = v_2/v_1$. For $m_{\text{top}} = 174.3$ GeV/c², $0.5 < \tan\beta < 2.4$ has been excluded by the LEP Higgs searches. A different value of the top quark mass will lead to different exclusion bounds on $\tan\beta$.

The total cross-section for scalar Higgs production including massive quark loops has been calculated at next-to-leading order (NLO) in perturbative QCD [70, 91, 100]. The corresponding calculation for Higgs production in the MSSM can be found in Ref. [92]. In the Heavy Quark Effective Theory (HQET) [82, 81, 101], the top quark mass is assumed to be much heavier than the Higgs boson mass and all relevant energy scales. Assuming the HQET total inclusive cross-sections have been calculated at NLO for scalar [69] and pseudoscalar production [71, 83] and also at NNLO for scalar [74–76, 102] and for pseudoscalar [77, 78, 102] production, see also [72, 73]. The use of the HQET significantly simplifies the computation of higher order QCD effects and has been shown to accurately reproduce the exact NLO rate at the LHC for $pp \rightarrow H$ [70, 91] for a Higgs mass less than 1 TeV/c² if the LO massive results are multiplied by the NLO K-factor obtained in the HQET.

In this paper we concentrate on the Higgs plus one jet ($gg \rightarrow g\Phi$, $qg \rightarrow q\Phi$, and $q\bar{q} \rightarrow g\Phi$) production processes since they are important for the experimental detection of the Higgs. Here Φ represents either the SM Higgs, H , or the MSSM scalars, h^0 and H^0 , or the MSSM pseudoscalar A^0 . The production of the SM Higgs plus one jet process has been calculated exactly at LO in [103, 104] with the inclusion of heavy quark loops. The production rate in the MSSM for the lightest scalar plus one jet was recently calculated in LO including SUSY loop effects, which can be significant for light SUSY squarks and gluinos [105]. The NLO QCD corrections to the Higgs plus one jet process have only been computed in the HQET, since the full virtual corrections would require the evaluation of massive two-loop integrals for a $2 \rightarrow 2$ reaction. The differential cross-section for the production of a scalar Higgs boson plus one jet in the HQET at NLO has been calculated previously by [68, 72, 73, 79, 80, 106] and the integrated rate was shown to increase substantially from the lowest order rate. The pseudoscalar case has been presented in [107] and in [108].

We present the calculation of the Higgs plus one jet process where we include both top and bottom quark loops with the full quark mass dependence. This is done for the SM Higgs and for the lightest scalar and pseudoscalar Higgs bosons of the MSSM. The contributions of loops with bottom quarks can be important for large values of $\tan\beta$ in the MSSM. We also address the region of validity of the HQET predictions for these reactions.

In Section (4.2), the limit of the partonic matrix elements in the HQET

$$|\mathcal{M}|^2 = |c_t^\Phi \mathcal{M}_t + c_b^\Phi \mathcal{M}_b|^2$$

Φ		
H	$c_t^H = 1$ $c_b^H = 1$	$ \mathcal{M} ^2 = \mathcal{M}_t ^2 + \mathcal{M}_b ^2 + 2\text{Re}(\mathcal{M}_t \mathcal{M}_b^*)$
h^0	$c_t^{h^0} = \cos \alpha / \sin \beta$ $c_b^{h^0} = -\sin \alpha / \cos \beta$	$ \mathcal{M} ^2 = \frac{\cos^2 \alpha}{\sin^2 \beta} \mathcal{M}_t ^2 + \frac{\sin^2 \alpha}{\cos^2 \beta} \mathcal{M}_b ^2 - 2 \frac{\sin \alpha \cos \alpha}{\sin \beta \cos \beta} \text{Re}(\mathcal{M}_t \mathcal{M}_b^*)$
H^0	$c_t^{H^0} = \sin \alpha / \sin \beta$ $c_b^{H^0} = \cos \alpha / \cos \beta$	$ \mathcal{M} ^2 = \frac{\sin^2 \alpha}{\sin^2 \beta} \mathcal{M}_t ^2 + \frac{\cos^2 \alpha}{\cos^2 \beta} \mathcal{M}_b ^2 + 2 \frac{\sin \alpha \cos \alpha}{\sin \beta \cos \beta} \text{Re}(\mathcal{M}_t \mathcal{M}_b^*)$
A^0	$c_t^{A^0} = \cot \beta$ $c_b^{A^0} = \tan \beta$	$ \mathcal{M} ^2 = \frac{1}{\tan^2 \beta} \mathcal{M}_t ^2 + \tan^2 \beta \mathcal{M}_b ^2 + 2\text{Re}(\mathcal{M}_t \mathcal{M}_b^*)$

Table 4.1: Higgs-fermion couplings in the MSSM and the dependence of the matrix element-squared on the couplings. \mathcal{M}_t and \mathcal{M}_b represent contributions from top- and bottom- quark loops, respectively. The α parameter is the angle that diagonalizes the CP-even Higgs squared-mass matrix.

and in the small quark mass limit are explored. In Section (4.3), the Higgs plus jet matrix elements are given and our computational techniques are described. Section (4.4) summarizes our notation for the hadronic differential cross-sections. Section (4.5) contains numerical results for differential cross-sections at the Tevatron and LHC, as well as integrated results with cuts in transverse momentum, p_t , and rapidity, y . Analytic results for the matrix elements are given in two Appendices.

4.2 Partonic Processes - Heavy Quark Effective Theory

In the limit where the top quark mass is much heavier than all the energy scales in the problem, only the top quark coupling to gluons is numerically significant and this limit provides a good approximation to Standard Model Higgs production matrix elements. The HQET limit for scalar Higgs production has been extensively studied in the literature. This limit is especially useful for deriving higher order QCD corrections since the massive top quark loops that couple the Higgs boson to gluons reduce to effective vertices. The Feynman

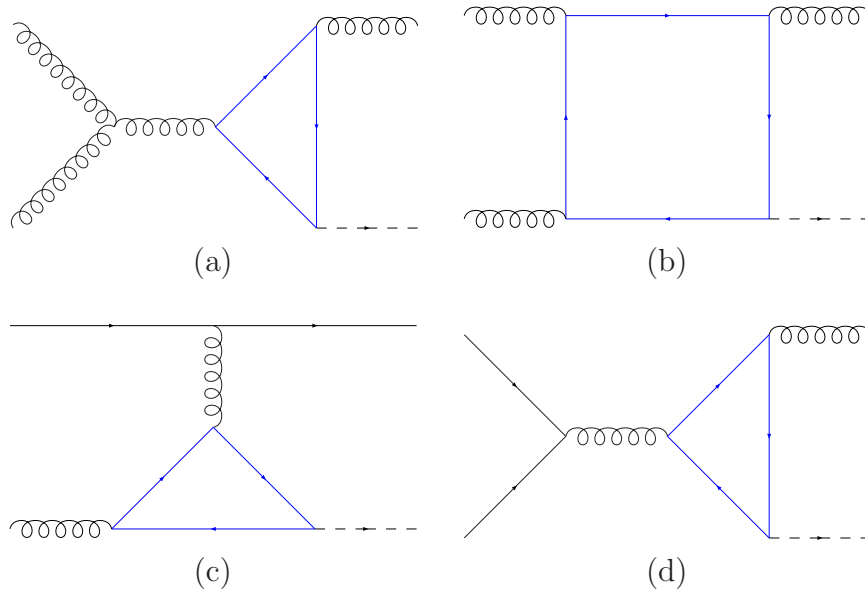


Figure 4.1: Sample Higgs plus one jet diagrams. Figures 4.1a,b are the gg diagrams, 4.1c is the $q\bar{q}$ channel, and 4.1d is the $q\bar{q}$ channel. All quarks contribute to the loops. The crossed and charge conjugate diagrams are not shown. There are a total of 12 gg diagrams and 2 for each of the $q\bar{q}$ and $q\bar{q}$ sub-processes.

rules can be derived from an effective Lagrangian density [69, 70, 74, 81, 82, 91],

$$\mathcal{L}_{\text{eff}}^H = -g_H \frac{H}{4v} \mathcal{C}_H(\alpha_s) \mathcal{O}_H, \quad \mathcal{O}_H = G_{\mu\nu}^a G^{a,\mu\nu}, \quad (4.1)$$

where $g_H = 1$ in the Standard Model and $v = 246$ GeV. \mathcal{O}_H generates vertices which couple the Higgs boson to two, three, and four gluons. In the large m_{top} limit, the coefficient \mathcal{C}_H can be evaluated as a power series in α_s [70, 81, 82, 90, 91, 109, 110]

$$\mathcal{C}_H(\alpha_s^{(5)}(\mu_r^2)) = -\frac{\alpha_s^{(5)}(\mu_r^2)}{3\pi} \left[1 + \frac{11\alpha_s^{(5)}(\mu_r^2)}{4\pi} + \dots \right], \quad (4.2)$$

where $\alpha_s^{(5)}(\mu_r^2)$ is evaluated at the scale μ_r in a 5 flavor scheme.

For comparison, we consider a pseudoscalar Higgs boson with a coupling to fermions given by,

$$\mathcal{L}_{\text{eff}}^{A^0} = -ig_A \frac{A^0}{v} m_i \bar{\psi}_i \gamma_5 \psi_i. \quad (4.3)$$

In the large m_{top} limit, the interactions of the pseudoscalar with gluons can be found from the effective Lagrangian¹ [67, 75, 93]

$$\mathcal{L}_{\text{eff}}^{A^0} = -g_A \frac{A^0}{v} (C_{A_1}(\alpha_s) \mathcal{O}_1 + C_{A_2}(\alpha_s) \mathcal{O}_2), \quad (4.4)$$

$$\mathcal{O}_1 = \epsilon_{\mu\nu\lambda\sigma} G_a^{\mu\nu} G_a^{\lambda\sigma}, \quad \mathcal{O}_2 = \partial^\mu \sum_{i=0}^{n_f} \bar{q}_i \gamma_\mu \gamma_5 q_i, \quad (4.5)$$

where $G_a^{\mu\nu}$ is the gluon field strength tensor. The process independent coefficient functions are

$$C_{A_1} = -\frac{\alpha_s(\mu_r^2)}{16\pi}, \quad C_{A_2} = \mathcal{O}(\alpha_s^2). \quad (4.6)$$

We consider $g_A = 1$ and examine the differences between differential cross-sections for the production of a SM scalar Higgs boson and a pseudoscalar Higgs boson with the couplings of Eq. (4.3), when the bosons are produced in association with a jet.

¹There is some confusion over the coupling constant for the pseudoscalar case in the literature. The correct coupling is found in Ref. [71]. There is an extra factor of 1/4 in Ref. [67] leading to a cross-section 16 times too small for the pseudoscalar case. It seems that the 1/4 from the effective Lagrangian was incorporated into the coupling constant by mistake. The Feynman rules in both papers are correct if the coupling constant from the Ref. [71] paper is used.

It is also of interest to compare the production rates for a Higgs boson plus a jet in the MSSM. The effective Lagrangians in this case are found by making the replacements in Eqs. (4.1) and (4.5),

$$\begin{aligned} g_H &\rightarrow c_t^{h^0} \\ g_A &\rightarrow c_t^{A^0}, \end{aligned} \tag{4.7}$$

where $c_t^{h^0}$ and $c_t^{A^0}$ are given in Table (4.1). (We neglect contributions from SUSY particles such as the bottom squarks and gluinos, and therefore assume that the SUSY particle masses are much larger than m_{top} and m_Φ . These genuine SUSY contributions can be important for light squark and gluino masses [105].) When the bottom quark becomes important, the HQET breaks down as a reliable calculational tool. This occurs in the MSSM when $\tan\beta$ becomes large and the bottom quark couplings are enhanced.

4.3 Partonic Processes - Full Theory

There are three channels associated with Higgs plus one jet production: gluon fusion, quark-gluon scattering, and quark-antiquark annihilation. Representative Feynman diagrams are shown in Fig. (4.1). At the LHC where $\sqrt{S} = 14$ TeV the gluon fusion and quark-gluon channels are the most important, with the quark-antiquark channel adding a negligible amount to the process. However all three channels are important at the Tevatron where $\sqrt{S} = 1.96$ TeV.

The calculation of the matrix elements was carried out in both $n = 4 - 2\epsilon$ dimensions and 4-dimensions. The γ_5 in the pseudoscalar calculation was treated using the Akyeampong-Delbourgo prescription [111–113] for the γ_5 -matrix. In this scheme the γ_5 is exchanged for a Levi-Civita tensor contracted with four γ -matrices. After the trace, the tensor loop integrals were reduced to scalar integrals using the usual Passarino-Veltman [114] reduction techniques.

4.3.1 Gluon fusion ($gg \rightarrow g\Phi$)

The gluon fusion channel is the most important channel at the LHC. The momentum distribution in this process is assigned with all momentum incoming,

$$g(p_1^{\mu_1, a_1}) + g(p_2^{\mu_2, a_2}) \rightarrow g(-p_3^{\mu_3, a_3}) + \Phi(-p_5), \tag{4.8}$$

where μ_i are Lorentz indices and a_i are color indices. The Mandelstam variables used in the partonic system are

$$\hat{s} = (p_1 + p_2)^2, \quad \hat{t} = (p_1 + p_5)^2, \quad \hat{u} = (p_2 + p_5)^2, \quad Q^2 = m_\Phi^2. \tag{4.9}$$

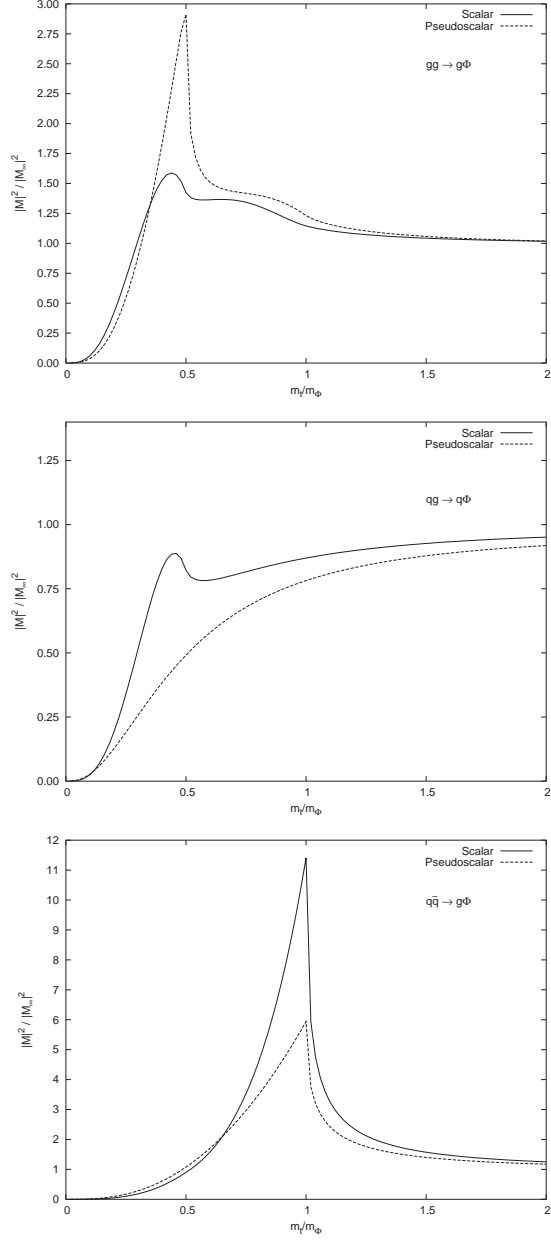


Figure 4.2: The squared matrix elements, $|\mathcal{M}|^2$, evaluated at $\hat{s} = 4m_\Phi^2$ and $\hat{u} = \hat{t}$ for the three different channels, $(gg, q\bar{q}, q\bar{q})$, normalized to the squared matrix elements in the HQET for scalar and pseudoscalar (with $g_A = 1$) Higgs plus jet production. We include only the top quark loops. The solid line is the scalar, whereas the dashed line is the pseudoscalar.

The matrix elements, including the gluon polarization vectors, can be written

$$\mathcal{M}^{gg} = \epsilon^{\mu_1}(p_1)\epsilon^{\mu_2}(p_2)\epsilon^{\mu_3}(p_3)\mathcal{M}_{\mu_1\mu_2\mu_3}^{gg}. \quad (4.10)$$

The Ward-Takahashi identities let us check the gauge invariance of the sub-process. In the gluon fusion case, these can be written as

$$\begin{aligned} p_1^{\mu_1}\epsilon^{\mu_2}(p_2)\epsilon^{\mu_3}(p_3)\mathcal{M}_{\mu_1\mu_2\mu_3}^{gg} &= \epsilon^{\mu_1}(p_1)p_2^{\mu_2}\epsilon^{\mu_3}(p_3)\mathcal{M}_{\mu_1\mu_2\mu_3}^{gg} \\ &= \epsilon^{\mu_1}(p_1)\epsilon^{\mu_2}(p_2)p_3^{\mu_3}\mathcal{M}_{\mu_1\mu_2\mu_3}^{gg} = 0, \end{aligned} \quad (4.11)$$

giving us a strong check on the algebraic results. Analytic results for the matrix element squared for $gg \rightarrow gA^0$ are given in Appendix A, see also Appendix C in [91], while those for $gg \rightarrow gH$ can be found in Refs. [103, 104].

4.3.2 Quark-antiquark annihilation ($q\bar{q} \rightarrow g\Phi$)

For this sub-process, the momentum, color, and Lorentz structure was assigned as follows

$$q(p_1) + \bar{q}(p_2) \rightarrow g(-p_3^{\mu_3, \alpha_3}) + \Phi(-p_5). \quad (4.12)$$

The matrix elements satisfy

$$\mathcal{M}^{q\bar{q}} = \epsilon^{\mu_3}(p_3)\mathcal{M}_{\mu_3}^{q\bar{q}}, \quad p_3^{\mu_3}\mathcal{M}_{\mu_3}^{q\bar{q}} = 0. \quad (4.13)$$

Analytic results for $q\bar{q} \rightarrow gA^0$ are given in Appendix B, see also Appendix C in [91], while those for $q\bar{q} \rightarrow gH$ can be found in Refs. [103, 104]. The results for quark-gluon scattering can be found by crossing.

4.3.3 HQET Matrix Elements

The 4-dimensional color-spin averaged matrix elements for Higgs boson plus one jet production in the $m_{\text{top}} \rightarrow \infty$ limit are presented here for completeness. These matrix elements obey the same crossing relations as the full matrix elements,

$$|\mathcal{M}(\hat{s}, \hat{t}, \hat{u})|_{qg \rightarrow g\Phi}^2 = -|\mathcal{M}(\hat{u}, \hat{t}, \hat{s})|_{q\bar{q} \rightarrow g\Phi}^2. \quad (4.14)$$

The matrix elements in the large m_{top} HQET limit can be written [91, 103, 104, 108],

$$\overline{\sum} |\mathcal{M}|_{gg \rightarrow g\Phi}^2 = A_\Phi \frac{N_c}{4(N_c^2 - 1)} \frac{\hat{s}^4 + \hat{t}^4 + \hat{u}^4 + Q^8}{\hat{s}\hat{t}\hat{u}} \quad (4.15)$$

$$\overline{\sum} |\mathcal{M}|_{qg \rightarrow q\Phi}^2 = -A_\Phi \frac{1}{8N_c} \frac{\hat{s}^2 + \hat{t}^2}{\hat{u}} \quad (4.16)$$

$$\overline{\sum} |\mathcal{M}|_{q\bar{q} \rightarrow g\Phi}^2 = A_\Phi \frac{(N_c^2 - 1)}{8N_c^2} \frac{\hat{u}^2 + \hat{t}^2}{\hat{s}}, \quad (4.17)$$

where,

$$\begin{aligned} A_H &= \left(\frac{\alpha_s}{3\pi v} \right)^2 (4\pi\alpha_s) g_H^2 \\ A_A &= \left(\frac{\alpha_s}{2\pi v} \right)^2 (4\pi\alpha_s) g_A^2 \end{aligned} \quad (4.18)$$

and $g_H = 1$ for the SM and g_Φ is given in Eq. (4.7) for the MSSM. The bar implies a sum and average over colors and spins. The exact matrix elements squared as compared with the HQET matrix elements are shown in Fig. (4.2) for both the SM scalar, which are in excellent agreement with the plots in [104], and for a pseudoscalar with $g_A = 1$. In this plot, the mass of the Higgs was set to $m_\Phi = 100 \text{ GeV}/c^2$ and the mass of the top quark was varied. In these plots, two thresholds can be observed. Each threshold occurs when an imaginary part of the matrix elements turns on or off. If we examine Eq. (4.58) for $q\bar{q} \rightarrow gA^0$ we clearly see that the imaginary part contains the difference of two step functions

$$\theta(\hat{s} - 4m_{\text{top}}^2) - \theta(M_{A^0}^2 - 4m_{\text{top}}^2), \quad (4.19)$$

so the first threshold occurs at $2m_{\text{top}} = M_{A^0}$ and the second at $2m_{\text{top}} = \sqrt{\hat{s}}$. Since we choose $\hat{s} = 4M_{A^0}^2$ for the plot this implies that these thresholds occur at $m_{\text{top}}/m_\Phi = 0.5$ and 1 respectively. The imaginary part is finite between these cusps. Similar phenomena occur in the other reactions. However when the squared matrix elements contain several terms the onset of the imaginary parts is not always visible. The reactions $gg \rightarrow q\Phi$ do not have \hat{s} channels so they only have cusps at $m_{\text{top}}/m_\Phi = 0.5$. Finally the $gg \rightarrow g\Phi$ channels show both cusps. Note that the reason the cusps do not appear exactly at 0.5 and 1 is due to our choice of points in m_{top}/m_Φ .

These ratios show that when the heavy quark becomes heavier than $m_{\text{top}} \sim \frac{1}{2}m_\Phi$ the HQET is a reasonable approximation to the matrix elements with a top loop only. In the MSSM, however, the usefulness of the HQET is limited to small values of $\tan\beta$ where the bottom quark contribution can be neglected.

4.3.4 Small Quark Mass Limit

When the quark mass in the loop is much smaller than the Higgs mass and the energy scale, the small quark mass limit $m_f \rightarrow 0$ is relevant. This is the case for the bottom quark contribution in the large $\tan\beta$ limit of the MSSM. The matrix elements in this limit behave as

$$|\mathcal{M}|^2 \sim m_f^4 \log^4(m_f^2/\mu^2), \quad (4.20)$$

where $\mu \gg m_f$. Exact expressions in the small quark mass limit are given in Appendix B.

4.4 Observables

Generically, we can write a $2 \rightarrow 2$ differential observable as

$$\hat{s}^2 \frac{d^2 \hat{\sigma}}{d\hat{t} d\hat{u}} = \frac{1}{16\pi} \overline{\sum} |\mathcal{M}|^2, \quad (4.21)$$

where the bar implies a sum and average over colors and spins. To relate the hadronic differential distributions to the partonic differential distributions we need to perform a convolution with the parton distribution functions.

The hadronic process can be written as

$$H_1(P_1) + H_2(P_2) \rightarrow j(-p_3) + \Phi(-p_5) \quad (4.22)$$

where the j represents the gluon or the quark jet in the sub-process of interest. In the hadronic system, we can write

$$S = (P_1 + P_2)^2, \quad T = (P_1 + p_5)^2, \quad U = (P_2 + p_5)^2. \quad (4.23)$$

This translates into the partonic system (with momentum fractions x_1 and x_2) as

$$p_1 = x_1 P_1, \quad p_2 = x_2 P_2, \quad (4.24)$$

$$\hat{s} = x_1 x_2 S, \quad \hat{t} = x_1(T - Q^2) + Q^2, \quad \hat{u} = x_2(U - Q^2) + Q^2 \quad (4.25)$$

$$x_{1,\min} = \frac{-U}{S + T - Q^2}, \quad x_{2,\min} = \frac{-x_1(T - Q^2) - Q^2}{x_1 S + U - Q^2}, \quad (4.26)$$

where $Q^2 = m_\Phi^2$. The hadronic variables can be written in terms of the transverse momentum and rapidity

$$T = Q^2 - \sqrt{S} \sqrt{p_t^2 + Q^2} \cosh y + \sqrt{S} \sqrt{p_t^2 + Q^2} \sinh y \quad (4.27)$$

$$U = Q^2 - \sqrt{S} \sqrt{p_t^2 + Q^2} \cosh y - \sqrt{S} \sqrt{p_t^2 + Q^2} \sinh y. \quad (4.28)$$

The hadronic differential cross-section is,

$$S^2 \frac{d^2 \sigma^{H_1 H_2}}{dT dU} = \sum_{ab} \int_{x_{1,\min}}^1 \frac{dx_1}{x_1} \int_{x_{2,\min}}^1 \frac{dx_2}{x_2} f_a^{H_1}(x_1, \mu_f^2) f_b^{H_2}(x_2, \mu_f^2) \hat{s}^2 \frac{d^2 \hat{\sigma}_{ab}}{d\hat{t} d\hat{u}}. \quad (4.29)$$

Upon further integration we obtain the single differential p_t and rapidity distributions with the kinematic limits,

$$p_{t,\max} = \frac{1}{2} \frac{S - Q^2}{\sqrt{S}}, \quad y_{\max} = \frac{1}{2} \ln \left(\frac{1 + S_Q}{1 - S_Q} \right), \quad (4.30)$$

$$\text{where } S_Q = \sqrt{1 - \frac{4S(p_t^2 + Q^2)}{(S + Q^2)^2}}. \quad (4.31)$$

4.5 Numerical Results

We present our calculations for the CERN LHC with $\sqrt{S} = 14$ TeV and the Fermilab Tevatron with $\sqrt{S} = 1.96$ TeV. We use the CTEQ6.1L parton distribution functions [84] with $\Lambda_5^{\text{LO}} = 165.2$ MeV and a one loop running coupling constant with $\alpha_s(M_Z) = 0.1298$. For the differential distributions, the full kinematic rapidity and p_t are used and the factorization and renormalization scales are set equal to,

$$\mu_r = \mu_f = \sqrt{Q^2 + p_t^2}. \quad (4.32)$$

We use pole masses with $m_{\text{top}} = 174.3$ GeV/ c^2 and $m_{\text{bot}} = 4.5$ GeV/ c^2 . For the integrated cross-section we require the p_t of the Higgs and the jet to satisfy $p_{t,\min} > 30$ GeV/ c in the rapidity region $|y| < 2.5$ and replace p_t by $p_{t,\min}$ in Eq. (4.32) for the renormalization and factorization scales.

4.5.1 Standard Model

The transverse momentum distributions of the SM Higgs boson for all the separate channels are shown in Fig. (4.3) for the LHC. For a SM Higgs boson with $M_H = 120$ GeV/ c^2 , the cross-section for Higgs plus one jet is approximately 12.3 pb when both the top and bottom quarks are included in the calculation. Although the bottom quark contribution alone is only 0.05 pb, the top-bottom interference lowers the cross-section by approximately 8.25% from 13.4 pb when only the top quark is included, see [115]. This lowering of the cross-section may be visible at the LHC. As shown in Fig. (4.4), the full theory and the HQET agree very well at small to moderate p_t for both the scalar [103, 106] and the pseudoscalar differential distributions.

4.5.2 Minimal Supersymmetric Standard Model

The MSSM is a special case of the 2HDM. In the MSSM, the up- and down-type quarks become massive from different Higgs doublets and the ratio of the two VEVs is parameterized by $\tan \beta = v_2/v_1$. As shown in Table (4.1), up- and

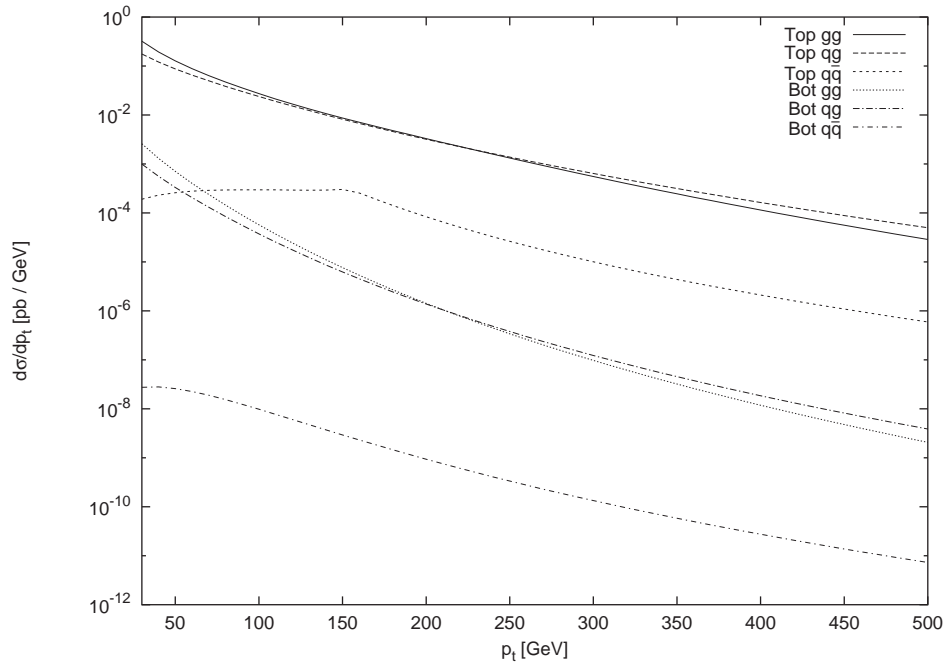


Figure 4.3: Transverse momentum distributions for the SM Higgs boson plus one jet production at the LHC with $M_H = 120 \text{ GeV}/c^2$ for the different channels. The curves labeled ‘Top’ (‘Bot’) include *only* the top (bottom) quark loops.

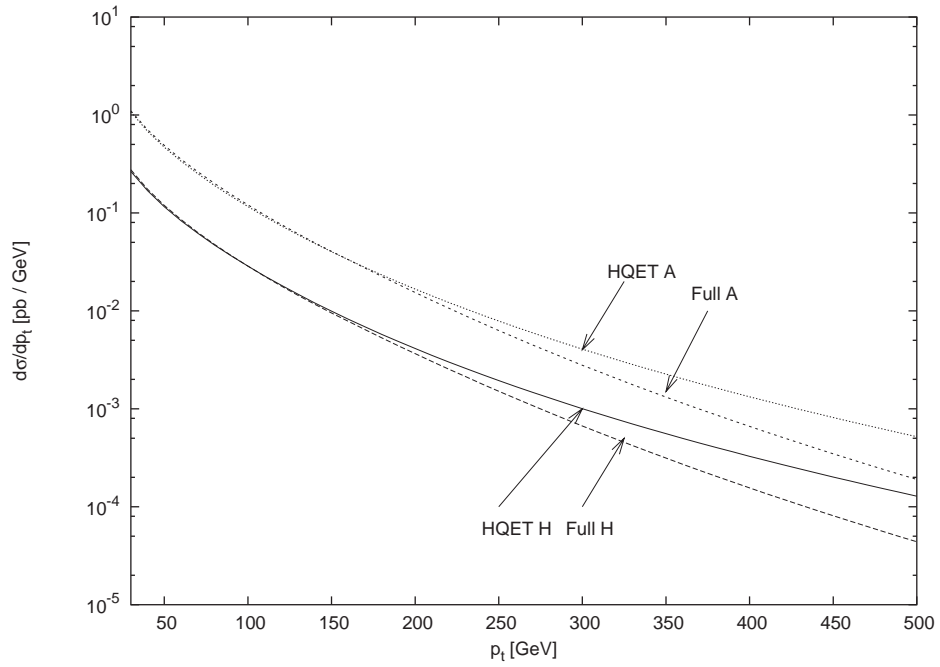


Figure 4.4: Transverse momentum distributions for the SM Higgs (H) plus one jet and for a pseudoscalar (A^0) plus one jet in the full theory with only the top-quark loops included and in the HQET at the LHC for $M_\Phi = 120 \text{ GeV}/c^2$. We assume $g_A = 1$.

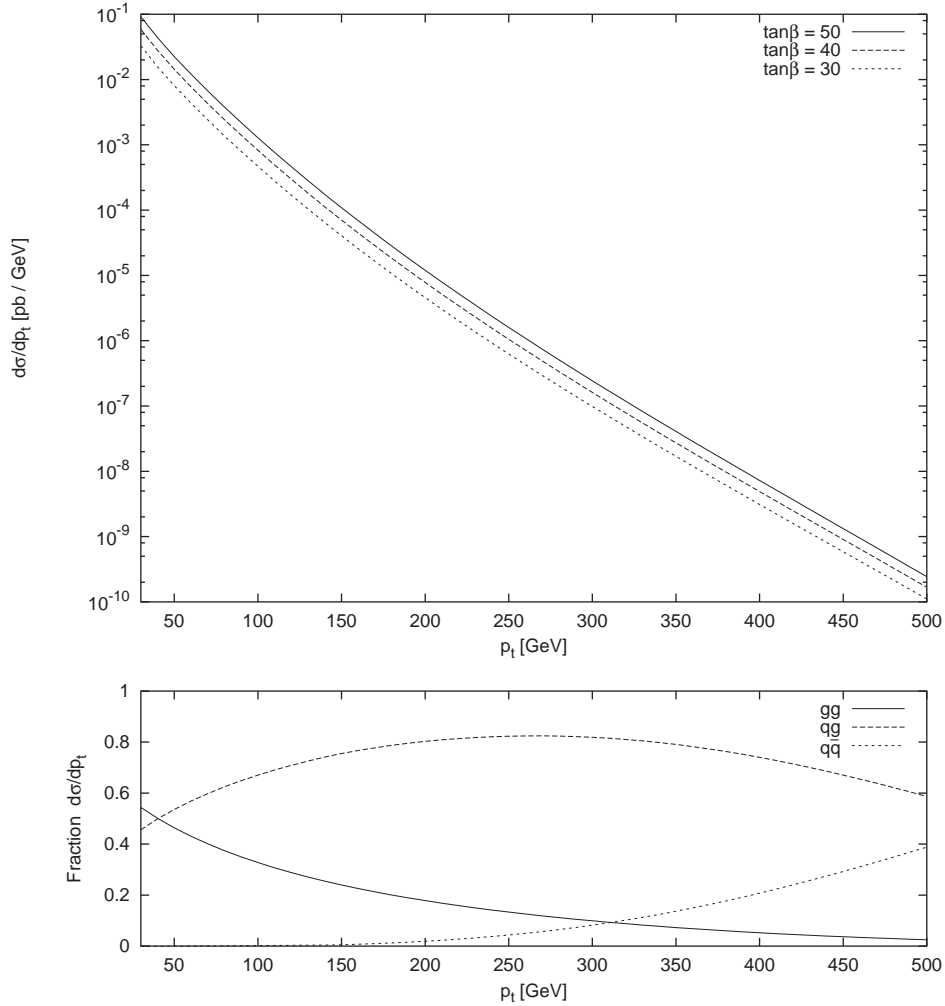


Figure 4.5: The transverse momentum distributions for the MSSM pseudo-scalar Higgs boson for $\tan\beta = 30, 40, 50$ and $M_{A^0} = 120 \text{ GeV}/c^2$ at the Tevatron including the top and bottom quark loops. The top, middle, and bottom lines in the top graph are the curves for $\tan\beta = 50, 40, 30$ respectively. Below is the fraction of the process that comes from each of the different channels. The curves at $p_t = 250 \text{ GeV}/c$ from top to bottom are the $q\bar{q}$, $g\bar{g}$, and $q\bar{q}$ channels respectively.

down-type quarks couple differently to the Higgs bosons of the MSSM. The α parameter is the angle that is introduced to diagonalize the mass eigenstates of the CP-even Higgs squared-mass matrix to obtain the physical states. The program HDECAY [86] was used to determine the mass of the lightest scalar and the α mixing parameter once the values of M_{A^0} and $\tan\beta$ were chosen. The SUSY Higgs mixing parameter was set to $\mu = 300 \text{ GeV}/c^2$, the gluino mass to $\mu_2 = 200 \text{ GeV}/c^2$, all the SUSY breaking masses to $1 \text{ TeV}/c^2$, and the soft breaking term to $1.5 \text{ TeV}/c^2$.

At the Tevatron, there is a very small signal for the SM Higgs boson. The cross-section for a SM Higgs boson plus one jet with $M_H = 120 \text{ GeV}/c^2$ at lowest order in QCD is approximately 0.1 pb. For $\tan\beta \sim 30$ the cross-section for a $120 \text{ GeV}/c^2$ pseudoscalar Higgs in the MSSM is about twice as large as for a $120 \text{ GeV}/c^2$ SM Higgs at the Tevatron and continues to grow with $\tan\beta$. The differential cross-section for pseudoscalar plus jet production at the Tevatron is shown in Fig. (4.5). At the Tevatron, the large $\tan\beta$ region is completely dominated by bottom quark loops where the HQET is of little use.

For the LHC, the entire $\tan\beta$ region is experimentally accessible. In the small $\tan\beta$ region, the cross-section is well approximated by the HQET limit and the bottom quark contribution can be neglected. However, there are regions where both the top and bottom quark loops are important. The results are summarized in Figs. (4.6) and (4.7). These plots use the full theory matrix elements. For pseudoscalar plus jet production, including only the top quark loop underestimates the total cross-section by 9.5% at $\tan\beta = 4$ and the discrepancy becomes larger as $\tan\beta$ grows. Including only the bottom quark underestimates the total cross-section by 5.6% at $\tan\beta = 8$ and becomes a better approximation as $\tan\beta$ increases. The total cross-section for the MSSM lightest scalar plus jet production receives an important contribution from the interference between the top- and bottom-quark loops over a large range of $\tan\beta$.

4.6 Conclusions

We calculated the differential distributions and cross-sections for the SM Higgs, H , the MSSM scalar Higgs boson, h^0 , and pseudoscalar boson, A^0 , plus one jet production at the Tevatron and LHC. We included both the top and bottom quark loops and investigated the validity of the Heavy Quark Effective Theory (HQET) limit and the light quark mass limit. For large $\tan\beta$, the HQET fails and the complete result with all mass dependences is needed.

The NLO QCD corrections for Higgs plus jet [79, 80, 106] and pseudoscalar plus jet [107] production have been previously found in the large m_{top} limit.

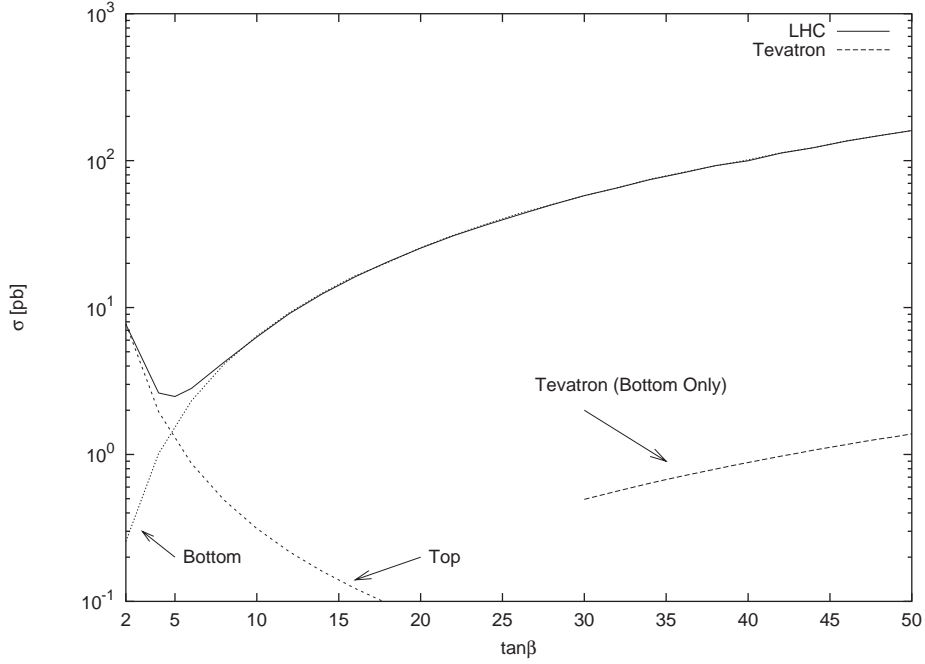


Figure 4.6: Cross-section for the production of the MSSM pseudoscalar Higgs boson plus one jet for different values of $\tan\beta$ at the LHC for $M_{A^0} = 120 \text{ GeV}/c^2$ integrated for $p_t > 30 \text{ GeV}/c$ using the full theory matrix elements. The top and bottom labels show what the contribution of the top and bottom quark would be alone. In the region $4 < \tan\beta < 8$ the total cross-section is not represented well by either the top or bottom matrix elements alone. In the experimentally accessible region, the total cross-section at the Tevatron is dominated by the bottom loop so only the bottom contribution is shown for $\tan\beta > 30$.

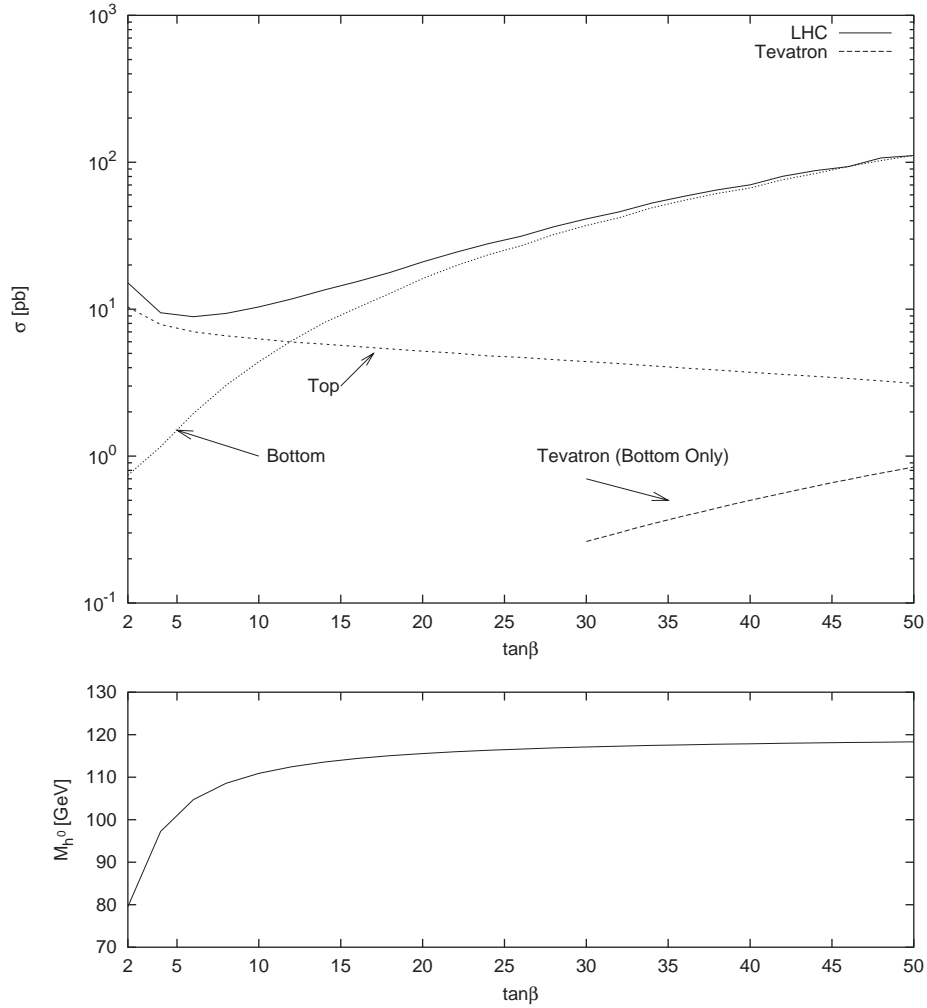


Figure 4.7: Cross-section for the production of the MSSM lightest scalar Higgs boson plus one jet for different values of $\tan\beta$ integrated for $p_t > 30$ GeV/c using the full theory matrix elements. The top and bottom labels show what the contributions of the top and bottom quark would be alone. In the experimentally accessible region, the total cross-section at the Tevatron is dominated by the bottom loop, so only the bottom contribution is shown for $\tan\beta > 30$. Below is the corresponding mass of the lightest scalar for $M_{A^0} = 120$ GeV/c².

Our results make it clear that these can only be applied to the MSSM in certain regions. At large $\tan\beta$, using the bottom-quark only is a very good approximation in the MSSM. At small $\tan\beta$ the MSSM pseudoscalar is top-quark loop dominated, whereas the lightest scalar in the MSSM still receives important contributions from both the top- and bottom-quarks over a much broader range of $\tan\beta$. This can be seen as the effective suppression of the $c_t^{h^0}$ coupling and enhancement of the $c_b^{h^0}$ coupling at small $\tan\beta$ where the interference between the two terms is still playing an important role.

Acknowledgments

B. Field would like to thank W. Kilgore for discussions on the pseudoscalar coupling as well as A. Field-Pollatou, N. Christensen and J. Ellis for helpful comments and suggestions. The work of B. Field and J. Smith is supported in part by the National Science Foundation grant PHY-0098527. The work of S. Dawson is supported by the U.S. Department of Energy under grant DE-AC02-98CH10886.

Appendix A: Pseudoscalar Matrix Elements

For the $q\bar{q} \rightarrow gA^0$ sub-process, the (spin and color averaged) matrix elements squared are particularly simple because the presence of a γ_5 makes the traces much smaller than in the scalar case. They can be written in terms of the integrals presented in [104],

$$\overline{\sum} |\mathcal{M}|_{q\bar{q} \rightarrow gA^0}^2 = \frac{16m_f^4}{\hat{s}} \left(\frac{(4\pi\alpha_s(\mu_r^2))^3}{4N_c^2 v^2} \right) |C_1(\hat{s})|^2 [\hat{s}^2 - 2\hat{t}_1\hat{u}_1 + Q^4], \quad (4.33)$$

where the new variables are defined

$$\hat{s}_1 = \hat{s} - Q^2, \quad \hat{t}_1 = \hat{t} - Q^2, \quad \hat{u}_1 = \hat{u} - Q^2. \quad (4.34)$$

It is easy to see that $\hat{s}_1 = -(\hat{t} + \hat{u})$ and so on.

In these expressions we use the notation of [104]. The C_1 loop integral that appears in the calculation is the usual triangle integral with two massive legs. For $p_1^2 = 0$, $p_2^2 = Q^2 = m_\Phi^2$, $p_{12} = p_1 + p_2$ and $p_{12}^2 = \hat{s}$, the triangle integral is defined as

$$C_1(\hat{s}) = C_1(p_1, p_2) \quad (4.35)$$

$$= \frac{1}{i\pi^2} \int \frac{d^4q}{[q^2 - m_f^2][(q + p_1)^2 - m_f^2][(q + p_{12})^2 - m_f^2]}. \quad (4.36)$$

The box integrals with $p_1^2 = p_2^2 = p_3^2 = 0$, and $p_{123}^2 = (p_1 + p_2 + p_3)^2 = Q^2$ are defined as

$$\begin{aligned} D(\hat{s}, \hat{t}) &= D(p_1, p_2, p_3) \\ &= \frac{1}{i\pi^2} \int \frac{d^4q}{[q^2 - m_f^2][(q+p_1)^2 - m_f^2][(q+p_{12})^2 - m_f^2][(q+p_{123})^2 - m_f^2]}. \end{aligned} \quad (4.37)$$

It is easy to see that the box integrals satisfy the relation $D(\hat{x}, \hat{y}) = D(\hat{y}, \hat{x})$. The computer package FF [116] was used to evaluate the scalar integrals.

For the $gg \rightarrow gA^0$ sub-process, the (spin and color averaged) matrix element squared can be written in the symmetric form,

$$\begin{aligned} \overline{\sum} |\mathcal{M}|_{gg \rightarrow gA^0}^2 &= \sum_f \frac{m_f^4 (4\pi\alpha_s(\mu_r^2))^3}{v^2(N_c^2 - 1)^2} \left\{ F(\hat{s}, \hat{t}, \hat{u}) + F(\hat{s}, \hat{u}, \hat{t}) + \right. \\ &\quad \left. F(\hat{u}, \hat{s}, \hat{t}) + F(\hat{u}, \hat{t}, \hat{s}) + \right. \\ &\quad \left. F(\hat{t}, \hat{u}, \hat{s}) + F(\hat{t}, \hat{s}, \hat{u}) \right\} \end{aligned} \quad (4.38)$$

where

$$\begin{aligned} F(\hat{s}, \hat{t}, \hat{u}) &= -2 \operatorname{Re} \left(C_1(\hat{u}) D^*(\hat{u}, \hat{s}) \right) \left[\hat{s}_1 \left(\frac{\hat{s}Q^2}{\hat{t}} + \hat{u} \right) - \hat{s}\hat{t} - \frac{\hat{s}^3}{\hat{t}} \right] \\ &\quad - \frac{1}{2} \operatorname{Re} \left(D(\hat{s}, \hat{t}) D^*(\hat{u}, \hat{s}) \right) \left[\hat{t}_1(\hat{s}^2 + \hat{s}\hat{t}) \right] \\ &\quad + 2 \operatorname{Re} \left(C_1(\hat{t}) C_1^*(\hat{u}) \right) \left[\frac{\hat{t}^2 - \hat{t}_1 Q^2}{\hat{s}} + Q^2 \left(\frac{Q^4 + 2\hat{s}\hat{s}_1}{\hat{u}\hat{t}} \right) + \hat{t} - 3Q^2 + 4\hat{s} \right] \\ &\quad - |C_1(\hat{u})|^2 \left[\frac{Q^6 \hat{u}_1}{\hat{s}\hat{t}\hat{u}} + \frac{\hat{s}^2 + Q^4}{\hat{t}} + \frac{\hat{t}^2 + Q^4}{\hat{s}} - \frac{4\hat{s}\hat{t} - 3Q^4}{\hat{u}} - 3Q^2 \right] \\ &\quad + \operatorname{Re} \left(C_1(\hat{u}) D^*(\hat{s}, \hat{t}) \right) \left[\hat{s}\hat{t} - \hat{s}_1 \hat{t}_1 + Q^2 \left(\frac{\hat{s}_1^2 + \hat{s}^2}{\hat{u}} \right) \right] \\ &\quad - \frac{1}{4} |D(\hat{s}, \hat{t})|^2 \left(2(\hat{s}^3 + \hat{t}^3) - \frac{\hat{s}^2 \hat{t}^2}{\hat{u}} + \frac{\hat{s}\hat{t}}{\hat{u}^2} \left[(\hat{s} + \hat{t})^3 - 2\hat{s}\hat{t}\hat{u} \right] \right). \end{aligned} \quad (4.39)$$

Appendix B: Analytic Limits of Matrix Elements

The partonic cross-section for $q\bar{q} \rightarrow g\Phi$ is

$$\frac{d\hat{\sigma}}{d\hat{t}} = \frac{1}{16\pi\hat{s}^2} \frac{1}{36} |\mathcal{M}|_{q\bar{q} \rightarrow g\Phi}^2, \quad (4.40)$$

where the spin and color average is explicitly given,

$$|\overline{\mathcal{M}}|_{q\bar{q} \rightarrow g\Phi}^2 \equiv \frac{1}{36} |\mathcal{M}|_{q\bar{q} \rightarrow g\Phi}^2. \quad (4.41)$$

For a scalar Higgs,

$$|\mathcal{M}|_{q\bar{q} \rightarrow gH}^2 = \frac{16\alpha_s^3 \hat{t}^2 + \hat{u}^2}{\pi v^2 \hat{s}} |A_{q\bar{q}}^H|^2, \quad (4.42)$$

and

$$A_{q\bar{q}}^H = \sum_j \left\{ \frac{m_j^2}{\hat{s} - M_H^2} \left[2 - \frac{2\hat{s}}{\hat{s} - M_H^2} \left(I_1(\hat{s}/m_j^2) - I_1(M_H^2/m_j^2) \right) \right. \right. \\ \left. \left. + \left(1 + \frac{4m_j^2}{\hat{s} - M_H^2} \right) \left(I_2(\hat{s}/m_j^2) - I_2(M_H^2/m_j^2) \right) \right] \right\}, \quad (4.43)$$

where m_j is the fermion mass in the loop. The integrals are defined by:

$$I_1(a) = \int_0^1 dx \log(1 - ax(1-x)), \quad (4.44)$$

$$I_2(a) = \int_0^1 \frac{dx}{x} \log(1 - ax(1-x)). \quad (4.45)$$

In the large fermion mass limit, $m_j \rightarrow \infty$, [104, 103]

$$A_{q\bar{q}}^H \rightarrow -\frac{1}{3} \left(1 + \frac{1}{120} \frac{11\hat{s} + 7M_H^2}{m_j^2} + \dots \right). \quad (4.46)$$

In the small fermion mass limit, $m_j \rightarrow 0$, [104]

$$A_{q\bar{q}}^H \rightarrow A_{q\bar{q}}^{Hr} + iA_{q\bar{q}}^{Hi}, \quad (4.47)$$

$$A_{q\bar{q}}^{Hr} \rightarrow \frac{2m_j^2}{\hat{s} - M_H^2} \left\{ 1 + \Lambda_s \left(-\frac{\hat{s}}{\hat{s} - M_H^2} \right. \right. \\ \left. \left. + \frac{1}{4} \left(1 + \frac{4m_j^2}{\hat{s} - M_H^2} \right) \left[\Lambda_s - 2 \log \left(\frac{m_j^2}{M_H^2} \right) \right] \right) \right\}, \quad (4.48)$$

$$A_{q\bar{q}}^{Hi} \rightarrow -\frac{m_j^2 \pi}{\hat{s} - M_H^2} \left(1 + \frac{4m_j^2}{\hat{s} - M_H^2} \right) \Lambda_s, \quad (4.49)$$

where $\Lambda_s = \log(\hat{s}/M_H^2)$.

The result for $qg \rightarrow q\Phi$ can be found from crossing,

$$\frac{d\hat{\sigma}}{d\hat{t}} = \frac{1}{16\pi\hat{s}^2} \left(\frac{1}{96} \right) |M|_{qg \rightarrow q\Phi}^2, \quad (4.50)$$

and

$$|\mathcal{M}(\hat{s}, \hat{t}, \hat{u})|_{q\bar{q} \rightarrow g\Phi}^2 = -|\mathcal{M}(\hat{u}, \hat{t}, \hat{s})|_{q\bar{q} \rightarrow g\Phi}^2. \quad (4.51)$$

In the large fermion mass limit, $m_j \rightarrow \infty$ [104, 103],

$$A_{q\bar{q}}^H \rightarrow -\frac{1}{3} \left(1 + \frac{1}{120} \frac{11\hat{u} + 7M_H^2}{m_j^2} + \dots \right) \quad (4.52)$$

In the small fermion mass limit, $m_j \rightarrow 0$,

$$A_{q\bar{q}}^H \rightarrow A_{q\bar{q}}^{Hr} + iA_{q\bar{q}}^{Hi} \quad (4.53)$$

$$A_{q\bar{q}}^{Hr} \rightarrow \frac{2m_j^2}{\hat{u} - M_H^2} \left\{ 1 + \Lambda_u \left(-\frac{\hat{u}}{\hat{u} - M_H^2} + \frac{1}{4} \left(1 + \frac{4m_j^2}{\hat{u} - M_H^2} \right) \left[\Lambda_u - 2 \log \left(\frac{m_j^2}{M_H^2} \right) \right] \right) \right\}, \quad (4.54)$$

$$A_{q\bar{q}}^{Hi} \rightarrow -\frac{2m_j^2 \hat{u} \pi}{(\hat{u} - M_H^2)^2}, \quad (4.55)$$

where $\Lambda_u = \log(|\hat{u}|/M_H^2)$.

The results for pseudoscalar production are found assuming the $\bar{\psi}\psi A^0$ coupling given in Eq. (4.3). The form factor for

$$g(p_1^{\mu_1, a_1}) + g(p_2^{\mu_2, a_2}) \rightarrow A^0(p_5), \quad (4.56)$$

with all moment outgoing and $p_1^2 = 0$, $p_5^2 = M_{A^0}^2$, $(p_1 + p_5)^2 = \hat{s}$, is given by

$$i\Gamma^{\mu_1, \mu_2}(p_1, p_2, p_5) = -\frac{\alpha_s}{2\pi} \frac{g_A m_j^2}{v} \delta_{a_1 a_2} \epsilon^{\alpha\beta\mu_1\mu_2} p_5^\alpha p_2^\beta \times \frac{1}{\hat{s} - M_{A^0}^2} \left\{ I_2(\hat{s}/m_j^2) - I_2(M_{A^0}^2/m_j^2) \right\}. \quad (4.57)$$

The differential cross-section for $q\bar{q} \rightarrow gA^0$ is given by Eq. (4.40), with

$$|\mathcal{M}|_{q\bar{q} \rightarrow gA^0}^2 = \frac{\alpha_s^3}{\pi} g_A^2 \sum_j \frac{4m_j^4}{\hat{s}v^2} \left(1 + \frac{2\hat{t}\hat{u}}{(\hat{s} - M_{A^0}^2)^2} \right) \left| I_2(\hat{s}/m_j^2) - I_2(M_{A^0}^2/m_j^2) \right|^2. \quad (4.58)$$

In the large fermion mass limit, $m_j \rightarrow \infty$ [108],

$$|\mathcal{M}|_{q\bar{q} \rightarrow gA^0}^2 \rightarrow \frac{\alpha_s^3}{\pi} g_A^2 \frac{1}{\hat{s}v^2} \left(2\hat{t}\hat{u} + (\hat{s} - M_{A^0}^2)^2 \right) \left[1 + \frac{\hat{s} + M_{A^0}^2}{6m_j^2} + \dots \right]. \quad (4.59)$$

In the small fermion mass limit, $m_j \rightarrow 0$,

$$\begin{aligned}
|\mathcal{M}|_{q\bar{q} \rightarrow gA^0}^2 &\rightarrow \frac{\alpha_s^3}{\pi} g_A^2 \frac{1}{\hat{s} v^2} \left(1 + \frac{2\hat{t}\hat{u}}{(\hat{s} - M_{A^0}^2)^2} \right) m_j^4 \\
&\times \Lambda_s^2 \left\{ \left[\Lambda_s - 2 \log \left(\frac{m_j^2}{M_{A^0}^2} \right) \right]^2 + 4\pi^2 \right\}, \tag{4.60}
\end{aligned}$$

where $\Lambda_s = \log(\hat{s}/M_{A^0}^2)$.

Part II

Resummation and the Higgs Boson

Chapter 5

Next-to-leading Log Resummation of Scalar and Pseudoscalar Higgs Boson Differential Cross-Sections at the LHC and Tevatron

The region of small transverse momentum in $q\bar{q}$ - and gg -initiated processes must be studied in the framework of resummation to account for the large, logarithmically-enhanced contributions to physical observables. In this paper, we will calculate the fixed order next-to-leading order (NLO) perturbative total and differential cross-sections for both a Standard Model (SM) scalar Higgs boson and the Minimal Supersymmetric Standard Model's (MSSM) pseudoscalar Higgs boson in the Heavy Quark Effective Theory (HQET) where the mass of the top quark is taken to be infinite. Resummation coefficients $B_g^{(2)}, C_{gg}^{(2)}$ for the total cross-section resummation for the pseudoscalar case are given, as well as $\bar{C}_{gg}^{(1)}$ for the differential cross-section.

5.1 Introduction

The discovery of one or more Higgs bosons is the central research interest for high energy physics programs at hadron colliders around the world. Beyond the phenomenology of the Standard Model (SM) Higgs boson, the Minimal Supersymmetric Standard Model (MSSM) which is a special case of the Two Higgs Doublet Model (2HDM) is of particular interest to theorists. For a review see Ref. [64, 117].

Very recently, a new central value for the top quark mass was reported [118]. This changed the exclusion limits on the SM Higgs boson, putting its central mass value from precision electroweak fits at $117 \text{ GeV}/c^2$. This is exciting because this value is above the exclusion limits from the LEP direct searches which exclude the mass of a SM-like Higgs boson below approximately $114 \text{ GeV}/c^2$ [99]. In the MSSM there are five physical Higgs bosons; a light and a heavy scalar (h^0, H^0), two charged scalars (H^\pm), and a CP-odd pseudoscalar (A^0). The mass of the pseudoscalar is excluded [119] from being lighter than $92 \text{ GeV}/c^2$. The ratio between the vacuum expectation values (VEVs) of the two neutral Higgs bosons of the MSSM is defined as $\tan\beta = v_2/v_1$. For $m_{\text{top}} = 174.3 \text{ GeV}/c^2$, $0.5 < \tan\beta < 2.4$ has been excluded by the LEP Higgs searches. The bounds on $\tan\beta$ will change as the central value of the top mass changes. A full analysis of the $\tan\beta$ exclusion bounds for the new top mass of $m_{\text{top}} = 178.0 \text{ GeV}/c^2$ is not yet available. In this paper, we will leave $\tan\beta = 1$ so that the pseudoscalar results can easily be scaled by an appropriate number of interest to the reader, and the mass of the Higgs bosons will be set to $M_\Phi = 120 \text{ GeV}/c^2$, where Φ is the Higgs boson of interest.

In the context of resummation, the literature has focused on the scalar Higgs boson [106, 110, 120–132]. This paper will provide resummation coefficients for the pseudoscalar Higgs boson for the total cross-section and differential distributions. Our calculations are done in the Heavy Quark Effective Theory (HQET) where the mass of the top quark is taken to be infinite. The role of the bottom quark in pseudoscalar production becomes dominant at large $\tan\beta$. In order to correctly take the bottom quark into account at this order, massive resummation coefficients will have to be determined. This will be reserved for another discussion.

In Section (5.2), we will introduce the Heavy Quark Effective Theory (HQET) in which our calculations were performed. In Section (5.3), we will introduce our resummation conventions and present our new results for pseudoscalar resummation. Finally, in Section (5.4) we will present our numeric results for the differential distributions for the SM scalar and MSSM pseudoscalar Higgs boson at the Large Hadron Collider (LHC) and Tevatron in the HQET.

5.2 Heavy Quark Effective Theory

Higgs phenomenology in QCD lends itself well to the use of Heavy Quark Effective Theory (HQET). When only the top quark is considered in calculations, it is possible to replace the top quark loops by an effective vertex when the other quarks are ignored. The role of the bottom quark in Higgs

physics has recently been examined in great detail [133, 134], but will not be included in this paper. The Lagrangian that describes this effective vertex can be derived from the $gg \rightarrow \Phi$ (where Φ is a Higgs boson of interest) triangle diagram [135–138] and letting the mass of the quark become infinitely heavy at the end of the calculation [139–141]. The Higgs of interest could be the SM scalar Higgs, or the pseudoscalar Higgs of the MSSM. In principle, the light and heavy scalar Higgs of the MSSM can be included in this formalism in place of the SM Higgs by multiplying by the appropriate coupling factor. However, supersymmetric corrections within the MSSM will not be included in this paper, only SM QCD corrections will be included.

The HQET method allows for the inclusion of the $\mathcal{O}(\epsilon)$ terms which are important for deriving resummation coefficients. This program leads to the effective Lagrangian in $d = 4 - 2\epsilon$ dimensions for a scalar Higgs boson

$$\mathcal{L}_{\text{eff}}^H = -\frac{1}{4}g_H H G_{\mu\nu}^a G^{a,\mu\nu} \left(\frac{4\pi\mu_r^2}{m_{\text{top}}^2} \right)^\epsilon \Gamma(1 + \epsilon) \quad (5.1)$$

where $g_H = \alpha_s/3\pi v$ is the coupling of the effective vertex at LO, $G^{a,\mu\nu}$ is the field-strength tensor for the gluons, μ_r is the renormalization scale, and the vacuum expectation value (VEV) of the Higgs is defined as $v^2 = (\sqrt{2}G_F)^{-1} \simeq 246$ GeV. The effective coupling receives order by order corrections that have been calculated [90, 110] previously. The appearance of the top quark mass in this expression hints that the corrections to the effective coupling at higher order may include logarithmic corrections including the top quark mass, which is the case. Alternatively, we can define $1/v^2 = 6422.91$ pb, which is convenient in cross-section calculations. This effective Lagrangian generates effective vertices with two, three, and four gluons with a scalar Higgs boson. The Feynman rules for a scalar Higgs can be found in the literature [66].

When a pseudoscalar Higgs boson is considered, the effective Lagrangian changes due to the γ_5 coupling and can be written

$$\mathcal{L}_{\text{eff}}^{A^0} = \frac{1}{4}g_{A^0} A^0 G_{\mu\nu}^a \tilde{G}^{a,\mu\nu} \left(\frac{4\pi\mu_r^2}{m_{\text{top}}^2} \right)^\epsilon \Gamma(1 + \epsilon) \quad (5.2)$$

where $g_{A^0} = \alpha_s/2\pi v$ is the coupling of the effective vertex. The $\tilde{G}^{a,\mu\nu} = 1/2 \epsilon^{\mu\nu\rho\sigma} G_{\rho\sigma}^a$ operator is the dual of the usual gluon field-strength tensor. It is important to note that the four gluon plus pseudoscalar Higgs vertex is absent in this effective Lagrangian as its Feynman rule is proportional to a completely antisymmetric combination of structure functions and therefore vanishes. It should be noted that this is the LO effective Lagrangian, and that a second operator begins to contribute at higher orders. A complete discussion can be found in Ref. [93]. The Feynman rules for the pseudoscalar can be found in

the literature [71]. The Feynman rules listed in this reference should be used with $g_{A^0} = \alpha_s/2\pi v$ to avoid a spurious extra factor of 1/4.

If we define $z = M_\Phi^2/\hat{s}$ where \hat{s} is the partonic center of momentum energy squared, the partonic total cross-section for Higgs production (either scalar or pseudoscalar written here generically as Φ) from the fusion of two partons a and b can be written as a series expansion in α_s as

$$\begin{aligned}\hat{\sigma}(ab \rightarrow \Phi + X) &= \hat{\sigma}_0^\Phi \Delta_{ab \rightarrow \Phi} \\ &= \hat{\sigma}_0^\Phi \left(\delta_{ag} \delta_{bg} \delta(1-z) + \frac{\alpha_s}{\pi} \Delta_{ab \rightarrow \Phi}^{(1)}(z) \right. \\ &\quad \left. + \left(\frac{\alpha_s}{\pi} \right)^2 \Delta_{ab \rightarrow \Phi}^{(2)}(z) + \mathcal{O}(\alpha_s^3) + \dots \right),\end{aligned}\quad (5.3)$$

where $\hat{\sigma}_0^\Phi$ is the LO partonic total cross-section, and the $\Delta_{ab \rightarrow \Phi}^{(n)}(z)$ coefficients are higher order corrections.

The NNLO corrections for both the scalar and pseudoscalar Higgs bosons have been calculated in the HQET [74, 77, 102]. Although the next-to-leading order corrections have been calculated in several places [69–71, 79, 91, 107, 121, 123], there are some discrepancies in the literature that we would like to clear up in this paper. For this reason, we will explicitly calculate the NLO corrections for the gg initial state. The importance of this particular channel, beyond its relevance to high-energy hadron collisions, will be addressed later. The partonic cross-section at NLO has to be written as the sum of the real emissions, the virtual corrections, the charge renormalization, and Altarelli-Parisi subtractions as follows

$$\hat{\sigma}_{\text{NLO}} = \hat{\sigma}_{\text{real}} + \hat{\sigma}_{\text{virt}} + \hat{\sigma}_{\text{ren}} + \hat{\sigma}_{\text{AP}}. \quad (5.4)$$

Although a few very thorough treatments for the scalar case exist in the literature [69, 70], we will re-derive them here to highlight differences in the pseudoscalar case, where an exhaustive treatment is missing. We will follow closely the discussion in these references. We will see that only the gg channel will play a role in the resummation formalism.

5.2.1 Scalar Higgs Matrix Elements

Suppressing $\mathcal{O}(\epsilon)$ terms for now, the matrix elements for scalar Higgs production in the HQET can be written as [69–71, 79, 91, 107, 121, 123]

$$\mathcal{M}(g(p_1^{\mu,A}) + g(p_2^{\nu,B}) \rightarrow H) = -\frac{\alpha_s}{3\pi v} \delta^{AB} \left(\eta^{\mu\nu} \frac{M_H^2}{2} - p_1^\nu p_2^\mu \right) \epsilon_\mu(p_1) \epsilon_\nu(p_2). \quad (5.5)$$

Here $AB(\mu\nu)$ are the color (Lorentz) indices of the incoming gluons. When the matrix elements are squared, the contraction of the delta functions yields a factor of $\delta^{AB}\delta_{AB} = N_c^2 - 1 = 8$, the contraction of the metric yields $\eta^{\mu\nu}\eta_{\mu\nu} = d$. This yields the squared matrix elements (before any color-spin averaging)

$$|\mathcal{M}(gg \rightarrow H)|^2 = \frac{\alpha_s^2 M_H^4 (N_c^2 - 1)}{16\pi^2 v^2} \left(\frac{4\pi\mu_r^2}{m_{\text{top}}^2} \right)^{2\epsilon} \Gamma^2(1 + \epsilon)(1 - \epsilon). \quad (5.6)$$

In this $2 \rightarrow 1$ process, it is easiest to calculate the decay width of the Higgs and convert that to a partonic total cross-section. We need to color and spin average the matrix elements squared noting that the gluon-gluon initial state must be averaged over $4(1 - \epsilon)^2$ transverse polarizations. We can write the partonic cross-section in terms of the decay width and simply add $\delta(1 - z)$ since $z = M_H^2/\hat{s} = 1$ at threshold, so that [69]

$$\begin{aligned} \hat{\sigma}_0^H(gg \rightarrow H) &= \frac{\pi^2}{8M_H^3} \Gamma(H \rightarrow gg) \\ &= \left(\frac{\alpha_s}{\pi} \right)^2 \frac{\pi}{576v^2} \left(\frac{4\pi\mu_r^2}{m_{\text{top}}^2} \right)^{2\epsilon} \frac{\Gamma^2(1 + \epsilon)}{1 - \epsilon}. \end{aligned} \quad (5.7)$$

This factor (with its ϵ dependence) will be pulled from each of the higher order correction factors. The LO cross-section in the HQET starts at $\mathcal{O}(\alpha_s^2)$.

Radiative Corrections

At the next order in perturbation theory, there are qg and $q\bar{q}$ initial state processes. However, as we will see later, we are only interested in the gg initial state, so we will only calculate the NLO corrections to the gg initial state process.

The real contributions at NLO to the gg initial state come from the process $gg \rightarrow gH$ which was originally calculated in the $\epsilon \rightarrow 0$ limit in the full theory including a finite mass top quark in Ref. [103,104]. We can write the amplitude as,

$$g(p_1^{A,\mu}) + g(p_2^{B,\nu}) \rightarrow g(-p_3^{C,\sigma}) + H(-p_5) \quad (5.8)$$

If we define the partonic (with hats) kinematic variables in terms of the Higgs momentum so that our differential cross-section can be written in terms of the Higgs transverse momentum as $\hat{s} = (p_1 + p_2)^2$, $\hat{t} = (p_1 + p_5)^2$, and $\hat{u} = (p_2 + p_5)^2$. The matrix elements take the symmetric form [69–71, 79, 91,

107, 121, 123]

$$\begin{aligned}
|\mathcal{M}(gg \rightarrow gH)|^2 &= \frac{\alpha_s^3 4N_c(N_c^2 - 1)}{v^2 9\pi} \left(\frac{4\pi\mu_r^2}{m_{\text{top}}^2} \right)^{2\epsilon} \Gamma^2(1 + \epsilon) \\
&\times \left\{ \left[\frac{M_H^8 + \hat{s}^4 + \hat{t}^4 + \hat{u}^4}{\hat{s}\hat{t}\hat{u}} \right] (1 - 2\epsilon) \right. \\
&\quad \left. + \frac{\epsilon}{2} \left[\frac{(M_H^4 + \hat{s}^2 + \hat{t}^2 + \hat{u}^2)^2}{\hat{s}\hat{t}\hat{u}} \right] \right\}. \tag{5.9}
\end{aligned}$$

Color and spin averaging gives an additional factor of $1/256/(1 - \epsilon)^2$. By pulling out the LO cross-section from the expression, we can write the properly averaged matrix elements (where the overbar corresponds to color and spin averaging)

$$\begin{aligned}
|\overline{\mathcal{M}}(gg \rightarrow gH)|^2 &= \hat{\sigma}_0^H \frac{\alpha_s}{\pi} \frac{N_c(N_c^2 - 1)}{1 - \epsilon} \left\{ \left[\frac{M_H^8 + \hat{s}^4 + \hat{t}^4 + \hat{u}^4}{\hat{s}\hat{t}\hat{u}} \right] (1 - 2\epsilon) \right. \\
&\quad \left. + \frac{\epsilon}{2} \left[\frac{(M_H^4 + \hat{s}^2 + \hat{t}^2 + \hat{u}^2)^2}{\hat{s}\hat{t}\hat{u}} \right] \right\}. \tag{5.10}
\end{aligned}$$

First, let us find the differential cross-section. The LO differential cross-section involves $2 \rightarrow 2$ kinematics and can be written with the $4 - 2\epsilon$ phase space dimensions as [123]

$$\frac{d\hat{\sigma}^H}{d\hat{t}} = \frac{1}{16\pi\hat{s}^2} \left(\frac{4\pi\mu_r^2}{M_H^2} \right)^\epsilon \frac{1}{\Gamma(1 - \epsilon)} \left(\frac{\hat{s}M_H^2}{\hat{u}\hat{t}} \right)^\epsilon |\overline{\mathcal{M}}|^2. \tag{5.11}$$

As we will see in Sec. (5.3), it is the small p_t behavior of this expression that we will be interested in. If we insert the expression $\hat{u}\hat{t} = \hat{s}p_t^2$ and drop the terms proportional to p_t , we find an expression for the differential cross-section in the small p_t limit. Once we have changed variables, we find the partonic differential cross-section in the small p_t region (where we are suppressing the trivial rapidity dependence)

$$\frac{d\hat{\sigma}^H}{dp_t^2} = \hat{\sigma}_0^H \frac{\alpha_s}{\pi} \left(\frac{4\pi\mu_r^2}{M_H^2} \right)^\epsilon \frac{z}{(1 - \epsilon)\Gamma(1 - \epsilon)} \left(\frac{M_H^2}{p_t^2} \right)^\epsilon \left[C_A \frac{1}{p_t^2} \ln \left(\frac{M_H^2}{p_t^2} \right) - \beta_0 \frac{1}{p_t^2} \right]. \tag{5.12}$$

We will see that this representation will make it particularly simple to extract the resummation coefficients $A_g^{(1)}$ and $B_g^{(1)}$ for the differential distribution. These coefficients will be the same for the total cross-section as well. Turning our attention back to the expression we had for the matrix elements squared, we would like to calculate the real corrections for the NLO total partonic cross-section. The matrix elements for the real emission needs to be integrated and can be written as [69]

$$\hat{\sigma} = \frac{1}{2\hat{s}} \int |\overline{\mathcal{M}}|^2 d\text{PS}_2. \quad (5.13)$$

For a $2 \rightarrow 2$ process, this can be done by introducing the following parameterization for the angular integration. If we write the scattering angle θ as $\cos \theta = 2\omega - 1$, this maps the θ integration to an ω integration between 0 and 1. We can express the kinematic invariants as follows

$$\hat{t} = -\hat{s}(1-z)(1-\omega), \quad \hat{u} = -\hat{s}(1-z)\omega, \quad (5.14)$$

and do the phase space integrations using the following parameterization

$$d\text{PS}_2 = \frac{1}{8\pi} \left(\frac{4\pi\mu_r^2}{\hat{s}} \right)^\epsilon \frac{(1-z)^{1-2\epsilon}}{\Gamma(1-\epsilon)} \int_0^1 \omega^{-\epsilon} (1-\omega)^{-\epsilon} d\omega \quad (5.15)$$

which reduces the angular integration into repeated applications of Euler's beta function integral, where additional integer powers of ω and $(1-\omega)$ are introduced from the kinematic variables \hat{t} and \hat{u} ,

$$\int_0^1 d\omega \omega^\alpha (1-\omega)^\beta = \frac{\Gamma(1+\alpha)\Gamma(1+\beta)}{\Gamma(2+\alpha+\beta)}. \quad (5.16)$$

Turning our attention back to the real emissions, we find the color and spin averaged partonic total cross-section, after regulating the singularity at $z = 1$ with a plus distribution, can be written as

$$\begin{aligned} \hat{\sigma}_{\text{real}}^H &= \hat{\sigma}_0^H \left(\frac{\alpha_s}{\pi} \right) \left(\frac{4\pi\mu_r^2}{\hat{s}} \right)^\epsilon \Gamma(1+\epsilon) \\ &\times C_A \left\{ \left[\frac{1}{\epsilon^2} + \frac{1}{\epsilon} + 1 - 2\zeta_2 \right] \delta(1-z) \right. \\ &\quad - \frac{2z}{\epsilon} \left[z\mathcal{D}_0(z) + \frac{1-z}{z} + z(1-z) \right] - \frac{11}{6}(1-z)^3 \\ &\quad + 2 \left[1 + z^4 + (1-z)^4 \right] \mathcal{D}_1(z) \\ &\quad \left. - 2 \left[1 - z + 2z^2 + z^4 \mathcal{D}_0(z) \right] \right\} + \mathcal{O}(\epsilon), \quad (5.17) \end{aligned}$$

where the plus prescription is defined as usual

$$\int_0^1 dx f(x)[g(x)]_+ = \int_0^1 dx g(x)[f(x) - f(1)], \quad (5.18)$$

and we have introduced the common abbreviation

$$\mathcal{D}_n(z) \equiv \left(\frac{\ln^n(1-z)}{1-z} \right)_+. \quad (5.19)$$

Virtual Corrections

Next, we must calculate the virtual contributions. There are two diagrams with gluon loops (a gluon triangle and a four point incoming state as can be seen in Ref. [69]), and can be calculated directly. We can write the integrated virtual contribution that contributes at α_s^3 to the total partonic cross-section in the same fashion as the real emissions [69–71, 79, 91, 107, 121, 123]

$$\hat{\sigma}_{\text{virt}} = \hat{\sigma}_0 \left(\frac{\alpha_s}{\pi} \right) \left(\frac{4\pi\mu_r^2}{M_H^2} \right)^\epsilon \Gamma(1 + \epsilon) C_A \left\{ \left[-\frac{1}{\epsilon^2} - \frac{1}{\epsilon} + \frac{5}{6} + 4\zeta_2 \right] \delta(1 - z) \right\}. \quad (5.20)$$

As expected, the ϵ^2 singularities cancel between the real emission and virtual graphs. It will turn out that the differences between the fixed order results for the scalar and the pseudoscalar come from different virtual corrections. These virtual contributions will be needed to cancel some ϵ poles in the expression we will derive to determine the process dependent resummation coefficients, in particular $C_{gg}^{(1)}$ for the differential distribution.

Total cross-section

The remaining $1/\epsilon$ singularities must be removed to find the partonic total cross-section. The poles are cancelled in the charge (coupling) renormalization and the Altarelli-Parisi subtraction. Understanding the charge renormalization tells us why it was so important to have the $\mathcal{O}(\epsilon)$ terms of the lowest order cross-section. We can see that the counter-term can be written [69, 70]

$$\hat{\sigma}_{\text{ren}} = (4Z_g)\hat{\sigma}_0, \quad Z_g = -\frac{\alpha_s}{\epsilon}(4\pi)^{\epsilon-1}\Gamma(1 + \epsilon)\beta_0, \quad \beta_0 = \frac{11}{6}C_A - \frac{2}{3}n_f T_R, \quad (5.21)$$

where $n_f = 5$ since the top quark has been integrated out. These equations hold with the $\overline{\text{MS}}$ renormalization conditions.

The Altarelli-Parisi subtraction factors out the soft and collinear singularities into the PDFs much like the factorization process separates the short and long distance physics in hadron-hadron scattering. This cancels the rest of the $1/\epsilon$ poles and gives us the final expression for the total cross-section

$$\begin{aligned} \hat{\sigma}_{\text{NLO}}(gg \rightarrow H + X) = & \hat{\sigma}_0^H \left\{ \delta(1 - z) + \left(\frac{\alpha_s}{\pi} \right) \left[\left(\frac{11}{6}C_A + 2C_A\zeta_2 \right) \delta(1 - z) \right. \right. \\ & - \frac{11}{6}C_A(1 - z)^3 + 2C_A \left[1 + z^4 + (1 - z)^4 \right] \mathcal{D}_1(z) \\ & \left. \left. + 2C_A \left(z^2 \mathcal{D}_0(z) + (1 - z) + z^2(1 - z) \right) \ln \frac{M_H^2}{z\mu^2} \right] \right\} + \mathcal{O}(\epsilon). \quad (5.22) \end{aligned}$$

Our expressions for the resummation coefficients show their full color dependence. It is sufficient to notice at this stage that the term proportional to the $\delta(1-z)$ in the correction can be evaluated as $11/2 + \pi^2$ when we use

$$C_A = N_c, \quad C_F = \frac{N_c^2 - 1}{2N_c}, \quad T_R = \frac{1}{2}. \quad (5.23)$$

5.2.2 Pseudoscalar Higgs Matrix Elements

There are many reasons for our primary interest to be the pseudoscalar Higgs boson. In the MSSM, the exact roles the top and bottom quarks play in the differential cross-section is complicated [134]. However, in much of the parameter space in the MSSM, the cross-section for the pseudoscalar is larger than the lightest scalar Higgs boson in the MSSM. If supersymmetry does exist in nature, the pseudoscalar Higgs may be the first Higgs boson discovered due to its larger cross-section. If supersymmetry becomes important only at very high scales, then seeing a pseudoscalar Higgs would be the first evidence of supersymmetry in nature. This leads us to investigate in detail pseudoscalar resummation.

We should also mention that because of the importance of the bottom quark in calculations involving the MSSM pseudoscalar (and the lightest scalar Higgs in the MSSM as well) when the parameter $\tan\beta$ is large is systematically ignored in these calculations. To remedy this situation, one would have to calculate the resummation coefficients in the full theory. In principle, these coefficients can be extracted from Ref. [91]. However, these results have not been published.

The difference in the lowest order (LO) partonic cross-section of the pseudoscalar Higgs boson and the scalar Higgs boson can be traced to the difference in the effective couplings g_H and g_{A^0} and a factor of $9/4$. This can be written as [71]

$$\begin{aligned} \hat{\sigma}_0^{A^0}(gg \rightarrow A^0) &= \frac{9}{4} \hat{\sigma}_0^H(gg \rightarrow H) \\ &= \left(\frac{\alpha_s}{\pi}\right)^2 \frac{\pi}{256v^2} \left(\frac{4\pi\mu_r^2}{m_{\text{top}}^2}\right)^{2\epsilon} \frac{\Gamma^2(1+\epsilon)}{1-\epsilon} \delta(1-z). \end{aligned} \quad (5.24)$$

Upon the expansion of the $\mathcal{O}(\epsilon)$ terms, we see they do not effect the final answer as expected at the lowest order.

Radiative Corrections

The matrix elements for the production of the pseudoscalar in the HQET are slightly more complicated in $d = 4 - 2\epsilon$ dimensions due to the presence of the

intrinsically 4-dimensional Levi-Civita tensor in the Feynman rules [71] coming from the $\tilde{G}^{a,\mu\nu}$ term in the effective Lagrangian. There are several conventions for handling this problem [111–113, 142]. We have chosen the scheme defined in Ref. [111–113].

For the radiative corrections, we can separate all the vectors into 4- and $(d-4)$ -dimensional components. We label the $(d-4)$ -dimensional components of the vectors with a twiddle. We can take the incoming momentum to be 4-dimensional as a convenient choice of frame, which simplifies the results considerably [71].

The (un-averaged) matrix elements can be written,

$$|\mathcal{M}(gg \rightarrow gA^0)|^2 = \frac{\alpha_s^3 N_c(N_c^2 - 1)}{v^2 \pi} \left(\frac{4\pi\mu_r^2}{m_{\text{top}}^2} \right)^{2\epsilon} \Gamma^2(1 + \epsilon) \times \left\{ \left[\frac{M_{A^0}^8 + \hat{s}^4 + \hat{t}^4 + \hat{u}^4}{\hat{s}\hat{t}\hat{u}} \right] + \frac{2\hat{s}(\hat{t}^2 + \hat{u}^2)(\tilde{p}_3 \cdot \tilde{p}_3 \hat{s} - \hat{t}\hat{u}\epsilon)}{\hat{t}^2\hat{u}^2} \right\}. \quad (5.25)$$

We can see that the $\epsilon \rightarrow 0$ corrections are identical in the scalar and pseudoscalar case for the real emissions. We can also see that the residual difference is not only proportional to ϵ , but rather proportional to ϵ and the $(d-4)$ -dimensional component of the p_3 vector, which vanishes in the 4-dimensional limit.

From this analysis, we can see that the real part of the differential cross-section for the pseudoscalar Higgs boson will be identical to the scalar case in Equation (5.12) with a 9/4 difference in normalization.

Virtual Corrections

The virtual corrections to the pseudoscalar have the same diagrams as the scalar at this order, but there is a slight difference in the result. This difference is due to the fact that the diagram with the four point gluon vertex vanishes due to the antisymmetry of the ggA^0 vertex in the effective theory. The integrated result is

$$\hat{\sigma}_{\text{virt}}^{A^0} = \hat{\sigma}_0^{A^0} \left(\frac{\alpha_s}{\pi} \right) \left(\frac{4\pi\mu_r^2}{M_H^2} \right)^\epsilon \Gamma(1 + \epsilon) C_A \left\{ \left[-\frac{1}{\epsilon^2} - \frac{1}{\epsilon} + 2 + 4\zeta_2 \right] \delta(1 - z) \right\}. \quad (5.26)$$

We can see that although the pole terms are the same, the finite terms have changed slightly because of the “missing” diagram.

Total cross-section

When we combine our pseudoscalar results, we find that the total partonic cross-section that is identical to the scalar case with the exception of the small numeric difference in the $\delta(1-z)$ term. The expression changes from $11/6C_A + 2C_A\zeta_2 \rightarrow 2C_A + 2C_A\zeta_2$ in the pseudoscalar case. Here we see the factor $11/2 \rightarrow 6$, which would seem to be a small difference, but it is mostly a coincidence of the SU_3 Casimir invariants.

The partonic cross-section can be written as

$$\begin{aligned} \hat{\sigma}_{\text{NLO}}^{A^0}(gg \rightarrow A^0 + X) = & \hat{\sigma}_0^{A^0} \left\{ \delta(1-z) + \left(\frac{\alpha_s}{\pi} \right) \left[\left(2C_A + 2C_A\zeta_2 \right) \delta(1-z) \right. \right. \\ & - \frac{11}{6}C_A(1-z)^3 + 2C_A \left[1 + z^4 + (1-z)^4 \right] \mathcal{D}_1(z) \\ & \left. \left. + 2C_A \left(z^2 \mathcal{D}_0(z) + (1-z) + z^2(1-z) \right) \ln \frac{M_H^2}{z\mu^2} \right] \right\} + \mathcal{O}(\epsilon). \quad (5.27) \end{aligned}$$

Now that we have expressions for the total partonic cross-sections for both the scalar and the pseudoscalar Higgs boson we see that the only difference between the two lies in the correction proportional to $\delta(1-z)$ at NLO and in the normalization. This difference in the $\delta(1-z)$ factors is numerically small and is α_s suppressed, leaving us to believe that the primary difference is going to be factor of $9/4$ in the LO partonic cross-sections.

5.3 Resummation

To introduce the machinery behind resummation [143–145], we need to define the hadronic cross-section. This is the convolution of parton distribution functions (PDFs) with the partonic cross-section

$$\begin{aligned} \sigma(S, M_\Phi^2) = & \sum_{a,b} \int_{x_{1,\min}}^1 dx_1 \int_{x_{2,\min}}^1 dx_2 f_{a/h_1}(x_1, \mu_f) f_{b/h_2}(x_2, \mu_f) \\ & \times \int_0^1 dz z \hat{\sigma}_0^\Phi \Delta_{ab \rightarrow \Phi}(z, \mu_r, \mu_f) \quad (5.28) \end{aligned}$$

where μ_r and μ_f are the renormalization and factorization scales respectively, and f_{a/h_1} is the parton distribution function for finding a parton a in hadron h_1 . We must also remember that there is a $\delta(1-z)$ in the definition of the LO cross-section $\hat{\sigma}_0^\Phi$. The minimum partonic energy fraction $x_{(1,2),\min}$ is defined so that there is enough center of momentum energy to create the desired final state particles. A similar equation can be written for the differential distribution.

Implicitly, the partonic cross-section contains logarithmic corrections that are formally singular at threshold ($z \rightarrow 1$). The differential cross-section contains corrections that are singular as the transverse momentum of the Higgs particle vanishes. They can be written in the form

$$\text{threshold} \sim \alpha_s^n \frac{\ln^{2n-1}(1-z)}{(1-z)}, \quad \text{recoil} \sim \frac{\alpha_s^n}{p_t^2} \ln^{2n-1} \frac{M_\Phi^2}{p_t^2}, \quad (5.29)$$

and various powers of these combinations. It can be seen then that the normal fixed order cross-section calculation diverges (in one direction or the other) at small p_t due to large logarithms, and therefore it is not reliable in this region. The systematic way of handling these formally divergent terms at small p_t is known as resummation. Because of this divergent behavior, one is not usually able to integrate the differential cross-section all the way down to $p_t = 0$ or to reliably understand the differential cross-section in the experimentally interesting small p_t region. Resummation coefficients can be determined for both differential distributions and total-cross sections to address this problem.

5.3.1 Formalism

The resummation formalism allows the small p_t cross-section to be written as a power series in both universal and process dependent coefficients. We write the resummed differential cross-section for a $c\bar{c} \rightarrow \Phi$ process (where c in this case represents a gluon or a quark)

$$\begin{aligned} \frac{d\sigma^{\text{resum}}}{dp_t^2 dy d\phi} &= \sum_{a,b} \int_{x_{1,\min}}^1 dx_1 \int_{x_{2,\min}}^1 dx_2 \int_0^\infty db \frac{b}{2} J_0(bp_t) \\ &\times f_{a/h_1}(x_1, b_0/b) f_{b/h_2}(x_2, b_0/b) \frac{S}{Q^2} W_{ab}(x_1 x_2 S; Q, b, \phi), \end{aligned} \quad (5.30)$$

with,

$$\begin{aligned} W_{ab}(s; Q, b, \phi) &= \sum_c \int_0^1 dz_1 \int_0^1 dz_2 \bar{C}_{ca}(\alpha_s(b_0/b), z_1) \bar{C}_{\bar{c}b}(\alpha_s(b_0/b), z_2) \\ &\times \delta(Q^2 - z_1 z_2 s) \frac{d\sigma_{\bar{c}c}^{LO}}{d\phi} S_c(Q, b), \end{aligned} \quad (5.31)$$

where the Higgs mass $M_\Phi^2 = Q^2$, $d\phi$ is the phase space of the system under consideration, and $\hat{\sigma}_{\bar{c}c}^{(LO)}$ is the lowest order cross-section with a $c\bar{c}$ initial state which is therefore defined at $p_t = 0$. The constant b_0 is written in terms of the Euler-Mascheroni constant $\gamma_E = 0.57721\dots$ as $b_0 = 2e^{-\gamma_E}$. In the resummation formalism only the gg and $q\bar{q}$ initial states are needed to determine

the hadronic differential distribution at small p_t . The qg initial states are accounted for in the cross terms in the convolution. The coefficients C_{ab} are process dependent and can be written as power series to be described below. $J_0(bp_t)$ is the first order Bessel function. The Sudakov form factor S_c , which makes the integration over the Bessel function convergent, can be written as

$$S_c(Q, b) = \exp \left\{ - \int_{b_0^2/b^2}^{Q^2} \frac{dq^2}{q^2} \left[A_c(\alpha_s(q)) \ln \frac{Q^2}{q^2} + B_c(\alpha_s(q)) \right] \right\}. \quad (5.32)$$

The coefficient functions A_c , B_c , and C_{ab} can be written as power series in α_s as

$$A_c(\alpha_s) = \sum_{n=1}^{\infty} \left(\frac{\alpha_s}{\pi} \right)^n A_c^{(n)}, \quad B_c(\alpha_s) = \sum_{n=1}^{\infty} \left(\frac{\alpha_s}{\pi} \right)^n B_c^{(n)}, \quad (5.33)$$

$$\bar{C}_{ab}(\alpha_s, z) = \delta_{ab} \delta(1-z) + \sum_{n=1}^{\infty} \left(\frac{\alpha_s}{\pi} \right)^n \bar{C}_{ab}^{(n)}(z). \quad (5.34)$$

The $A_c^{(1)}$, $A_c^{(2)}$, and $B_c^{(1)}$ coefficients have been shown to be universal. There are several conventions in the literature as to whether to expand in terms of α_s/π or $\alpha_s/2\pi$ (or even $\alpha_s/4\pi$ in Ref. [102]). We have chosen to expand in α_s/π . It would seem that several typos exist in the literature due to this numeric expansion factor. We have derived the previously unknown coefficients $B_g^{(2)}$, $C_{gg}^{(1)}$ and $C_{gg}^{(2)}$ for pseudoscalar Higgs production for the total cross-section and the $\bar{C}_{gg}^{(1)}$ for the differential cross-section resummation given below. Here we must stop to address a question of notation. It is unfortunate that we have the same notation for the resummation coefficients for both the p_t resummation and the total cross-section resummation. It would be convenient to use a calligraphic font for the p_t coefficients, but several authors have used this font in other contexts dealing with resummation. Therefore, we will put bars over the resummation coefficients for differential cross-sections even if they are identical to the coefficients for the total cross-section resummation.

To determine the $\bar{C}^{(n)}$ coefficients for the differential cross-section, one must understand the meaning of the resummation formula. We can expand Equation (5.30) order by order in α_s and compare to the perturbative calculation to read off the coefficients [127]. To extract the coefficients from the perturbative results, we need to integrate the differential cross-section around $p_t = 0$ paying careful attention to the use of the Altarelli-Parisi splitting functions near $p_t = 0$ as follows

$$\Delta\hat{\sigma} = \int_0^{q_t^2} dp_t^2 \frac{d\hat{\sigma}}{dp_t^2}. \quad (5.35)$$

This expression will contain ϵ poles and virtual corrections at the next order will be needed to be added to find a finite expression. This is demonstrated later in this paper. One should also be careful to use this formula with other quantities that show the same rapidity dependence. When we expand to $\mathcal{O}(\alpha_s)$, we can see that the NLL coefficients emerge as follows for a $c\bar{c}$ initial state

$$\Delta\hat{\sigma}_{c\bar{c}} = 1 + \frac{\alpha_s}{\pi} \left[-\frac{\bar{A}_c^{(1)}}{2} \ln^2\left(\frac{M_\Phi^2}{q_t^2}\right) - \bar{B}_c^{(1)} \ln\left(\frac{M_\Phi^2}{q_t^2}\right) + 2\bar{C}_{c\bar{c}}^{(1)} \right]. \quad (5.36)$$

In principle, it is possible to continue this process to higher orders to obtain the needed coefficients for the differential cross-section. The NLO corrections to the differential cross-section are known [79, 106], however the NNLO differential cross-section for Higgs production is currently unknown. However, the total cross-section is known to NNLO, so the resummation coefficients for the total cross-section can be determined to NNLL. The NLO differential cross-section in Ref. [106] has been written in terms of the p_t of the Higgs boson for the scalar case, and could in principle be used in part to extract the NNLO process dependent $\bar{C}_{gg}^{(2)}$ coefficient for the differential cross-section for the scalar Higgs boson, advancing the resummed expressions ahead of the fixed order calculation. This work has not yet been completed.

5.3.2 Matching

The resummation formalism is valid in the small p_t region. Fixed order perturbation theory is valid at moderate p_t where there are no large logarithms. The process of matching allows for a smooth transition between the two regions. The procedure is described in great detail and clarity in Ref. [146].

One can write the differential cross-section as the sum of three terms

$$\frac{d\sigma}{dp_t^2 dy} = \frac{d\sigma^{\text{resum}}}{dp_t^2 dy} + \frac{d\sigma^{\text{pert}}}{dp_t^2 dy} - \frac{d\sigma^{\text{asym}}}{dp_t^2 dy} \quad (5.37)$$

This equation is easy to understand. At low p_t , we have the resummed contribution since the latter contributions cancel. At high p_t we have the perturbative contribution when the resummed and asymptotic cancel. At small p_t we remove the terms from the perturbative expansion that are asymptotically divergent like $1/p_t^2$. This allows for a smooth transition between the two regions at all values of p_t . However, extracting the divergent pieces can be quite difficult analytically as one must express the differential cross-section in terms of p_t order by order. For a $2 \rightarrow 1$ process, the first order corrections have

$2 \rightarrow 2$ kinematics and this is relatively simple, but becomes more intractable for the higher order corrections.

In this paper, we are interested in the new coefficient functions, and determining where the distributions peak for the different colliders, so this treatment will be ignored. However, we will display the perturbative differential cross-section to guide the eye on what the transition must look like.

5.3.3 Higgs Resummation

One of the interesting facets for Higgs production is that there is only a gg initial state for this process in the HQET at order α_s^3 , so the other terms (a $q\bar{q}$ initial state) are zero explicitly. Without getting too far ahead of our discussion, we can see that the Mellin moments of the $q\bar{q}$ corrections at order α_s^4 strictly vanish on threshold due to the fact that there is no $q\bar{q}$ initial state at lowest order. This makes it possible to work in z -space with little additional effort due to the presence of the $\delta(1-z)$ terms in the $C_{gg}^{(n)}$ coefficients, which makes the convolution with the PDFs trivial.

An additional complication arises from evaluating the parton distribution functions at very low scales during the convolution. This is solved by what is known as the b_\star prescription [146, 147]. Here the b parameter is replaced by b_\star that has an infrared cut-off b_{\max} so that as b becomes large, $b_\star \rightarrow b_{\max}$, and the fraction b_0/b in Equation (5.30) never leaves the perturbative regime of the parton distribution function. Over the rest of the range $b_\star \approx b$. This can be achieved by in the following parametrization

$$b_\star = \frac{b}{\sqrt{1 + b^2/b_{\max}^2}}. \quad (5.38)$$

This construction may seem a little artificial, but it allows for the numeric integration of our differential cross-section and allows us to use what is known to make reasonable calculations.

In these calculations, we have set $b_{\max} = (2 \text{ GeV})^{-1}$. This is mostly determined by the limits of applicability for the PDFs implemented to obtain the hadronic cross-section. There are other non-perturbative correction factors that are employed [128, 129, 146], but as no data is available yet we have not included these factors in our analysis.

It is thus possible to determine the unknown coefficients to a given order in the resummation and perform the resummed calculation. The known coefficients for scalar Higgs production will be given later. To leading-log (LL) accuracy, only the $A_c^{(1)}$ term is needed. At next-to-leading log (NLL) accuracy one needs the $A_c^{(2)}$, $B_c^{(1)}$, and $C_{ab}^{(1)}$ coefficients. The state of the art currently

is NNLL where the $A_c^{(3)}$, $B_c^{(2)}$, and $C_{ab}^{(2)}$ coefficients are needed [127]. For a scalar Higgs, these terms have been recently calculated but are missing for a pseudoscalar Higgs. The $A_g^{(3)}$ term can now be determined thanks to the excellent recent work on the three-loop splitting functions [57, 58]. Previously, only a numeric estimate was available [148].

Let us begin by extracting the process dependent C_{ab} coefficients for the total cross-section. To extract the formally divergent pieces of the cross-section, consider the Mellin transform of the hadronic cross-section, $\sigma_N(M_\Phi^2)$. The N -moments in Mellin space are defined as

$$\sigma_N(M_\Phi^2) \equiv \int_0^1 dz z^{N-1} \sigma(z, M_\Phi^2) \quad (5.39)$$

The advantage of transforming to Mellin space is that the limit $z \rightarrow 1$ corresponds to the limit of $N \rightarrow \infty$. This allows for a systematic way of extracting the divergent terms, which diverge as $\ln(N)$ in Mellin space.

Before continuing, we should comment on which initial state channels contribute. In evaluating the the C_{ab} coefficients in the $N \rightarrow \infty$ limit we see that only the gg channel has finite contributions, all the other channels have Mellin moments are strictly zero on threshold. We could also see that in the HQET there are no $q\bar{q}$ or qg initial state that contribute at this order to the cross-section at $p_t = 0$. Although we have set up our formalism for the sum of several channels, we will now consider only the gg initial state channel.

The Mellin moments of the fixed order corrections allow us to determine the process dependent total cross-section $C_{gg}^{(n)}$ coefficients in a simple way. We find the Mellin moments of the fixed order corrections, $\Delta_{ab \rightarrow \Phi}^{(n)}$, with the package HARMPOL in FORM [149]. Some diverge as $\ln(N)$, most tend to zero as $N \rightarrow \infty$, and some finite pieces are left over. In this way, we can separate the formally divergent pieces from the finite contributions on threshold. With this we can identify the p_t divergent terms with the $\ln(N)$ divergent terms in the Mellin moment. We choose to absorb the extra powers of γ_E into our definition of $\tilde{N} = Ne^{\gamma_E}$ so that we do not have spurious factors of γ_E in our expressions. This seems to be appropriate as in the $\overline{\text{MS}}$ scheme the factors of γ_E are also absorbed. This being noted, we will continue to write our terms as $\ln(N)$ with no factors of γ_E .

Next-to-leading-log Differential Cross-section Coefficients

We are interested in determining the $C_{gg}^{(1)}$ coefficient for the scalar and pseudo-scalar Higgs boson. First, let us integrate the differential cross-section for the scalar around $p_t = 0$. We will label this contribution ‘real’ to note that this

integral is similar to the real emission corrections to the total cross-section. We find

$$\begin{aligned} \Delta\hat{\sigma}^{\text{real}} &= \hat{\sigma}_0^H \left(\frac{4\pi\mu_r^2}{M_H^2} \right)^\epsilon z\Gamma(1+\epsilon)(1+\epsilon)\frac{\alpha_s}{\pi} \\ &\times \left[\frac{C_A}{\epsilon^2} + \frac{\beta_0}{\epsilon} - \frac{C_A}{2} \ln^2\left(\frac{M_H^2}{q_t^2}\right) + \beta_0 \ln\left(\frac{M_H^2}{q_t^2}\right) + C_A - C_A\zeta_2 \right]. \end{aligned} \quad (5.40)$$

We have to add the total partonic cross-section virtual correction to this expression to cancel the ϵ poles. The pole proportional to the β_0 gets renormalized into the coupling like in the total cross-section calculation. Once these two expression are added together we find

$$\begin{aligned} \Delta\hat{\sigma} &= \hat{\sigma}_0^H z \left[1 + \frac{\alpha_s}{\pi} \left(-\frac{C_A}{2} \ln^2\left(\frac{M_H^2}{q_t^2}\right) \right. \right. \\ &\quad \left. \left. + \beta_0 \ln\left(\frac{M_H^2}{q_t^2}\right) + C_A + \frac{5}{6}C_A + 3C_A\zeta_2 \right) \right]. \end{aligned} \quad (5.41)$$

The coefficients can now be read off and agree with the literature [123]

$$\bar{A}_g^{(1),H} = C_A, \quad \bar{B}_g^{(1),H} = -\beta_0 = -\left(\frac{11}{6}C_A - \frac{2}{3}n_f T_R\right), \quad \bar{C}_{gg}^{(1),H} = \frac{11}{12}C_A + \frac{3}{2}C_A\zeta_2. \quad (5.42)$$

As noted earlier, the pseudoscalar Higgs has different virtual corrections from the scalar Higgs boson. This changes the $\bar{C}_{gg}^{(1)}$ coefficient for the pseudoscalar to

$$\bar{C}_{gg}^{(1),A^0} = C_A + \frac{3}{2}C_A\zeta_2. \quad (5.43)$$

The pseudoscalar $\bar{C}_{gg}^{(1)}$ coefficient is larger than the scalar coefficient by a factor of $1/12C_A$. This is a small numeric difference, and the NNLL coefficient have not been extracted for the differential distribution, although as we will see in the next section we might expect a larger difference to appear in the differential $\bar{C}_{gg}^{(2)}$ coefficient based on the differences in the $C_{gg}^{(2)}$ coefficients for the total cross-section.

Next-to-leading-log Total Cross-section Coefficients

Exact expressions for the fixed order NLO corrections to scalar and pseudoscalar Higgs production have been in the literature for some time. Leaving aside the Sudakov terms ($A^{(n)}$ and $B^{(n)}$), let us examine our expressions for the fixed order corrections to the partonic cross-section. We see that the NLO

corrections have organized themselves in terms of constant pieces proportional to $\delta(1 - z)$ from the soft and virtual corrections and additional logarithmic corrections. The Mellin moment of the $\delta(1 - z)$ is simply

$$\int_0^1 dz z^{N-1} \delta(1 - z) = 1. \quad (5.44)$$

So it is easy to see that all the constant terms proportional to $\delta(1 - z)$ contribute to the $C_{gg}^{(1)}$ term. Beyond these terms, the Mellin moments of the logarithmic corrections in the limit $N \rightarrow \infty$ can have finite pieces that also contribute. Once the expression for the correction term has been transformed into Mellin space, there are no terms proportional to $\delta(1 - z)$, but are only constant terms.

In presenting the expressions for the $C_{gg}^{(n)}$ terms, we mix the notation somewhat to allow the reader to see all the different contributions. We keep the $\ln(N)$ pieces that are formally divergent, we separate out the terms that were initially proportional to the $\delta(1 - z)$ for convenience, and we include the terms proportional to $\ln(M_\Phi^2/\mu^2)$ for completeness. We have set $\mu = \mu_r = \mu_f$ for simplicity. The finite pieces compose the $C_{gg}^{(n)}$ coefficients.

In the case of the scalar and pseudoscalar

$$\begin{aligned} \Delta_{N,gg}^{(1),H} &= \lim_{N \rightarrow \infty} \int_0^1 dz z^{N-1} \Delta_{gg \rightarrow H}^{(1)} \\ &= C_A \ln^2(N) - 2C_A \ln \frac{M_H^2}{\mu^2} \ln(N) + \left[\frac{11}{6} C_A + 2C_A \zeta_2 \right] + 2C_A \zeta_2, \end{aligned} \quad (5.45)$$

$$\begin{aligned} \Delta_{N,gg}^{(1),A^0} &= \lim_{N \rightarrow \infty} \int_0^1 dz z^{N-1} \Delta_{gg \rightarrow A^0}^{(1)} \\ &= C_A \ln^2(N) - 2C_A \ln \frac{M_{A^0}^2}{\mu^2} \ln(N) + \left[2C_A + 2C_A \zeta_2 \right] + 2C_A \zeta_2, \end{aligned} \quad (5.46)$$

where the terms in the square brackets are the terms that were proportional to the delta function in the expression for the NLO correction in Equations (5.22) and (5.27). We have used the convention of absorbing the extra factors of γ_E that appear in other expressions for the $C_{gg}^{(n)}$ coefficients.

Next-to-next-to-leading-log Total Cross-section Coefficients

Exact expressions for the fixed order NNLO corrections to scalar and pseudo-scalar Higgs production are known. The NNLO corrections to inclusive Higgs production have been explicitly calculated and presented for the scalar [74, 102]

and the pseudoscalar [77, 102]. Although the the color factors have been evaluated in [74, 77], they were found to agree perfectly with [102] once the color factors were evaluated.

This allowed for the determination of the $C_{gg}^{(2)}$ coefficient for both the scalar and pseudoscalar. The scalar result was compared with the literature value [131] and was found to be in perfect agreement once the factorization and renormalization scales were set equal to one another and the spurious factors of γ_E were absorbed. For completeness, we present the full expression, leaving the color dependence intact and showing the $\ln(N)$ contributions.

$$\begin{aligned}
\Delta_{N,gg}^{(2),H}(z) = & \left[2C_A^2 \ln^4(N) + \left[C_A^2 \left(\frac{11}{9} - 4 \ln \frac{M_H^2}{\mu^2} \right) - \frac{4}{9} n_f C_A T_R \right] \ln^3(N) \right. \\
& + \left[C_A^2 \left(\frac{157}{18} + 7\zeta_2 - \frac{11}{6} \ln \frac{M_H^2}{\mu^2} + 2 \ln^2 \frac{M_H^2}{\mu^2} \right) - 3C_A C_F \right. \\
& \quad \left. \left. - n_f C_A T_R \left(\frac{10}{9} - \frac{2}{3} \ln \frac{M_H^2}{\mu^2} \right) \right] \ln^2(N) \right. \\
& + \left[C_A^2 \left(\frac{101}{27} - \frac{7}{2} \zeta_3 - \left(7\zeta_2 + \frac{157}{18} \right) \ln \frac{M_H^2}{\mu^2} + \frac{11}{12} \ln^2 \frac{M_H^2}{\mu^2} \right) \right. \\
& \quad \left. + 3C_A C_F \ln \frac{M_H^2}{\mu^2} - n_f C_A T_R \left(\frac{28}{27} - \frac{10}{9} \ln \frac{M_H^2}{\mu^2} + \frac{1}{3} \ln^2 \frac{M_H^2}{\mu^2} \right) \right] \ln(N) \\
& + \left\{ C_A^2 \left(\frac{3187}{288} + \frac{157}{18} \zeta_2 - \frac{1}{20} \zeta_2^2 - \frac{55}{12} \zeta_3 + \frac{7}{8} \ln \frac{\mu^2}{m_{\text{top}}^2} \right) \right. \\
& \quad - \left[\frac{3}{2} + \frac{11}{6} \zeta_2 - \frac{19}{2} \zeta_3 \right] \ln \frac{M_H^2}{\mu^2} - 2\zeta_2 \ln^2 \frac{M_H^2}{\mu^2} \\
& \quad + \frac{9}{4} C_F^2 - \frac{1}{6} C_F T_R - \frac{5}{48} C_A T_R - C_A C_F \left(\frac{145}{24} + 3\zeta_2 + \frac{11}{8} \ln \frac{\mu^2}{m_{\text{top}}^2} \right) \\
& \quad - n_f T_R \left(C_A \left(\frac{1153}{216} + \frac{10}{9} \zeta_2 - \frac{5}{9} \zeta_3 \right) + C_F \left(\frac{3}{8} - \ln \frac{\mu^2}{m_{\text{top}}^2} \right) \right. \\
& \quad \left. \left. - \left[C_A - \frac{2}{3} \zeta_2 C_A - \frac{1}{2} C_F \right] \ln \frac{M_H^2}{\mu^2} \right) \right\} \\
& + C_A^2 \left[\frac{157}{18} \zeta_2 + \frac{29}{5} \zeta_2^2 + \frac{22}{9} \zeta_3 - \left(\frac{11}{6} \zeta_2 + 8\zeta_3 \right) \ln \frac{M_H^2}{\mu^2} + 2\zeta_2 \ln^2 \frac{M_H^2}{\mu^2} \right] \\
& - C_A C_F \left[3\zeta_2 \right] - n_f T_R C_A \left[\frac{10}{9} \zeta_2 + \frac{8}{9} \zeta_3 - \frac{2}{3} \zeta_2 \ln \frac{M_H^2}{\mu^2} \right] \tag{5.47}
\end{aligned}$$

The term in curly brackets all by itself was the piece proportional to $\delta(1-z)$ in the original NNLO correction. The NNLO correction used as input for the

Mellin moment can be found in Ref. [102]. One should carefully note that there are terms in the coefficient that are proportional to T_R , but not $n_f T_R$. These terms come from the higher order corrections to the g_H effective coupling where only the top quark is included in the derivation of the corrections [90, 110]. One of our novel results is the $C_{gg}^{(2)}$ factor of the pseudoscalar, which is very similar to the scalar case. The difference between the two coefficients can be written as

$$\begin{aligned}
\Delta_{N,gg}^{(2),A^0} - \Delta_{N,gg}^{(2),H} &= \left[\frac{C_A}{4} (3C_F - C_A) \right] \ln^2(N) - \left[(3C_F - C_A) \ln \frac{M_H^2}{\mu^2} \right] \ln(N) \\
&+ \left\{ \frac{C_A}{4} (3C_F - C_A) \zeta_2 + \left[\frac{n_f T_R}{4} (2 - C_F) \right. \right. \\
&+ \frac{C_A}{32} (11C_F - 7C_A) \left. \right] \ln \frac{\mu^2}{m_{\text{top}}^2} \\
&- \left[\frac{n_f T_R}{24} (C_A + 3C_F) + \frac{5}{48} C_A^2 \right] \ln \frac{M_H^2}{\mu^2} \\
&+ \frac{n_f T_R}{32} \left(3C_F - \frac{17}{3} C_A - 8 \right) \\
&+ \frac{C_A}{96} \left(145C_F + \frac{5}{2} T_R - \frac{223}{12} C_A \right) + \frac{C_F}{8} \left(\frac{1}{3} T_R - \frac{9}{2} C_F \right) \left. \right\} \\
&+ \frac{C_A}{4} (3C_F - C_A) \zeta_2. \tag{5.48}
\end{aligned}$$

Finally, as we have the NLO corrections for each of the processes, we can compute the $B_g^{(2)}$ coefficients for each of them. The scalar case matches its value in the literature [131] and the pseudoscalar result is new. They are

$$B^{(2),H} = C_A^2 \left(\frac{23}{24} + \frac{11}{3} \zeta_2 - \frac{3}{2} \zeta_3 \right) + n_f T_R C_F - n_f T_R C_A \left(\frac{1}{6} + \frac{4}{3} \zeta_2 \right) - \frac{11}{18} C_F C_A, \tag{5.49}$$

$$B^{(2),A^0} = C_A^2 \left(\frac{1}{2} + \frac{11}{3} \zeta_2 - \frac{3}{2} \zeta_3 \right) + \frac{1}{2} n_f T_R C_F - n_f T_R C_A \frac{4}{3} \zeta_2. \tag{5.50}$$

5.4 Results and Conclusions

Although we have shown the explicit differences in the scalar and pseudoscalar functions, they are numerically quite small. Also, as the differences in the corrections become greater, they are suppressed more in α_s , leaving the

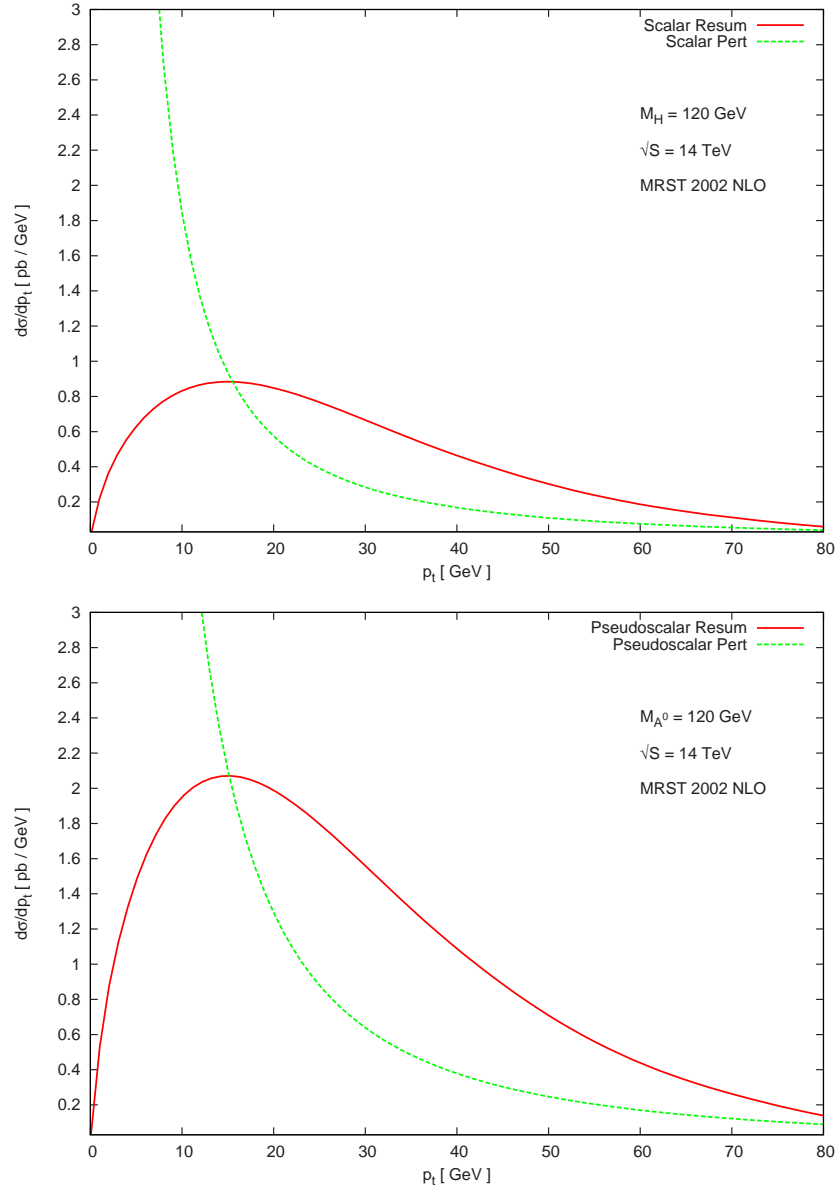


Figure 5.1: The transverse momentum spectrum for the scalar and pseudo-scalar Higgs boson at the LHC for $|y| \leq 2.5$. The p_t distribution peaks at approximately 15 GeV. The resummed curve is the NLL resummation, and the perturbative curve is the NLO fixed order calculation. The NLO fixed order calculation diverges in the negative direction at small p_t . This piece of the differential cross-section is not shown for clarity. These two curves cross at approximately $p_t = 100$ GeV/c and stay very close thereafter.

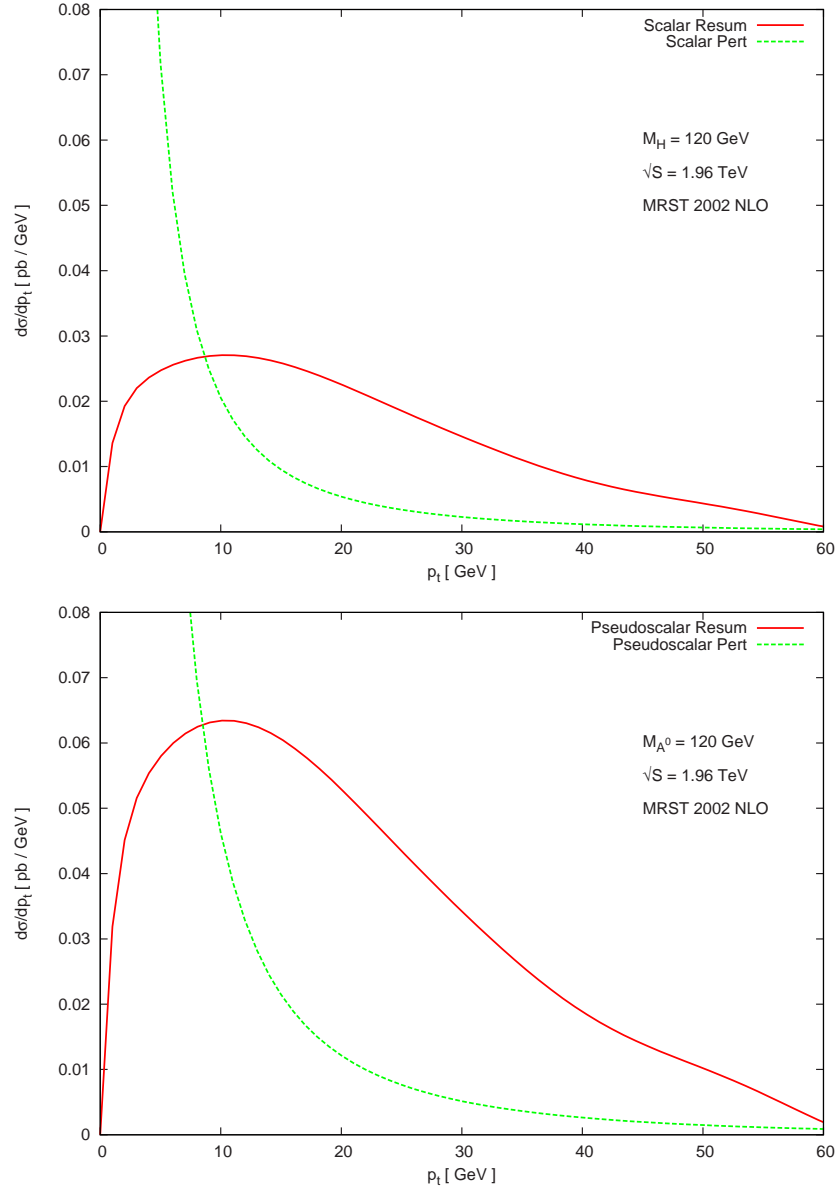


Figure 5.2: The transverse momentum spectrum for the scalar and pseudo-scalar Higgs boson at the Tevatron for $|y| \leq 2.5$. The p_t distribution peaks at approximately 10 GeV. The resummed curve is the NLL resummation, and the perturbative curve is the NLO fixed order calculation. The NLO fixed order calculation diverges in the negative direction at small p_t . This piece of the differential cross-section is not shown for clarity. These two curves cross at approximately $p_t = 80$ GeV/c and stay very close thereafter.

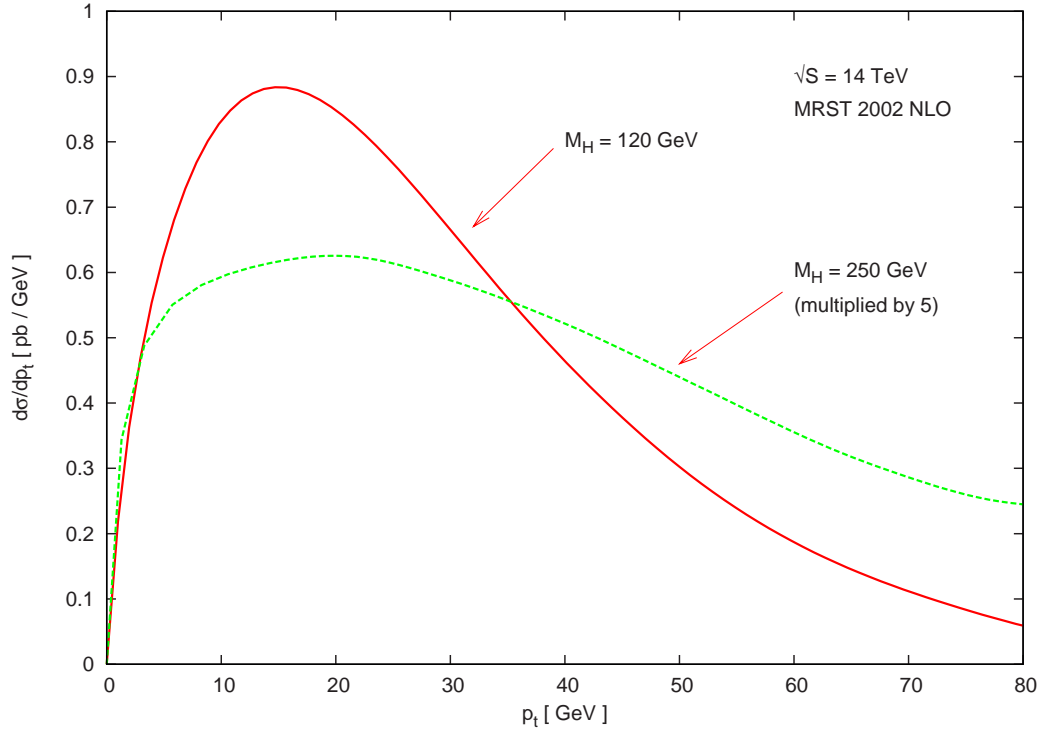


Figure 5.3: The effects of increasing Higgs mass on the transverse momentum spectrum at the LHC for $|y| \leq 2.5$. The $M_H = 250 \text{ GeV}/c^2$ curve peaks at approximately $23 \text{ GeV}/c$. We can clearly see that the resummed curve peaks at higher p_t with increasing Higgs mass and that the width of the resummed distribution becomes wider with increasing Higgs mass.

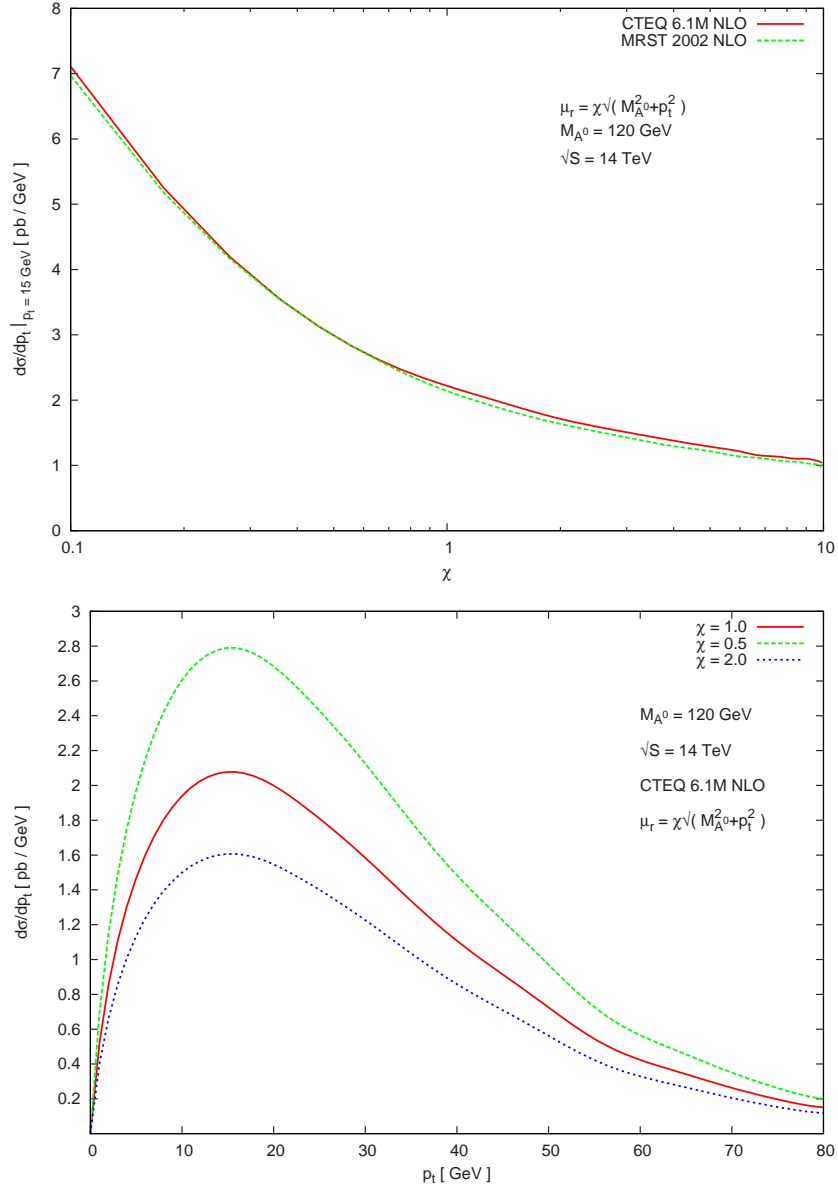


Figure 5.4: This is the scale uncertainty in the transverse momentum spectrum for the pseudoscalar Higgs boson. The upper figure shows the variation on the differential cross-section at its peak near 15 GeV/c over a scale variation of an order of magnitude. The upper figure shows both the MRST and CTEQ parton distribution function. The lower figure shows the variation over the whole spectrum when the scale is varied by a factor of two. It is easy to see that the largest scale uncertainty is at the peak value.

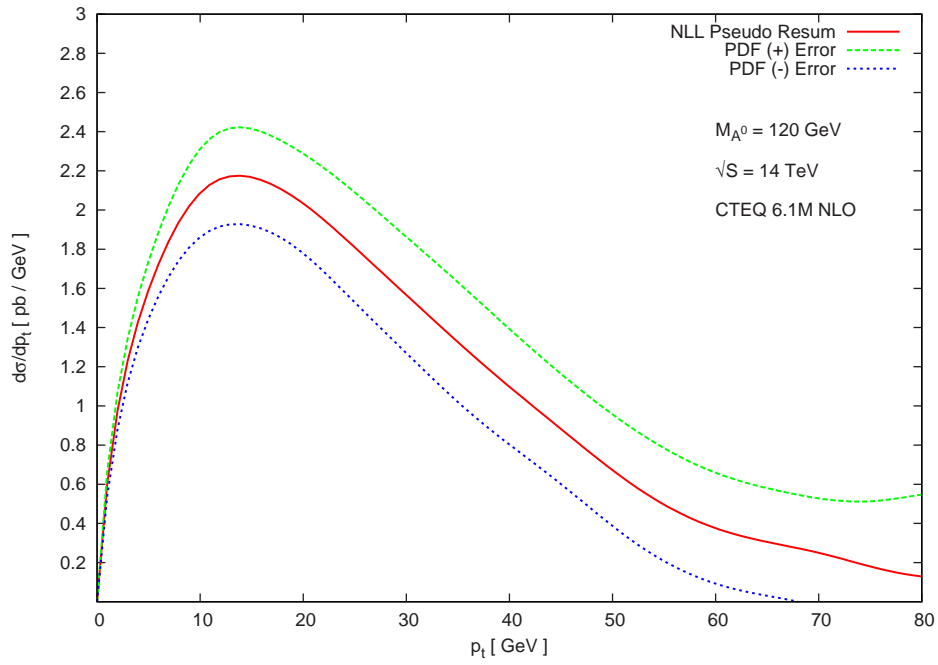


Figure 5.5: The uncertainty due to the parton distribution functions for the CTEQ 6.1M parton distribution functions. The resummation is done for the gg initial state only and therefore has the largest PDF uncertainty. A $q\bar{q}$ initial state would have a smaller PDF uncertainty.

predominant difference in the resummed cross-section is the same factor of 9/4 that appears in the LO cross-section. We are also interested in where the resummed p_t distribution peaks at the LHC and Tevatron, so we integrated the differential cross-sections numerically for a rapidity $|y| \leq 2.5$.

We implemented the MRST2002 NLO updated parton distribution functions [150, 151] and the MRST2001 LO parton distribution functions [152] in our analysis as well as the CTEQ 6.1M NLO parton distribution functions [84, 153]. We have taken the renormalization and factorization scales to be identical and set equal to $\mu^2 = M_\Phi^2 + p_t^2$. It should be noted that this choice of scale suppresses the width of the resummation peak as p_t grows due to the running of the coupling constant becoming smaller as the scale increases, but the effect is not a significant one. The LO cross-section “normalization factor” in the resummation formalism also shows p_t dependence for the same reason when this scale is used.

Our numerical results for the LHC were created with $\sqrt{S} = 14$ TeV and the Tevatron with $\sqrt{S} = 1.96$ TeV and a Higgs mass of 120 GeV/c². We used an NLO one-loop $\alpha_s(M_Z) = 0.1197$ consistent with the MRST2002 NLO updated parton distribution functions and $\alpha_s(M_Z) = 0.118$ for the CTEQ 6.1M NLO parton distribution functions. The p_t distributions for the scalar and pseudoscalar Higgs bosons at the LHC are shown in Figure 5.1 and Figure (5.2) shows the same figures for the Tevatron. It would appear that in both cases the factor of 9/4 difference in the LO cross-sections is the dominant difference in the small p_t region. The perturbative curves are from the same computer code that generated the differential cross-sections in Ref. [102].

The average transverse momentum and transverse momentum squared at the LHC for a 120 GeV/c² scalar and pseudoscalar Higgs boson with $p_t = 0 - 80$ GeV/c are $\langle p_t \rangle \simeq 27.5$ GeV/c and $\langle p_t^2 \rangle^{1/2} \simeq 32.7$ GeV/c with a peak value at 15 GeV/c. At the Tevatron the average transverse momentum and transverse momentum squared for the scalar and pseudoscalar Higgs boson with $p_t = 0 - 60$ GeV/c are $\langle p_t \rangle \simeq 20$ GeV/c and $\langle p_t^2 \rangle^{1/2} \simeq 24$ GeV/c with a peak value at 10 GeV/c. These values should be used with caution as they depend on the PDFs used in the analysis.

We are interested in what happens when a much heavier Higgs boson is considered. This would be the case if one were interested in a heavy SM Higgs, the heavy scalar H^0 in the MSSM, or a heavy pseudoscalar Higgs. We also ran our code for a Higgs with a mass of 250 GeV/c². We found a few interesting trends. The peak in the differential distribution moved to a higher p_t as expected [128] and the width of the peak became much broader. The width of the peak is interesting because it is telling us something about the decay width for the Higgs. The scale of the cross-section also dropped considerably

as one would expect for a heavier final state particle. As the mass of the Higgs became very heavy, it became hard to distinguish a discernable peak in the distribution as it became very wide. As we can see in Figure (5.3), this is a pronounced effect. The resummed curve becomes so broad that it does not cross the fixed order differential cross-section until very high transverse momentum.

There is a great deal of interest in understanding the uncertainties associated with the differential cross-section. Although it is common to look at the scale dependence of a total cross-section for scalar Higgs production [154], we would like to see how our results are effected by changes in the scale factor μ and the uncertainty in the parton distribution functions for the differential cross-section.

In Figure (5.4), the upper graph shows the scale dependence of the peak of the distribution when the scale factor is varied by a factor of ten. The lower graph in the same figure shows how the entire distribution changes when the scale is changed by a factor of two. From this lower graph is it easy to see that the peak of the distribution has the most sensitivity to the scale parameter. We define a prefactor to our renormalization scale to allow it to be varied with ease. We define $\mu^2 = \chi^2(M_\Phi^2 + p_t^2)$. When the scale factor is changed by a factor of ten lower ($\chi = 0.1$) the peak increased by a factor of approximately 3.1 and when the scale factor is increased by a factor of ten higher ($\chi = 10$) the peak of the distribution is lowered by factor of approximately 0.46. When the scale is only varied over a more reasonable factor of two, then the peak moves by approximately 25%. The overall scale dependence is very close to $\alpha_s^2(\mu)$ running as expected from the σ_0^{LO} prefactor in the resummation formalism. Overall, we can see that the shape of the distribution is not effected greatly by the change in the scale parameter, only its magnitude is changed significantly.

It is well known that the CTEQ gluon distribution is higher at small x than the MRST sets which can be seen in the upper graph in Figure (5.4), but the effect is quite small. Otherwise, the two distributions are very similar and can be considered interchangeable in this analysis.

In Figure (5.5), the uncertainty due to the parton distribution functions is shown. At the peak of the distribution, we see an uncertainty of approximately 10%. Considering only scale variations of a factor of two would lead us to believe that there is still approximately a 35% uncertainty in the differential cross-section at its peak. The uncertainty would be slightly lower at other values of the transverse momentum due to the scale μ and larger at higher values of the transverse momentum due to the PDF uncertainty.

In this paper, we have calculated the resummation coefficients for pseudo-scalar Higgs boson production for both the total cross-section, presenting the

$B_g^{(2)}$, $C_{gg}^{(1)}$, and $C_{gg}^{(2)}$ coefficients, and the differential cross-section, presenting the $\bar{C}_{gg}^{(1)}$ coefficient. We have also shown the effects of increasing the mass of the Higgs boson on the resummed differential cross-section and performed an analysis of the uncertainties associated with the renormalization scale and the parton distribution functions.

Acknowledgments

I would like to thank J. Smith, S. Dawson, J. Vermaseren, W. Vogelsang, G. Stermann, N. Christensen, and A. Field-Pollatou for all their help and comments during the several stages of this paper. The author is supported in part by the National Science Foundation grant PHY-0098527.

Appendix: Harmonic Polynomials

Finding the Mellin moments of the fixed order total cross-section corrections has been made considerably simpler with the HARMPOL package in FORM [149]. In order to use this powerful package, it is necessary to express the polylogarithmic expressions in terms of harmonic polylogarithms [155, 156].

Harmonic polylogarithms are defined recursively in three classes for each weight. To make this clear, let us define three functions

$$f(-1; x) = \frac{1}{1+x}, \quad f(0; x) = \frac{1}{x}, \quad f(1; x) = \frac{1}{1-x}, \quad (5.51)$$

so we can define the weight $w = 1$ harmonic polylogarithms as

$$H(a; x) = \int_0^x dx' f(a; x'). \quad (5.52)$$

Thus the first three harmonic polylogarithms can be written explicitly as

$$H(-1; x) = \ln(1+x), \quad H(0; x) = \ln(x), \quad H(1; x) = -\ln(1-x). \quad (5.53)$$

For higher weight harmonic polylogarithms, we need to generalize the notation. The w -dimensional vector \vec{m}_w should be broken into the first index and the rest of the vector as $\vec{m}_w = (a, \vec{m}_{w-1})$. This gives us a general expression for the rest of the harmonic polylogarithms recursively,

$$H(\vec{0}_w; x) = \frac{1}{w!} \ln^w x, \quad H(\vec{m}_w; x) = \int_0^x dx' f(a; x') H(\vec{m}_{w-1}; x'). \quad (5.54)$$

Although it is easy to find the harmonic polylogarithmic expression for the logarithms and dilogarithms, some further work is needed for the dilogarithms

with quadratic arguments and the trilogarithms that appear in the NNLO corrections. The dilogarithms can be simplified in a very straightforward way using well known relationships. To list them briefly the most useful expressions are

$$-\text{Li}_2(1-x^2) = 2[\text{Li}_2(x) + \text{Li}_2(-x) + \ln(x) \ln(1-x^2)] - \zeta_2 \quad (5.55)$$

$$-\text{Li}_2(1-x) = \text{Li}_2(x) + \ln(x) \ln(1-x) - \zeta_2 \quad (5.56)$$

$$\text{Li}_2(x) = \text{H}(0, 1; x) = \text{H}_2(x) \quad (5.57)$$

$$-\text{Li}_2(-x) = \text{H}(0, -1; x) = \text{H}_{-2}(x) \quad (5.58)$$

Fewer relationships exist for the trilogarithms. It proved to be very challenging to remove three of the trilogarithmic expressions simultaneously from the NNLO corrections. The following expressions were derived from the polylogarithm literature [157,158] and are presented here for future reference (using the notation for the Harmonic polylogarithms of Ref. [156]). That allows one to express the NNLO corrections completely in terms of Harmonic polylog-

rithms,

$$\begin{aligned}
\operatorname{Li}_3\left(\frac{+(1-x)}{1+x}\right) - \operatorname{Li}_3\left(\frac{-(1-x)}{1+x}\right) &= 2\operatorname{Li}_3(1-x) + 2\operatorname{Li}_3\left(\frac{1}{1+x}\right) \\
&\quad - \frac{1}{2}\operatorname{Li}_3(1-x^2) - \frac{7}{4}\zeta_3 \\
&\quad + \zeta_2 \ln(1+x) - \frac{1}{3}\ln^3(1+x), \tag{5.59}
\end{aligned}$$

$$\begin{aligned}
\operatorname{Li}_3\left(\frac{x}{1+x}\right) &= \frac{1}{6}\left[\ln^3\left(\frac{1+x}{x}\right) + \ln^3(1+x)\right] - \left(\frac{\zeta_2}{2}\right. \\
&\quad \left. + \frac{\ln^2(x)}{4}\right)\left[2\ln(1+x) - \ln(x)\right] \\
&\quad - \frac{1}{2}\left[\operatorname{Li}_3\left(-\frac{1}{x}\right) + \operatorname{Li}_3(-x)\right] \\
&\quad - \operatorname{Li}_3\left(\frac{1}{1+x}\right) + \zeta_3, \tag{5.60}
\end{aligned}$$

$$\begin{aligned}
\operatorname{Li}_3\left(\frac{1}{1+x}\right) &= \frac{1}{2}\ln^2(1+x)\ln(x) \\
&\quad - \ln(1+x)\left[\operatorname{Li}_2(-x)\right. \\
&\quad \left. + \ln(x)\ln(1+x) - \zeta_2\right] + \zeta_2 \\
&\quad - \operatorname{H}_{-2,-1}(x) + \zeta_2 \ln(1+x) \\
&\quad + \frac{1}{6}\left[\ln^3(1+x) - 18\zeta_2 \ln(1+x)\right], \tag{5.61}
\end{aligned}$$

$$\begin{aligned}
\operatorname{Li}_3\left(\frac{-(1-x)}{x}\right) &= -\operatorname{Li}_3(1-x) - \operatorname{Li}_3(x) + \zeta_3 + \zeta_2 \ln(1-x) \\
&\quad - \frac{1}{2}\ln(x)\ln^2(1-x) + \frac{1}{6}\ln^3(1-x) \\
&\quad - \zeta_2 \ln\left(\frac{1-x}{x}\right) - \frac{1}{6}\ln^3\left(\frac{1-x}{x}\right), \tag{5.62}
\end{aligned}$$

and,

$$\begin{aligned} \text{Li}_3\left(\frac{-(1-x^2)}{x^2}\right) &= -\text{Li}_3(1-x^2) - 4\left[\text{Li}_3(x) + \text{Li}_3(-x)\right] \\ &\quad + \zeta_3 + \zeta_2 \ln(1-x^2) - \ln(x) \ln^2(1-x^2) \\ &\quad + \frac{1}{6} \ln^3(1-x^2) - \zeta_2 \ln\left(\frac{1-x^2}{x^2}\right) - \frac{1}{6} \ln^3\left(\frac{1-x^2}{x^2}\right), \end{aligned} \quad (5.63)$$

$$\begin{aligned} \text{Li}_3(1-x^2) &= \ln(x) \ln^2(1-x^2) + \text{Li}_2(1-x^2) \ln(1-x^2) \\ &\quad + \zeta_3 - 2\left[\text{H}_{2,1}(x) - \text{H}_{-2,1}(x)\right], \end{aligned} \quad (5.64)$$

$$\begin{aligned} \text{Li}_3(1-x) &= \frac{1}{2} \ln(x) \ln^2(1-x) + \ln(1-x) \text{Li}_2(1-x) \\ &\quad + \zeta_3 - \text{H}_{2,1}(x), \end{aligned} \quad (5.65)$$

$$\text{Li}_3\left(-\frac{1}{x}\right) = \text{Li}_3(-x) + \zeta_2 \ln(x) + \frac{1}{6} \ln^3(x), \quad (5.66)$$

$$\text{Li}_3(x) = \text{H}_3(x), \quad (5.67)$$

$$-\text{Li}_3(-x) = \text{H}_{-3}(x), \quad (5.68)$$

$$-S_{1,2}(1-x) = \text{Li}_3(x) + \ln(x) \text{Li}_2(x) + \frac{1}{2} \ln(1-x) \ln^2(x) + \zeta_3, \quad (5.69)$$

$$-S_{1,2}(-x) = \text{H}_{-2,-1}(x). \quad (5.70)$$

It was also necessary to linearize all the arguments of the natural logs and to partial fraction the inverse powers of $1-x^2$. With these above expressions, it was possible to use HARMPOL to find the Mellin moments of the correction factors. Although most of these expressions were verified numerically, it should be emphasized that these expressions were derived so that they would be valid at $x \leq 1$, which is where they would be evaluated on threshold. In some regions these expressions would pick up imaginary pieces, but since we are interested in corrections to a partonic cross-section our expression must stay real.

Using these expressions, the NNLO corrections in Refs. [74, 77, 102] can be reduced to Harmonic polylogarithms so their moments can be easily found.

Chapter 6

Higgs Boson Resummation via Bottom-Quark Fusion

We study the resummed differential cross-sections for Higgs production via bottom-quark fusion. The region of small transverse momentum must be studied in the framework of resummation to account for the large, logarithmically-enhanced contributions to physical observables. Resummation offers the most reliable theoretical prediction for the transverse momentum spectrum. Knowledge of the position, magnitude, and distribution about the peak of the transverse momentum can help shape the details of an experimental search. Coefficients for the resummation of the total cross-section for Higgs Boson production in $b\bar{b}$ initial state processes are given in an appendix.

6.1 Introduction

Previous calculations of the resummation of total and differential cross-sections for the inclusive production of a Higgs boson have concentrated on the gluon-gluon initial state [106, 120–130, 159–161]. In the Standard Model (SM), the gluon-gluon initial state gives the largest contribution to the total and differential cross-sections, but this is not always the case in extensions of the SM. In the Minimal Supersymmetric Standard Model (MSSM) the bottom-quark fusion mechanism can be greatly enhanced. In fact, for values of $\tan\beta > 7$ (which will be defined below), bottom-quark fusion is the dominant production mechanism at both the Tevatron and the LHC [134].

The transverse momentum (p_t) spectrum of a particle produced in a collider collision is an experimental observable that needs to be treated with care to assure reliable predictions across a broad range of transverse momentums. Understanding the p_t -spectrum of an observed process allows for the compari-

son of signal to background events. It can also help in improving experimental cuts at the LHC to improve background rejection [162]. The separation between small- p_t and large- p_t is usually determined by the condition $p_t \geq M_H$. The large- p_t behavior is described well by a perturbative expansion whereas the small- p_t behavior needs to be described in the framework of resummation. The convergence of the perturbative expansion in the small- p_t region is spoiled by the presence of large logarithms that need to be systematically resummed to all orders in α_s . It is this small- p_t behavior and resummation for the process of inclusive Higgs production from bottom-quark fusion that is studied in this article.

A resummed differential cross-section reliably predicts the distribution of small transverse momenta for a particle in a production process. This is of great experimental interest because whereas the Higgs is easiest to identify when it is produced with significant p_t , a typical p_t distribution peaks at smaller values of the p_t than are typically observed. The location of the differential peak will be of great importance at the LHC as it is below the projected p_t threshold for a trigger event, which implies that many of the signal events would never be recorded. The shape, magnitude, and distribution around the peak of the p_t spectrum in the small- p_t region will strongly influence the details of the experimental trigger and search strategies [163,164]. It is also important to use the properties of the p_t spectrum to separate the background from the signal once events have been recorded.

The MSSM contains two Higgs doublets, one giving mass to up-type quarks and the other to down-type quarks. The associated vacuum expectation values (VEVs) are labeled v_u and v_d respectively, and define the MSSM parameter $\tan\beta \equiv v_u/v_d$. In the MSSM, there are five physical Higgs boson mass eigenstates. In this article, we are interested in the neutral Higgs bosons $\{h^0, H^0, A^0\}$ which we will call Φ generically.

In contrast to the SM, the bottom-quark Yukawa couplings in the MSSM can be enhanced with respect to the top-quark Yukawa coupling. In the SM, the ratio of the $t\bar{t}\Phi$ and $b\bar{b}\Phi$ couplings is given at tree-level by $\lambda_t^{\text{SM}}/\lambda_b^{\text{SM}} = m_t/m_b \approx 35$. In the MSSM, the couplings depend on the value of $\tan\beta$. At leading order,

$$\frac{\lambda_t^{\text{MSSM}}}{\lambda_b^{\text{MSSM}}} = f_\Phi \frac{1}{\tan\beta} \cdot \frac{m_t}{m_b}, \quad (6.1)$$

with

$$f_\Phi = \begin{cases} -\cot\alpha, & \Phi = h^0 \\ \tan\alpha, & \Phi = H^0 \\ \cot\beta, & \Phi = A^0 \end{cases} \quad (6.2)$$

where α is the mixing angle between the weak and the mass eigenstates of the neutral scalars. Given the mass of the pseudoscalar M_{A^0} and $\tan\beta$, the angle

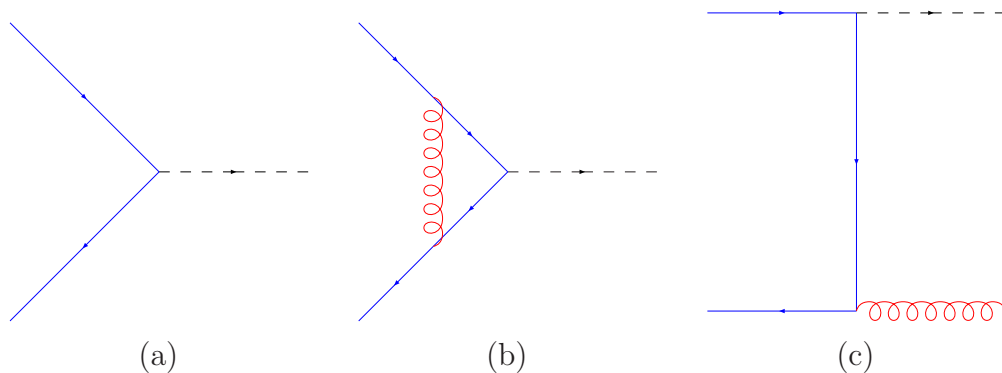


Figure 6.1: Diagrams needed for the $b\bar{b}$ initial state resummed differential cross-section. Figure 6.1a is the lowest order production channel and couples differently for different Higgs bosons. Figure 6.1b is the virtual correction to the lowest order process. Figure 6.1c is the lowest order graph contributing to the differential cross-section. The crossed graph is not shown.

α can be determined given reasonable assumptions for the masses of the other supersymmetric particles in the spectrum [117]. The form of f_Φ shows us that the production of the pseudoscalar due to bottom-quark fusion is enhanced by a factor of $\tan^2\beta$. This makes the bottom-quark initial state an interesting study.

Previously [161], we calculated in detail the resummation coefficients for a differential cross-section for the scalar and pseudoscalar Higgs boson from the gluon-gluon initial state. In this article, we will calculate the resummation coefficients needed for the resummation of the $b\bar{b}$ initial state for the scalar and pseudoscalar Higgs bosons in the same manner as the gluon-gluon channel in Ref. [161]. We will leave the bottom-quark–Higgs coupling set equal to the SM value so that the reader can scale the results to whatever coupling value is of interest.

6.2 Setup

In our analysis, we employed the CTEQ6.1M bottom-quark parton distribution [84, 165–167] with $\alpha_s(M_Z) = 0.118$ and set the mass of the Higgs boson $M_\Phi = 120$ GeV.

We have employed the five-flavor-number scheme counting the bottom quark as an initial state using the bottom-quark parton distributions as encoded in the CTEQ PDF set. The bottom-quark distribution contains all the collinear terms from the splitting of gluons into $b\bar{b}$ pairs [84, 133, 168–172]. This

scheme sets the perturbative expansion as $(\alpha_s \log(m_b^2/M_\Phi^2))^n$ and allows us to resum these large, logarithmically-enhanced contributions.

6.3 Resummation

The result of the resummation formalism is a series of numeric coefficients (some of which are scale dependent) that encode the small p_t behavior of the production process. These coefficients are generically labeled $\bar{A}_b^{(n)}$, $\bar{B}_b^{(n)}$, and $\bar{C}_{b\bar{b}}^{(n)}$ and are used in the differential resummation formalism [143–145] as described below.

The basic equation for the resummation of a differential cross-section can be written for the $b\bar{b}$ initial state as

$$\begin{aligned} \frac{d\sigma^{\text{resum}}}{dp_t^2 dy d\phi} &= \int_{x_{1,\min}}^1 dx_1 \int_{x_{2,\min}}^1 dx_2 \int_0^\infty db \frac{b}{2} J_0(bp_t) \\ &\times f_{b/h_1}(x_1, b_0/b) f_{\bar{b}/h_2}(x_2, b_0/b) \frac{S}{Q^2} W_{b\bar{b}}(x_1 x_2 S; Q, b, \phi), \end{aligned} \quad (6.3)$$

$$\begin{aligned} W_{b\bar{b}}(s; Q, b, \phi) &= \int_0^1 dz_1 \int_0^1 dz_2 \bar{C}_{b\bar{b}}(\alpha_s(b_0/b), z_1) \bar{C}_{b\bar{b}}(\alpha_s(b_0/b), z_2) \\ &\times \delta(Q^2 - z_1 z_2 s) \frac{d\sigma_{b\bar{b}}^{LO}}{d\phi} S_b(Q, b), \end{aligned} \quad (6.4)$$

where the Higgs mass $M_\Phi^2 = Q^2$, $d\phi$ is the phase space of the system under consideration, and $\hat{\sigma}_{b\bar{b}}^{(LO)}$ is the lowest order cross-section for the $b\bar{b}$ initial state. It is important not to confuse the bottom-quark parton and the impact parameter b in these equations. The constant b_0 is written in terms of the Euler-Mascheroni constant $\gamma_E = 0.57721\dots$ as $b_0 = 2e^{-\gamma_E}$. The coefficients $\bar{C}_{b\bar{b}}$ are process dependent and can be written as power series to be described below. $J_0(bp_t)$ is the first order Bessel function. The delta function before the partonic differential cross-section in Eqn. (6.4) is a threshold condition. The Sudakov form factor S_b , which makes the integration over the Bessel function convergent, can be written as

$$S_b(Q, b) = \exp \left\{ - \int_{b_0^2/b^2}^{Q^2} \frac{dq^2}{q^2} \left[\bar{A}_b(\alpha_s(q)) \ln \frac{Q^2}{q^2} + \bar{B}_b(\alpha_s(q)) \right] \right\}. \quad (6.5)$$

The coefficient functions \bar{A}_b , \bar{B}_b , and $\bar{C}_{b\bar{b}}$ can be written as power series in α_s as

$$\bar{A}/\bar{B}_b(\alpha_s) = \sum_{n=1}^{\infty} \left(\frac{\alpha_s}{\pi} \right)^n \bar{A}/\bar{B}_b^{(n)}, \quad (6.6)$$

$$\bar{C}_{b\bar{b}}(\alpha_s, z) = \delta(1-z) + \sum_{n=1}^{\infty} \left(\frac{\alpha_s}{\pi} \right)^n \bar{C}_{b\bar{b}}^{(n)}(z). \quad (6.7)$$

The resummation formalism needs the lowest order total cross-section as a normalization factor, $b\bar{b} \rightarrow \Phi$ in this case. Following Ref. [133], we will ignore the bottom-quark mass except in the Yukawa coupling with the Higgs boson. Although the pseudoscalar Higgs couples to quarks with a γ_5 , there are no differences in the matrix elements for the different neutral Higgs bosons at lowest order (modulo the MSSM coupling factor) when the bottom-quark mass is neglected.

It is important to use the $\overline{\text{MS}}$ running mass for the bottom-quark in our calculation as the difference from the pole mass at the scales involved is considerable [174, 173]. In the SM, the bottom-quark Yukawa coupling is $\lambda_b^{\text{SM}} = \sqrt{2}\bar{m}_b/v$, where v is the SM VEV and is approximately equal to 246 GeV and \bar{m}_b is the $\overline{\text{MS}}$ running mass. We have set the bottom-quark mass $\bar{m}_b(\bar{m}_b) = 4.62$ GeV in our calculations. The NLO running of the bottom-quark mass corresponds to $\bar{m}_b(M_\Phi = 120 \text{ GeV}) = 3.23$ GeV. Because the quark mass comes into the cross-section squared, this is a significant effect. The coupling in the MSSM can be written

$$\lambda_b^{\text{MSSM}} = \begin{cases} -\sqrt{2} \frac{\bar{m}_b \sin \alpha}{v \cos \beta}, & \Phi = h^0 \\ \sqrt{2} \frac{\bar{m}_b \cos \alpha}{v \cos \beta}, & \Phi = H^0 \\ \sqrt{2} \frac{\bar{m}_b}{v} \tan \beta, & \Phi = A^0. \end{cases} \quad (6.8)$$

The spin- and color-averaged total partonic cross-section (see Fig. 6.1a) for the leading order subprocess, $b\bar{b} \rightarrow \Phi$, can be easily written

$$\hat{\sigma}_0^{\text{SM}} = \frac{6\pi}{4N_c^2} \frac{\bar{m}_b^2}{v^2} \frac{1}{M_\Phi^2} \delta(1-z), \quad (6.9)$$

where $z = M_\Phi^2/\hat{s}$, \hat{s} is the partonic center-of-momentum energy, and the number of colors $N_c = 3$. We also need the LO differential cross-section (Fig. 6.1c) for the next-to-leading log (NLL) resummation coefficients for the differential cross-section. If we remove the $\delta(1-z)$ factor from our prefactor $\hat{\sigma}_0$,

then we can write the spin- and color-averaged differential cross-section for $b(p_1)\bar{b}(p_2) \rightarrow g(-p_3)\Phi(-p_5)$ as

$$\begin{aligned}\frac{d\hat{\sigma}}{d\hat{t}} &= \hat{\sigma}_0 \left(\frac{\alpha_s}{\pi} \right) \frac{C_F}{2} \left(\frac{M_\Phi^4 + \hat{s}^2}{\hat{s}\hat{t}\hat{u}} \right) \\ &= \hat{\sigma}_0 \left(\frac{\alpha_s}{\pi} \right) \frac{C_F}{2} \frac{1}{p_t^2} \left[1 + z^2 \right].\end{aligned}\quad (6.10)$$

where $C_F = (N_c^2 - 1)/2N_c$, and the kinematic variables are defined as $\hat{s} = (p_1 + p_2)^2$, $\hat{t} = (p_1 + p_5)^2$, $\hat{u} = (p_2 + p_5)^2$, and $M_\Phi^2 = p_5^2$. In the second line of Equation (6.10), we have written the differential cross-section in terms of $\hat{u}\hat{t} = \hat{s}p_t^2$ for the $2 \rightarrow 2$ process.

To find the resummation coefficients for a differential cross-sections [121, 123, 127, 161] we integrate the differential cross-section around $p_t = 0$

$$\Delta\hat{\sigma} = \int_0^{q_t^2} dp_t^2 \frac{d\hat{\sigma}}{dp_t^2} \quad (6.11)$$

and label this result ‘real’ as it is similar to the real corrections to the LO total cross-section. The q_t in this integral is an arbitrary small transverse momentum used to extract the resummation coefficients. Working in $N = 4 - 2\epsilon$ dimensions for the $b\bar{b} \rightarrow \Phi$ process we find

$$\Delta\hat{\sigma}^{\text{real}} = \hat{\sigma}_0 z \frac{\alpha_s}{\pi} \left[\frac{C_F}{\epsilon^2} + \frac{3C_F}{2\epsilon} - \frac{C_F}{2} \ln^2 \left(\frac{M_\Phi^2}{q_t^2} \right) + \frac{3}{2} C_F \ln \left(\frac{M_\Phi^2}{q_t^2} \right) + C_F - C_F \zeta_2 \right]. \quad (6.12)$$

To regularize this result, we need to add the virtual corrections that are shown in Fig. 6.1b. These corrections are very similar to Drell-Yan corrections [175]. The virtual corrections can be written as

$$\Delta\hat{\sigma}_{\text{virt}} = \hat{\sigma}_0 \left(\frac{\alpha_s}{\pi} \right) \left[-\frac{C_F}{\epsilon^2} - \frac{3C_F}{2\epsilon} - C_F + 2C_F \zeta_2 \right]. \quad (6.13)$$

In the Drell-Yan case, the $-C_F$ factor would be $-4C_F$. When the two results are added together the resummation coefficients are easily read off from the expression. The total expression is

$$\Delta\hat{\sigma} = \hat{\sigma}_0 z \left[1 + \frac{\alpha_s}{\pi} \left(-\frac{C_F}{2} \ln^2 \left(\frac{M_\Phi^2}{q_t^2} \right) + \frac{3}{2} C_F \ln \left(\frac{M_\Phi^2}{q_t^2} \right) + C_F \zeta_2 \right) \right]. \quad (6.14)$$

and we can compare this to the expansion of our expression in Equation (6.3) in terms of the resummation coefficients

$$\Delta\hat{\sigma}_{b\bar{b}} = 1 + \frac{\alpha_s}{\pi} \left[-\frac{\bar{A}_b^{(1)}}{2} \ln^2 \left(\frac{M_\Phi^2}{q_t^2} \right) - \bar{B}_b^{(1)} \ln \left(\frac{M_\Phi^2}{q_t^2} \right) + 2\bar{C}_{b\bar{b}}^{(1)} \right]. \quad (6.15)$$

Keeping the notation of Ref. [161], we write the differential resummation coefficients with an overbar. We can read off the next-to-leading log (NLL) bottom-quark resummation coefficients in the threshold limit ($z \rightarrow 1$) as required by Eqn. (6.4) as

$$\bar{A}_b^{(1)} = C_F, \quad \bar{B}_b^{(1)} = -\frac{3}{2}C_F, \quad \bar{C}_{bb}^{(1)} = \frac{1}{2}C_F\zeta_2. \quad (6.16)$$

In contrast to Z^0/W^\pm production and Drell-Yan processes [175, 146] with quarks in the initial state, the $\bar{C}^{(1)}$ coefficient is positive.

We can also determine the NNLL $\bar{A}^{(2)}$ and $\bar{B}^{(2)}$ coefficients. We find

$$\bar{A}_b^{(2)} = \frac{1}{2}C_F \left(C_A \left(\frac{67}{18} - \zeta_2 \right) - \frac{10}{9}n_f T_R \right) \quad (6.17)$$

$$\begin{aligned} \bar{B}_b^{(2)} = & C_F^2 \left(\frac{3}{2}\zeta_2 - 3\zeta_3 - \frac{3}{16} \right) - C_A C_F \left(\frac{11}{18}\zeta_2 - \frac{3}{2}\zeta_3 + \frac{13}{16} \right) \\ & - n_f C_F T_R \left(\frac{1}{4} + \frac{2}{9}\zeta_2 \right) \end{aligned} \quad (6.18)$$

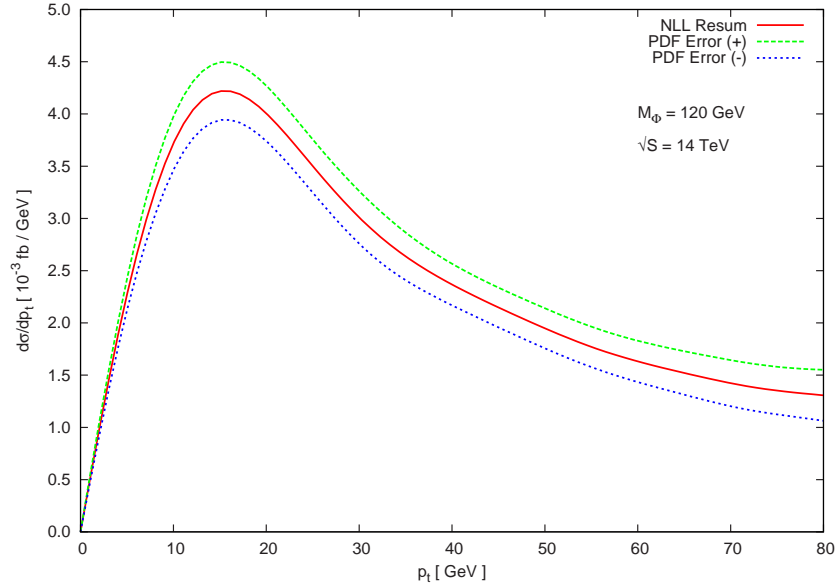
for $\bar{A}^{(2)}$ and $\bar{B}^{(2)}$.

A similar study was presented in Ref. [176] that contained the differential resummation coefficients $\bar{A}_b^{(1)}$, $\bar{A}_b^{(2)}$, and $\bar{B}_b^{(1)}$. Although our notation differs somewhat from that in the previous reference, it proved to be very useful for comparison. There are several novel contributions in this study, including the presentation of the Mellin moments $\Delta_{bb}^{(1)}$ and $\Delta_{bb}^{(2)}$ in the appendix and the differential resummation coefficient $\bar{B}_b^{(2)}$.

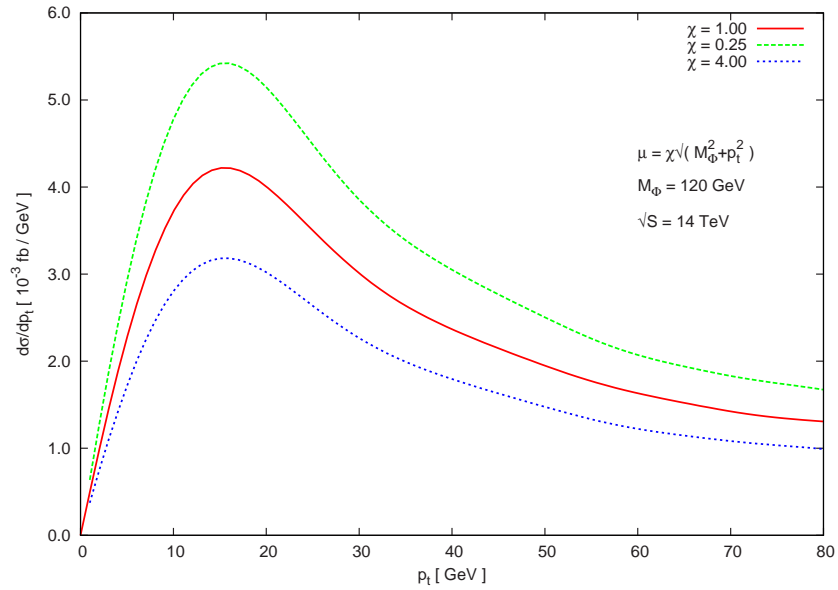
We present the full set of differential resummation coefficients $\bar{A}_b^{(1)}$, $\bar{A}_b^{(2)}$, $\bar{B}_b^{(1)}$, and $\bar{B}_b^{(2)}$ as well as the process dependent coefficients $\bar{C}_{bb}^{(1)}$, $\Delta_{bb}^{(1)}$, and $\Delta_{bb}^{(2)}$ with their full scale dependence. The $\bar{B}^{(1)}$, $\bar{A}^{(1)}$, and $\bar{A}^{(2)}$ coefficients agrees with a previous calculation as does $\bar{C}_{bb}^{(1)}$.

6.4 Results and Conclusions

The differential resummation coefficients and the position of the peak of the differential cross-section is of great interest to the experimental community involved with Higgs research at the LHC, particularly for a low mass Higgs. In this article, we studied a Higgs with $M_\Phi = 120$ GeV using the formalism presented in Eqn. (6.3). Here the Higgs will decay primarily into $b\bar{b}$ pairs that can be tagged. Knowing where the peak of the differential distribution lies, especially if it is below the p_t of a typical trigger event is important for experimental searches.



(a)



(b)

Figure 6.2: Figure 6.2a shows the errors associated with the CTEQ6.1M PDF set. The variation is approximately 8 – 12%. Figure 6.2b show the variation of the renormalization and factorization scale for a factor of 1/4 and 4. These scales were chosen because there has been great interest [169–172] in the scale $\mu = M_\Phi/4$. We find this variation to be approximately 20%.

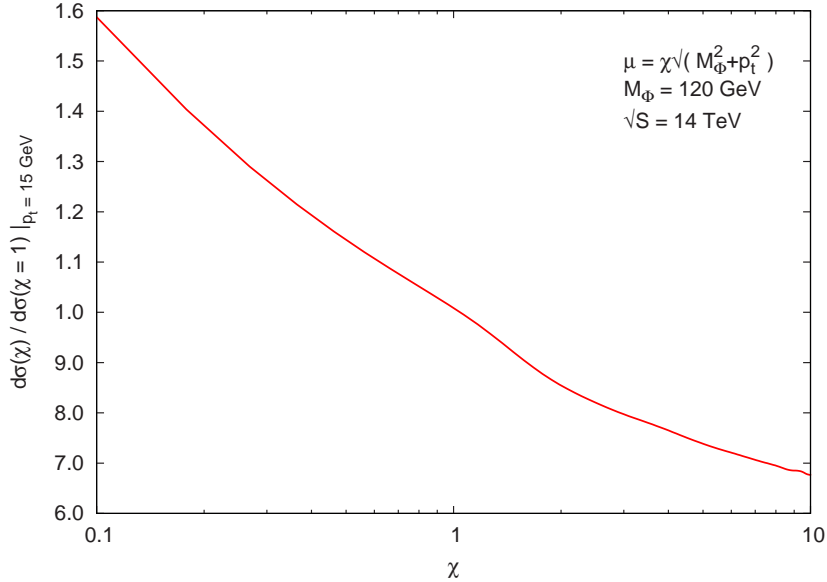


Figure 6.3: The movement of the peak of the differential distribution (at 15 GeV) for a variation in the scale by a factor of 10.

The results of our calculations can be found in Figure 6.2. We have done our analysis for the LHC (a proton-proton collider at $\sqrt{S} = 14$ TeV). We find that the differential distribution at the LHC peaks at a transverse momentum of approximately 15 GeV for $M_\Phi = 120$ GeV. We find that the magnitude of the differential cross-section is an excellent match with previously published results [174, 176, 173]. The results for the Tevatron are similar, but are smaller by a factor of 60 and the peak moves to a transverse momentum of approximately 13 GeV in the differential distribution. The position of the peak is dependent on the mass of the Higgs boson. The peak moves to higher values of p_t as the mass becomes heavier.

A study of the PDF and scale uncertainties in the calculation show that the uncertainty due to the choice of the PDF set is approximately 8 – 12% when the entire set of CTEQ6.1M uncertainty PDFs are considered [84]. At the peak of the distribution, the uncertainty is approximately 10% due to the PDFs. When the scale is varied by a factor of four, we see a variation in the differential cross-section of approximately 20%. This would give us a combined uncertainty of roughly 30 – 35%, which is slightly better than the gluon-gluon channel [161] uncertainty in the differential distribution. However, when the scale is only varied by a factor of two (as was the case for the gluon-gluon channel), the total uncertainty drops to approximately 25%.

We have calculated the resummation coefficients needed for NLL inclusive Higgs production via bottom-quark fusion in the SM and the MSSM for the differential cross-section and for the NNLL resummation for the total cross-section. We find a smaller uncertainty in the bottom-quark initial state than the gluon-gluon initial state.

Acknowledgments

The author would like to acknowledge the help and comments of J. Smith, S. Dawson, G. Sterman, W. Vogelsong, F. Olness, and A. Field-Pollatou. I would also like to thank W. Kilgore and R. Harlander for supplying the output of their calculation [133] including its scale dependence. The author is supported in part by the National Science Foundation grant PHY-0354776 and under DOE Contract No. DE-AC02-98CH10886.

Appendix: Total Cross-Section Resummation Coefficients

Let us turn to determining the $\bar{C}^{(1)}$ and $\bar{C}^{(2)}$ coefficients for the total cross-section resummation, although total cross-sections will not be presented in this article. The total cross-section coefficients were determined in the course of the study and will be presented here for convenience and completeness. Care has been taken to keep both the renormalization and factorization scales explicit in these results.

To extract the formally divergent pieces of the total cross-section, consider the Mellin transform of the hadronic cross-section, $\sigma_N(M_\Phi^2)$. The N -moments in Mellin space are defined as

$$\sigma_N(M_\Phi^2) \equiv \int_0^1 dz z^{N-1} \sigma(z, M_\Phi^2) \quad (6.19)$$

The advantage of transforming to Mellin space is that the limit $z \rightarrow 1$ corresponds to the limit of $N \rightarrow \infty$. This allows for a systematic way of extracting the divergent terms, which diverge as $\ln(N)$ in Mellin space. This allows for the presentation of the finite and divergent pieces of the Mellin moments in a systematic way.

Using the results of Ref. [133], we take the Mellin moments of the corrections in the limit $N \rightarrow \infty$ ($z \rightarrow 1$ in z -space). The NLO corrections are easy to color decompose due to the presence of only one color factor [161]. Leaving the terms that were originally proportional to the $\delta(1-z)$ factor inside curly brackets, we find

$$\Delta_{bb}^{(1)} = \left[2C_F \right] \ln^2(N) + \left[2C_F \ln \frac{M_\Phi^2}{\mu_f^2} \right] \ln(N) + \left\{ 2C_F \zeta_2 - C_F + 2 \ln \frac{\mu_r^2}{\mu_f^2} \right\} + 2C_F \zeta_2 \quad (6.20)$$

where we have given both the renormalization scale μ_r and the factorization scale μ_f dependence in the results. We define the color factors in the usual way as $C_A = N_c$ and $C_F = (N_c^2 - 1)/2N_c$.

In contrast to NLO, the NNLO corrections contain a mix of color factors (both C_A and C_F appear). Although it is easy to see that the factor proportional to $\ln^4(N)$ should clearly be $2C_F^2$, no unique color decomposition from the results provided in Ref. [133] can be determined for all the terms in the expression. However, the numeric result (here the number of light flavors $n_f = 5$) can be written

$$\begin{aligned} \Delta_{bb}^{(2)} = & \left[\frac{32}{9} \right] \ln^4(N) + \left[\frac{44}{9} - \frac{8}{27} n_f + \frac{64}{9} \ln \frac{M_\Phi^2}{\mu_f^2} \right] \ln^3(N) \\ & + \left[\frac{34}{3} + \frac{92}{9} \zeta_2 - \frac{20}{27} n_f + \left(\frac{38}{3} - \frac{4}{9} n_f \right) \ln \frac{M_\Phi^2}{\mu_r^2} - \frac{16}{3} \ln \frac{M_\Phi^2}{\mu_f^2} + \frac{32}{9} \ln^2 \frac{M_\Phi^2}{\mu_f^2} \right] \ln^2(N) \\ & + \left[\frac{404}{27} - 14\zeta_3 - \frac{56}{81} n_f + \left(\frac{34}{3} + \frac{92}{9} \zeta_2 - \frac{20}{27} n_f \right) \ln \frac{M_\Phi^2}{\mu_f^2} - \left(9 - \frac{2}{9} n_f \right) \ln^2 \frac{M_\Phi^2}{\mu_f^2} \right. \\ & + \left. \left(\frac{38}{3} - \frac{4}{9} n_f \right) \ln \frac{M_\Phi^2}{\mu_r^2} \ln \frac{M_\Phi^2}{\mu_f^2} \right] \ln(N) + \left\{ \frac{115}{18} + \frac{58}{9} \zeta_2 - \frac{26}{3} \zeta_3 - \frac{19}{18} \zeta_4 \right. \\ & + \left. \left(\frac{2}{27} - \frac{10}{27} \zeta_2 + \frac{2}{3} \zeta_3 \right) n_f + \left(\frac{25}{12} + \frac{38}{3} \zeta_2 \right) \ln \frac{M_\Phi^2}{\mu_r^2} - \left(\frac{1}{18} + \frac{4}{9} \zeta_2 \right) n_f \ln \frac{M_\Phi^2}{\mu_r^2} \right. \\ & + \left. \left(\frac{11}{12} - 10\zeta_2 - \frac{122}{9} \zeta_3 \right) \ln \frac{M_\Phi^2}{\mu_f^2} + \left(\frac{1}{18} + \frac{4}{9} \zeta_2 \right) n_f \ln \frac{M_\Phi^2}{\mu_f^2} \right. \\ & + \left. \left(\frac{19}{4} - \frac{1}{6} n_f \right) \ln^2 \frac{M_\Phi^2}{\mu_r^2} + \left(\frac{19}{4} - \frac{32}{9} \zeta_2 - \frac{1}{6} n_f \right) \ln^2 \frac{M_\Phi^2}{\mu_f^2} \right. \\ & + \left. \left(\frac{1}{3} n_f - \frac{19}{2} \right) \ln \frac{M_\Phi^2}{\mu_r^2} \ln \frac{M_\Phi^2}{\mu_f^2} \right\} + \frac{34}{3} \zeta_2 + \frac{88}{9} \zeta_3 + \frac{364}{45} \zeta_2^2 - \left(\frac{20}{27} \zeta_2 + \frac{16}{27} \zeta_3 \right) n_f \\ & + \left(\frac{38}{3} \zeta_2 - \frac{4}{9} \zeta_2 n_f \right) \ln \frac{M_\Phi^2}{\mu_r^2} - \left(\frac{16}{3} \zeta_2 - \frac{128}{9} \zeta_3 \right) \ln \frac{M_\Phi^2}{\mu_f^2} + \frac{32}{9} \zeta_2 \ln^2 \frac{M_\Phi^2}{\mu_f^2}. \quad (6.21) \end{aligned}$$

Bibliography

- [1] James Glanz, The New York Times,
“Swiss Physicists Face Decision in Race for Atomic Prize”, 6 Sept 2000.
“On a Particle’s Trail, Physicists Seek Time”, 4 Nov 2000.
“So Boson Arrives At the Party...”, 4 Nov 2000.
“Race to Find Basis of Mass Still On as Lab Retires Device”, 9 Nov 2000.
“Physicists Give Themselves One Last Try at Tantalizing Discovery”,
15 Nov 2000.
“Second Look Back Doubts On Finding Key Particle”, 11 July 2001.
- [2] H. N. Brown *et al.* [Muon g-2 Collaboration], Phys. Rev. Lett. **86**, 2227 (2001) [arXiv:hep-ex/0102017].
- [3] F. J. Yndurain, arXiv:hep-ph/0102312.
- [4] M. Hayakawa and T. Kinoshita, arXiv:hep-ph/0112102.
- [5] P. de Bernardis *et al.* [Boomerang Collaboration], Nature **404**, 955 (2000) [arXiv:astro-ph/0004404].
- [6] P. de Bernardis *et al.* [Boomerang Collaboration], arXiv:astro-ph/0011469.
- [7] J. C. Mather *et al.*, Astrophys. J. **354**, L37 (1990).
- [8] D. N. Spergel *et al.*, Astrophys. J. Suppl. **148**, 175 (2003) [arXiv:astro-ph/0302209].
- [9] Y. Fukuda *et al.* [Super-Kamiokande Collaboration], Phys. Rev. Lett. **81**, 1562 (1998) [arXiv:hep-ex/9807003].
- [10] C. Itzykson and J. B. Zuber, “Quantum Field Theory,” Mcgraw-Hill (1980).

- [11] B. De Wit and J. Smith, “Field Theory In Particle Physics. Vol. 1,” North-Holland (1986).
- [12] G. Sterman, “An Introduction to quantum field theory,” Cambridge Univ. Press (1993).
- [13] M. J. G. Veltman, “Diagrammatica: The Path to Feynman rules,” Cambridge Univ. Press (1994).
- [14] M. E. Peskin and D. V. Schroeder, “An Introduction to quantum field theory,” Addison-Wesley (1995).
- [15] S. Weinberg, Phys. Rev. Lett. **19**, 1264 (1967).
- [16] A. Salam, p. 367 of *Elementary Particle Theory*, ed. N. Svartholm (Almqvist and Wiksells, Stockholm, 1969).
- [17] S. L. Glashow, J. Iliopoulos and L. Maiani, Phys. Rev. D **2**, 1285 (1970).
- [18] H. V. Klapdor-Kleingrothaus, A. Dietz, H. L. Harney and I. V. Krivosheina, Mod. Phys. Lett. A **16**, 2409 (2001) [arXiv:hep-ph/0201231].
- [19] C. E. Aalseth *et al.*, Mod. Phys. Lett. A **17**, 1475 (2002) [arXiv:hep-ex/0202018].
- [20] N. Cabibbo, Phys. Rev. Lett. **10**, 531 (1963).
- [21] M. Kobayashi and T. Maskawa, Prog. Theor. Phys. **49**, 652 (1973).
- [22] C. N. Yang and R. L. Mills, Phys. Rev. **96**, 191 (1954).
- [23] Y. Nambu and G. Jona-Lasinio, Phys. Rev. **122**, 345 (1961).
- [24] J. Goldstone, A. Salam and S. Weinberg, Phys. Rev. **127**, 965 (1962).
- [25] P. W. Higgs, Phys. Lett. **12**, 132 (1964).
- [26] P. W. Higgs, Phys. Rev. Lett. **13**, 508 (1964).
- [27] P. W. Higgs, Phys. Rev. **145**, 1156 (1966).
- [28] F. Englert and R. Brout, Phys. Rev. Lett. **13**, 321 (1964).
- [29] G. S. Guralnik, C. R. Hagen and T. W. B. Kibble, Phys. Rev. Lett. **13**, 585 (1964).

- [30] T. W. B. Kibble, Phys. Rev. **155**, 1554 (1967).
- [31] P. W. Anderson, Phys. Rev. **130**, 439 (1963).
- [32] LEP Electroweak Working Group
<http://lepewwg.web.cern.ch/LEPEWWG/>
- [33] T. Appelquist and J. Carazzone, Phys. Rev. D **11**, 2856 (1975).
- [34] T. Hambye and K. Riesselmann, Phys. Rev. D **55**, 7255 (1997)
[arXiv:hep-ph/9610272].
- [35] M. Sher, Phys. Rept. **179**, 273 (1989).
- [36] K. Riesselmann, arXiv:hep-ph/9711456.
- [37] E. Sellmeier, Ann. Phys. (Leipz.) **143**, 272 (1871).
- [38] W. Strutt (Lord Rayleigh), Philos. Mag. **41**, 107 (1871).
- [39] R.G. Newton, Amer. J. Phys. **44**, 639 (1976).
- [40] B. W. Lee, C. Quigg and H. B. Thacker, Phys. Rev. D **16**, 1519 (1977).
- [41] J. C. Ward, Phys. Rev. **77**, 293 (1950).
- [42] J. C. Ward, Phys. Rev. **78**, 182 (1950).
- [43] Y. Takahashi, Nuovo Cim. **6**, 371 (1957).
- [44] J. C. Taylor, Nucl. Phys. B **33**, 436 (1971).
- [45] A. A. Slavnov, Theor. Math. Phys. **10**, 99 (1972) [Teor. Mat. Fiz. **10**, 153 (1972)].
- [46] G. Zweig, CERN-TH-412
- [47] M. Gell-Mann, Phys. Lett. **8**, 214 (1964).
- [48] S. Stepanyan *et al.* [CLAS Collaboration], Phys. Rev. Lett. **91**, 252001 (2003) [arXiv:hep-ex/0307018].
- [49] J. C. Collins, D. E. Soper and G. Sterman, Nucl. Phys. B **261**, 104 (1985).
- [50] T. Kinoshita, J. Math. Phys. **3**, 650 (1962).

- [51] T. D. Lee and M. Nauenberg, Phys. Rev. **133**, B1549 (1964).
- [52] F. Bloch and A. Nordsieck, Phys. Rev. **52**, 54 (1937).
- [53] L. N. Lipatov, Sov. J. Nucl. Phys. **20**, 94 (1975) [Yad. Fiz. **20**, 181 (1974)].
- [54] V. N. Gribov and L. N. Lipatov, Yad. Fiz. **15**, 781 (1972) [Sov. J. Nucl. Phys. **15**, 438 (1972)].
- [55] G. Altarelli and G. Parisi, Nucl. Phys. B **126**, 298 (1977).
- [56] Y. L. Dokshitzer, Sov. Phys. JETP **46**, 641 (1977) [Zh. Eksp. Teor. Fiz. **73**, 1216 (1977)].
- [57] S. Moch, J. A. M. Vermaseren and A. Vogt, Nucl. Phys. B **688**, 101 (2004) [arXiv:hep-ph/0403192].
- [58] A. Vogt, S. Moch and J. A. M. Vermaseren, Nucl. Phys. B **691**, 129 (2004) [arXiv:hep-ph/0404111].
- [59] F. Maltoni website
<http://maltoni.home.cern.ch/maltoni/>
- [60] R. Barate *et al.* [ALEPH Collaboration], Phys. Lett. B **499**, 67 (2001) [arXiv:hep-ex/0011047].
- [61] M. Acciarri *et al.* [L3 Collaboration], Phys. Lett. B **495**, 18 (2000) [arXiv:hep-ex/0011043].
- [62] P. Abreu *et al.* [DELPHI Collaboration], Phys. Lett. B **499**, 23 (2001) [arXiv:hep-ex/0102036].
- [63] G. Abbiendi *et al.* [OPAL Collaboration], Phys. Lett. B **499**, 38 (2001) [arXiv:hep-ex/0101014].
- [64] J. F. Gunion, H. E. Haber, G. L. Kane and S. Dawson, “The Higgs Hunter’s Guide”, (Addison-Wesley, Reading, MA, 1990), Erratum *ibid.* [arXiv:hep-ph/9302272].
- [65] [LEP Higgs Working Group], arXiv:hep-ex/0107030.
- [66] R. P. Kauffman, S. V. Desai and D. Risal, Phys. Rev. D **55**, 4005 (1997) [Erratum-*ibid.* D **58**, 119901 (1998)] [arXiv:hep-ph/9610541]. Further typos were found and corrected in Ref. [79].

- [67] R. P. Kauffman and S. V. Desai, Phys. Rev. D **59**, 057504 (1999) [arXiv:hep-ph/9808286].
- [68] V. Del Duca, W. Kilgore, C. Oleari, C. Schmidt and D. Zeppenfeld, Nucl. Phys. B **616**, 367 (2001) [arXiv:hep-ph/0108030].
- [69] S. Dawson, Nucl. Phys. B **359**, 283 (1991).
- [70] A. Djouadi, M. Spira and P. M. Zerwas, Phys. Lett. B **264**, 440 (1991).
- [71] R. P. Kauffman and W. Schaffer, Phys. Rev. D **49**, 551 (1994) [arXiv:hep-ph/9305279].
- [72] S. Catani, D. de Florian and M. Grazzini, JHEP **0105**, 025 (2001) [arXiv:hep-ph/0102227].
- [73] S. Catani, D. de Florian and M. Grazzini, JHEP **0201**, 015 (2002) [arXiv:hep-ph/0111164].
- [74] R. V. Harlander and W. B. Kilgore, Phys. Rev. D **64**, 013015 (2001) [arXiv:hep-ph/0102241].
- [75] R. V. Harlander and W. B. Kilgore, Phys. Rev. Lett. **88**, 201801 (2002) [arXiv:hep-ph/0201206].
- [76] C. Anastasiou and K. Melnikov, Nucl. Phys. B **646**, 220 (2002) [arXiv:hep-ph/0207004].
- [77] R. V. Harlander and W. B. Kilgore, JHEP **0210**, 017 (2002) [arXiv:hep-ph/0208096].
- [78] C. Anastasiou and K. Melnikov, Phys. Rev. D **67**, 037501 (2003) [arXiv:hep-ph/0208115].
- [79] V. Ravindran, J. Smith and W. L. Van Neerven, Nucl. Phys. B **634**, 247 (2002) [arXiv:hep-ph/0201114].
- [80] D. de Florian, M. Grazzini and Z. Kunszt, Phys. Rev. Lett. **82**, 5209 (1999) [arXiv:hep-ph/9902483].
- [81] M. A. Shifman, A. I. Vainshtein, M. B. Voloshin and V. I. Zakharov, Sov. J. Nucl. Phys. **30**, 711 (1979) [Yad. Fiz. **30**, 1368 (1979)].
- [82] B. A. Kniehl and M. Spira, Z. Phys. C **69**, 77 (1995) [arXiv:hep-ph/9505225].

- [83] A. Djouadi, M. Spira and P. M. Zerwas, Phys. Lett. B **311**, 255 (1993) [arXiv:hep-ph/9305335].
- [84] J. Pumplin, D. R. Stump, J. Huston, H. L. Lai, P. Nadolsky and W. K. Tung, JHEP **0207**, 012 (2002) [arXiv:hep-ph/0201195].
- [85] J. F. Gunion and X. G. He, Phys. Rev. Lett. **76**, 4468 (1996) [arXiv:hep-ph/9602226].
- [86] A. Djouadi, J. Kalinowski and M. Spira, Comput. Phys. Commun. **108**, 56 (1998) [arXiv:hep-ph/9704448].
- [87] [LEP Higgs Working Group for Higgs boson searches], arXiv:hep-ex/0107029.
- [88] [LEP Higgs Working Group], arXiv:hep-ex/0107030.
- [89] K. Hagiwara *et al.* [Particle Data Group], Phys. Rev. D **66**, 010001 (2002).
- [90] K. G. Chetyrkin, B. A. Kniehl and M. Steinhauser, Phys. Rev. Lett. **79**, 2184 (1997) [arXiv:hep-ph/9706430].
- [91] M. Spira, A. Djouadi, D. Graudenz and P. M. Zerwas, Nucl. Phys. B **453**, 17 (1995) [arXiv:hep-ph/9504378].
- [92] M. Spira, A. Djouadi, D. Graudenz and P. M. Zerwas, Phys. Lett. B **318**, 347 (1993).
- [93] K. G. Chetyrkin, B. A. Kniehl, M. Steinhauser and W. A. Bardeen, Nucl. Phys. B **535**, 3 (1998) [arXiv:hep-ph/9807241].
- [94] S. L. Adler and W. A. Bardeen, Phys. Rev. **182**, 1517 (1969).
- [95] R. V. Harlander, Phys. Lett. B **492**, 74 (2000) [arXiv:hep-ph/0007289].
- [96] A. D. Martin, R. G. Roberts, W. J. Stirling and R. S. Thorne, Eur. Phys. J. C **4**, 463 (1998) [arXiv:hep-ph/9803445].
- [97] A. D. Martin, R. G. Roberts, W. J. Stirling and R. S. Thorne, Eur. Phys. J. C **14**, 133 (2000) [arXiv:hep-ph/9907231].
- [98] B. Field, Phys. Rev. D **66**, 114007 (2002) [arXiv:hep-ph/0208262].
- [99] R. Barate *et al.* [ALEPH Collaboration], Phys. Lett. B **565**, 61 (2003) [arXiv:hep-ex/0306033].

- [100] D. Graudenz, M. Spira and P. M. Zerwas, Phys. Rev. Lett. **70**, 1372 (1993).
- [101] J. R. Ellis, M. K. Gaillard and D. V. Nanopoulos, Nucl. Phys. B **106**, 292 (1976).
- [102] V. Ravindran, J. Smith and W. L. van Neerven, Nucl. Phys. B **665**, 325 (2003) [arXiv:hep-ph/0302135].
- [103] R. K. Ellis, I. Hinchliffe, M. Soldate and J. J. van der Bij, Nucl. Phys. B **297**, 221 (1988).
- [104] U. Baur and E. W. N. Glover, Nucl. Phys. B **339**, 38 (1990).
- [105] O. Brein and W. Hollik, Phys. Rev. D **68**, 095006 (2003) [arXiv:hep-ph/0305321].
- [106] C. J. Glosser and C. R. Schmidt, JHEP **0212**, 016 (2002) [arXiv:hep-ph/0209248].
- [107] B. Field, J. Smith, M. E. Tejeda-Yeomans and W. L. van Neerven, Phys. Lett. B **551**, 137 (2003) [arXiv:hep-ph/0210369].
- [108] C. Kao, Phys. Lett. B **328**, 420 (1994) [arXiv:hep-ph/9310206].
- [109] K. G. Chetyrkin, B. A. Kniehl and M. Steinhauser, Nucl. Phys. B **510**, 61 (1998) [arXiv:hep-ph/9708255].
- [110] M. Krämer, E. Laenen and M. Spira, Nucl. Phys. B **511**, 523 (1998) [arXiv:hep-ph/9611272].
- [111] D. A. Akyeampong and R. Delbourgo, Nuovo Cim. A **17**, 578 (1973).
- [112] D. A. Akyeampong and R. Delbourgo, Nuovo Cim. A **18**, 94 (1973).
- [113] D. A. Akyeampong and R. Delbourgo, Nuovo Cim. A **19**, 219 (1974).
- [114] G. Passarino and M. J. G. Veltman, Nucl. Phys. B **160**, 151 (1979).
- [115] S. Dawson, in *Proc. of the APS/DPF/DPB Summer Study on the Future of Particle Physics (Snowmass 2001)* ed. N. Graf, eConf **C010630**, P124 (2001) [arXiv:hep-ph/0111226].
- [116] G. J. van Oldenborgh, Comput. Phys. Commun. **66**, 1 (1991).. Rev. D **66**, 114007 (2002) [arXiv:hep-ph/0208262].

- [117] M. Carena and H. E. Haber, Prog. Part. Nucl. Phys. **50**, 63 (2003) [arXiv:hep-ph/0208209].
- [118] Tevatron Electroweak Working Group [D0 Collaboration], arXiv:hep-ex/0404010.
- [119] J. Fernandez [DELPHI Collaboration], eConf **C030626**, FRAP09 (2003) [arXiv:hep-ex/0307002].
- [120] S. Catani and L. Trentadue, Nucl. Phys. B **327**, 323 (1989).
- [121] R. P. Kauffman, Phys. Rev. D **44**, 1415 (1991).
- [122] C. P. Yuan, Phys. Lett. B **283**, 395 (1992).
- [123] R. P. Kauffman, Phys. Rev. D **45**, 1512 (1992).
- [124] S. Catani, M. L. Mangano, P. Nason and L. Trentadue, Nucl. Phys. B **478**, 273 (1996) [arXiv:hep-ph/9604351].
- [125] C. Balazs and C. P. Yuan, Phys. Lett. B **478**, 192 (2000) [arXiv:hep-ph/0001103].
- [126] D. de Florian and M. Grazzini, Phys. Rev. Lett. **85**, 4678 (2000) [arXiv:hep-ph/0008152].
- [127] D. de Florian and M. Grazzini, Nucl. Phys. B **616**, 247 (2001) [arXiv:hep-ph/0108273].
- [128] E. L. Berger and J.-w. Qiu, Phys. Rev. D **67**, 034026 (2003) [arXiv:hep-ph/0210135].
- [129] E. L. Berger and J.-w. Qiu, Phys. Rev. Lett. **91**, 222003 (2003) [arXiv:hep-ph/0304267].
- [130] G. Bozzi, S. Catani, D. de Florian and M. Grazzini, Phys. Lett. B **564**, 65 (2003) [arXiv:hep-ph/0302104].
- [131] S. Catani, D. de Florian, M. Grazzini and P. Nason, JHEP **0307**, 028 (2003) [arXiv:hep-ph/0306211].
- [132] A. Kulesza, G. Sterman and W. Vogelsang, Phys. Rev. D **69**, 014012 (2004) [arXiv:hep-ph/0309264].
- [133] R. V. Harlander and W. B. Kilgore, Phys. Rev. D **68**, 013001 (2003) [arXiv:hep-ph/0304035].

- [134] B. Field, S. Dawson and J. Smith, Phys. Rev. D **69**, 074013 (2004) [arXiv:hep-ph/0311199].
- [135] F. Wilczek, Phys. Rev. Lett. **39**, 1304 (1977).
- [136] J. R. Ellis, M. K. Gaillard, D. V. Nanopoulos and C. T. Sachrajda, Phys. Lett. B **83**, 339 (1979).
- [137] H. M. Georgi, S. L. Glashow, M. E. Machacek and D. V. Nanopoulos, Collisions,” Phys. Rev. Lett. **40**, 692 (1978).
- [138] T. G. Rizzo, Phys. Rev. D **22**, 178 (1980) [Addendum-ibid. D **22**, 1824 (1980)].
- [139] M. A. Shifman, A. I. Vainshtein, M. B. Voloshin and V. I. Zakharov, Sov. J. Nucl. Phys. **30**, 711 (1979) [Yad. Fiz. **30**, 1368 (1979)].
- [140] A. I. Vainshtein, V. I. Zakharov and M. A. Shifman, Sov. Phys. Usp. **23**, 429 (1980) [Usp. Fiz. Nauk **131**, 537 (1980)].
- [141] M. B. Voloshin, Sov. J. Nucl. Phys. **45**, 122 (1987) [Yad. Fiz. **45**, 190 (1987)].
- [142] G. 't Hooft and M. J. G. Veltman, Nucl. Phys. B **44**, 189 (1972).
- [143] J. C. Collins and D. E. Soper, Nucl. Phys. B **193**, 381 (1981) [Erratum-ibid. B **213**, 545 (1983)].
- [144] J. C. Collins and D. E. Soper, Nucl. Phys. B **197**, 446 (1982).
- [145] J. C. Collins, D. E. Soper and G. Sterman, Nucl. Phys. B **250**, 199 (1985).
- [146] P. B. Arnold and R. P. Kauffman, Nucl. Phys. B **349**, 381 (1991).
- [147] C. T. H. Davies and W. J. Stirling, Nucl. Phys. B **244**, 337 (1984).
- [148] A. Vogt, Phys. Lett. B **497**, 228 (2001) [arXiv:hep-ph/0010146].
- [149] J. A. M. Vermaseren, arXiv:math-ph/0010025.
- [150] A. D. Martin, R. G. Roberts, W. J. Stirling and R. S. Thorne, Eur. Phys. J. C **28**, 455 (2003) [arXiv:hep-ph/0211080].
- [151] A. D. Martin, R. G. Roberts, W. J. Stirling and R. S. Thorne, arXiv:hep-ph/0308087.

- [152] A. D. Martin, R. G. Roberts, W. J. Stirling and R. S. Thorne, Phys. Lett. B **531**, 216 (2002) [arXiv:hep-ph/0201127].
- [153] D. Stump, J. Huston, J. Pumplin, W. K. Tung, H. L. Lai, S. Kuhlmann and J. F. Owens, JHEP **0310**, 046 (2003) [arXiv:hep-ph/0303013].
- [154] A. Djouadi and S. Ferrag, Phys. Lett. B **586**, 345 (2004) [arXiv:hep-ph/0310209].
- [155] J. A. M. Vermaseren, Int. J. Mod. Phys. A **14**, 2037 (1999) [arXiv:hep-ph/9806280].
- [156] E. Remiddi and J. A. M. Vermaseren, Int. J. Mod. Phys. A **15**, 725 (2000) [arXiv:hep-ph/9905237].
- [157] L. Lewin, “Dilogarithms and Associated Functions”, (North Holland, 1958).
- [158] L. Lewin, “Polylogarithms and Associated Functions”, (North Holland, 1981).
- [159] D. L. Rainwater, M. Spira and D. Zeppenfeld, arXiv:hep-ph/0203187.
- [160] J. Campbell *et al.*, arXiv:hep-ph/0405302.
- [161] B. Field, Phys. Rev. D **70**, 054008 (2004) [arXiv:hep-ph/0405219].
- [162] K. A. Assamagan *et al.* [Higgs Working Group Collaboration], arXiv:hep-ph/0406152.
- [163] S. Abdullin, M. Dubinin, V. Ilyin, D. Kovalenko, V. Savrin and N. Stepanov, Phys. Lett. B **431**, 410 (1998) [arXiv:hep-ph/9805341].
- [164] C. Balazs, P. Nadolsky, C. Schmidt and C. P. Yuan, Phys. Lett. B **489**, 157 (2000) [arXiv:hep-ph/9905551].
- [165] F. I. Olness and W. K. Tung, Nucl. Phys. B **308**, 813 (1988).
- [166] R. M. Barnett, H. E. Haber and D. E. Soper, Nucl. Phys. B **306**, 697 (1988).
- [167] F. I. Olness, R. J. Scalise and W. K. Tung, Phys. Rev. D **59**, 014506 (1999) [arXiv:hep-ph/9712494].
- [168] D. A. Dicus and S. Willenbrock, Phys. Rev. D **39**, 751 (1989).

- [169] F. Maltoni, Z. Sullivan and S. Willenbrock, Phys. Rev. D **67**, 093005 (2003) [arXiv:hep-ph/0301033].
- [170] E. Boos and T. Plehn, Phys. Rev. D **69**, 094005 (2004) [arXiv:hep-ph/0304034].
- [171] S. Dittmaier, M. Kramer and M. Spira, arXiv:hep-ph/0309204.
- [172] S. Dawson, C. B. Jackson, L. Reina and D. Wackerath, arXiv:hep-ph/0408077.
- [173] J. Campbell, R. K. Ellis, F. Maltoni and S. Willenbrock, Phys. Rev. D **67**, 095002 (2003) [arXiv:hep-ph/0204093].
- [174] D. Dicus, T. Stelzer, Z. Sullivan and S. Willenbrock, Phys. Rev. D **59**, 094016 (1999) [arXiv:hep-ph/9811492].
- [175] G. Altarelli, R. K. Ellis and G. Martinelli, Nucl. Phys. B **157**, 461 (1979).
- [176] C. Balazs, H. J. He and C. P. Yuan, Phys. Rev. D **60**, 114001 (1999) [arXiv:hep-ph/9812263].
- [177] V. D. Barger and R. J. N. Phillips, “Collider Physics, *Frontiers in Physics 71*,” Addison-Wesley (1987).
- [178] E. Bycking and K. Kajantie, “Particle Kinematics,” John Wiley & Sons (1973).

Appendix A

Cross-sections and widths

A.1 Cross-section

The definition of a cross-section can be written in very general terms as

$$d\sigma = \frac{1}{2E_{\mathcal{A}}E_{\mathcal{B}}|v_{\mathcal{A}} - v_{\mathcal{B}}|} \left(\prod_f \frac{d^3p_f}{(2\pi)^3} \frac{1}{2E_f} \right) \times |\mathcal{M}(p_{\mathcal{A}}, p_{\mathcal{B}} \rightarrow \{p_f\})|^2 (2\pi)^4 \delta^{(4)}(p_{\mathcal{A}} + p_{\mathcal{B}} - \sum_f p_f). \quad (\text{A.1})$$

However, this equation is usually far too general to be very useful. We are more interested in a few special cases. Notably, $2 \rightarrow 2$ scattering can be solved completely because there is no free angular dependence left to the cross-section.

$$\frac{d\sigma}{dt} = \frac{1}{16\pi} \frac{|\mathcal{M}|^2}{\lambda(s, m_1^2, m_2^2)}, \quad (\text{A.2})$$

where

$$\lambda(x, y, z) = x^2 + y^2 + z^2 - 2xy - 2xz - 2yz, \quad (\text{A.3})$$

is known as the triangular function¹ or sometimes the Källén function in the literature. For our special case, it can also be written as

$$\lambda(s, m_1^2, m_2^2) = \{s - (m_1 + m_2)^2\} \{s - (m_1 - m_2)^2\}. \quad (\text{A.4})$$

Excellent references on how to correctly understand cross-sections and the complexity of phase space integrals as well as how to generalize cross-sections to problems that can be solved by a computer are in the literature [11,177,178].

¹ $\sqrt{-\lambda(x, y, z)}/4$ is the area of a triangle with sides \sqrt{x} , \sqrt{y} , and \sqrt{z} .

A.2 Width

The definition of a decay width of an unstable particle into several final states can be written,

$$d\Gamma = \frac{1}{2m_{\mathcal{A}}} \left(\prod_f \frac{d^3 p_f}{(2\pi)^3} \frac{1}{2E_f} \right) \times |\mathcal{M}(m_{\mathcal{A}} \rightarrow \{p_f\})|^2 (2\pi)^4 \delta^{(4)}(p_{\mathcal{A}} - \sum_f p_f). \quad (\text{A.5})$$

Once again, we are mostly interested in the decay of a single particle into two particles. The $1 \rightarrow 2$ decay can be written as

$$\Gamma(A \rightarrow BC) = \frac{N}{16\pi} \frac{\lambda^{1/2}(M_A^2, M_B^2, M_C^2)}{M_A^3} |\mathcal{M}|^2, \quad (\text{A.6})$$

where $N = 1/2$ if B and C are identical particles and $N = 1$ otherwise.

Appendix B

The Clifford Algebra

Some Clifford algebras that we use in physics are the Pauli matrices and the Dirac γ matrices. The Dirac matrices are often written as defined by the space-time metric, $g^{\mu\nu}$ ($\eta^{\mu\nu}$ in this work). This is not necessary however and may confuse their relationship. A Clifford algebra is more general than the metric.

So-called “modern” books tend to look down upon the Pauli metric (with an imaginary fourth or zeroth component in its four vectors) as being too old-fashioned. However, when one introduces the signed Minkowski metric to calculations there is a choice to be made about the sign of the metric, mostly negative or mostly positive. Most physicists tend to pick a metric and keep it with an almost religious fervor.

Perhaps a great deal could be said as to why its important to learn about the differences in the metrics, but the most practical is that the computer program FORM does its traces and contractions in the Pauli metric. One is free to use whatever metric is convenient as long as one understands the output of third party programs. This is what lead to the sign error in the $(g - 2)_\mu$ calculation, a difference in the definition of the γ_5 between the two conventions that is clearly part of the FORM documentation.

A detailed discussion of the differences and translations between the different conventions can be found in Appendix B of Ref. [11] and Appendix F of Ref. [13].

B.1 Algebra and Group Theory

The Clifford algebra¹ is introduced in the Dirac equation for a free particle in physics,

$$[i\gamma^\mu p_\mu - m]\psi = 0. \quad (\text{B.1})$$

Starting in Euclidean space and the definition of the Clifford algebra,

$$\gamma^i \gamma^j + \gamma^j \gamma^i = 2\delta^{ij} \mathbb{1}, \quad (\text{B.2})$$

we want to find all the inequivalent irreducible representations (irreps) for the algebra that are faithful (they are 1:1 and onto in their homotopy) under the restrictions that

1. $i = j$, $\gamma_i^2 = \mathbb{1}$ (γ_i are Hermitian)
2. $i \neq j$, $\gamma_i \gamma_j = -\gamma_j \gamma_i$, and
3. $(-\mathbb{1})\gamma_i = \gamma_i(-\mathbb{1})$.

There may be more than one irrep of a given group labelled by the index ν . So we can write the dimension of the ν^{th} irrep, d_ν . We also know that if we define the commutator subgroup (an invariant subgroup), C , then the factor group G/C is abelian and the order of G/C is equal to the number of inequivalent one-dimensional irreps.

From these restrictions, we can build a complete set of all the independent group elements. We have

$$\begin{aligned} & \pm \mathbb{1}, \\ & \pm \gamma_i, \quad 1 \leq i \leq d, \\ & \pm \gamma_i \gamma_j, \quad 1 \leq i < j \leq d, \\ & \vdots \\ & \pm \gamma_i \gamma_j \cdots \gamma_d, \end{aligned}$$

where the \pm signs denote separate group elements, not one group element with all its signs changed. In order to guarantee that the algebra satisfies the group relations, we have to pick the representation of the group such that $\mathcal{D}(e) = \mathcal{D}(1) = \mathbb{1}$. We can now count the elements to find the order of the group,

$$g = 2 \sum_{k=0}^d \binom{d}{k} = 2^{d+1}. \quad (\text{B.3})$$

¹Named after W.K. Clifford (1845 – 1879). Clifford was a contemporary of Hermann Grassmann (1809 – 1877) and coined the phrase “mind-stuff.”

d	d_ν	
2	2	Pauli matrices
4	4	Dirac matrices
6	8	⋮
8	16	

Table B.1: Clifford algebras in even dimensions.

Furthermore, we know from group theory that the number of inequivalent irreps is equal to the number of classes (r) and the sum of $(d_\nu)^2$ for all ν is equal to the order of the group. Now we can construct the irreps in even dimensions (we'll use them to build the odd dimensions in a moment). We find

$$d_\nu = 2^{d/2}, \quad r = 2^d + 1, \quad d = \text{even}. \quad (\text{B.4})$$

So for the first few dimensions we have the results of Table (B.1). We will skip the proof that this irrep is faithful and simply state that it is in even dimensions.

For the odd dimensions we find,

$$d_\nu = 2^{(d-1)/2}, \quad r = 2^d + 2, \quad d = \text{odd}. \quad (\text{B.5})$$

This is where the problem arises. We have two irreps that are not one-dimensional and are left with two faithful irreps to the algebra that are not faithful to the group. This leads to a problem defining the equivalent of the γ_5 matrix in odd dimensions. By construction we can show that it would be equal to both the identity matrix and the negative identity matrix and therefore does not exist. Since some definitions of the γ_5 involve the Levi-Cevita tensor, we could also say that you cannot write down a completely anti-symmetric object in an odd number of dimensions.

We conclude with writing down the explicit form for the representations of the Clifford algebra in all even dimensions. If we remember that the third Pauli matrix can be written as the product of the other two ($\sigma_1\sigma_2 = i\sigma_3$), then we are ready.

$$d = 2, \quad \mathcal{D}(\gamma_1) = \sigma_1, \quad \mathcal{D}(\gamma_2) = \sigma_2. \quad (\text{B.6})$$

In $d = 2n$ dimensions we have

$$\mathcal{D}(\gamma_i) = \underbrace{\sigma_3 \otimes \cdots \otimes \sigma_3}_{i-1} \otimes \underbrace{\sigma_1}_i \otimes \underbrace{\mathbb{1} \otimes \cdots \otimes \mathbb{1}}_{n-i}, \quad i = 1 \dots n, \quad (\text{B.7})$$

$$\mathcal{D}(\gamma_{n+i}) = \underbrace{\sigma_3 \otimes \cdots \otimes \sigma_3}_{i-1} \otimes \underbrace{\sigma_2}_{n+i} \otimes \underbrace{\mathbb{1} \otimes \cdots \otimes \mathbb{1}}_{n-i}, \quad i = 1 \dots n. \quad (\text{B.8})$$

If we use the same normalization as the Pauli matrices we would define $\gamma_1\gamma_2\gamma_3\gamma_4 = i\gamma_5$, which we are certainly free to do. In this respect, there is no *extra* factor of i . However, several conventions exist in the literature including the Itzykson and Zuber (or chiral) representation and the Bjorken and Drell convention. Also, some authors count the matrices from $i = 0, 1, 2, 3$ and some $i = 1, 2, 3, 4$.

Appendix C

Group Theory

We will briefly review the details of the $SU(2)$ and $SU(3)$ groups for reference in building SM like models.

C.1 $SU(2)$

The $SU(2)$ group is the group of all unitary 2×2 matrices with unit determinant. The group elements are defined as $T_a = \sigma_a/2$, where σ_a are the Pauli matrices. The Lie algebra is defined as

$$[T_a, T_b] = -i\epsilon_{abc}T_c, \quad (\text{C.1})$$

where $\epsilon_{123} = +1$.

C.2 $SU(3)$

The $SU(3)$ group is the group of all unitary 3×3 matrices with unit determinant. These matrices are sometimes called the Gell-Mann matrices. We define the generators $T_a = \lambda_a/2$ and the Lie algebra as

$$[T_a, T_b] = if_{abc}T_c. \quad (\text{C.2})$$

We also have,

$$\{T_a, T_b\} = \frac{4}{3}\delta_{ab}\mathbb{1} + 2d_{abc}\lambda_c. \quad (\text{C.3})$$

The structure constants f_{abc} are anti-symmetric and d_{abc} are symmetric. The non-vanishing coefficients are listed in Table (C.1).

abc	f_{abc}	abc	d_{abc}	abc	d_{abc}
123	1	118	$1/\sqrt{3}$	355	+1/2
147	1/2	146	1/2	366	-1/2
156	-1/2	157	1/2	377	-1/2
246	1/2	228	$1/\sqrt{3}$	448	$-1/(2\sqrt{3})$
257	1/2	247	-1/2	558	$-1/(2\sqrt{3})$
345	1/2	256	1/2	668	$-1/(2\sqrt{3})$
367	-1/2	338	$1/\sqrt{3}$	778	$-1/(2\sqrt{3})$
458	$\sqrt{3}/2$	344	1/2	888	$-1/\sqrt{3}$
678	$\sqrt{3}/2$				

Table C.1: Non-vanishing $SU(3)$ structure constants.

Appendix D

Loop Integrals

Radiative corrections rely on our ability to do loop integrals. Loop integrals are done by first combining the denominators of an integral and then decomposing the resulting expressions into scalar integrals.

D.1 Feynman parametrization

In order to use many of the results in dimensional regularization, one must first combine the denominators in a loop integral into one denominator. This is done through the introduction of Feynman parameters.

For two denominators, it is very easy to show that,

$$\frac{1}{AB} = \int_0^1 dx \frac{1}{(Ax + B(1-x))^2}, \quad (\text{D.1})$$

which can be proved simply by calculating the integral. For three denominators, we have the expression,

$$\frac{1}{ABC} = 2 \int_0^1 dx \int_0^{1-x} \frac{1}{(Ax + By + (1-x-y)C)^3}. \quad (\text{D.2})$$

This can be generalized, and proven by induction, to the formula,

$$\begin{aligned} \frac{1}{A_1^{\alpha_1} A_2^{\alpha_2} \cdots A_n^{\alpha_n}} &= \frac{\Gamma(\alpha_1 + \alpha_2 + \cdots + \alpha_n)}{\Gamma(\alpha_1)\Gamma(\alpha_2)\cdots\Gamma(\alpha_n)} \\ &\times \int_0^1 dx_1 \cdots dx_n \frac{x_1^{\alpha_1-1} x_2^{\alpha_2-1} \cdots x_n^{\alpha_n-1} \delta(1-x_1-x_2-\cdots-x_n)}{(x_1 A_1 + x_2 A_2 + \cdots + x_n A_n)^{\alpha_1+\alpha_2+\cdots+\alpha_n}}. \end{aligned} \quad (\text{D.3})$$

D.2 Tensor Reduction

We also need to decompose our integrals into scalar integral by removing all the free tensor indices in the numerator. This is often a very error-prone task that can only be completely done on the case of one loop diagrams. Two loop diagrams need a different method to be solved.

Simply put, all the tensor indices are contracted with the basis vectors available (the particle momenta in our case) and expanded in terms of unknown functions which are then solved for by means of Gram determinants. More information can be found in Ref. [114].

Appendix E

Mathematical Reference

Many special functions appear in particle physics. Here we collect some of their properties as a reference tool.

E.1 Euler Gamma

To see the poles of the Gamma function, consider this definition by Euler,

$$\Gamma(z) = \lim_{n \rightarrow \infty} \frac{1 \cdot 2 \cdot 3 \cdots n}{z(z+1)(z+2) \cdots (z+n)} n^z. \quad (\text{E.1})$$

$$\Gamma(1+z) = z\Gamma(z) \quad (\text{E.2})$$

$$\Gamma(n) = (n-1)!, \quad n \text{ integer} \quad (\text{E.3})$$

$$\Gamma(1/2) = \sqrt{\pi} \quad (\text{E.4})$$

Euler-Mascheroni constant¹

$$\gamma_E = \lim_{n \rightarrow \infty} 1 + \frac{1}{2} + \frac{1}{3} + \cdots + \frac{1}{n} - \ln n = 0.577215 \dots \quad (\text{E.5})$$

E.2 Beta function

$$B(p, q) = \frac{\Gamma(p)\Gamma(q)}{\Gamma(p+q)} \quad (\text{E.6})$$

¹Although this constant has been calculated to thousands of decimal places, the fraction 228/395 is good to six decimal places.

E.3 Dilogarithms

Integration of Feynman parameters often lead to Dilogarithms. The best references on Dilogarithms are Refs. [157, 158].

$$\text{Li}_2(z) = \frac{z}{1^2} + \frac{z^2}{2^2} + \frac{z^3}{3^2} + \dots, \quad |z| \leq 1 \quad (\text{E.7})$$

$$= - \int_0^z dz \frac{\ln(1-z)}{z} \quad (\text{E.8})$$

E.4 Expansions

$$\begin{aligned} \Gamma(1 + \epsilon) = 1 - \gamma_E \epsilon + \frac{1}{2} \left(\gamma_E^2 + \zeta_2 \right) \epsilon^2 \\ - \frac{1}{6} \left(\gamma_E^3 + 3\gamma_E \zeta_2 - \psi^{(2)}(1) \right) \epsilon^3 + \dots \end{aligned} \quad (\text{E.9})$$

Index

- α_s , 28
- approximate symmetry, 6
- Bloch-Nordsieck theorem, 34
- CKM Matrix, 4
- dimensional regularization, 26
- effective Lagrangian, 54, 65, 82, 103
- electroweak symmetry breaking, 9
- exact symmetry, 5
- factorization, 30, 34
- Feynman rules
 - QCD, 20
- FORM, 116, 128, 156
- gauge invariance, 6–9
- ghosts, 22
- Goldstone boson, 9, 11
- Goldstone fermion, 9
- HDECAY, 59, 92
- Higgs mechanism, 10–13
- Higgs mass
 - experimental limits, 18
 - theoretical bounds, 14
- HQET, 47, 54, 65, 79, 102
- kinematics, 67
- Kinoshita-Lee-Nauenberg theorem,
 - 34
- Landau pole, 15
- MSSM, 44, 59, 79, 88, 132
- Nambu-Goldstone theorem, 9
- neutrino masses, 4
- physical observable, 39, 55
- physical observables, 87
- QCD, 24–30
- quark model, 24
- renormalization, 27
- resummation, 40, 111–120
 - Higgs, 115–120, 135–138
 - matching, 114
- Standard Model, 2, 88
 - Lagrangian, 2, 19
- supersymmetry, 41
- Ward-Takahashi identities, 24, 85
- weak mixing angle, 12
- Wigner-Weyl symmetry, *see* exact symmetry
- Yukawa coupling, 13